Étude expérimentale et modélisation de l'oxydation partielle du méthane en gaz de synthèse sur réacteur catalytique monolitique à temps court

Elena Leonidovna E. L. Gubanova

N° d'ordre : 204 - 2008 Année 2008

THESE

présentée

devant l'UNIVERSITE CLAUDE BERNARD - LYON 1

pour l'obtention

du DIPLOME DE DOCTORAT

Spécialité : Chimie - Génie des procédés

(arrêté du 7 août 2006)

présentée et soutenue publiquement le 7 novembre 2008

par

Elena Leonidovna GUBANOVA

ETUDE EXPERIMENTALE ET MODELISATION DE L'OXYDATION PARTIELLE DU METHANE EN GAZ DE SYNTHESE SUR REACTEUR CATALYTIQUE MONOLITHIQUE A TEMPS COURT

Directeurs de thèse :

Claude MIRODATOS
Vladislav SADYKOV

JURY :

M. Claude DE BELLEFON (Président de jury)
M. Alain KIENNEMANN (Rapporteur)
M. Claude MIRODATOS
M. Vladislav A. SADYKOV
M. Alexander G. STEPANOV (Rapporteur)
M. André C. VAN VEEN

UNIVERSITE CLAUDE BERNARD - LYON I

Président de l'Université	**M. le Professeur L. COLLET**
Vice-président du Conseil Scientifique	M. le Professeur J.F. MORNEX
Vice-président du Conseil d'Administration	M. le Professeur J. LIETO
Vice-président du Conseil des Etudes et de la Vie Universitaire	M. le Professeur D. SIMON
Secrétaire Général	M. G. GAY

SECTEUR SANTE

Composantes

UFR de Médecine Lyon R.T.H. Laënnec	Directeur : M. le Professeur P. COCHAT
UFR de Médecine Lyon Grange-Blanche	Directeur : M. le Professeur X. MARTIN
UFR de Médecine Lyon-Nord	Directeur : M. le Professeur J. ETIENNE
UFR de Médecine Lyon-Sud	Directeur : M. le Professeur F.N. GILLY
UFR d'Odontologie	Directeur : M. O. ROBIN
Institut des Sciences Pharmaceutiques et Biologiques	Directeur : M. le Professeur F. LOCHER
Institut Techniques de Réadaptation	Directeur : M. le Professeur MATILLON
Département de Formation et Centre de Recherche en Biologie Humaine	Directeur : M. le Professeur P. FARGE

SECTEUR SCIENCES

Composantes

UFR de Physique	Directeur : Mme. le Professeur S. FLECK
UFR de Biologie	Directeur : M. le Professeur H. PINON
UFR de Mécanique	Directeur : M. le Professeur H. BEN HADID
UFR de Génie Electrique et des Procédés	Directeur : M. le Professeur G. CLERC
UFR Sciences de la Terre	Directeur : M. le Professeur P. HANTZPERGUE
UFR de Mathématiques	Directeur : M. le Professeur A. GOLDMAN
UFR d'Informatique	Directeur : M. le Professeur S. AKKOUCHE
UFR de Chimie Biochimie	Directeur : Mme. le Professeur H. PARROT
UFR STAPS	Directeur : M. C. COLLIGNON
Observatoire de Lyon	Directeur : M. le Professeur R. BACON
Institut des Sciences et des Techniques de l'Ingénieur de Lyon	Directeur : M. le Professeur J. LIETO
IUT A	Directeur : M. le Professeur M. C. COULET
IUT B	Directeur : M. le Professeur R. LAMARTINE
Institut de Science Financière et d'Assurances	Directeur : M. le Professeur J.C. AUGROS

REMERCIEMENTS

Je voudrais tout d'abord remercier tous les membres du jury et particulièrement Alexander G. Stepanov et Alain Kiennemann qui m'ont fait l'honneur de juger ce manuscrit comme rapporteurs.

Ensuite, je tiens à remercier Claude Mirodatos pour la confiance qu'il m'a accordée pour la réalisation de ce travail. Je me souviendrai longtemps de son dynamisme et de ses compétences scientifiques, sans oublier son support pour résoudre des défis administratifs d'une thèse en cotutelle. Je veux aussi remercier particulièrement André van Veen pour m'avoir fait profiter de ses nombreuses connaissances dans des domaines très variés. Il a su me faire découvrir de nombreux aspects de mon métier! Je tiens à remercier également Vladislav A. Sadykov pour m'avoir apporté beaucoup de connaissances en catalyse et tout son support du coté russe!

Aussi, je souhaite remercier quelques personnes en particulier Yves Schuurman pour nos nombreuses discussions et son aide avec la modélisation ou encore Erwan Milin, Natalia Sazonova, Louis Olivier et Gabriella Fogassy pour leurs nombreux efforts de traduction et des accompagnements pour résoudre des problèmes du quotidien et pratiques.

Finalement, mes remerciements se tournent vers « celles du 4éme étage », à l'administration (accueil), le service analyse et tout le personnel de l'IRCELYON. Je garde bien évidement le meilleur pour la fin avec tout le groupe « Ingénierie », ceux qui sont déjà partis, ceux qui vont bientôt partir, ceux qui restent : « Je vous souhaite tous mes vœux de réussite personnelle d'abord et professionnelle ensuite… ». Grâce à vous, cette une et demi année passée à l'IRCELYON restera de très bons souvenirs pour moi et vous y êtes tous pour quelque chose.

A vous tous donc, à tous ceux qui ne se retrouvent pas dans ces quelques lignes ou que j'aurais malencontreusement oubliés :

MERCI !!!

Table of Contents

CHAPTER I

Introduction

I.1. General information on processes for the synthesis gas generation

Methane is the main component of natural gas, being forecasted to outlast crude oil by a significant time span (around 60 years) [1]. Nevertheless, the gas industry is currently in a relatively underdeveloped state. Furthermore, natural gas is abundant in many locations around the world [2]. Currently, the use of natural gas as feedstock for chemical or fuels synthesis is regaining significant interest due to the recent rise in supply costs for oil. This marks a major reversal of the recent past situation where the use of gas for chemical synthesis was considered uneconomical because of high costs of natural gas storage and transportation from the remote reservoirs where it is most abundant. Methods to enhance the value of natural gas, either by synthesizing more valuable chemicals or more readily transportable products, have been investigated, particularly in the last 20 years, but yields tended to be too low to compete with oil caused by selectivity issues during methane activation where the added value products are more reactive than methane as reactant.

At present where alternatives for direct methane upgrading did not leave the laboratory stage, the only industrial route for converting methane into more valuable chemicals is the process route via synthesis gas. However, commonly synthesis gas production costs represent the major share of costs given that high investments have to be undertaken to install a pressurized high temperature unit for steam or auto-thermal reforming. Several synthesis gas production methods are available, depending on purpose of industrial application. As shown in Table I.1, synthesis gas can come from steam reforming, oxy-reforming or decomposition of methanol (mainly used in hydrogen production for fuel cells [3,4], because methanol is easy to transport and has a high energy density). Nevertheless, methanol is synthesized from synthesis gas produced from coal or natural gas and this route of synthesis gas production cannot be considered as a primary source.

Using methane to prepare synthesis gas can proceed according to three processes that attract greatest industrial interest: The steam reforming (***Eq.I.1***), the dry reforming with carbon dioxide (***Eq.I.2***) and the partial oxidation with oxygen or air (***Eq.I.3***), together with the associated (reverse) water gas shift equilibrium allowing to adjust the H_2 / CO ratio (***Eq.I.4***).

Steam reforming:

$$CH_4 + H_2O \rightarrow CO + 3H_2 \qquad \Delta H^{\theta}_{298} = +206 kJmol^{-1} \qquad \textbf{Eq.I.1}$$

Dry reforming:

$$CH_4 + CO_2 \rightarrow 2CO + 2H_2 \qquad \Delta H^{\theta}_{298} = +247 kJmol^{-1} \qquad \textbf{Eq.I.2}$$

Partial oxidation:

$$CH_4 + 0.5O_2 \rightarrow CO + 2H_2 \qquad \Delta H^{\theta}_{298} = -38 kJmol^{-1} \qquad \textbf{Eq.I.3}$$

Reverse water gas shift / water gas shift equilibrium:

$$CO_2 + H_2 \leftrightarrow CO + H_2O \qquad \Delta H^{\theta}_{298} = +41 kJmol^{-1} \qquad \textbf{Eq.I.4}$$

It should be stressed, that recently renewed attention has been focused onto the partial oxidation of methane (POM) to syngas due to its potential advantages over conventional steam reforming of methane to syngas [5,6,7,8]: POM produces syngas with a lowered H_2/CO ratio (H_2/CO ≈ 2) suitable for methanol (MeOH) synthesis or Fischer-Tropsch (F-T) process; the POM reaction is slightly exothermic and thus would be much more energy-efficient than the highly endothermic steam reforming of methane; smaller reactors (or higher throughput) would be possible because high methane conversion and selectivities to CO and H_2 may be achieved by POM at short contact time ($\leq 10^{-2}$s) [9].

Table I.1: *Comparison of syngas production via different routes*

Process name	Reaction	ΔH_{298} / kJ mol^{-1}	Industrial application	Advantages	Associated challenges
CH_4 steam reforming	$CH_4+H_2O=CO+3H_2$	206	H_2 production, synthesis gas production	Low (moderate) catalyst coking, suitable for high-pressure processes, easy separation of products	High H_2/CO ratio, needs separation for follow-up F-T or MeOH synthesis, energy (capital) intensive process
CH_4 / CO_2 reforming (dry reforming)	$CO_2+CH_4=2CO+2H_2$	247	Synthesis gas or H_2 production	Uses of two greenhouse gases, i.e. CH_4 + CO_2, as feedstock, high availability of mixtures in some gas fields	Energy-intensive process, low H_2/CO ratio, more H_2 is needed for a follow-up F-T or MeOH process, facile catalysts coking
CH_4 partial oxidation (oxy-reforming)	$CH_4+0.5O_2 \rightarrow CO+2H_2$	-36	Synthesis gas or H_2 production	Mild exothermic reaction, energy saving, H_2/CO ~ 2 (suitable for methanol or F-T synthesis)	A hot-spot may occur in the catalyst bed
Methanol steam reforming	$CH_3OH+H_2O=CO_2+3H_2$	49	H_2 production	Low reforming temperature, High yield of H_2	Not from a primary source, energy-intensive process
Methanol oxy-reforming	$CH_3OH+0.5O_2 \rightarrow CO_2+2H_2$	-192	H_2 production	Exothermic reaction, Low reaction temperature saves energy (or heat exchanger) costs	Not from a primary source, a hot-spot may occur in the catalyst bed

I.1.1. Steam reforming

Steam reforming (SR) of natural gas offers an efficient, economical, and widely used process for hydrogen production, and provides near-and mid-term energy security and environmental benefits. The efficiency of the large-scale steam reforming process with sophisticated heat recovery is about 65% to 75%, among the highest of current commercially available production methods. However, the related devices to ensure the heat recovery cause extensive capital costs from the huge need of investments. Natural gas is a convenient, easy to handle, hydrogen feedstock with a high hydrogen-to-carbon monoxide ratio (3:1). It is also widely available from sources in the U.S., Canada, Russia etc.. The cost of hydrogen produced by SR strongly depends on natural gas prices and is currently the least expensive among all large-scale hydrogen production technologies. A well-developed natural gas infrastructure already exists in the world, a key factor that makes hydrogen production from natural gas attractive. The principal reactions involved in catalytic SR are the formerly mentioned steam reforming of methane (***Eq.I.1***) and in combination with the water gas shift reaction (reverse ***Eq.I.4***) the conversion of methane with maximum hydrogen yield (***Eq.I.5***).

Steam reforming with maximum hydrogen yield:

$$CH_4 + 2H_2O \leftrightarrow CO_2 + 4H_2 \qquad \Delta H^{\theta}_{298} = +165 kJmol^{-1} \qquad \textbf{Eq.I.5}$$

Both steam reforming reactions (***Eq.I.1*** and ***Eq.I.5***) are strongly endothermic, and both lead to significant increases in molar flow rates, i.e. volume expansion, as the reaction proceeds. Equilibrium conversion of both reforming reactions therefore benefit from high temperatures and low pressures, whereas the water-gas shift (WGS) reaction (reverse ***Eq.I.4***), being exothermic and having no change in the number of moles, benefits thermodynamically from lower temperatures and is independent of pressure. The overall endothermic and reversible process is usually carried out in parallel vertical fixed bed catalyst tubes, suspended within huge high-temperature (typically >850^{o}C) furnaces, coupled with pressure swing adsorption (PSA) for hydrogen purification.

I.1.2. Dry reforming

Reforming of methane with CO_2 (***Eq.I.2***) is another alternative route with important advantages for some applications since the H_2:CO product ratio being produced is 1:1 or less. A lower H_2:CO product ratio is preferred for the production of oxygenated compounds (via oxo-synthesis or hydroformylation), and it also introduces the possibility to adjust the H_2:CO ratio to desired values of different applications combining the steam reforming, partial oxidation, and dry reforming reactions. It can be considered also as a "greener" process, which may reduce CO_2 emissions, as long as a sufficient heat source is available. The dry reforming was first studied by Fischer and Tropsch in 1928 over base metal catalysts [10], and more recently studies on this reaction have identified a number of typical catalysts, including Fe [11], Co [12], Ni [13,14,15], being of interest from the industrial point of view. Numerous studies have demonstrated that noble metal catalysts exhibit better activity and suffer less of carbon deposition [16,17,18,19]. The dry reforming reaction is more endothermic than steam reforming, and could take up excess energy of the partial oxidation. Generally, a suitable adjustment between exothermic and endothermic reactions can be predicted from thermodynamic equilibrium calculations. The stoichiometric reaction of methane and carbon dioxide over the group VIII transition metals at 780°C and ambient pressure, gives synthesis gas selectivities of around 90%, with methane and carbon dioxide conversions greater than 85%, with carbon deposition being also predicted. The major drawback of this reaction, however, is the rapid deactivation caused by carbon deposition via the Boudouard reaction ($2CO \leftrightarrow C + CO_2$) and/or CH_4 decomposition.

I.1.3. Catalytic partial oxidation of methane (CPOM)

Catalytic partial oxidation of methane (CPOM) is an advantageous route for synthesis gas production for both economical and technical reasons: It makes the process less energy-intensive and capital cost–intensive because of its slight exothermic nature, and the lower H_2:CO ratio (of about 2) is more favorable with respect to downstream processes such as methanol synthesis and Fischer–Tropsch synthesis of higher hydrocarbons. In addition, a fuel processor based on partial oxidation of methane could provide a low cost and compact system, with fast start-up and the capability to follow load variations more adequate for fuel cell electric vehicles [20].

In CPOM, methane reacts directly with oxygen or air to form CO and H_2 in the one-step reaction (***Eq.I.3***). CPOM is much faster than reforming reactions, suggesting that a single stage

process for syngas generation would be a viable alternative to steam reforming and could also result in smaller reactors and higher throughput. The extreme reaction conditions (reaction temperatures around 1000°C) result in very high reactions rates and thus extremely short residence times in the millisecond range [21] suffice to obtain the desired conversion. Nevertheless, despite decades of extensive research, the reaction is still poorly understood to date. Many engineering problems such as heat and mass transfer issues and sparse kinetic information present still obstacles for reactor simulation and optimization. As well as for engineering reasons, proper kinetic measurements would benefit to the development of improved catalysts and these are also required for a clear understanding of the reaction mechanism.

I.2. Proposed mechanism for the CPOM

Methane can be converted to synthesis gas either via the direct or indirect reaction schemes. According to the indirect reaction scheme, part of methane is combusted towards CO_2 and H_2O in a well oxygen supplied zone (***Eq.I.6***). Reforming of the remaining methane with CO_2 and H_2O takes subsequently place producing CO and H_2 (***Eq.I.1-2***).

$$CH_4 + 2O_2 \leftrightarrow CO_2 + 2H_2O \qquad \Delta H^{\theta}_{298} = -801 kJmol^{-1} \qquad \textbf{Eq.I.6}$$

On the other hand, it has been shown that under certain conditions over certain catalysts, the direct formation of synthesis gas from methane and oxygen is possible [22,23,24]. This strongly depends on the availability of oxygen on the catalyst surface and on the oxygen-surface bond-strength [22]. The problem with industrial implementation of synthesis gas production through this route is the reactivity between oxygen and the primary products - carbon monoxide and hydrogen to form carbon dioxide and water [25]. This limits the possible yields of synthesis gas from the direct reaction between methane and oxygen at lower temperatures. In this context it should be noted that demonstrating the direct formation of synthesis gas involved among others the Temporal Analysis of Products (TAP) method [24] capable to probe the catalyst performance without significant mass and heat transfer issues.

Recent research has been directed towards reaction between methane and solid oxygen carriers. A recent study has shown that oxygen in solid oxidized platinum has high activity for

methane oxidation to syngas and at the same time a low activity for the oxidation of hydrogen and carbon monoxide [24]. Oxygen bound or dissolved in a solid platinum matrix was found to be less reactive than oxygen supplied from a gas phase and thereby largely increasing the syngas selectivity. It was proposed that this finding relates to the favorably balanced ratio of diffusion rate of oxygen in platinum and the residence times of reacting species on the surface adjusting the availability of oxygen on the surfaces so that the reaction proceeds with stoichiometrically favorable quantities for the syngas generation. However, platinum is a rather expensive material and large volumes necessary to establish a sufficient oxygen reservoir exclude any applicable catalyst development with platinum-only systems. Cerium and ceria-zirconia oxides have been shown to have a high oxygen storage capacity and suitable release characteristics in many applications [26,27,28,29]. Otsuka et. al. [28,30] have studied the reaction between methane and cerium oxide and found that synthesis gas indeed can be formed. Physical mixing with platinum black had a large effect on the conversion of methane.

I.3. Short-contact-time CPOM reactors

The catalytic partial oxidation of methane to synthesis gas in short contact time reactors is generally addressed as a potentially attractive method for natural gas conversion. CH_4 conversion close to unity and 90% selectivity to H_2 and CO can be reached by oxidizing CH_4 over Rh or Pt structured catalysts at high reaction temperatures (830°C), at contact times of 10^{-2} to 10^{-4} s and with autothermal reactor configurations [73]. Autothermal operating conditions yield significant economic, energetic and environmental benefits [31]. The presence of a catalyst allows to achieve high yields and large throughput with small reactor sizes and lower operating temperatures; simplicity and compactness of the reactor reduce its heat capacity and improve its dynamic response. All these features make the CPO process ideal for small to medium scale decentralized production of H_2 and syngas. Though extremely flexible, the process is highly complex. Short contact time reactors work under severe conditions, with very high gas hourly space velocity (GHSV) and temperatures, complex fluid pattern and a strong coupling of heat and mass transfer with surface and possibly gas phase kinetics [32]. These factors make the understanding of the process kinetics, a pre-requisite for any design application, a challenging task.

As shown in paragraph I.2, two distinct mechanisms are proposed for explaining the formation of syngas: the direct pathway with formation CO and H_2 and the indirect one where the total oxidation of methane is followed by reforming reactions with syngas formation. In the literature, depending on the sampling technique, the type of reactor and operating conditions, different product distributions were obtained and different mechanisms were thus inferred, either direct [33,34], indirect [35,36] or mixed [37]. Many factors were speculated to govern the reaction pathway, namely pressure, temperature, change in noble metal oxidation state [38,39] and nature of the support [39,40]. This makes the distinction between the direct and indirect formation of syngas difficult. In addition, the kinetics of the catalytic partial oxidation of methane cannot be determined in a straightforward way. First of all, the CPO reaction is extremely fast, which indicates that mass-transport limitations are likely to occur. Also, nonselective, exothermic oxidation reactions can lead to severe heat-transport limitations, resulting in high catalyst temperatures. In most kinetic studies, however, heat-transfer resistances are not taken into account, since only gas-phase temperatures are measured.

Several experimental reactor configurations have been used to study the reaction kinetics of CPO at short contact times and high temperatures. These configurations have in common that, in contrast to fixed beds, the catalytic material is present in a structured way. A catalytic annular reactor was applied by Beretta et all. [41]. To study the intrinsic kinetics of CPO reaction in the presence of heat-transport limitations, de Smet et all. [42] developed an experimental reactor, containing a single Pt gauze catalyst. Heat-transport limitations were taken into account explicitly in this reactor, since the catalyst temperature was measured directly using a thermocouple spot-welded to the Pt gauze. It was demonstrated that experiments could not be performed at conditions where both conversions and selectivities are determined by the chemical phenomena alone. Therefore, taking into account the relevant transport phenomena, de Smet et al. [42] developed a reactor model to obtain the intrinsic kinetic parameters of the CPO reaction on a Pt gauze [43]. Other authors [73,37,44,45] studied the process under relevant practical conditions, using either autothermal or non-adiabatic reactors and different geometries of the catalyst support (spheres, honeycombs or metal foams). Typically, in these studies the reaction mechanism is inferred from the outlet concentrations. Such an approach is claimed to be not fully rigorous for the mechanism analysis, since frequently both a direct and indirect scheme can equally justify the data.

I.4. Overview of catalysts proposed for the CPOM process

After nearly 100 years of development, three main types of catalysts have been investigated for the partial oxidation of methane to synthesis gas. They are supported nickel, cobalt or iron catalyst; supported noble metal catalyst; and transition metal carbide catalysts [46]. Some of these catalyst systems will be discussed in more detail.

I.4.1. The base metals catalytic system

The earliest work on catalytic partial oxidation was performed by Liander [47], Padovani and Franchetti [48], and Prettre et. al. [49] who found that synthesis gas with a product ratio $H_2/CO=2$ could be produced at 730 – 930°C and 1 atm. over supported nickel catalysts. Most researchers since have come to similar conclusions to these early results; nickel is highly active for synthesis gas production, but it also catalyses carbon formation. To decrease the carbon deposition and increase the stability of the support and thus to extend the catalyst lifetime, much work has been done on the modification of supports.

Choudhary and co-workers [50,51,52,53] have studied nickel catalysts supported over ytterbium oxide, CaO, TiO_2, ZrO_2, ThO_2, UO_2 and rare earth oxide modified alumina supports. They found that the NiO containing MgO, CaO, rare earth oxides on alumina catalysts showed high catalytic activity in the process at a very short contact time.

Effect of supports on the catalytic activity has been investigated for Ni supported on Al_2O_3, SiO_2-Al_2O_3, SiO_2- ZrO_2, and zeolite H-Y. Acidity of supports (SiO_2-Al_2O_3, zeolite H-Y) was shown to reduce the catalytic activity. The fact was explained by the long time required to reduce Ni on the acid supports [54]. In any case, the products distribution shows that complete oxidation followed by steam or CO_2 (or both) reforming reactions could occur on these types of catalysts. The indirect mechanism appears to be the typical one for high temperatures (above 700°C). At low temperatures, methoxy species (OCH_3) are formed first on the reduced surface (e.g., Co/MgO), which decompose to CO or CO_2 and H_2O [53].

The addition of rare earth metal oxide or alkaline metal oxide to alumina or the use of rare-earth oxides as support can restrict carbon deposition [55,56,57,58,59]. Nickel catalysts supported with rare earth oxide- and alkaline metal oxide-modified alumina have been tested for 500 hours without observable decrease in methane conversion, CO and H_2 selectivity [60]. The

promotion of the rare earth oxide addition on the catalyst support is probably due to its capability to act as oxygen or oxygen - containing compounds storage, which can help in oxidizing the deposited surface carbon. It is also believed that the presence of rare earth oxide such as CeO_2 can stabilize the support and prevent it from sintering during the high-temperature reaction.

Perovskites, the composite oxides of alkali-earth (rare-earth) and transition metals with a general formula ABO_3, establish a vast class of catalytic systems for oxidation reforming of hydrocarbons. The perovskite structure is depicted in Figure I.1, where the alkali-earth cation (A) is symbolized in red color, the transition metal cation (B) is depicted in green color and the oxygen anion is represented with blue color.

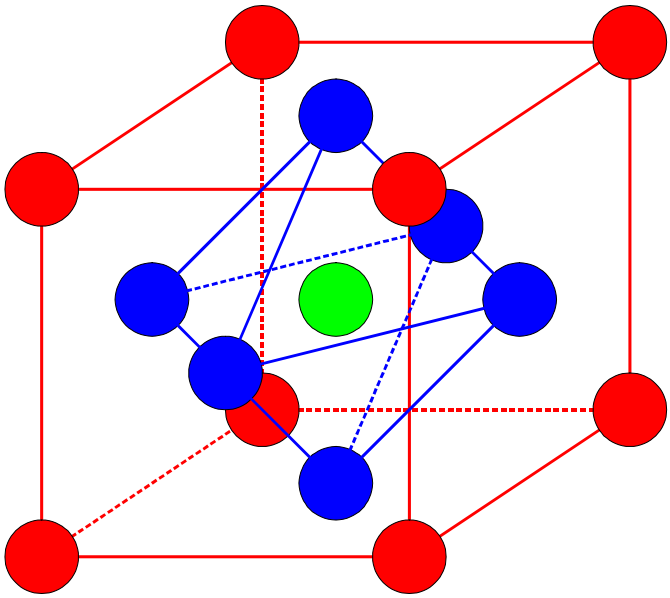

Figure I.1: *Schematic of the unit cell in the perovskite structure.*

Briefly, the transition metal cation B is in the octahedral surrounding of oxygen anions and in the cubic centre of the big cation A. This cation itself is surrounded by 12 oxygen ions. A dense packing is provided with the layers AO_3 constituted by oxygen anions and A cations. Lattice defects are formed, if A or B cations are replaced by cations with different charge. Activity of perovskite for the different catalytic reactions has been intensively investigated since 1970. Catalytic activity seems to correlate with the density of different lattice defects [61]. However, there is still an ongoing debate nowadays [62]. Among the different methods to synthesize Ni-based perovskites the acetate [63], citrate, gelation, impregnation [64] methods are the most popular. Some authors suggest [65] using ceria oxide for improving resistance of

Ni/Al_2O_3 catalyst to both sintering ability and coke formation. Cerium is supposed to weaken a strong bond of Ni with aluminum oxide. This prevents Ni diffusion in the aluminum oxide lattice followed by migration to the catalyst surface. Nickel crystallites formed on the surface without cerium are generally susceptible to the carbon deposition. Due to lanthanum Ni and lanthanides - based perovskites have a high basicity and Ni dispersion [63]. Z. Zhang, X.E. Verykios [66] have investigated Ni/La_2O_3 in the steam and CO_2 reforming of methane. It was shown that the catalyst was highly resistant to the coke deposition. The same fact was confirmed by P. Chen et. al. [67] for the partial oxidation and CO_2 reforming of methane over the four-component La and Ni-based catalyst. In this case the tendency for coke deposition is reduced due to low metallic Ni content on the catalyst surface. Metallic Ni is capable to promote the homolytic decomposition of C-H bond followed by coke formation. Moreover, triple-charged La and Cr cations improve the oxygen anions mobility in the lattice and stabilize Ni in the state of 1+ or 2+ [67].

I.4.2. Group VIII transition metals

Green and co-workers showed that high yields of synthesis gas can be obtained over nearly all the noble metal catalysts used, as well as over the rare earth ruthenium pyrochlores [46]. For, example, under reaction conditions of 780°C and 1 bar, for stoichiometric partial oxidation with air, they obtained methane conversions ~ 94%, with carbon monoxide and hydrogen selectivities of 97% and 99%, respectively, at complete oxygen conversion [68,69,70,71]. Further, all the catalysts catalyze the partial oxidation reaction to thermodynamic equilibrium, ignoring elemental carbon formation. No carbon deposition was seen on these catalysts and a study by Claridge et al. has shown that the relative order of carbon formation is Ni > Pd >>Rh, Ru, Ir, Pt [72].

Hickman and Schmidt [73] studied platinum group metals supported extruded monoliths, foams and metal gauzes. Rh-containing catalysts ensure higher HC conversions and syngas selectivities (up to 90%) as compared with Pt-containing ones, especially at high GHSV and pressures up to 5 atm [74,75,76]. For gauzes, oxygen conversion was incomplete and hydrogen selectivity low [77]. As demonstrated by O'Connor et al, [78], ceramic foam monolithic catalysts (80 ppi) with supported secondary alumina layer and Rh (5 wt.%) ensure more than 95% conversion of cyclohexane, n-hexane and isooctane in the mixture with air in the autothermal regime at short contact times, even in the case when up to 25% of toluene was added. Syngas

yield only weakly varied with GHSV in the range of 30000/h –300000/h. In the patent of Johnson Matthey [79] a catalytic process of the hydrogen generation is described by autothermal reforming of hydrocarbons including contact of the mixture of hydrocarbon, oxygen-containing gas and steam with catalyst comprised of the thermally stable support from the mixture of ceria and zirconia oxides with supported Rh. Hydrocarbons can be either linear or branched with the carbon number from 1 to 15, including methane, isooctane, naphta, liquefied petroleum gas, reformulated gasoline and diesel oil.

As follows from analysis of published data, the most promising type of a catalyst for this application is a monolith catalyst containing precious metals combined with mixed active component. The catalyst being developed at Argonne National Laboratory and produced by Süd-Chemie Inc. contains a transition metal supported on an oxide-ion-conducting substrate, such as ceria, zirconia or lanthanum gallate, that has been doped with a small amount of non-reducible element, such as gadolinium, samarium or zirconium [80]. Various transition metals supported on doped ceria have exhibited excellent isooctane reforming activity between 500 and 800^{o}C with high fuel conversion and H_2 selectivity. Among the metals investigated (Ni, Co, Ru, Pd, Fe, Cu, Ag), all metals, except for Ag, exhibit a conversion above 95 % at T > 600°C , and all metals exhibit 100 % conversion at 700°C. At T < 600°C, conversion decreases more rapidly for first-row transition metals (in particular Ni and Co), than for the second row (Ru) and third row (Pt, Pd) transition metals. The second- and third-row transition metals exhibit a higher selectivity to H_2 (>60%) than the first-row transition metals at T > 650°C. At T < 600°C, the H_2 selectivity decreases to <50% for all metals except Ni and Ru [81].

I.5. Complex CeO_2-ZrO_2 mixed oxides

Ceria-zirconia is one of the main components of current new generation of three-way catalysts (TWC) for the treatment of noxious pollutions from car exhaust [82] and transformation of hydrocarbons or oxygenates into syngas by partial oxidation or autothermal reforming [83,84], solid oxide fuel cells anodes [85] etc. It has gradually replaced pure cerium oxide (CeO_2) which characteristics in terms of specific surface area and their stability under reactive atmosphere were not adequate to sustain the high degree of conversion and the thermal resistance required for catalytic converters to meet the more severe regulations in terms of emissions of CO, NO_x and

hydrocarbons. It has been used in the formulations of car exhaust catalysts since the early 1990s and this is evidenced by an almost exponential increase in the number of publications devoted to the catalytic features of this system in the last few years, following the first publications in the open literature in 1993 [86,87]. The main features, which contribute to the success of ceria-zirconia, are:

- A higher thermal resistance as compared with conventional CeO_2-containing TWC;
- A higher reduction efficiency of the redox couple Ce^{4+} - Ce^{3+};
- Good oxygen storage / release capacity.

These features bring to an overall higher degree of conversion especially at low temperature, during start up, where the majority of emissions are produced. Most of the recent literature on this topic has focused on the study of the redox properties, related to the oxygen storage capacity, thermal stability and interaction with noble metals which will be discuss in more detail further.

I.5.1. Phase diagram of CeO_2–ZrO_2

Before entering into the details of the properties of the CeO_2–ZrO_2 mixed oxides the appearance of the phase diagram will be briefly discussed. Until present days the exact appearance of this diagram is still a subject of debate and extensive work of several research groups [88,89,90,91,92,93,94]. The main reason is that besides the thermodynamically stable phases, a number of metastable phases have been presented in the literature.

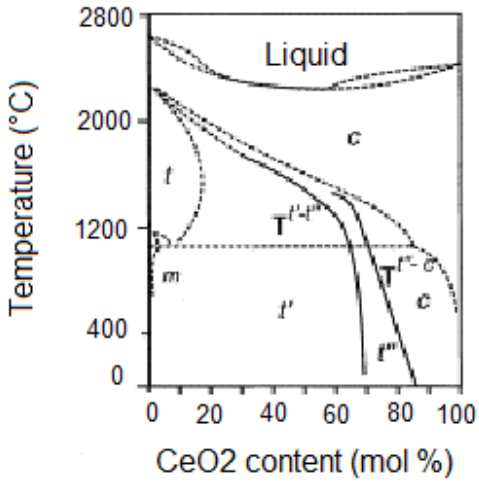

Figure I.2: *Phase diagram of the CeO_2-ZrO_2* [89].

As shown in Figure I.2, below 1000°C the phase diagram shows a monophase region of monoclinic (*m*) symmetry for CeO_2 molar contents less than ≈ 10%, while for CeO_2 contents higher than 80% cubic (*c*) phase was reported [93]. In the intermediate region, the true nature of CeO_2-ZrO_2.phase diagram is still unclear. In this region indeed a number of stable and metastable phases of tetragonal symmetry are observed [91]. According to Yashima et al. [89,90,94] three different *t, t'* and *t''* phases can be distinguished on the bases of XRD and Raman characterization. The *t*-form is a stable one formed through a diffusional phase decomposition, the *t'*-form is obtained through a diffusionless transition and it is metastable, while the *t''*-form is an intermediate between *t'* and *c*. It shows no tetragonality and it exhibits an oxygen displacement from ideal fluorite sites. The typical schematic of the unit cell in the fluorite structure is presented in Figure I.3. The *t''* phase is often referred to as a cubic phase because its XRD pattern is indexed in the cubic Fm3m space group [95]. This is due to the fact that the cation sublattice prevalently generates the XRD pattern. For clarity, the characteristics of all the phases are summarized in Table I.2.

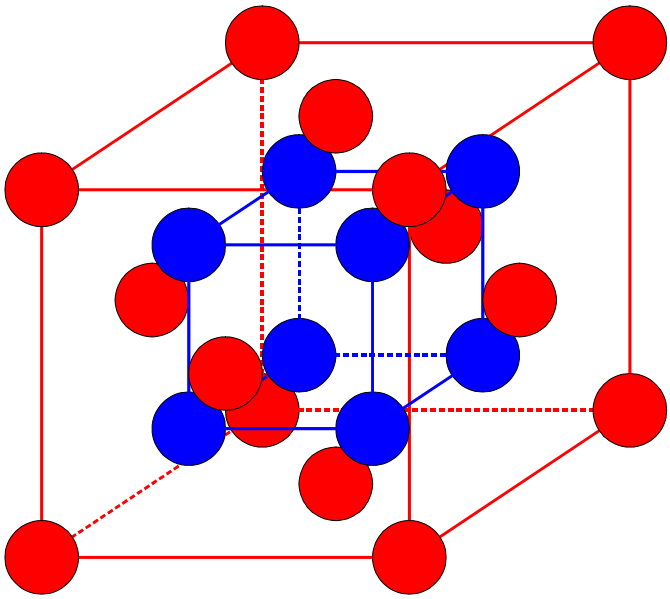

Figure I.3: *Schematic of the unit cell in the fluorite structure.*

Table I.2: *Classification of the phases in the CeO_2-ZrO_2 binary system* [94].

Phase	Composition range (mol% Ce)	Tetragonality[a]	Space group
Monoclinic (m)	0-10	-	$P2_1/c$
Tetragonal (t)	10-30	>1	$P4_2/nmc$
Tetragonal (t')	30-65	>1	$P4_2/nmc$
Tetragonal (t'')	65-80	1	$P4_2/nmc$
Cubic (c)	80-100	1	Fm3m

The phase boundaries as indicated in Figure I.2 should be considered as very approximative due to the fact that in the case of the metastable tetragonal phases, the kind of distortion from the fluorite type structure is highly sensitive to the particle size. Yashima et. al. observed that the t'' phase is formed for CeO_2 contents above 65 mol%, while P. Fornasiero et. al. reported the formation of the same phase for a $Ce_{0.5}Zr_{0.5}O_2$ sample [95].

It should be noted that specific compounds have also been proposed to exist in the CeO_2-ZrO_2 system: tetragonal $Ce_2Zr_3O_{10}$ [96] and cubic Ce_3ZrO_8 [97]. The existence of the former compound, however, has not been confirmed [93]. Finally, in the discussion of the features of the

[a] Defined as axial ratio c/a.

CeO_2-ZrO_2 phase diagrams, it must be considered that upon reduction of the CeO_2-ZrO_2 mixed oxides a still different situation is observed [98] and the presence of different phases was inferred [99].

I.5.2. Methods of preparation of complex mixed oxide

The presence of metastable phases in the phase diagram immediately points out the critical importance of the method of synthesis of mixed oxides and the relevance of the kinetic liability/inertness towards phase separation.

Several different preparation methods of CeO_2-ZrO_2 were described in literature. Main synthesis methods of this kind of system are high temperature sintering [100], co-precipitation [101], high-energy milling [102] and sol-gel techniques [95]. Some known preparation methods have some disadvantages leading to samples with very low specific surface areas not suitable for catalyst supports (high temperature sintering) or too high specific surface areas collapsing later employing the catalyst at high temperatures (sol-gel techniques). However, the main disadvantage of most of the former methods is in homogeneity in the metal ion distribution that could be a reason for forming not single-phase samples and, as a consequence, a low ionic conductivity. Traditional preparation methods of catalyst could lead also to segregation of components with formation of separate phase or micro-heterogeneous solid solutions. A method, which can help to solve the problem of homogeneity, is the Pechini method.

According to the patent [103] establishing this synthesis procedure, the Pechini method makes use of α-hydrooxicarbonic acid (such as citric acid), which is necessary for complexation of different cations. In the presence of polybasic alcohol, for example the ethylene glycol, these complexes react with alcohol forming organic esters and water as products. At heating of this mixture, the polyesterification happens, which is the reason of the uniform distribution of metallic ions in the entirely organic matrix [104]. After that the solution is heated for removing a surplus of solvent, and as intermediate product the solid resin is formed. Because of its very high viscosity and very strong interactions due to complexes formation, metal ions “freeze” in solid polymeric grid in the same uniform state [105]. In the end of preparation the solid resin is combusted under air for removing organic residues.

The sequence of mixing reactants, water : citric acid : ethylene glycol ratio and the nature of used metal precursors (more preferable are nitrates, which allow very easy removal of the

anions to the benefit of oxides formation during calcination) play a very important role in solid synthesis process according to the Pechini method [106].

The formation of the polymeric structure prevents a segregation process of cations of metals, especially in multicomponent systems [107]. One of the striking advantages of this method of preparation is the formation of a crystalline phase at low temperatures being the reason of yielding small particles with higher specific surface area and, therefore, a higher reactivity [104].

I.6. Thermal stability of CeO_2-ZrO_2 oxide

The thermal stability of CeO_2 is a critical point in determining its promotion effects. Industrial research has spent significant efforts on finding the solution for improving the thermal stability, oxygen storage capacity (OSC) and metal-support interactions by modification of the CeO_2 synthesis and by looking for different types of promoters and stabilizers. The addition of ZrO_2 always aimed at increasing the thermal stability of CeO_2, which easily sinters above 800°C, particularly under a reducing atmosphere [108]. Since 1990s, the evidence has been reported in the open literature concerning the use of CeO_2-ZrO_2 mixed oxides in problems of efficiency of structural doping of CeO_2 by ZrO_2 in improving the redox and catalytic properties of CeO_2 [86,87]. The improved stability of CeO_2-ZrO_2 mixed oxides compared to CeO_2 is now a well-established fact [82,101,109] and justifies their general use for three-way catalysis applications. OSC is recognized to improve the catalytic activity, and generally speaking, it is related to capacity of a system to release or to retake oxygen, during the different rich or lean phases that occur during the regulation of the exhaust gases composition. For ceria support, several factors contribute to decrease the OSC during aging, and sintering may be one of the important causes for the OSC loss [110]. However, it was found for ceria-zirconia mixed oxides, that an aging or a reduction treatment at high temperature is beneficial for OSC [95,111].

An investigation of the effects of ZrO_2 content on thermal stability suggested $Ce_{0.8}Zr_{0.2}O_2$ as suitable composition [112]; in contrast, ZrO_2-rich compositions were found to be more thermally stable compared to CeO_2-rich in other studies [113]. Using a polymeric precursor route for the synthesis of the mixed oxides, the lowest sintering was observed for a $Ce_{0.5}Zr_{0.5}O_2$ composition [114]. Of great importance, a single phase $Ce_{0.2}Zr_{0.8}O_2$ solid solution with high thermal stability featured very different redox behavior as a function of redox pretreatments

compared to that of a poor thermal stability, indicating the importance of textural properties on the chemical behavior [115] Clearly, a rational for deriving the effects of the composition on thermal stability is needed.

It was found that sintering behavior is strongly affected by the pore structure of the material itself. Both the pore curvature and pore radius are extremely important factors, larger pores with negative pore curvature preventing sintering of the materials [116]. Researchers from Rhodia recently demonstrated the importance of the initial texture on the thermal stability. They showed that by the bimodal – fractal type of pore distribution, a remarkably high thermal stability could be conferred to these mixed oxides. It is observed that when the porous solid is sintered at high temperatures, pores with small radii tend to both annihilate and grow. Accordingly, they partially act as a reservoir to the secondary network of the macro-pores generated by the synthesis, which is nearly unaffected by the thermal treatment. In such a way, a final texture consisting of a network of very large pores is produced, which confers a significant BET area to the product after calcination at very high temperatures. It is also noted that the presence of such a stable pore network, generated by the synthesis, minimizes encapsulation of the precious metal particles upon ageing [117], which is a typical drawback of $Ce_xZr_{1-x}O_2$ with poor textural stability [116].

It was shown that the mode of preparation strongly affects the thermal stability of these mixed oxides, in addition to the effects of dopants [118,119,120]. Thus, researchers from Ford observed remarkably high thermal stability, which was distinguished for a $Ce_{0.5}Zr_{0.5}O_2$ (20-30 $m^2\ g^{-1}$ after calcination at 1050°C for 12h) using a cellulose template for the synthesis of the solid solution; such synthesis conferred a filamentous-like morphology to the mixed oxide particles. Whereas no general rule seems derivable from the literature data as far as the best composition and textural properties are concerned, indications are available, which suggest that use of ZrO_2–rich compositions and dopants with large ionic radii are factors enhancing thermal stability of CeO_2-containing mixed oxides; on the contrary small dopants increase the rate of sintering [117]. For example, addition of Y_2O_3 or MgO to ZrO_2-rich $Ce_xZr_{1-x}O_2$ decreases the grain size of the material with respect to parent $Ce_xZr_{1-x}O_2$ in the sintering process [121,122].

One of the alternative ways for improving thermal stability of CeO_2-based oxide is that using high-surface-area Al_2O_3 generates a homogeneous nanosized supported mixed oxide. The investigations that were done two decades ago reported that the interaction of CeO_2 with Al_2O_3 favors formation of highly dispersed CeO_2 particles at the surface and, upon aging, $CeAlO_3$ is

formed [123,124]. It also was shown that using Al_2O_3 as support for CeO_2-based mixed oxide can provide high textural stability particularly under reducing conditions; however, re-oxidation of such reduced species is not easy, resulting in deterioration of the OSC. Only recently, there has been a renewed interest in this area, focused on the preparation that could help to find solution to prevent the unfavorable interaction of CeO_2 with Al_2O_3 leading to formation of $CeAlO_3$, hence, deterioration of its redox properties and characterization of nanostructured $Ce_xZr_{1-x}O_2/Al_2O_3$ materials.

An analysis of the data in the literature shows that addition of Al_2O_3 to $Ce_xZr_{1-x}O_2$ mixed oxide significantly increases its thermal stability with respect to the unsupported oxide. As above discussed, synthesis strategies have important influence on the characteristics of the obtained solid. Reasonably good textural properties were observed for the unsupported oxide even after calcination in high temperatures range (1000-1100°C). For example a simple co-impregnation of ceria and zirconia precursors on the surface of Al_2O_3 led to high thermal stabilities with surface areas as high as 60-80 m^2 g^{-1} after calcination at 1000-1100°C for 5-100 h, provided that appropriate impregnation methodology is used, e.g. citrate precursors method [125,126,127]. Several studies suggested sol-gel or microemulsion synthesis as reasonable routes leading to materials with good compositional homogeneity, even for materials with intermediate $Ce_xZr_{1-x}O_2$ compositions [128,129,130]. It was found that such material is typically stable to 900°C without segregation of the components. Moreover, ZrO_2-rich nanostructured $Ce_xZr_{1-x}O_2/Al_2O_3$ was shown to maintain structural integrity even at 1100°C, consistent with the stability of the *t*-phase [127].

It should be stressed at this point that discussion still exists, whether the presence of a homogeneous solid solution is really a strict requisite to achieve good properties like efficient OSC. Generally speaking, the presence of compositional nanosized non-homogeneities favors accelerated phase segregation for calcination at and above 1000°C, allowing their detection by conventional XRD technique [131,132]. More important, the CeO_2-rich component (about 80 mol%), which is formed by the phase segregation, is a readily sintering material compared to other $Ce_xZr_{1-x}O_2$ compositions [133] and this may crucially affect the dynamic-OSC [126]. This property, which is measured under cycling feed stream compositions (typically alternating pulses of CO and O_2), is closely related to the suitability in three way catalyst application and is expected to play a major role in the partial oxidation of methane as well. The decline in dynamic-

OSC is probably linked to the extent of surface area losses of the material [101]. It is also important to underline that nanodomain non-homogeneities can, in principle, escape from proper detection, even in calcined samples. Structural characterization and detection of phase homogeneity in these nanodispersed materials is in fact prone to several difficulties [134].

The interactions in the $Ce_xZr_{1-x}O_2$ and Al_2O_3 nanostructured system are quite complex and depend on a number of factors, calcination temperature included. First it is observed that zirconia is sparingly soluble in Al_2O_3, which, as dictated by the phase diagram, leads to segregation of ZrO_2 from the Al_2O_3 phase on calcination [135,136]. On the other hand, by impregnation of ZrO_2 onto Al_2O_3, remarkable high thermal stability could be achieved leading to a BET area of 50 m^2 g^{-1} after calcination at 1200°C; this was attributed to the ability of ZrO_2 to spread over the Al_2O_3 surface, thus suppressing its transformation to the α-phase [137]. As for what ceria is concerned, this component strongly interacts with Al_2O_3 leading to formation of $CeAlO_3$. This interaction is particularly effective under reducing conditions, on the other hand, the presence of bi- and tri-dimensional patches/clusters of CeO_2 have been detected over the Al_2O_3 surface, leading to different interaction with the Al_2O_3 support [138], and, hence, redox activity [26]. Accordingly, one can expect that whereas ZrO_2 tends preferentially to segregate from the Al_2O_3 phase, this can be only partially true for the CeO_2 phase. Consistently, the presence of $CeAlO_3$ phase has been detected in a redox-aged $Ce_{0.6}Zr_{0.4}O_2/Al_2O_3$ sample [139].

These observations suggest that the interactions in this three-component system are rather complex. In a recent detailed characterization of a series of $Ce_xZr_{1-x}O_2/Al_2O_3$ nanostructured oxides, prepared by impregnation with varying the composition and loading of the solid solution, evidence was found that a fraction of ceria is in the Ce (III) oxidation state, higher amounts of Ce(III) being found as the amount of the supported $Ce_{0.2}Zr_{0.8}O_2$ phase was decreased from 70 to 7 wt%. Significantly, the degree of stabilization of the BET surface area is affected by the loading of the supported phase. The maximum degree of stabilization was achieved at the lowest loading employed (Figure I.4).

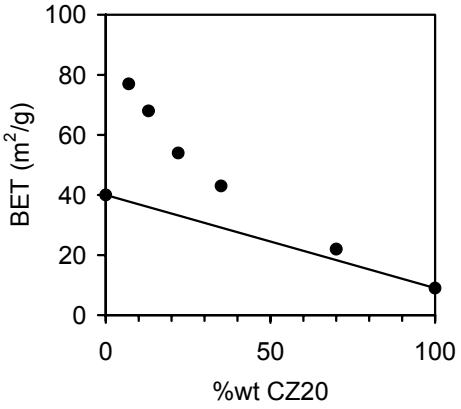

Figure I.4: *Effects of the $Ce_{0.2}Zr_{0.8}O_2$ loading on the BET area of $Ce_{0.2}Zr_{0.8}O_2$(YY)/Al_2O_3 nanostructured oxide calcined at 1100°C for 5 h (the straight line represents the BET area of a non interacting physical mixture)* [127].

The comparison with thermal stabilities reported for CeO_2/Al_2O_3 and ZrO_2/Al_2O_3 systems is rather interesting: Piras et al. [140] found almost no variation of the BET surface area in CeO_2/Al_2O_3 composite materials calcined at 1100°C as the CeO_2 content was varied from 3 to 15 wt%. Similarly, constant surface areas were observed for ZrO_2 loading between 0.43 and 14.8 wt% on impregnated ZrO_2-Al_2O_3 systems, after calcination at 1100°C [137]. This clearly points out a synergic stabilization of the textural properties due to the simultaneous presence of both the Zr and Ce component in this nanocomposite system. Consistently, a mutual interaction between the $Ce_{0.2}Zr_{0.8}O_2$ and Al_2O_3 phases has been detected as denoted by a decrease of the cell parameters with decreasing the amount of the $Ce_{0.2}Zr_{0.8}O_2$ phase, which suggested some incorporation of alumina species in the $Ce_{0.2}Zr_{0.8}O_2$ phase [127].

I.7. Redox properties of CeO_2-ZrO_2 oxides

Evidence for the importance of ZrO_2 in modifying the redox behavior of CeO_2 was first reported in open literature by Japanese authors [86,87]. Formation of a mixed oxide $Ce_xZr_{1-x}O_2$ by a co-precipitation method decreased the temperature of the bulk reduction from 830 to about 630°C [87]. This shift was observed even in nearly fully sintered $Ce_xZr_{1-x}O_2$ solid solutions [86,87], provided that catalytic amounts of noble metal were deposited on the powder to provide centers able to efficiently activate and dissociate hydrogen; these hydrogen species are then

spilled to the support favoring its reduction at 430-630°C, depending on the amount of ZrO_2 inserted in the lattice. A huge amount of work was devoted to investigation of this system, with the aim of identifying the best composition and properties (structure) of the $Ce_xZr_{1-x}O_2$ mixed oxide, leading to best performances. The lowest reduction temperature and the highest degree of reducibility are typically considered as desirable properties. In principle, one should consider that the desirable options for these catalytic redox oxides should also include the rate of the oxygen transfer, and, possibly, the ability to tune the redox property according to the requirements of the specific catalytic reaction considered.

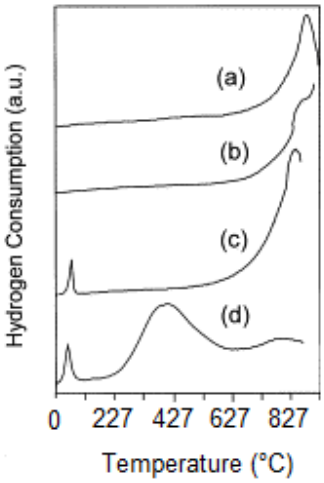

Figure I.5: *The temperature programmed reduction (TPR) profiles of LSA samples: (a) CeO_2, (b) $Ce_{0.6}Zr_{0.4}O_2$, (c) 0.5 wt% Rh/CeO_2, and (d) 0.5 wt% $Rh/Ce_{0.6}Zr_{0.4}O_2$* [141].

In the beginning of 90s, Ranga et al. reported an unusual observation [141] that the reduction occurred at very mild temperatures (330–430°C) in the bulk of Rh-loaded CeO_2–ZrO_2 solid solutions despite the fact that these systems were prepared by a solid state synthesis. This synthesis, which consists of firing a mixture of oxides at 1600°C, produces dense ceramic materials with a very low surface area (LSA, $\approx 1\ m^2\ g^{-1}$). The ability of the sintered Rh/CeO_2–ZrO_2 solid solutions to undergo reduction at mild temperatures is exemplified in Figure I.5, which reports the TPR profiles for Rh-loaded and metal-free $Ce_{0.6}Zr_{0.4}O_2$. The comparison of the TPR traces of the Rh-loaded CeO_2 and $Ce_{0.6}Zr_{0.4}O_2$ immediately reveals that there is a strong reduction peak at ca. 430°C in the ZrO_2-containing catalyst, which is missing in the other systems. This feature is attributed to the promotion of the reduction in the bulk of the mixed oxide, since surface effects can be excluded in these samples.

As far as the low temperature reduction is concerned, a remarkable observation was that a sequence of redox treatments, including a high temperature reduction (HTR, typically 1000°C) and, as shown later, also a high temperature oxidation (HTO, typically 1000°C), leads to temperature profiles with reduction at temperatures as low as 180-330°C [111,115], at least for single-phase solid solutions [142,143]. Typically, for a sintered $Ce_xZr_{1-x}O_2$, the sequence HTR

followed by a low temperature oxidation (LTO, typically 180-430°C) induces a low temperature reduction, but this favorable redox behavior is aversely modified [144] when the HTR is followed by a HTO instead of LTO. This is exemplified in Figure I.6.

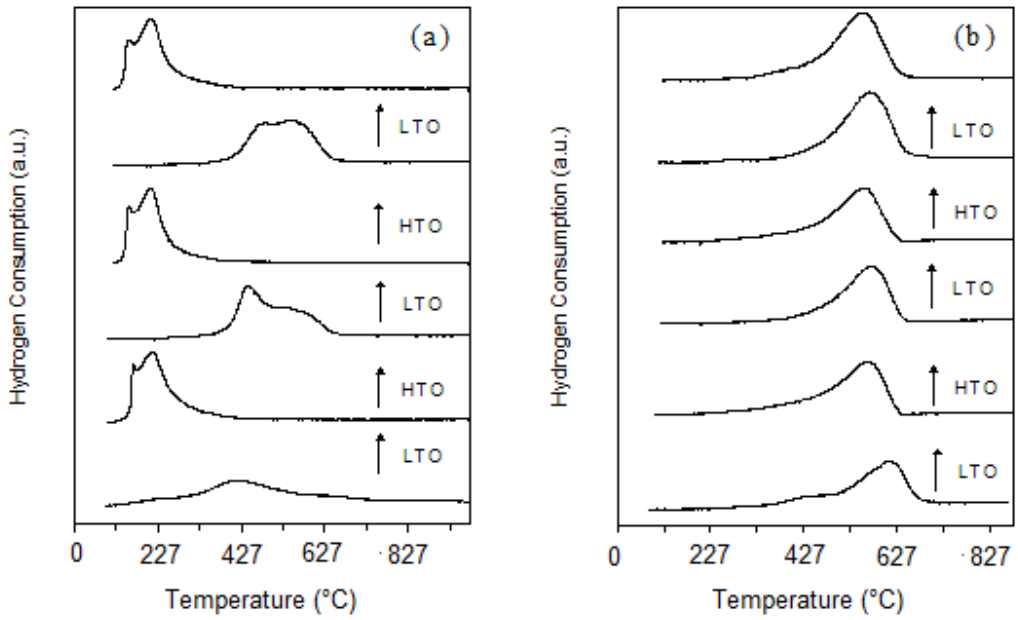

Figure I.6: *Effects of pre-treatments (HTO at 1000°C and LTO at 430°C) of the temperature programmed reduction profiles of (a) texturally-unstable and (b) texturally-stable* $Ce_{0.2}Zr_{0.8}O_2$ *solid solutions. Both materials were calcined at 1000°C for 5 h before the experiment resulting in BET surface areas of respectively 4 and 22* $m^2 g^{-1}$ [115].

Clearly the observation that reduction of the sintered samples may occur at a temperature as low as ca. 230°C compared to ca. 630°C in the high surface area sample is a very unusual feature. It is just the opposite of what is the typical redox behavior of the traditional CeO_2 OSC promoter. This prompted flourishing activity aimed at identifying the origin of such phenomenon.

Otsuka-Yao-Matsui et al., using ceramic type of $Ce_xZr_{1-x}O_2$ mixed oxides, investigated these phenomena in detail and reported the formation of ordered $Ce_xZr_{1-x}O_2$ solid solutions upon redox ageing [145,146,147]. When HTO is applied to the ordered phase, an order-disorder transition occurs, leading to high temperature reduction profiles, associated with the disordered solid solution. Other researchers have confirmed these results showing that when the

homogeneity and order of the solid solution are improved, the OSC increases [148,149]; computational support to the formation of ordered phase was also reported [150].

In fact, the dependence of the reduction behavior of the CeO_2–ZrO_2 mixed oxides upon textural properties is rather intriguing. For example, for the $Ce_{0.5}Zr_{0.5}O_2$ composition the following TPR behavior was observed: a single peak at 680°C [109] and two peaks at 610 and 730°C for surface areas of, respectively, 22 and 64 $m^2\ g^{-1}$) [95]. In another investigation two peaks at 530 and 730°C were found [87]. In contrast, the ultimate degree of reduction is approximately constant, e.g. a composition of $Ce_{0.5}Zr_{0.5}O_{1.85}$ is obtained after a reduction at 1000°C [95, 109]. Furthermore, the treatment under H_2 in the TPR leads to a strong sintering of the mixed oxides and the surface area drops to or below 10 $m^2\ g^{-1}$, which as shown in Figure I.7, leading to a decrease in the reduction temperature compared to the fresh, high surface sample (HSA) [95, 111]. This effect is even more remarkable in the presence of the supported noble metal where the reduction of the aged samples occurs at a temperature as low as 170°C for Rh. Clearly, both textural and structural factors govern the redox behavior of these mixed oxides. It is also worth noting that conventional characterization methods may fail in determining the presence of micro-domains in the mixed oxide, which in turn affect the redox behavior [151].

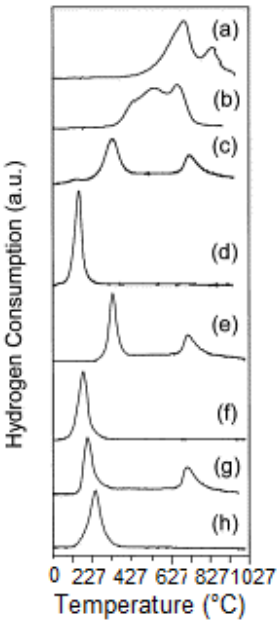

Figure I.7: *TPR profiles of fresh and recycled / oxidized at 430°C samples: $Ce_{0.5}Zr_{0.5}O_2$ (a) fresh, (b) recycled; $Rh/Ce_{0.5}Zr_{0.5}O_2$ (c) fresh, (d) recycled; $Pt/Ce_{0.5}Zr_{0.5}O_2$ (e) fresh, (f) recycled; $Pd/Ce_{0.5}Zr_{0.5}O_2$ (g) fresh, (h) recycled* [95,111].

A possible interpretation of the unusual redox behavior reported in Figure I.5 was given by the comparison of the Raman spectra of the fresh and aged $Ce_{0.5}Zr_{0.5}O_2$ (HSA). Both the fresh metal-free and Rh-loaded $Ce_{0.5}Zr_{0.5}O_2$ (HSA) featured a strong T_{2g} band at 465 cm^{-1} attributed to a total symmetric M–O (M=Zr, Ce) stretching mode whose intensity strongly decreased upon

ageing in TPR/oxidation processes. This was taken as an indication of a progressive breaking of the symmetry of the M–O bond leading to an oxygen sublattice of the type observed in the $Ce_{0.5}Zr_{0.5}O_2$ (LSA). This interpretation was further substantiated by the TPR profiles of the noble metal-loaded HSA $Ce_{0.5}Zr_{0.5}O_2$. In the presence of the noble metal, the hydrogen activation is unlikely to rate limit the reduction process. Consistently, spilling of H_2 to the support surface is responsible for the shift of the surface reduction from 500 to 130–180°C in the HSA CeO_2 in the presence of the noble metal [152]. Accordingly, the reduction peak observed at 610°C in the fresh $Ce_{0.5}Zr_{0.5}O_2$ (HSA) shifts to 230–430°C in the presence of Rh, Pt or Pd, leaving the peak at 830°C unaffected. The sintering occurring in the TPR modifies the oxygen sublattice, which increases the oxygen mobility in the bulk and shifts the whole reduction process to low temperatures.

Adachi and co-workers have pioneered an alternative approach to the design of low temperature OCS materials by subjecting the $Ce_xZr_{1-x}O_2$ materials to surface etching, using different reactants, i.e. chlorine or chlorine containing compounds, that could remove part of surface Zr (IV) species by an initial chlorination and subsequent volatilization with the aid of $AlCl_3$ [153], leading to a CeO_2-enriched surface. Such treated $Ce_xZr_{1-x}O_2$ mixed oxides, when prepared by an oxalate route, feature quite low temperature reduction profiles; most interesting is the fact that the improved property was quite stable even for extensive ageing and the materials did not experienced the adverse effect of the HTO. Unfortunately, also due to the high temperatures of the treatments favoring extensive sintering, these materials feature very low surface areas.

Comprehension of the reduction mechanism, however, is the true key that in principle allows one to design novel redox materials and, in this case, to tune their properties.

Investigation of the redox properties of $Ce_{0.5}Zr_{0.5}O_2$ with respect to CO as a reducing agent showed that surface processes limit the rate of reduction [154]. Accordingly, different surface processes have been identified in the dynamic OSC measurements, where significant CO dissociation can also occur [155]. In the case of H_2, the situation is more complex; a detailed TPR study, using deuterium as reducing agent [156], revealed the presence of the isotopic effect only for reduction processes occurring at high temperatures, typically above 280-430°C. The reason for such a behavior can be accounted for when the rate of oxygen migration from the bulk towards the surface of the $Ce_xZr_{1-x}O_2$ particle is calculated (Figure I.8): surface processes limit

the rate of reduction only at temperatures where the rate of oxygen migration exceeds that of the reduction. Furthermore, hydrogen scrambling, i.e. the activation of D_2 at the surface, always precedes the irreversible reduction, i.e. water evolution, and it is sensitive to the pre-treatments in the same fashion as the TPR behavior illustrated in Figure I.4: a TPR/MO pre-treatment leads to low temperature scrambling, whereas TPR/SO moves the scrambling process to high temperatures.

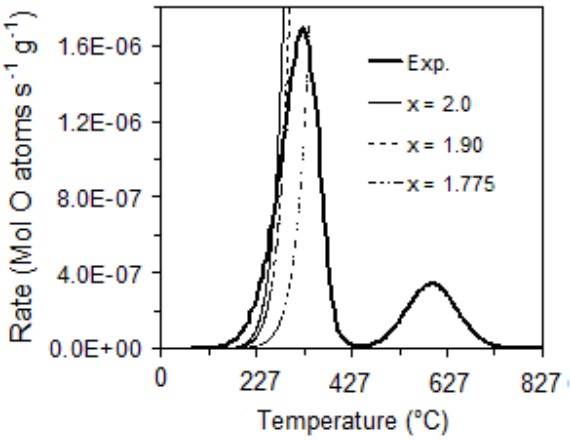

Figure I.8: *Comparison of the experimental reduction rate of a $Ce_{0.5}Zr_{0.5}O_2$ solid solution subjected to a TPR/MO pre-treatment and the calculated rate of oxygen migration from the bulk towards the particle surface calculated for different degrees of reduction* [156].

The redox behavior of ternary CeO_2–ZrO_2 systems using tri-valent oxides as dopants was also investigated [157]. Ga^{3+}, Y^{3+} and La^{3+} were inserted into the $Ce_{0.6}Zr_{0.4}O_2$ lattice [151] given that these cations have strongly varying sizes. The ionic radius of Y^{3+} (1.1015 Å) is very close to the critical one, Ga^{3+} (0.62 Å) and La^{3+} (1.18 Å) are, respectively, undersized and oversized ones. Conventionally, the critical radius is defined as the radius, which gives no expansion to the lattice upon substitution. Remarkable modifications of the TPR profiles were found, which can be summarized as follows:

1. An appropriate amount (2.5–5.0 mol%) of the tri-valent dopants is necessary to achieve a significant improvement of the reduction;
2. Among the cations investigated, the one whose ionic radius is closest to the critical radius of the $Ce_{0.6}Zr_{0.4}O_2$ is the most effective in promoting the reducibility at a low temperature;

3. The OSC measured after a low temperature reduction is improved by about 30% compared to the undoped sample. In contrast the total-OSC measured after a reduction at 1000°C is less affected (see above).

A remarkable point in all these investigations is that redox ageing often leads to improved TPR behavior at moderate temperatures (compare Figure I.7), suggesting a high thermal stability of the OSC in the CeO_2–ZrO_2 mixed oxides.

I.8. Ceria-based mixed oxides as oxygen storage component, role of dopants

The excellent oxygen storage behavior of ceria is the result of a unique and delicate balance between structural (phase formation), kinetic (rate at which redox changes among $Ce^{4+/3+}$ proceed) and textural (presence of surface cerium sites) factors. For the design of CeO_2 – based materials with high oxygen storage / transport capacity, it is therefore important to know the mechanism by which ceria stores, transports, i.e. lets diffusion in the bulk proceed, and releases oxygen. According to the mechanism and dynamics of oxygen storage, an increase in the number and mobility of oxygen vacancies should lead to a corresponding increase in the ability of the material to take up and release oxygen. Therefore any chemical modification of CeO_2 involving an increase in the number of structural defects (oxygen vacancies) should produce a material with a higher oxygen storage capacity. This is true providing that the chemical modification does not significantly reduce the number of active redox elements. In principle there are two ways in which one could operate to accomplish this. The first action is to promote ceria reduction [100], and the second approach is to chemically dope ceria with other transition or rare-earth elements [158]. Promotion of ceria reduction can be accomplished either by noble metal deposition or by chemically modifying ceria with one or more dopant [151].

The choice of the doping elements and of the amounts to be employed is a key factor in the design of modified ceria. The ability to substitute one cation by another one in a particular structure depends on several factors, such as the dimensions of the host/guest cations and the structural features of the pure oxide. Moreover, as was noted before, the preparation method can also have a strong influence on the stability and homogeneity of a solid solution. CeO_2 can easily form solid solutions with other rare earth elements and with transition metals. Of the rare earth elements, Pr and Tb are particularly suitable for making solid solutions with cerium [159,160].

The known structure of PrO_2 and TbO_2 is of the cubic fluorite type and the ionic radii of Pr^{4+} and Tb^{4+} are close to that of Ce^{4+} [161].

Regarding transition metals, CeO_2 can form solid solutions not only with ZrO_2 [94], but also with PbO_2 [162], CuO [163], MnO_x [164], although the range of stability and phase composition varies widely over these ions. With Cu^{2+} and $Mn^{3,4+}$, which have a smaller ionic radius, solid solutions that retain the fluorite structure are formed only in a limited compositional range. Conversely, although the ionic radius of Zr^{4+} (0.84 Å) is smaller than that of Ce^{4+} (0.97 Å), CeO_2 and ZrO_2 form solid solution quite easily and in a large composition range. Indeed, the use of Zr^{4+} as a dopant promotes the kinetics of Ce^{4+} reduction and enhances the oxygen storage capacity of ceria [82].

Generally speaking, the formation of mixed oxides or, better, solid solutions does not represent the only way to improve the properties of ceria, but also to improve the thermal behavior and the oxygen handling properties.

Summarizing literature data, there are sparse indications in the literature on the favorable role of dopants on thermal stability and also on the oxygen storage capacity (OSC) of the $Ce_xZr_{1-x}O_2$ materials, however, a rationale and a general description of their role is missing.

I.9. Effect of interactions between CeO_2-ZrO_2 mixed oxides and noble metals

Given some, but rather limited, catalytic action of the CeO_2-ZrO_2 mixed oxide itself, most of the catalytic processes employing $Ce_xZr_{1-x}O_2$ mixed oxides include a noble metal in the formulation of the active catalyst. Literature reports have been extensively showing that CeO_2 remarkably modifies the activity of supported metals [82]. Several aspects of the chemistry of noble metal (NM)/CeO_2-containing oxides have in fact been reviewed recently [165,166,167]. However, no general picture for the promotion effects of CeO_2 on the catalytic efficiency of supported noble metals exists currently [165,167]. This is due to the fact that too many factors appear to be operating, often simultaneously, when systems involving noble metal/CeO_2-based oxides are considered. In a recent critical discussion of the OSC properties, Kašpar et al. suggested that the capability of the CeO_2-based oxides to provide oxygen to or abstract it from the catalytic centre is perhaps a more general and appropriate definition of most of the CeO_2 functionalities related to the OSC property [168]. It is accepted as evident, that there is

immediately an extreme difficulty in defining the role and nature of the noble metal/$Ce_xZr_{1-x}O_2$ interactions, due to the remarkably modifiable chemical behavior of these systems outlined above. From phenomenological point of view, the strong metal – support interaction (SMSI) effect is characterized by number of features, which can be summarized as follows [82]:

- It is associated to reducible supports;
- It is induced by "high temperature", typically $T_{redn} \geq 450°C$, reduction treatments;
- Inherent to the onset of the SMSI state, the chemical properties of the dispersed metal phase are heavily disturbed: strong inhibition of its chemisorption properties and significant changes in its catalytic behavior occur;
- It is reversible, i.e., upon high–temperature reoxidation ($T_{redn} \leq 450°C$) followed by a mild reduction treatment, the conventional behavior of the supported metal phase may be recovered.

Anyway, the oxygen transfer capability is certainly an important aspect of the NM/$Ce_xZr_{1-x}O_2$ chemistry, but it does not include other intriguing catalytic properties of these systems. Generally speaking, it has been long recognized that NM/CeO_2-containing moieties are capable of exceptionally high activities [169,170], particularly under transient conditions, after being subjected to a HTR (at 450°C). This is due to the powerful ability of reduced CeO_{2-x}-moieties to abstract oxygen from simple oxygen containing molecules such as CO_2, CO, NO, etc. [171]. Role of surface and bulk oxygen vacancies, the latter favoring the high activity, has been evidenced [172]. In fact, the oxygen mobility in these systems is very high and differences of only about one order of magnitude between the oxygen diffusivity in the bulk and over the surface were found recently [173].

High catalytic activities were observed for these systems also under stationary reaction conditions [125,174], but these activities are generally dependent on the reaction temperature, high reaction temperatures often deactivating the catalyst activity. Even more intriguing are the findings reported by researchers from Johnson Matthey, who found that by co-precipitating NM and CeO_2-based oxides, the so-called normal support activation could be induced where the NM embedded within the support is capable of conferring catalytic activities to the support, which are even higher than those observed over conventionally impregnated catalysts [175].

All these examples clearly shown that the comprehension of the NM/$Ce_xZr_{1-x}O_2$ chemistry is by far less understood than that of simple oxides. There are several reasons for this; however,

one major difficulty is linked to the above-discussed variability of the properties of these mixed oxides.

I.10. Summary of literature overview

1. CPOM process advantages and challenges. The above literature overview indicated that the generation of synthesis gas by catalytic partial oxidation of methane at short contact time is a very promising alternative to the widely used, but energy demanding steam reforming of methane. The ratio H_2/CO of synthesis gas generated by CPOM is almost equal to 2, which is more convenient for synthesis of methanol and hydrocarbons by Fischer-Tropsch.

Another advantage of CPOM is the potential implementation of the process in small scale reactors at short contact times. Different research groups proposed a lot of different catalysts in literature for CPOM, but still most of them have disadvantages like carbon build–up, thermal and mechanic instability, not sufficiently high thermal conductivity and reaction rates. For this reason developing catalysts with better performance and thermo-mechanical properties is still a topical task for the future of this process.

2. Selected catalytic system: advantages and challenges. Catalysts employing CeO_2-ZrO_2 mixed oxides in their composition present today a promising perspective. However, if the cerium zirconium oxides with supported noble metals such as Pt are known from de-NO_x studies to selectively activate hydrocarbons, this has still to be demonstrated for the CPOM.

Most of the recent studies on this prospected system have been dedicated to the redox properties, related to the oxygen storage capacity or focused on the thermal stability and interaction with noble metals. It was revealed that one of the main advantageous features of ceria-zirconia is a high reduction efficiency of the redox couple Ce^{4+} - Ce^{3+}. Moreover it was shown that $Ce^{4+/3+}$ cations had a promotion effect of on the catalytic efficiency of supported noble metals (e.g. Pt). However, these effects and interaction still remain to be investigated in details.

3. Heat and oxygen management and doping effects. The formation of mixed oxides or, more precisely the establishment of solid solutions, does not only present a suitable way to

improve the properties of ceria, but it also improves the thermal behavior and the oxygen handling properties. Summarizing literature data, there are sparse indications in the literature on the favorable role of dopants on thermal stability and also on the oxygen storage capacity (OSC) of the $Ce_xZr_{1-x}O_2$ materials, however, a general description of their role is missing.

4. Engineering aspects. Concerning the literature dedicated to short-contact time reactor configuration for implementing of CPOM there are many propositions for lab scale devices for kinetic measurements on the CPOM reaction; however, these reactors employing catalyst gauzes or thin zone catalyst beds are not suitable to construct an industrial device. A monolith could be used in industry especially for the reason of good mass transfer properties and maintaining a low pressure drop at high reactant flow rates. On the other hand, for a proper determination of the optimal catalyst shape, for the dimensioning of a reactor to construct and optimization of process parameters, an adapted mathematical modeling is still needed.

I.11. Objectives of the thesis

As was noted above, the monolith shape is a very promising and convenient reactor configuration for an industrial implementation. For this reason, it was decided to study a single channel of a monolith as model configuration at lab scale. However, in order to analyze catalyst coating issues under conditions as realistic as possible, the channel used as lab model in the present study was designed with dimensions suitable for industrial implementation. On the other hand, testing requirements impose to down-scale reactant flow rates to some extent and there is a risk of mismatch in scale not present in the final application. In turn, at lab scale, great care has to be taken in order to minimize the influence of thermal effects and fluid dynamics, i.e. to reduce heat and mass transfer limitations. This last fact is very important for extracting relevant kinetic data, which might be used in the mathematical modeling.

Very frequently it is not possible to acquire enough kinetic data in a sufficiently wide parameter space in order to clearly discriminate kinetic models. It is well known that a fitting model description cannot prove that the reaction really proceeds according to the supposed mechanism, but that a mismatch in kinetic model prediction against experimental data might only exclude a potential mechanism. For this reason, it was decided to perform also a mechanistic study of the CPOM process over the selected catalyst. In this way, it might be

possible to select only the mathematical models, which are in agreement with the mechanistic information obtained independently.

On the basis of the literature overview and the above-mentioned prerequisites, the following main tasks can be formulated for this thesis work:

1. To study the effect of different dopants and process parameters on the catalytic performance of single monolith channels coated with doped CeO_2-ZrO_2 mixed oxides supporting Pt as noble or Ni as base metal.
2. To assess mechanistic features of CPOM over the most promising doped Pt/CeO_2-ZrO_2 catalyst, focusing on the relationship between CeO_2-ZrO_2 mixed oxides and supported Pt. For example, the main factors, such as surface or bulk (storage) effects, which control the state of Pt included in the catalyst composition. TAP reactor will be used as a key technique for accessing mechanistic insights.
3. To attempt building a kinetic model for the performance prediction of a single monolith channel reactor using the selected catalyst.

CHAPTER II

Experimental Techniques

II.1. Catalyst preparation

II.1.1. Powdered catalyst

Mixed oxides were prepared via the organic polymerized complex method, which is a modified version of the polymeric precursor method suggested by Pechini. The method allows preparing homogeneous complex oxides with perovskite and fluorite structure having well controlled properties and a high surface area [176,177].

For the preparation of $Gd_{0.3}Ce_{0.35}Zr_{0.35}O_x$ and $Pr_{0.3}Ce_{0.35}Zr_{0.35}O_x$ complex oxides, aqueous solutions of starting salts (nitrates of Ce and Pr), oxychloride of zirconium, citric acid (CA), ethylene glycol (EG), ethylene diamin (ED) were employed. The ethylene glycol and citric acid were used as complex formation reagents, ethylene diamine was chosen as additional complex builder. Reagents were used in the required molar ratio CA : EG : ED : Me ((Pr or Gd) + Ce + Zr) = 3.75 : 11.25 : 3.75 : 1. Despite the larger quantity of Pr or Gd added, these compounds will be referred to as dopands given that former studies had been using them in smaller quantities.

Citric acid was dissolved in ethylene glycol at a ratio of CA:EG=1:3 at 60°C. At the same time, aqueous nitrates of Ce ($Ce(NO_3)_3 \cdot 6H_2O$) and Pr ($Pr(NO_3)_3 \cdot 6H_2O$) were dissolved in 30 ml of distilled water adding a $ZrOCl_2$ solution thereafter. To this solution the solution of citric acid in ethylene glycol was added and the mixture was kept at 50°C during 72h for removing the solvent entirely. The product was further calcined for 4 h in air at 500°C. Pt (1.4 wt.%) was supported by incipient wetness impregnation with H_2PtCl_6 solution having a concentration of 9.2 mg/ml followed by drying and calcination for 2h at 500°C.

II.1.2. Monolithic catalyst

Monolithic catalysts were prepared based on structural substrates of separate triangular channels cut from an α-Al_2O_3 monolith. The wall thickness was 0.2 mm, the side width of the inside triangle amounted to 2.33 mm and the channel length was cut to 10 mm. After annealing at 1300°C the specific surface area of the corundum support was estimated to be 3 m^2/g. Layers of $Pr_{0.3}Ce_{0.35}Zr_{0.35}O_x$ and $Gd_{0.3}Ce_{0.35}Zr_{0.35}O_x$ complex mixed oxides were supported on these substrates by washcoating with water based suspensions. For the preparation of these suspensions, 5g of corresponding powders, i.e. ceria-zirconia mixed oxides doped either with Gd

or Pr, were dispersed in 60ml of distilled water and the resulting suspension was ultrasonically homogenized. Reaching a pH value of 3 and adjusting the viscosity of the suspension was accomplished by addition of nitric acid and polyethylene glycol, respectively.

To prepare another group of catalysts including metals such as La and Ni, first, the $Zr_{0.8}Ce_{0.2}O_x$ and, subsequently, $LaNiO_x$ ($LaNi_{0.9}Pt_{0.1}$) or Pt ($LaPtO_x$) were supported by incipient wetness impregnation. In the first step, a mixed solution of $Ce(NO_3)_3$ and $ZrOCl_2$, was used, and in the successive second - a mixed solution of La and Ni nitrates. Several consecutive impregnations, typically 4, were required to attain the active component content of 7-10 wt.%. After each impregnation, samples were dried and calcined at 900°C in air. Pt supporting involved a H_2PtCl_6 solution and incipient wetness impregnation to resemble as close as possible the preparation of powdered catalysts. Impregnation was followed by drying and calcination at 900°C in air. Compositions of catalysts with various active components are presented in Table II.1.

II.2. Characterization techniques

II.2.1. XRD (X-ray diffraction)

The crystallographic and real/defect structure of the synthesized mixed oxide support has a high impact on the oxygen mobility in the catalyst bulk which is important characteristics for the catalysts of partial oxidation of methane into syngas. XRD was used to elucidate the specificity of the structural properties of catalysts.

XRD patterns were obtained with an URD-6 diffractometer using Cu Kα monochromatic radiation (λ=1.5418 Å). The 2θ scanning region was 5-90°. The structural refinement has been carried out using PCW software.

II.2.2. Estimation of the catalysts specific surface area

To provide a high dispersion of supported platinum, complex oxide supports must possess reasonably high specific surface areas. However, high calcinations temperatures required for the phase formation could lead to considerable losses in specific surface area. In turn, estimation of the specific surface area was made according to the BET method.

The specific surface area (S_{sp}, m^2/g) of the samples was determined from the N_2 adsorption-desorption isotherms at -196°C by using the BET (Brunauer, Emmett, Teller) method [178]. Prior to surface area determination, the powders were outgased under vacuum conditions (10^{-5} torr) at 350°C for 4h.

Table II.1: *List of investigated catalysts*

Composition of active component (powder) and catalyst (powder supported onto substrate of monolith)	Oxide	Active component composition	
		Powder catalyst	Single channel of monolith
$LaNiO_x/ Zr_{0.8}Ce_{0.2}O_x/ Al_2O_3$	α - Al_2O_3		$LaNiO_x/ Zr_{0.8}Ce_{0.2}O_x$
0.4%Pt/ $LaNiO_x/ Zr_{0.8}Ce_{0.2}O_x/ Al_2O_3$			0.4%Pt/ $LaNiO_x/ Zr_{0.8}Ce_{0.2}O_x$
0.4%Pt/ $Zr_{0.8}Ce_{0.2}O_x/ Al_2O_3$			0.4%Pt/ $Zr_{0.8}Ce_{0.2}O_x$
0.4%Pt/ $La_2O_3/ Zr_{0.8}Ce_{0.2}O_x/ Al_2O_3$ Pt : La = 1:7			0.4%Pt/ $La_2O_3/ Zr_{0.8}Ce_{0.2}O_x$
1.8%Pt/ $Zr_{0.8}Ce_{0.2}O_x/ Al_2O_3$			1.8%Pt/ $Zr_{0.8}Ce_{0.2}O_x$
1.8%Pt/ $La_2O_3/ Zr_{0.8}Ce_{0.2}O_x/ Al_2O_3$ Pt : La = 1:1			1.8%Pt/ $La_2O_3/ Zr_{0.8}Ce_{0.2}O_x$
1.4%Pt /$Pr_{0.3}Ce_{0.35}Zr_{0.35}O_x/ Al_2O_3$			1.4%Pt /$Pr_{0.3}Ce_{0.35}Zr_{0.35}O_x$
1.4%Pt /$Gd_{0.3}Ce_{0.35}Zr_{0.35}O_x/ Al_2O_3$			1.4%Pt /$Gd_{0.3}Ce_{0.35}Zr_{0.35}O_x$
$Pr_{0.3}Ce_{0.35}Zr_{0.35}O_x/ Al_2O_3$			$Pr_{0.3}Ce_{0.35}Zr_{0.35}O_x$
$Gd_{0.3}Ce_{0.35}Zr_{0.35}O_x/ Al_2O_3$			$Gd_{0.3}Ce_{0.35}Zr_{0.35}O_x$
1.4% Pt/ Al_2O_3	γ - Al_2O_3	☺	
1.4%Pt /$Pr_{0.3}Ce_{0.35}Zr_{0.35}O_x$		☺	
1.4%Pt /$Gd_{0.3}Ce_{0.35}Zr_{0.35}O_x$		☺	
$Pr_{0.3}Ce_{0.35}Zr_{0.35}O_x$		☺	
$Gd_{0.3}Ce_{0.35}Zr_{0.35}O_x$		☺	

x accounts for the non-stoichiometry, but is generally a number close to 2.

☺ tags a sample in powder form.

II.2.3. TEM (Transmission electron microscopy) imaging

The catalyst characterization by transmission electron microscopy (TEM) [179] was performed with a JEOL 2010 microscope operating with 200kV and a maximum spatial resolution of 0.19 nm. The microscope is equipped with a LINK-ISIS detector for EDX analysis. The EDX analysis is based on measuring the energy of x-ray photons emitted by the sample under the impact of the incoming electron beam. The obtained spectrum is characteristic for the nature of the present elements and intensity of the peak for each element is proportional to its concentration. In the present case EDX was used to identify the nature of objects giving rise to contrast.

Sample preparation: The catalyst samples were milled, brought in suspension with absolute ethanol and stirred by ultrasounds to disperse the particle clusters. The obtained suspension was deposited on a freshly cut mica slice. The deposit was covered with carbon by evaporation and the carbon film is separated from the mica by immersion into a solution of water, acetone and hydrofluoric acid at intermediate concentration. Dissolving selectively the support, a fingerprint of the surface is obtained were the carbon filaments are preserved. The carbon film is washed and collected on a copper grid with less than 200 mesh, supporting in this way the overall carbon layer.

II.2.4. Laser granulometry

Recent literature [180] indicated that the adherence of catalytic coatings on substrates depends crucially on the particle size distribution of powders present in the coating suspension.

A Microtrac S3500 Series Particle Size Analyzer with tri-laser technology was used in order to determine the particle size distribution of the samples in the range of 0.3- 1000 μm. A spherical shape of particles was assumed. The percentage of particles having a certain size was measured as a fraction of the total solid volume.

II.2.5. Chemical Analysis

The chemical composition of catalysts was determined by elementary chemical analysis. The samples were treated in a mixture of $HF/HCl/HNO_3$ and H_2SO_4/HNO_3, subsequently. This mixture was evaporated and analyzed with a OES-ICP (SPECTRO) spectrophotometer.

II.2.6. FTIRS (Fourier transform infrared spectroscopy)

FTIRS [181] is a powerful technique to characterize adsorbates at catalytic surfaces or to investigate the catalytic surface itself observing the spectroscopic features of adsorbed probe molecules. The surface features of samples (the nature of surface centers in complex oxide supports and the state of supported Pt) were probed by FTIRS using CO as probe molecule adsorbed at -196°C. Spectra were recorded for samples pressed in wafers and pretreated in O_2 using a Shimadzu FTIR-8300 spectrometer with a resolution of 4 cm^{-1}.

II.2.7. RAMAN spectroscopy

The nature of the ceria zirconia solid solution in the catalyst was further investigated by RAMAN spectroscopy [181] focusing on lattice vibrations. The spectra were recorded using LabRAM HR spectrometer from Jobin Yvon. The relatively large focal length of 800 mm gives a relatively high resolution (0.3 cm^{-1}/pixel at 633) as compared to more standard bench-top instruments (e.g. 300 mm focal length). Mounting and positioning of samples was facilitated using the build-in optical microscope.

II.2.8. XPS (X-ray photoelectron spectroscopy)

XPS method was used to determine surface composition of elements and to receive information about the oxidation state of surface and sub-surface atoms.

XPS spectra were acquired using an ES-300 spectrometer (Kratos Analytical, UK) equipped with two anodes (AlK_α, 1486.6 eV and MgK_α, 1253.6 eV) operated at 50W to prevent reduction of Ce^{4+} in the surface layer. Samples were fixed on a holder by double-side scotch tape. Calibration of XP-spectra were made relatively E_b(C1s) = 284.8 eV [182]. Quantitative analysis of the samples was made using integral line intensities and factor of atomic sensitivities tabulated in [183].

II.2.9. O_2-TPD

O_2-TPD experiments were performed in the TAP reactor using oxygen saturation of the sample by a long train of pulses. A high temperature TAP reactor was charged with 20 mg of the

active phase of Gd and Pr doped CeZr catalysts in a sieve fraction of 100 to 200 microns sandwiched between inert quartz sections. Prior to experiments samples were heated to 800°C and pulses of an O_2/Ar mixture were introduced to remove residual carbon. To achieve a dynamic saturation of the surface by oxygen before TPD O_2 at desired temperature, $3.6 \cdot 10^{14}$ – $2.4 \cdot 10^{15}$ molecules/pulses of the O_2/Ar mixture were injected. The detection of the pulse responses at characteristic masses during TPD scanning experiments was accomplished with a quadruple mass-spectrometer.

II.3. Flow set-up for kinetic analysis (Boreskov Institute of Catalysis)

Kinetic transient and steady state experiments were carried out using a flow set-up consisting of feed sections; a reactor placed in the oven and a gas analysis system.

The gas supply of the bench test is performed by individual gas tanks (He, CH_4, N_2, H_2, O_2, CO_2). The feed pressure of gases in entering the installation is set to 3 bar using pressure reducers and their flow rate is controlled using mass flow meters.

The used reactor was a quartz tube with an internal diameter of 6mm.

The analysis system includes a GC “Cvet-500” and/or on-line IR absorbance sensor for CO, CO_2, CH_4, electrochemical one for O_2 and polarographic gas sensors for H_2.

The set-up could be used in two modes allowing to carry out experiments in transient and steady state regimes.

In **transient mode**, the installation operated according to the simple scheme presented in Figure II.1. Gases are distributed to two distinct gas lines that could be switched over:

- Line 1 allows to flow an inert gas (generally He) to the reactor system andto purge it. If needed, H_2 or O_2 can be admixed for feeding the reactor for catalyst reduction or oxidation treatment.
- Line 2 constitutes the line for feeding in normal operation all the reactants. This line carrying the inert gas (N_2) and all other gases was also used for calibration, after reactor by-pass.

6 ways valves with manual control make it possible to distribute gases towards the reactor, the analysis system or the vents.

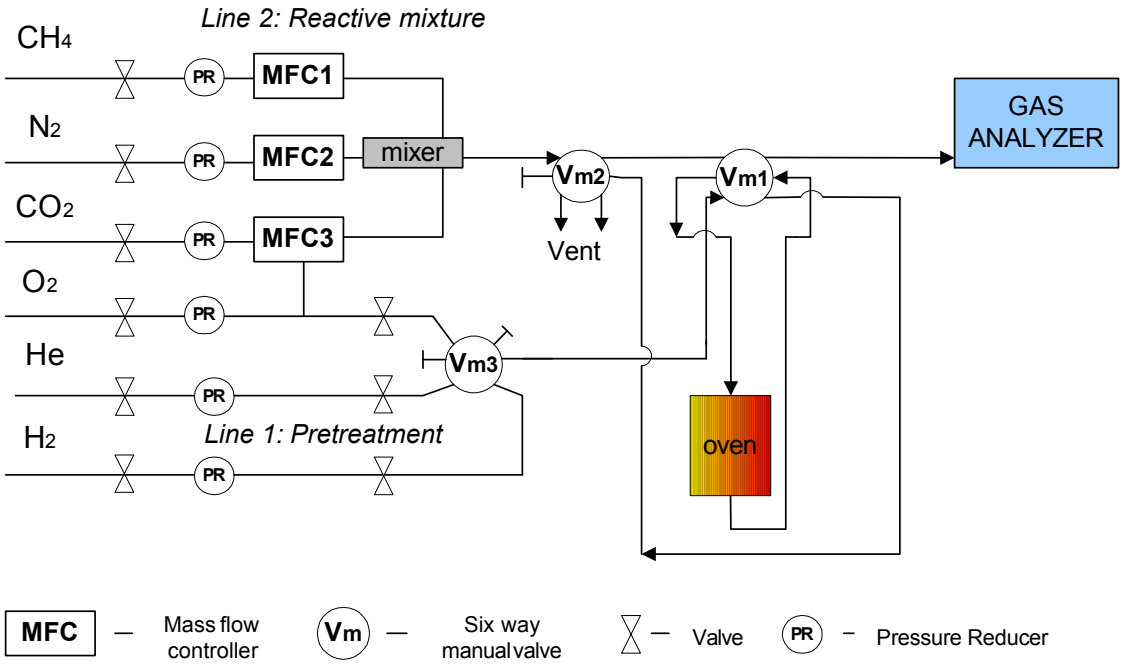

Figure II.1: Scheme of flow set-up for work in transient mode

- The scheme of the set-up in **steady-state mode** is shown in Figure II.2. Main parts of the installation in this mode are: two gas lines, a hot box where the feed is preheated and a gas analysis system.Line 1 allows sending an inert gas (generally He) to the reactor system and to purge it. If needed, H_2 or O_2 could be admixed feeding the reactor for catalyst reduction or oxidation treatment.
- Line 2 is used for feeding all reactants in normal operation as for transient operations.

The gas lines passed into a hot box containing one valve with manual control that allows directing the gas towards the reactor or directly to analysis (bypass) and two computer controlled valves allowed sampling of the gas mixture after the reactor for GC analysis or passed the gas stream towards in the vent. The temperature of the hot box was fixed at 120°C. The regulation of the oven temperature and measurement of catalyst temperatures was performed by the temperature regulator "Proterm".

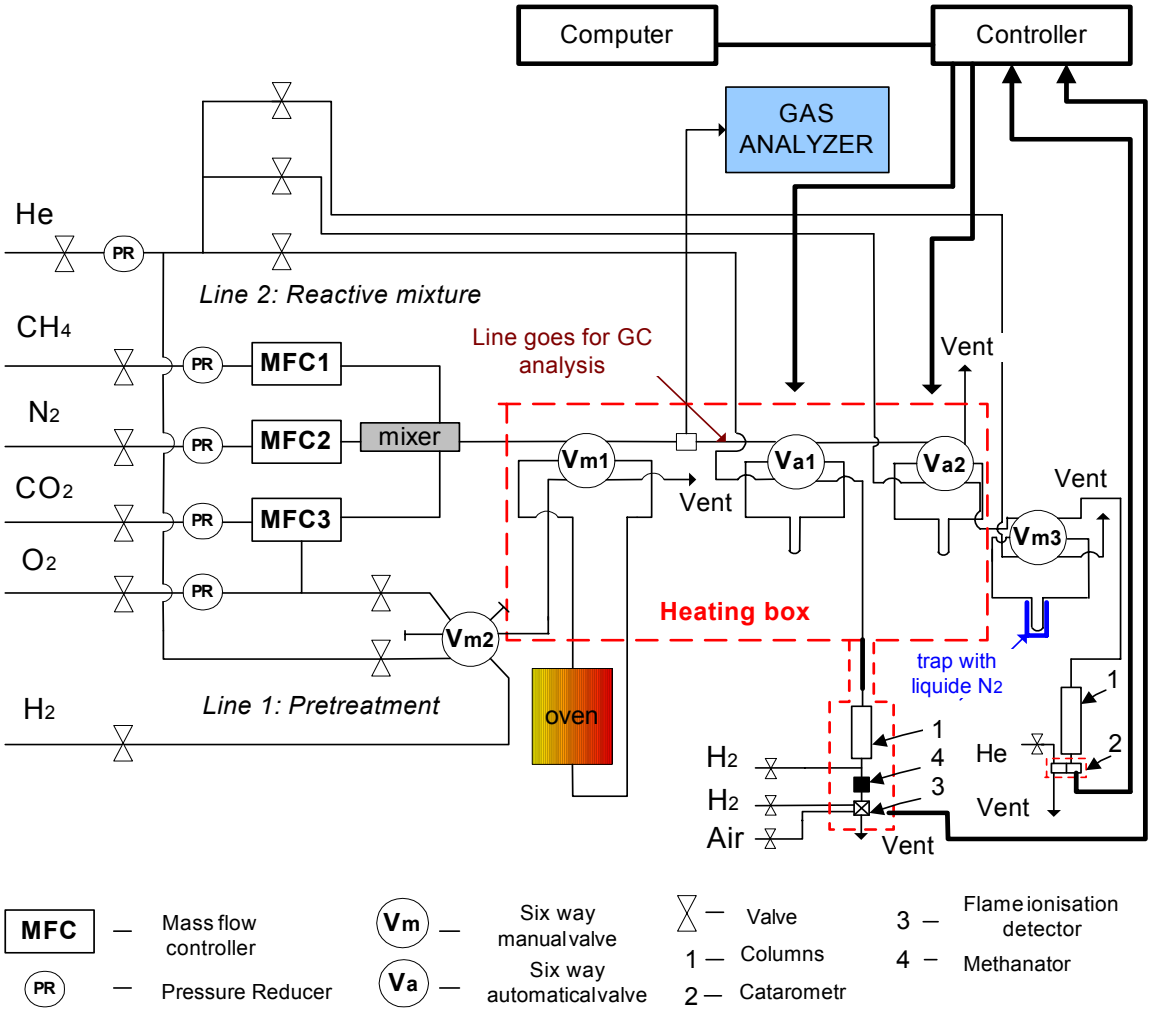

Figure II.2: *Scheme of flow set-up for work in steady state mode*

II.4. Flow set-up for complementary short contact time kinetic analysis (IRCELYON)

Analogous to the installation described previously, the main parts of this installation are: two feed sections; a hot box where the catalyst is placed in a reactor with pre- and main oven heating and a gas analysis system (Figure II.3).

The gas supply of the bench test is either ensured by a central gas supply system (H_2, O_2, N_2), or by individual gas tanks (Ar, CH_4, CO_2, He). Aiming at experiments with shorter contact time, the entire feeding section is made from 1/4'' inch stainless steel tubes (external diameter of

1.6 mm) and assembled with Swagelok type fittings to avoid excessive pressure drops at the required high flow rates. The pressure of gases entering the installation is set to 5 bar using pressure reducers and their flow is adjusted using Brooks 5850 TR mass flow controllers. The gases are distributed in two distinct gas lines that could be switched over:

- Line 1 allows sending an inert gas (generally N_2) to the reactor system and to purge it. If needed, H_2 could be admixed feeding the reactor for catalyst reduction treatment.
- Line 2 constitutes the line feeding all reactants in the normal operation mode. As the reactor could be bypassed, this line carrying the inert gas (N_2) and all other gases was also used for calibration.

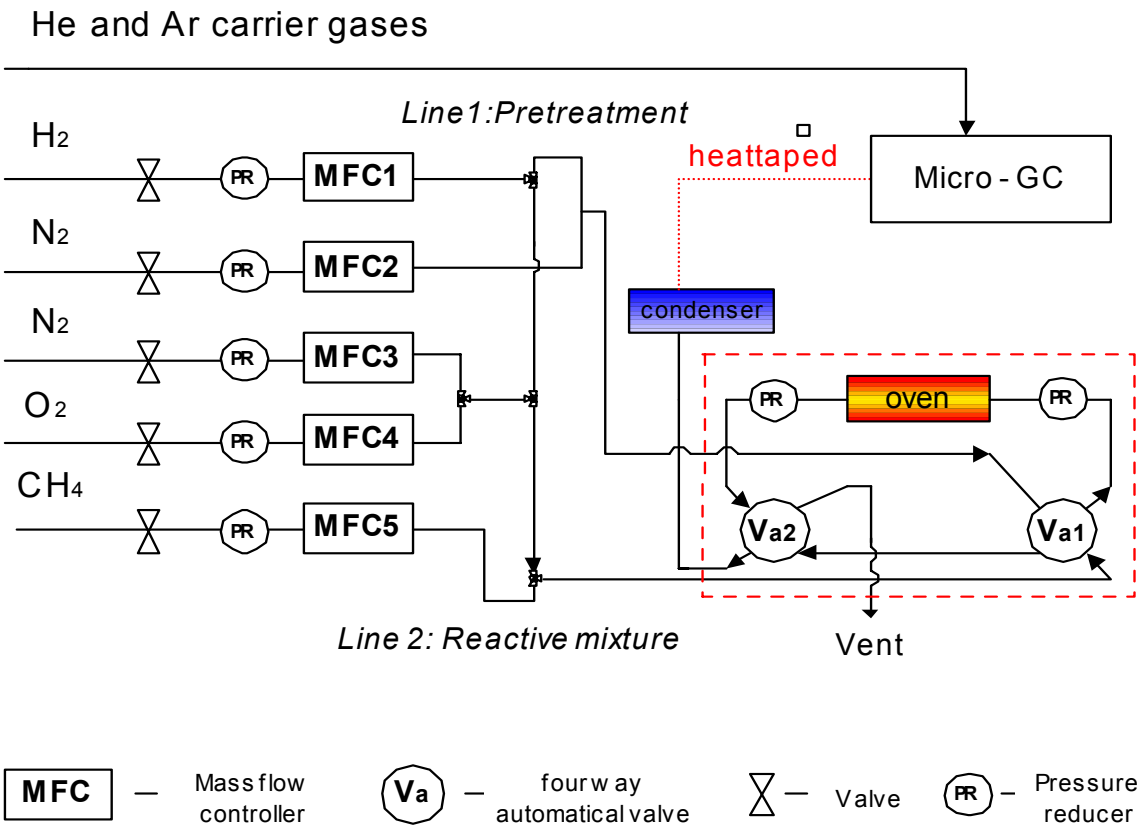

Figure II.3: *Scheme of the high flow set-up (IRCELYON)*

The gas lines passed in a hot box containing 1/4 inch Valco valves with computer controlled electric actuators making it possible to distribute gases towards the reactor, the analysis system or the vents. The temperature of the hot box was fixed to 130°C to avoid any condensation of the reaction products such as water.

Because of frequent changes to valve positions needed for adapting reaction conditions (reforming, purging, etc.), these valves were automated using a Labview program developed within in IRCELYON, which allowed also controlling the reactor temperature via a Eurotherm 2404 regulator, the preheating temperature via a West 6100+ controller and reactant flow rates via two Brooks 154 control units.

II.5. Temporal Analysis of Products (TAP) set-up (IRCELYON)

Transient experiments are a powerful tool for gaining insight into the mechanisms of complex catalytic reactions and allow deriving rate constants for the individual steps involved [184]. However, kinetic information is only obtained when the transient change proceeds rapidly enough and the system cannot relax to equilibrium at shorter time scale than monitored [185]. A conventional nonsteady-state reactor set-up operating at atmospheric pressure provides a time resolution of only about one second, limited by the way in which the perturbation is created and by the inevitable broadening of sharp responses that occurs in a flow system. In contrast, the Temporal Analysis of Products (TAP) reactor system allows fast transient experiments in the millisecond time regime with submillisecond signal sampling [186,187]. The construction of the TAP reactor system and the underlying experimental conditions are highly suitable for transient kinetic studies. However, it needs to be stressed that the catalyst sample remains under vacuum conditions having potentially impact on catalytic performances.

The TAP reactor system was originally developed to assist catalyst development and characterization at Monsanto [188]. Later, a new improved apparatus, called TAP-2 reactor system, has been introduced [189]. The critical difference between the TAP and TAP-2 reactor system is the positioning of the microreactor and the detector measuring the reactor effluent. In the TAP-2 system, both devices are physically much closer, and as a result the detection efficiency of the TAP-2 system is much higher.

The present work made use of the TAP-2 system schematically depicted in Figure II.4. The TAP-2 set-up consists of an ultra high vacuum system with high pumping speed and liquid nitrogen trap, a quadrupole mass spectrometer (QMS, item 3), a heated microreactor (item 2) and temperature controller, a heated valve/manifold assembly (item 1), a gas blending station and gas

blending oven for preparing reaction samples from gases and liquids, and a PC computer based control and data acquisition system.

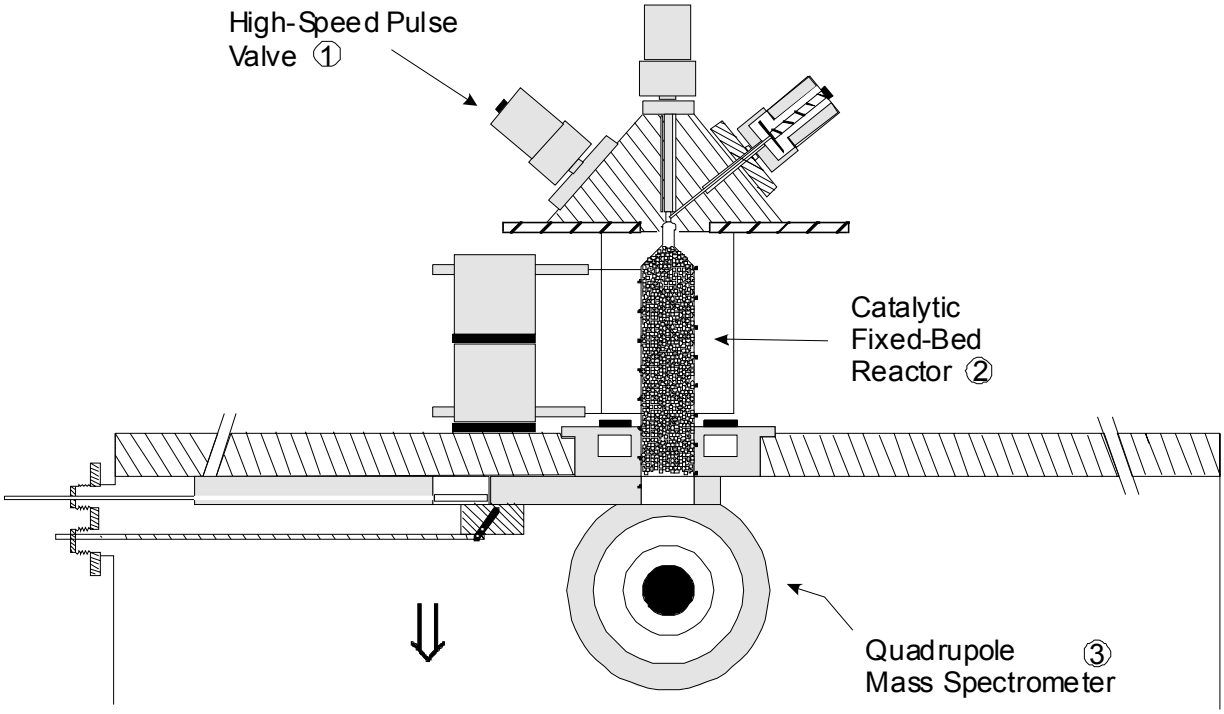

Figure II.4: *Schematic overview of the key parts in the TAP-2 installation*

The TAP-2 reactor system can be used to perform transient response and steady-flow experiments at pressures ranging from 10^{-6} to 2500 torr, and temperatures ranging from 300 to 1200K. However, the specific features of the TAP system are exhibited in the Knudsen domain in the course of vacuum transient experiments. The pulse intensities in vacuum experiments range from 10^{13} to 10^{18} molecules/pulse, with a pulse width < 2 ms, and a pulse frequency between 0.1 and 50 pulses/s. Such a time resolution is unique among other kinetic methods. Depending on the kind of information required, different experimental modes are used. These modes may be roughly divided into pulse experiments and investigations using a continuous gas feed (for an overview see Table II.2).

Table II.2: *Overview of the experimental modes and main information obtained*

Experiment	Obtained Information
Single-pulse technique	Diffusivities Heats of adsorption Product formation sequence Number of adsorption sites Education of reaction pathways
Sequential pulse technique	Lifetime of surface intermediates Education of reaction pathways
Flow experiment	Role of catalyst bulk-dissolved and lattice species in the reaction
Temperature-programmed desorption (TPD), Reaction (TPSR)	Thermal stability of intermediates Redox properties of solid oxide catalysts

II.6. Catalytic testing

II.6.1. Steady-state experiments

The testing of the catalysts in POM, steam (SR) and dry (DR) reforming was carried out in a plug-flow quartz reactor of 6 mm inner diameter. The space between the catalyst channel and the reactor walls was sealed enveloping the sample with α-Al_2O_3 fiber mat. The temperature of the catalytic bed varied in the range of 550-900°C. The catalysts were *in situ* pretreated at 900°C for 1 h in the oxygen (hydrogen) flow. The reaction mixture (POM: 1 –12 vol.% CH_4, 0.5-6% O_2, He (or N_2) – balance; SR: 3,5 –12 vol.% CH_4, H_2O:CH_4 =1, 1.8, 3, He – balance; DR: 7 vol.% CH_4, CO_2:CH_4 =1, N_2 – balance) was fed with the flow rate in the range of 5.5-84 l/h, i.e. at 1.0-15 ms contact time estimated from the flow rate and the volume of channel walls. Also, for SR and POM conducted with a diluted reaction mixture (1% CH_4), the temperature was measured by a thermocouple situated outside the reactor. For all other experiments, the inlet and outlet temperature of the catalyst channel were scanned during the testing. Blank experiments with corundum substrate (single channel without active component) catalyst and without it verified that homogeneous reactions did not occur under studied conditions. The reagents and reaction

products were analyzed by GC and on-line IR absorbance, electrochemical and polarographic gas sensors for different components.

II.6.2. Relaxation experiments

Using the same installation, relaxation experiments at atmospheric pressure were carried out in transient mode. After pretreatment oxygen was flushed out flowing He and then the He flow was substituted without interruption by the reaction feed with the desired composition. Control experiment showed that at high flow (up to 30 l/h) the purging time of a reactor with mounted single channel is not longer then 2-4sec.

The scheme of the reactor designed for a single-channel monolithic catalyst is presented in Figure II.5.

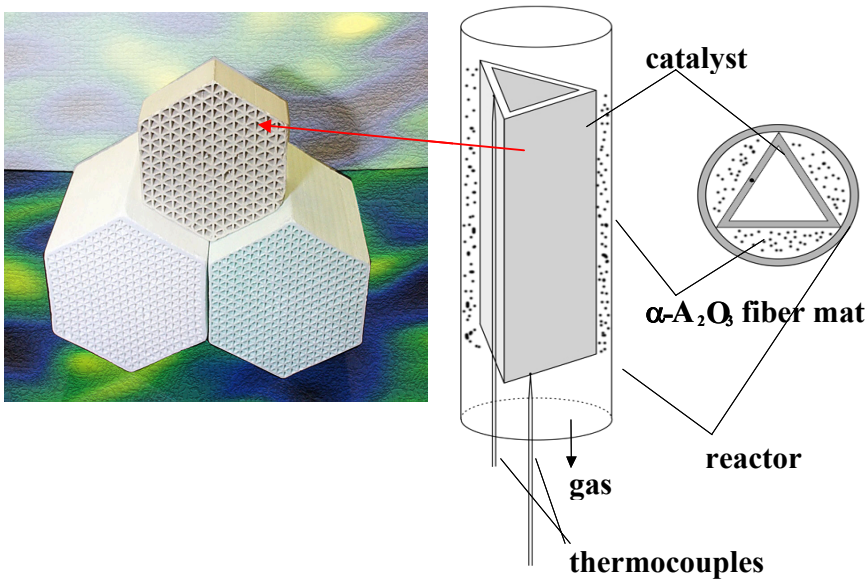

Figure II.5: *Monolithic catalyst and reactor scheme with a single channel*

II.6.3. Temporal Analysis of Products experiments (TAP)

The characterization of the oxygen–catalyst interaction and catalytically activity was performed with TPD using a high temperature version of the TAP reactor. For the sake of placing the catalyst well in the isothermal zone of the reactor, these experiments use 20 mg of a powdered catalyst samples sandwiched between inert quartz beds. Catalytic performance data on

the monolith channels were acquired with a high temperature variant of the TAP reactor charged with 10mm of the catalyst channel sandwiched between inert quartz sections.

All studies used Ar as a reference gas allowing precise quantitative exploitation of the mass spectrometer data. Prior to experiments the sample was heated to 800°C and pulses of an O_2/Ar mixture were introduced to remove residual carbon. Measurements concerning the catalytic performance were performed at a temperature of 700°C using pulses of a O_2/Ar and a CH_4/Ar mixture, in both cases in a ratio of 1:1. Experiments probing the catalytic performance were carried out in pump-probe mode injecting first oxygen and then methane with a short time lag. The pulse intensity of oxygen and methane was set to inject twice as much methane than oxygen using pulse sizes adjusted to $4.1 \cdot 10^{15}$ – $6.8 \cdot 10^{15}$ molecules per pulse. $3.6 \cdot 10^{14}$ – $2.4 \cdot 10^{15}$ molecules per pulse of the O_2 / Ar mixture were injected into the reactor preparing temperature programmed desorption (TPD) experiments when aiming at different temperatures on the dynamic saturation of the catalyst with oxygen. It should be stressed that after reaching the dynamic saturation at the desired temperature, pulsing was continued while decreasing the reactor temperature to 250°C presenting the starting temperature of each TPD run. The removal of weakly bound oxygen species was achieved by keeping the sample for about 10min under dynamic high vacuum prior to starting the heating ramp of 20°C/min.

The detection of the pulse responses and characteristic masses during scanning for TPD experiments was accomplished using a quadruple mass-spectrometer monitoring masses 32 (O_2), 15 (CH_4), 44 (CO_2), 28 (CO), 2 (H_2) and 40 (Ar). CO responses were obtained from m/e=28 subtracting the contribution of CO2 after proper deconvolution according to its fragmentation pattern.

II.6.4. Reactants and products analysis

II.6.4.1. Gas chromatography (BIC)

Gas chromatographic analysis of reactants and reaction products involved both a flame-ionization detector (FID) and thermal conductivity detector (TCD) attached to a GC “Cvet – 500”. Hydrogen and oxygen were analyzed with the TCD on a column with NaX molecular sieve at room temperature and a He carrier gas flow of 30 ml/min. Carbon monoxide, carbon dioxide and methane were first separated on a chromosorb-102 column at temperature 70^{o}C and then passed through a methanator (which was heated in H_2 flow up to 400^{o}C, with Ni-Cr catalyst) for

the transformation of CO and CO_2 to methane and finally individually detected on the FID. The selection of the gas sample for analysis was automated and controlled by computer. After start-up of the catalyst with a reactant mixture the first analysis for CO, CO_2 and CH_4 was taken after 60s, repeating subsequently analysis every 200 s. Analysis of O_2 and H_2 were taken with a periodicity of 410 s, and the first analysis starting at 120 s. From results of the analysis carbon and oxygen balances, selectivity and activity were calculated.

II.6.4.2. Gas chromatography (IRCELYON)

- In the case of a traditional chromatograph, the analysis of a gas containing hydrocarbons requires 10 to 60 min according to its complexity. The use of a μ-GC reduces this time: the sample is analyzed in less than 160 s. The study used a **Micro-GC 300** having 2 analytical modules: Module 1: Sieve molecular 5Å/10 m; Carrier gas: Ar (slightly lower sensitivity but reasonable linearity for the hydrogen response). Equipping the molecular sieve module with a backflush system prevents the accumulation of strongly interacting compounds like water, CO_2 and higher hydrocarbons on the column. In this context it should be stressed that the accumulation of compounds on a GC column leads to shifting retention times and may finally also cause damages to the column itself. Detection of: H_2, O_2, N_2, CH_4, CO.
- Module 2: PoraPLOT Q 8 m; Carrier gas: Helium. Detection of: N_2, CH_4, CO_2.

Because the μ-GC analyzes a small quantity of water vapor remaining after condensation, all gas lines, the injector, the columns and the detector are heated in order to avoid the condensation. The limit of detection is about of some ppm of the second module operating with He as carrier gas and about a factor 100 higher for the first module with Ar as carrier gas. Each calibration is performed by 7-10 points selected in the expected concentration range.

II.6.4.3. Mass Spectrometer

Mass spectrometry used as fast analysis method in the TAP installation is a powerful analytical technique that is used to identify unknown compounds, to quantify known compounds, and to elucidate the structure and chemical properties of molecules. Detection of compounds can be accomplished with very minute quantities (as little as 10^{-12}g, 10^{-15} moles for a compound of

mass 1000 Daltons[1]). This means that compounds can be identified at very low concentrations (one part in 10^{12}) in chemically complex mixtures.

The principle of an analysis by the mass spectrometer (*UTC 100C in our case*) is the bombardment of a small representative quantity of probe gas with low energy electrons (typical energies are in the range of 40 to 70 eV) at high vacuum conditions. Impact ionization creates hereby positively charged molecule and molecule fragment ions within the ion source. The gas phase ions are separated in the mass analyzer according to their mass-to-charge (m/z) ratios and then collected by a detector. In the detector the ion current is transcribed to a proportional electrical current. The data acquisition system records the magnitude of these electrical signals as a function of m/z and converts this information into a mass spectrum.

However, it occurs frequently that different probe constituents yield contributions at a given mass to charge ratio, like for example carbon monoxide and carbon dioxide at m/z = 28 (CO^+) or nitrogen and carbon dioxide at m/z = 28 (N_2^+ and CO^+). The data treatment becomes complex in those cases, as the obtained mass spectra need to be deconvoluted into the individual contributions. The deconvolution requires knowing the fragmentation pattern for sample constituents and the fact that individual contributions at one given m/z value are strictly additive to the overall measured ion current intensity. Hence, a first objective for an analysis by mass spectrometry is typically to identify, if possible, for every probe constituent a characteristic ion having at the given m/z value no (significant) contribution from other compounds (overlap). Next, a deconvolution strategy needs to be developed so that for each case at a given m/z value only a minimum of other contributions (from compounds with other overlap-free characteristic ions) need to be subtracted.

Table II.3: *Values of m/z ratio for different probe constituents resulted during the oxidation of methane*

Probe constituent	H_2	CH_4	H_2O	N_2	CO	O_2	Ar	CO_2
m/z	2	15	17, 18	28	28	32	36, 40	28, 44

[1] Dalton (Da) = a unit of mass defined as : 1 Da=(1/12) of the mass of a single atom of the isotope of carbon-12(^{12}C). This follows the accepted convention of defining the ^{12}C isotope as having exactly 12 mass units.

II.6.4.4. Quantitative exploitation of the mass spectrometer data

The quantitative exploitation of the mass spectrometer data makes use of the above mentioned strict proportionality of measured ion current intensity of a characteristic molecule (fragment) ion to the partial pressure of the compound. The intensity may be measured at a characteristic m/z value or may be calculated by unfolding contributions of different probe constituents. First, throughout all calculations ion current intensities are taken relative to that of the chosen inert standard at the chosen m/z value:

$$I^*_{a(i),m(j)} = \frac{I_{a(i),m(j)}}{I_{S,m(S)}} \qquad \textbf{Eq. II.1}$$

Next, the sensitivity coefficient is calculated from calibration experiments where the partial pressures, respective molar fractions or molar flows are known:

$$Sens_{a(i),m(j)} = I^*_{a(i),m(j)} \cdot \frac{n_S}{n_{a(i)}} = \frac{I_{a(i),m(j)}}{I_{S,m(S)}} \cdot \frac{n_S}{n_{a(i)}} \qquad \textbf{Eq. II.2}$$

In order to exploit an analysis by the mass spectrometer, the equation defining the sensitivity coefficient becomes rearranged, yielding an expression for the partial pressure, molar fraction or flow of the probe molecule as a function of the respective partial pressure, molar fraction or flow of the inert standard.

$$n_{a(i)} = I^*_{a(i),m(j)} \cdot \frac{n_S}{Sens_{a(i),m(j)}} = \frac{I_{a(i),m(j)}}{I_{S,m(S)}} \cdot \frac{n_S}{Sens_{a(i),m(j)}} \qquad \textbf{Eq. II.3}$$

A (recursive) deconvolution (unfolding of the different compound contributions to the ion current intensity at a given m/z value) can be accomplished recursively if the ion current intensity of interfering compounds is know at other m/e values without overlap.

$$I^*_{a(i),m(j)} = I^*_{common,m(j)} - \frac{Sens_{a(l),m(j)}}{Sens_{a(l),m(n)}} \cdot I^*_{a(l),m(n)} = \frac{I_{common,m(j)}}{I_{S,m(S)}} - \frac{Sens_{a(l),m(j)}}{Sens_{a(l),m(n)}} \cdot \frac{I_{a(l),m(n)}}{I_{S,m(S)}} \qquad \textbf{Eq. II.4}$$

After calculation of the partial pressures, molar fractions or flows of all relevant compounds, the estimation of conversion, selectivity and yield may proceed in the conventional way. However it is also possible to derive short-cut formulae making use of the formal definition of conversion and yield:

$$X_{a(i)} = \frac{n_{a(i),\text{influent}} - n_{a(i),\text{effluent}}}{n_{a(i),\text{influent}}} = 1 - \frac{n_{a(i),\text{effluent}}}{n_{a(i),\text{influent}}} \qquad \textbf{Eq. II.5}$$

Leads to:

$$X_{a(i)} = 1 - \frac{I^{*}_{a(i),m(j)} \cdot n_S}{Sens_{a(i),m(j)} \cdot n_{a(i),\text{influent}}} = 1 - \frac{I_{a(i),m(j)} \cdot n_S}{I_{S,m(S)} \cdot Sens_{a(i),m(j)} \cdot n_{a(i),\text{influent}}} \qquad \textbf{Eq. II.6}$$

Taking a general definition of the yield as:

$$Y_{a(j)} = \frac{-\nu_{a(i)} \left(n_{a(j),\text{effluent}} - n_{a(j),\text{influent}}\right)}{\nu_{a(j)} \cdot n_{a(i),\text{influent}}} \qquad \textbf{Eq. II.7}$$

Assuming that the product *a(j)* is not present in the feed, it is possible to derive the following equation:

$$Y_{a(j)} = \frac{-\nu_{a(i)}\ I^{*}_{a(j),m(j)} \cdot n_S}{\nu_{a(j)} \cdot Sens_{a(i),m(j)} \cdot n_{a(i),\text{influent}}} = \frac{-\nu_{a(i)}\ I_{a(j),m(j)} \cdot n_S}{\nu_{a(j)} \cdot I_{S,m(S)} \cdot Sens_{a(i),m(j)} \cdot n_{a(i),\text{influent}}} \qquad \textbf{Eq. II.8}$$

where $\nu_{a(i)}$ and $\nu_{a(j)}$ are the stoichiometric coefficients of reactants and reaction products, respectively, of ***Eqs. I.1 – I.3*** and ***I.6***:

$$CH_4 + 0.5O_2 = CO + 2H_2$$

$$CH_4 + 2O_2 = CO_2 + 2H_2O$$

$$CH_4 + CO_2 = 2CO + 2H_2$$

$$CH_4 + H_2O = CO + 3H_2$$

CHAPTER III

Selection of formulations for structured catalysts based on CeO_2-ZrO_2 mixed oxides

III.1. Context

The literature overview (Chapter I) outlined already that from the earliest work on catalytic partial oxidation, supported nickel catalysts are known as highly active for synthesis gas production. However, nickel based catalysts have shortcomings in terms of excessive carbon formation [45,46,47] leading to deactivation. Metallic Ni is capable to promote the homolytic cleavage of the C-H bond followed by coke formation form the resulting carbonaceous surface species (of carbide like structure) if these are not rapidly enough oxidized. The addition of La to the Ni-based catalyst was shown to provide a higher resistance to coke deposition [64,65]. It is claimed that triple-charged La cations improve the oxygen anions mobility in the lattice and stabilize Ni in the state of 1+ or 2+ [65] or that the surface decoration of nickel particles with La carbonate species present an additional mildly oxidizing pool to remove carbonaceous species prior to their accumulation [190]. Furthermore, the activity of nickel relates to its presence in metallic form [46,191], requiring thus to carefully adjust the degree of oxidation to a level where carbonaceous species are removed. Due to these drawbacks of Ni based system, the most promising types of catalyst for syngas production contain active components of precious metals combined with mixed oxides. As was noted in the literature review, the catalyst being developed at Argonne National Laboratory and produced by Süd-Chemie Inc. contains a transition metal supported on an oxide-ion-conducting substrate, such as ceria, zirconia or lanthanum gallate, being doped with a small amount of non-reducible elements, such as gadolinium, samarium or zirconium [78]. The objective of research presented in this chapter is to study this class of catalysts in more detail in order to select the most promising formulations for the CPOM reaction in short contact time reactors.

III.2. Comparative study of catalysts with different composition in the CPOM reaction

III.2.1. Systems based on $Zr_{0.8}Ce_{0.2}O_x$ / α-Al_2O_3 material

Catalysts based on Pt-promoted $LaNiO_x$/Ce-ZrO_x were recently shown to be efficient in CPOM [46,192,193]. However, as was noted above, formulas based on transition metals

supported on doped ceria are promising as well for CPOM. For this reason formulations containing Pt, La and / or Ni (pure or promoted by Pt) and Pt/Ce-Zr-(Pr, or Gd)-O were selected for comparison. Both groups of active components have been supported on corundum monolith channels for improving mass and heat transfer. In fact the high mass transfer rate in monolith channels is a major advantage in an industrial-scale reactor and an enhanced thermal stability of the studied system relates to a comparable high thermal conductivity along the channel axis in the flow direction. Obviously, by limiting hot spots formation in the inlet section, the latter contributes to preserve the high dispersion of the supported metal. Each of the tested catalysts comprising La and/or Ni is presented in Table III.1, with its reference denomination.

Table III.1. *List and compostion of selected catalysts investigated for CPOM*

Catalyst	Composition*
LaNi	$LaNiO_x$ / $Zr_{0.8}Ce_{0.2}O_x$ / α-Al_2O_3
LaNiPt	LaNiPt (0.4%Pt) / $Zr_{0.8}Ce_{0.2}O_x$ / α-Al_2O_3
0.4Pt	0.4%Pt / $Zr_{0.8}Ce_{0.2}O_x$ / α-Al_2O_3
0.4PtLa7	0.4%Pt+La(1:7) / $Zr_{0.8}Ce_{0.2}O_x$ / α-Al_2O_3
1.8Pt	1.8%Pt / $Zr_{0.8}Ce_{0.2}O_x$ / α-Al_2O_3
1.8PtLa1	1.8%Pt+La(1:1) / $Zr_{0.8}Ce_{0.2}O_x$ / α-Al_2O_3

* – all catalysts contained ~7% wt. $Zr_{0.8}Ce_{0.2}O_x$

The scheme of the set-up used for that catalyst screening (BIC) and the experimental operating conditions are described in Chapter II.

The conversion of methane and the selectivity towards CO and H_2 are presented in Figure III.1 and III.2 for the selected systems. As can be seen, the most active and selective system over the whole studied temperature range is unambiguously the $LaNiO_x$ / $Zr_{0.8}Ce_{0.2}O_x$ / α-Al_2O_3 catalyst (referred to as LaNi). Note that this ranking is relevant essentially at low and medium temperature. Moreover, this system was found not only active and selective but also highly stable on stream after a reduction pre-treatment as compared to the oxidising one [194]. It is now well known that the deep oxidation of methane mainly proceeds over Ni or Pt oxides whereas metallic

state is responsible for the synthesis gas formation [191,193]. Thus, in this study, all catalysts of the above mentioned group have been pre-reduced under hydrogen flow. Such a reduction pretreatment of fresh catalysts might ensure the required rapid start-up of syngas generators especially at low temperatures. For this reason, the catalyst being initially reduced will be denoted as "working" in the following part of the study.

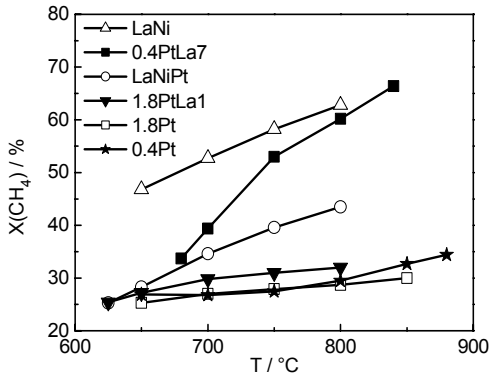

Figure III.1: *Methane conversion in CPOM over catalysts of different composition. Operating conditions: 7% CH_4 +3.5% O_2 in N_2. Contact time 8 ms.*

A B

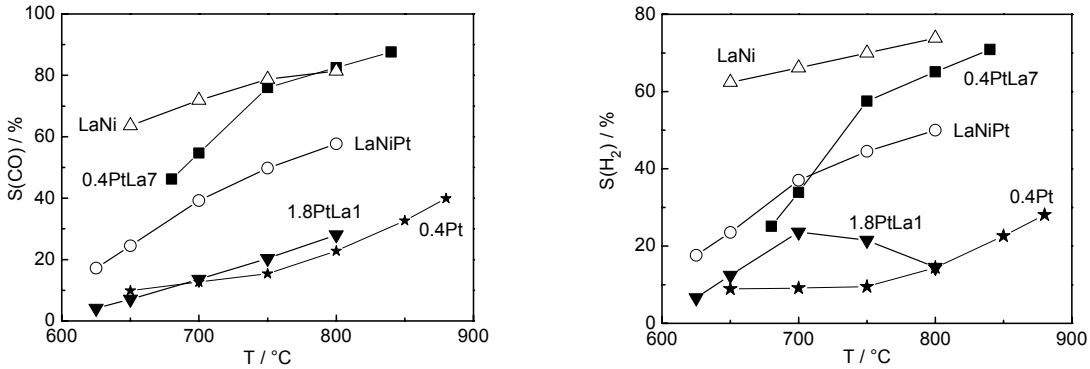

Figure III.2: *CO and H_2 selectivity in POM over catalysts of different composition. Operating conditions: 7% CH_4 + 3.5% O_2 in N_2. Contact time 8 ms.*

As also deduced from figures III.1 and III.2, the addition of Pt to $LaNiO_x$ decreases methane conversion and syngas selectivity. It can be assumed in a first approximation that oxygen is preferentially activated on Pt rather than on LaNi, resulting in a lower activity of the LaNi phase while the presence of oxygen on Pt would cause an over-oxidation of syngas to unselective products.

For the samples containing only Pt as active component as well as for the sample 0.4Pt, 1.8Pt and 1.8PtLa1, methane conversion does not exceed 35%, and the syngas selectivity remains low (Figure III.1 and III.2), again likely due to the complete oxidation induced by Pt.

For the catalyst 0.4PtLa7, a steep rise in methane conversion and syngas selectivity is observed by increasing temperature above 700°C where it reaches and even overpasses the performance of LaNi. Thus, the highest activity and syngas selectivity are observed for samples containing a large excess of La (LaNi, 0.4PtLa7 and LaNiPt), thus possessing the highest basicity. These results provide additional arguments for doping ceria-zirconia solid solutions by basic Gd or Pr cations thus controlling not only their oxygen mobility and red-ox properties but their acid-base properties as well.

III.2.2. Systems based on Pt/doped $Zr_{0.8}Ce_{0.2}O_x$ / α-Al_2O_3 material

The activity and selectivity of Pt/Ce-Zr-(Pr, or Gd)-O catalysts supported onto a corundum channel (Table III.2) were investigated either in oxidized or reduced state. The observed performances are presented in Figure III.3. For all catalysts doped either by Pr or Gd, the conversion of methane and selectivities to CO and H_2 are significantly higher after catalysts preoxidation. This feature is quite opposite to the trend above reported for the LaNi based formulations. Thus, the most efficient "working" state for a catalyst doped by Pr or Gd is the oxidized one, whereas Ni – based catalysts are more efficient under the reduced state.

Table III.2. *List and compostion of selected catalysts investigated for CPOM*

Catalyst	Composition*
PtPrCeZrO	1.4%Pt / $Pr_{0.3}Ce_{0.35}Zr_{0.35}O_x$ / α-Al_2O_3
PtGdCeZrO	1.4%Pt / $Gd_{0.3}Ce_{0.35}Zr_{0.35}O_x$ / α-Al_2O_3

* – all catalysts contained ~8% wt. $ZrO_{0.8}Ce_{0.2}O_2$

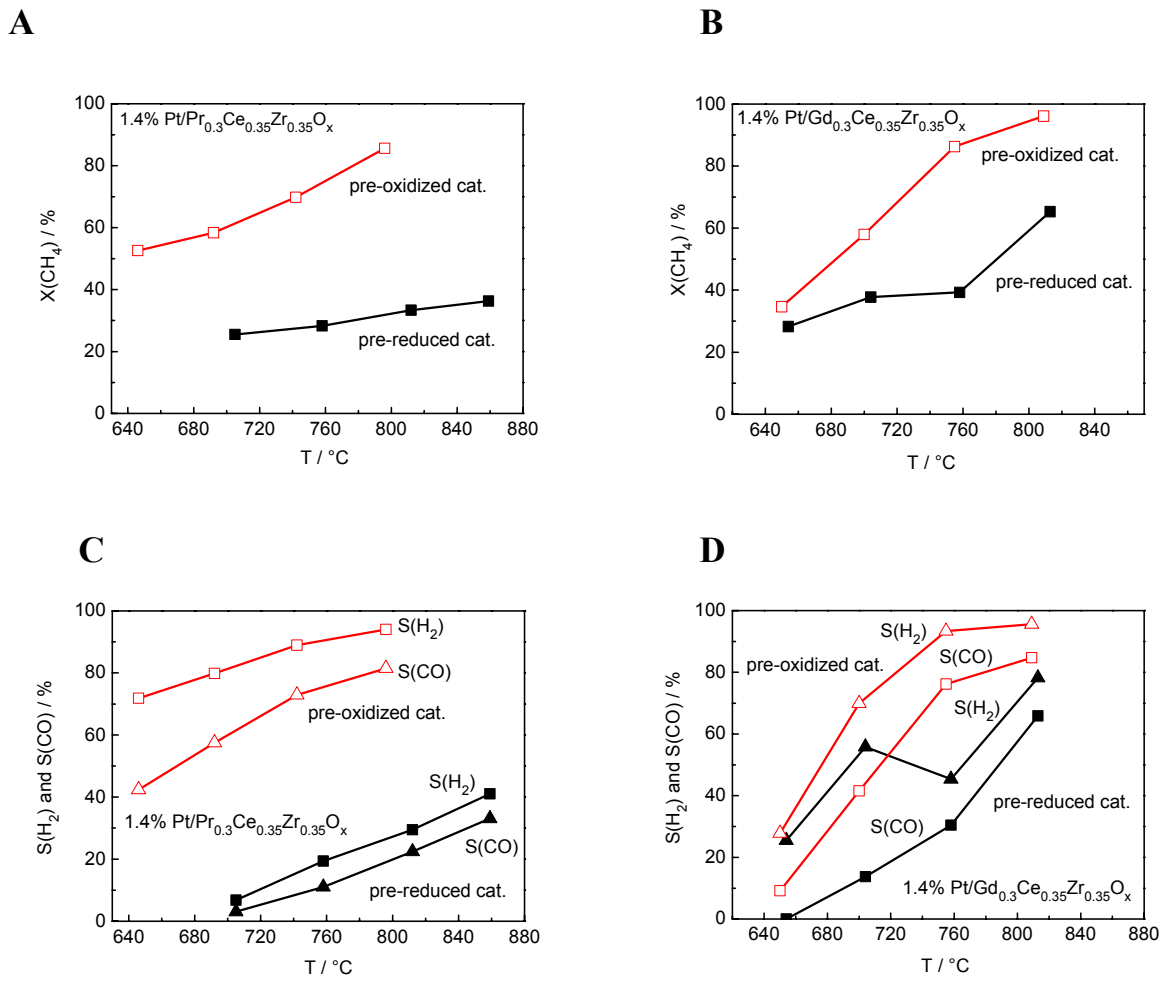

Figure III.3: *The activity and CO, H_2 selectivity in CPOM over PtPrCeZrO and PtGdCeZrO catalysts at either oxidized or reduced state. 7% CH_4 + 3.5% O_2 in N_2. Contact time 15 ms.*

However, within the perspective of designing a multi-purpose monolith-based syngas generator, it might be highly preferable to have a system working without any prereduction. As a matter of fact, this would require additional heating and would make the reformer design more complex. In addition, frequent start-up and shut-down sequences would necessitate to repeat this prereduction, which would slow down the operating process. In contrast, in the case of an oxidizing pre-treatment, a simple procedure would be to admit a lean methane/air mixture at a temperature sufficient for ignition and total combustion of the hydrocarbon. This would provide the heat required for the oxidizing pretreatment under the remaining oxygen flow.

For all the above reasons, the most promising systems are the catalysts doped by Gd or Pr, able to "work" in the oxidized state.

III.3. Dry reforming reaction on the PtPrCeZrO and PtGdCeZrO catalysts

The state of the catalyst surface, i.e. degree of surface reduction, oxygen reactivity at the surface and mobility in the bulk, surface coverage by carbonates and/or carboxylates are very important in the CPOM. All these factors could affect the mechanism of POM. Secondary reactions like steam (SR) and CO_2 or dry reforming (DR) have significant contribution to the overall performance in CPOM and might be considered as part of the reaction mechanism. For this reason the activity and selectivity of PtPrCeZrO and PtGdCeZrO catalysts supported on a monolith single channel have been also studied under dry reforming conditions at short contact times.

Figure III.4 and III.5 compare the temperature and contact time dependence for the two selected catalysts in the dry reforming reaction. Figure III.4 shows that the system doped with Pr is about two times more active than the Gd promoted one. However, even for the former catalyst, CH_4 and CO_2 conversions (maximum values at 780°C are 59 and 54% for CH_4 and CO_2, respectively) were lower than conversions in the catalytic partial oxidation. The difference between Pr and Gd doped systems could correlate to their respective bulk oxygen mobility. As will be seen later (Chapter IV), systems displaying a surface blocked by carbonates and/or carbon-containing complexes tend to have a slower oxygen mobility and therefore a lower activity. Hence, in order to investigate the surface basicity which might control the carbonate stability and coverages, the interaction between CO_2 and the two supports was studied in the TAP reactor, as will be presented in a subsequent chapter.

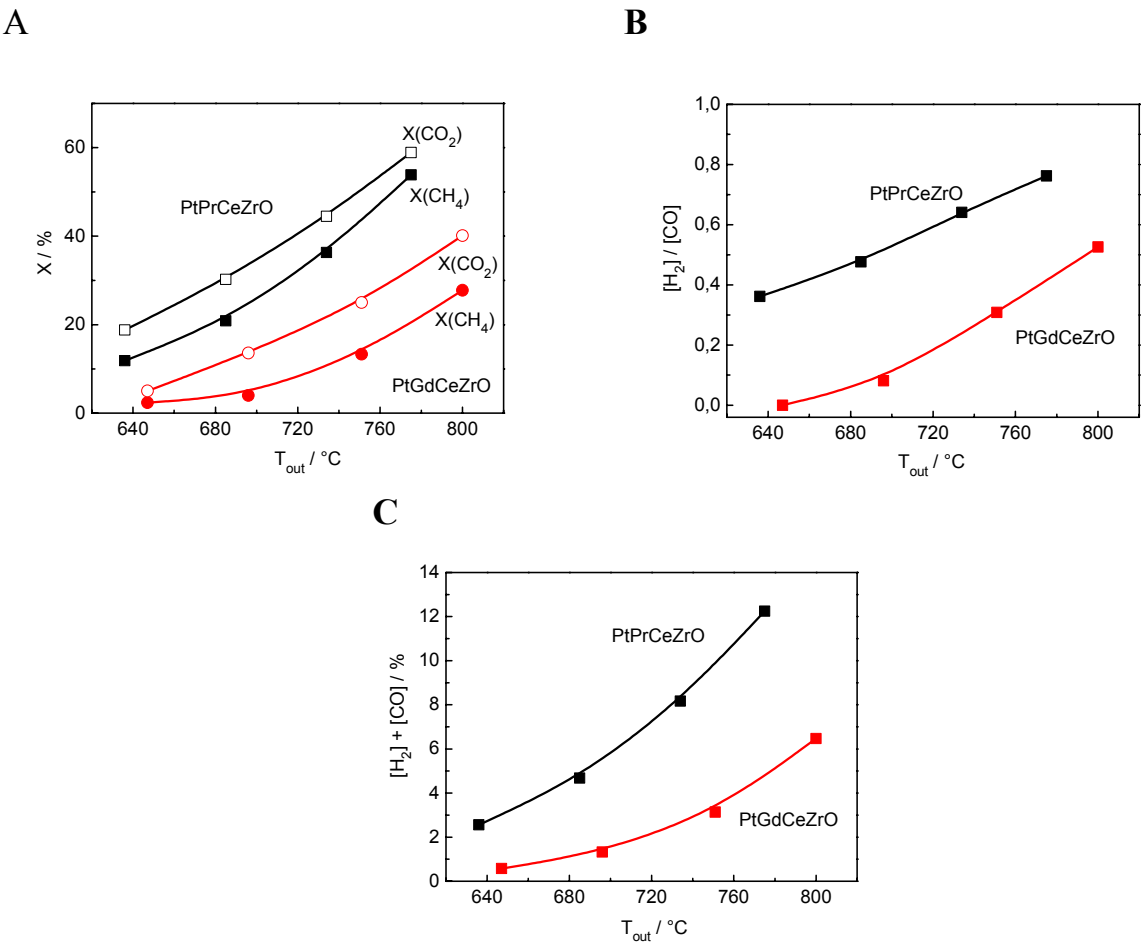

Figure III.4: *Temperature dependence of methane conversion, H_2/CO ratio and syngas content over PtPrCeZrO and PtGdCeZrO catalysts in DR reaction. The feed composition: 7% CH_4 + 7% CO_2 in N_2. Contact time 15 ms.*

The H_2-to-CO ratio for the highly active system doped with Pr approached the equilibrium value equal to 1 by increasing temperature and contact time (Figure III.4B and III.5B). The deviation from the equilibrium value at shorter contact times and lower temperature could be explained by a partial consumption of hydrogen (generated by the dissociation of methane) for CO_2 reduction into H_2O and CO; however for this case, the steam reforming of CO should not occur in the same time.

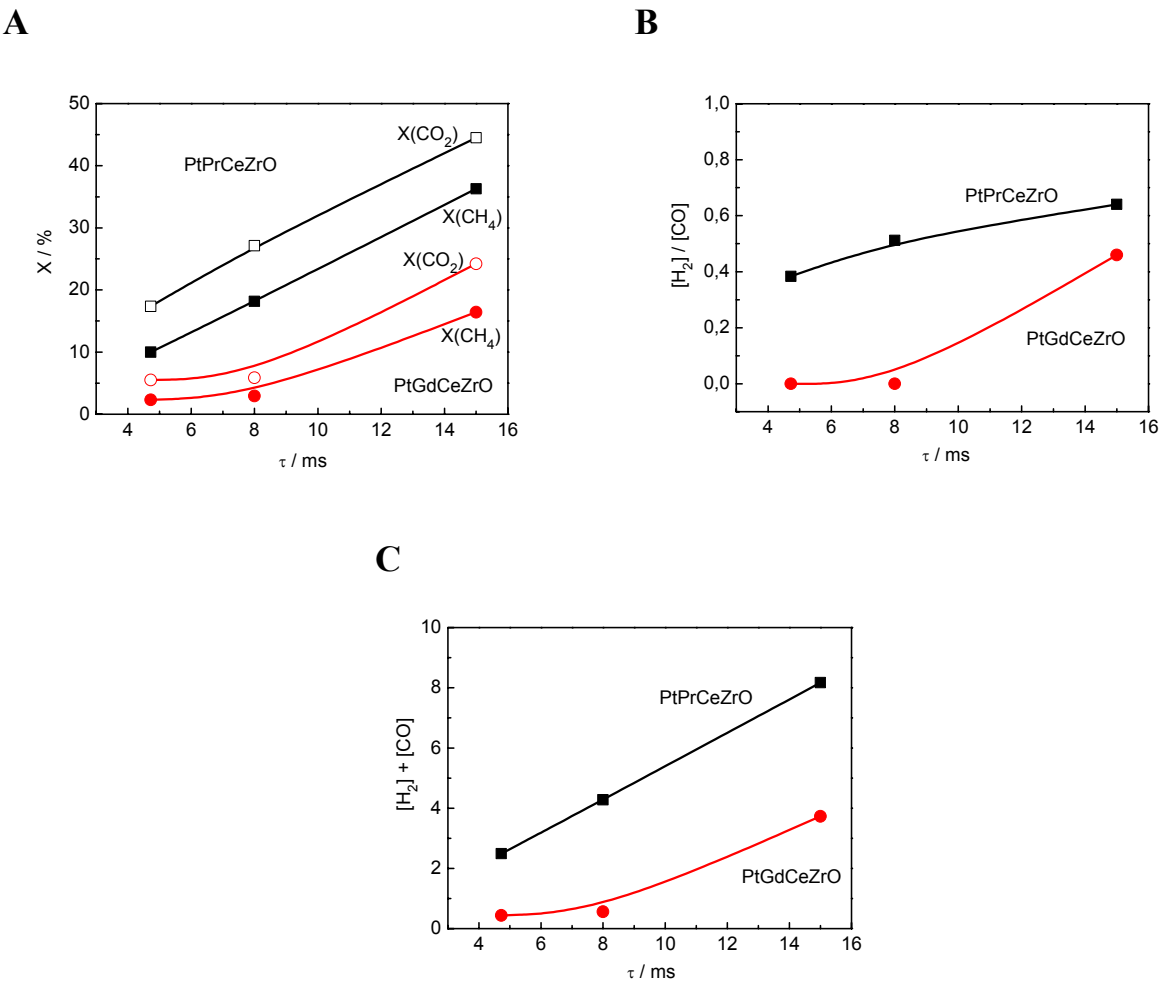

Figure III.5: *Contact time dependence of activity and product ratio/CO+H_2 sum over PtPrCeZrO and PtGdCeZrO catalysts in DR reaction at 750°C. The feed composition: 7% CH_4 + 7% CO_2 in N_2.*

The effect of initial methane concentration on methane conversion and H_2-to-CO ratio for the Gd doped catalyst is shown in Figure III.6. The methane conversion depends rather moderately and non-monotonously on reactants concentration in the feed. The higher CO_2 conversion compared to that of methane at smaller methane concentration in the feed could relates to an additional consumption of CO_2, e.g. by the reverse water-gas shift reaction proceeding with some of the formed H_2, or it could be a result of a stronger adsorption of CO_2 on the catalyst surface by carbonates and carbon-containing complexes. This would lead to a higher coverage and thus to a higher reaction probability and comparably a higher CO_2 conversion.

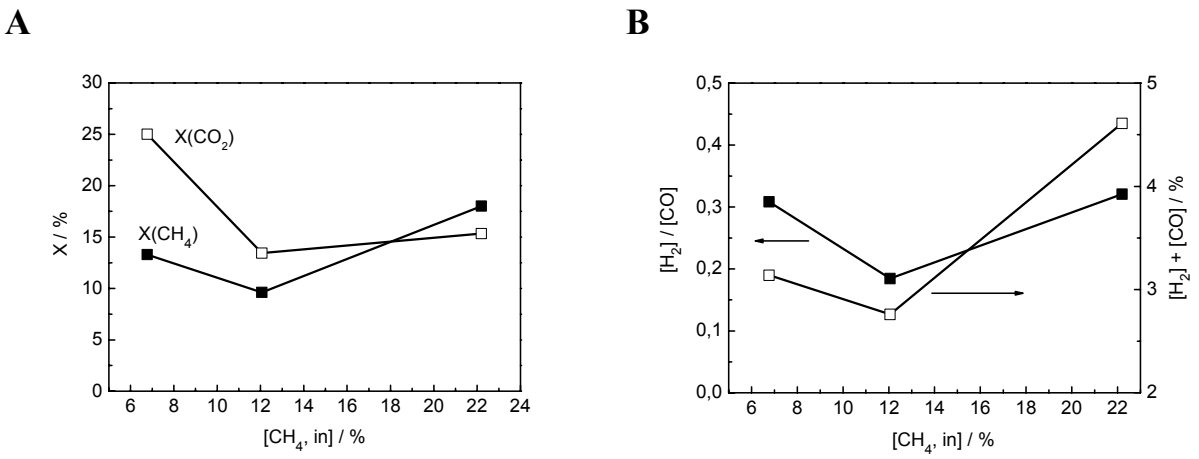

Figure III.6: *Effect of initial CH_4 concentration in the feed on activity and product ratio (sum) over PtGdCeZrO catalysts in DR reaction. The reactant ratio in the feed was kept constant at CH_4 / CO_2 = 1. Contact time 15 ms and 750°C.*

The main conclusion from the present study of DR over the Pr and Gd doped catalysts is that the former is more active and selective in the process. In addition, it will come from the next chapters that the observed trend in activity is in a good agreement with the lattice oxygen mobility and reactivity.

III.4. Effect of steady state reaction conditions on the TPR and TPO characteristics

The present part of the work aims at investigating the surface oxygen reactivity, and more precisely its influence on surface hydroxylation and carbonatation by using the temperature-programmed reduction with methane (TPR) and the temperature-programmed oxidation by oxygen (TPO). In order to characterize the state of the catalyst surface, which would correspond to the CPOM operation, the respective TPR and TPO investigations on PtPrCeZrO and PtGdCeZrO monoliths were performed after achieving the steady state in POM (and dry reforming) reaction.

Before the TPR and TPO experiments, the catalysts were pretreated in oxygen at 700°C for 30 min, then heated to 750°C and contacted with different initial reactant concentrations until

reaching the stationary state. The following feed compositions were used for establishing the POM steady-state before performing the TPR and TPO, respectively:

- TPR: 3.5% CH_4 + 1.75% O_2 or 5% CH_4 + 2.5% O_2 or 10% CH_4 + 5% O_2 and N_2 - balance;
- TPO: 10% CH_4 + 5% O_2 or 20% CH_4 + 10% O_2 or 10% CH_4 + 10% CO_2 or 20% CH_4 + 20% CO_2 and N_2 - balance.

After reaching the stationary state under reaction conditions, the reactor was flushed with water free He (cleared in a cryogenic trap), and cooled down to the starting temperature of TPR (200°C) or TPO (100°C) experiments. Then the feed was introduced with a composition of 1% CH_4 + 99% N_2 for TPR or: 1% O_2 + 99% N_2 for TPO. The temperature ramp was 5°C/min up to 850°C and after reaching that temperature the sample was kept isotherm during the next 70min. The contact time for TPR and TPO were kept at 15ms and 42.5ms and flow rate 94ml/min and 33ml/min, respectively.

III.4.1. Temperature-programmed reduction by methane

After CPOM carried out under 10% CH_4 + 5% O_2 (N_2-balance) feed composition, the TPR profiles reported in Figure III.7A-B are quite similar for both catalysts. However, for Gd - doped catalyst CO_2 and CO released already at 321°C and 524°C while for catalyst with Pr at 389°C and 545°C, respectively. Another feature of the Pr - doped catalyst is a relatively slow CO formation as compared to the catalyst with Gd. These data suggest that the PtGdCeZrO catalyst contains more available and reactive oxygen than the PtPrCeZrO catalyst. This last observation corresponds to O_2 – TPD results described in Chapter IV.

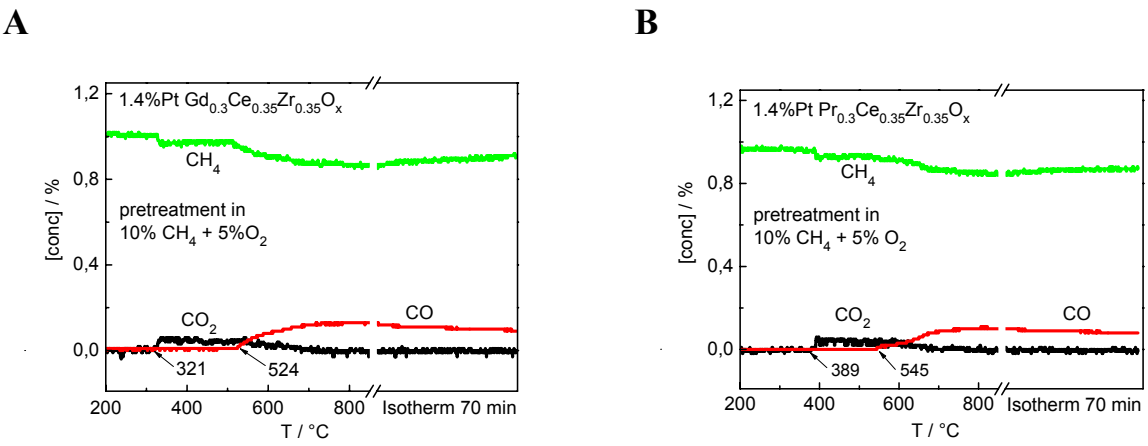

Figure III.7: *Temperature – programmed reduction by mixture 1% CH_4 (N_2 - balance) over single channel with PtGdCeZrO (A) and PtPrCeZrO (B) active component. Catalyst was tested after using in the CPOM with a feed of 10% CH_4 + 5% O_2 (N_2 - balance).*

III.4.2. Effect of steady state reaction conditions on the TPR characteristics

In this part, the TPR profiles were compared after steady state CPOM reaction carried out with different feed composition (3.5, 5, 10%CH_4 at CH_4/O_2=2 and N_2 - balance) at 750°C and 15ms for the PtPrCeZrO catalyst.

Table III.4: *Inlet and outlet temperature of the catalytic monolith channel during the CPOM reaction and methane conversion during the further TPR experiments*

Feed composition of steady state experiment*	T inlet, °C	T outlet, °C	XCH_4 (TPR), %
3.5%CH_4 + 1.75%O_2	770	752	24
5%CH_4+2.5%O_2	775	752	11
10%CH_4+5%O_2	825	750	13

* - all mixtures were diluted by nitrogen

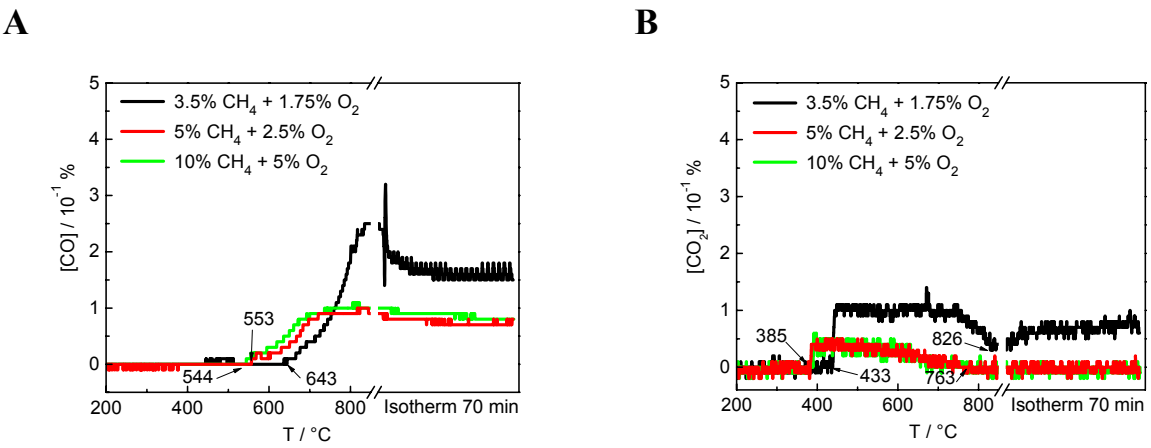

Figure III.8: *Influence of feed composition during the CPOM pre- reaction on the CO (A) and CO_2 (B) release observed during the TPR over PtPrCeZrO single channel. Reduction feed 1% CH_4 + 99% N_2. Contact time 15ms.*

Figure III.8 shows the TPR CO and CO_2 profiles, while no hydrogen traces were detected in these experiments. After CPOM carried out with the lowest reactant partial pressures, TPR data show higher CO and CO_2 production (Fig. III.8 A-B) and methane conversion (Table III.4). This can be explained changes in the surface state of the catalyst in steady state CPOM process. As can be seen from Table III.4, in CPOM reaction the inlet temperature of catalyst is strongly related to the feed composition, while the outlet temperature does not change significantly: the higher the feed concentration, the higher the channel inlet temperature. Since the oxygen desorption will be favored at high temperature, it can be inferred that the catalyst surface under CPOM concentrated feed will be more reduced than oxidized. That statement might explain the trends above reported for TPR experiments.

In fact, it should be noted that degree of surface oxidation under CPOM steady-state declines even under isothermal conditions and constant oxygen-to-methane ratio upon increasing concentration. This relates to the fact that the rate of reduction is usually first order with respect to the hydrocarbon while the order of oxygen in the rate expression for the reoxidation is usually zero or close to zero.

III.4.3. Temperature-programmed oxidation by oxygen

The TPO investigations were carried out to study the catalytic surface and probe for the presence of methane decomposition products, i.e. carbonaceous species, which could be formed

during CPOM and DR reactions. The TPO was carried out only on the PtGdCeZrO channel. Before TPO, the catalyst was brought to CPOM steady state at 750°C and contact time 42.5 ms using feeds of different composition for CPOM and DR reactions, namely 10% CH_4 + 5% O_2, 20% CH_4 + 10% O_2 and 10% CH_4 + 10% CO_2, 20% CH_4 + 20% CO_2, respectively.

As can be seen in Fig. III.9a-b, after both reactions (CPOM and DR) the accumulation of strongly bound carbon containing adspecies is reavealed by the CO_2 release between 550 and 750°C. Note however that a much lager amount of carbonaceous species, (carbonates and carboxylate forms) is detected on the catalytic surface, which was brought to steady state under dry reforming conditions, with even two types of adspecies, the most stable being decomposed/oxidized only around 750°C, i.e. at the temperature of the DR reaction. Such a carbonatation expected for basic surfaces is assumed to inhibit the oxygen diffusion from bulk to the surface and on the surface towards the interfaces bordering the Pt particles. This effect might explain the relatively slow transformation of activated methane fragments (CH_x) to synthesis gas and the observed decrease in activity.

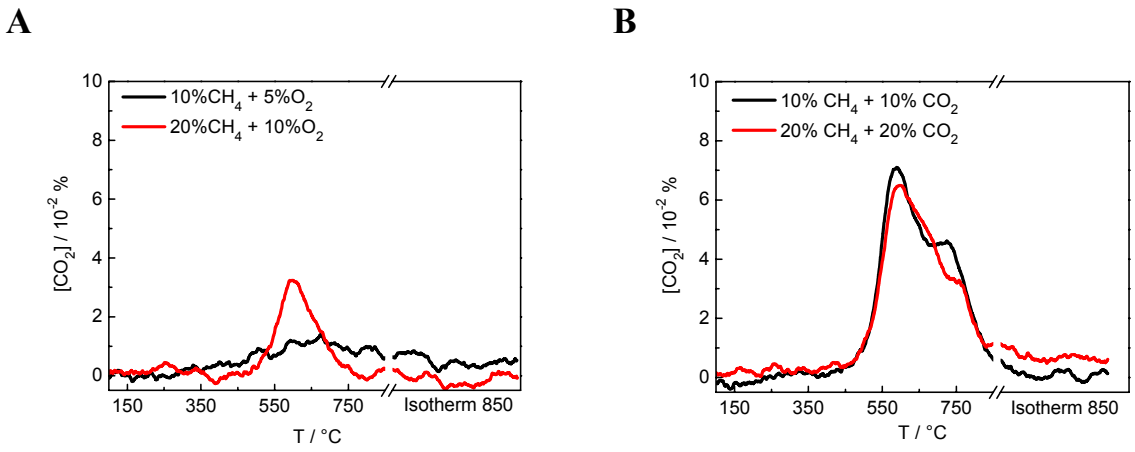

Figure III.9: *Temperature–programmed oxidation (TPO) carried out for Gd doped catalyst after CPOM (A) and DR (B) reactions with the feeds: A – 10% CH_4 + 5% O_2, 20% CH_4 + 10% O_2 and B - 10% CH_4 +10% CO_2, 20% CH_4 + 20% CO_2.*

III.5. Conclusions

The catalytic partial oxidation of methane has been studied over single channels of corundum monolith coated with catalysts based on ceria-zirconia forming a solid solution with either pure or Pt promoted lanthanum nickelate, as well as Pt-supported over Pr or Gd - doped ceria-zirconia. After a systematic screening, including the effects of oxidizing or reducing pre-treatments, the Pr and Gd - doped catalysts were determined as highly performing for the CPOM application and especially well adapted for a robust and easy to handle syngas generator, working at short contact time, high temperature and little demanding in term of required pretreatment. .

As a side reaction also involved in the CPOM, the dry reforming was studied for the two selected PtPrCeZrO and PtGdCeZrO systems as well. The influence of key process parameters such as temperature, contact time and initial concentration of reactants in the feed on the DR reaction were identified. The catalyst doped by Pr was found to present the highest activity and selectivity in the reaction. This property might be related to a non inhibited bulk/surface mobility of oxygen in these systems, which will be discussed in more details in the subchapter IV.1.1.

The state of the catalyst surface under steady-state regime for CPOM and DR reactions has been investigated by TPR and TPO experiments. TPR profiles indicated that a highly concentrated feed (high partial pressures) in the CPOM reaction tend to reduce (oxygen depletion) the catalytic surface. TPO experiments carried out on samples after steady-state CPOM or DR revealed the formation of some strongly bounded carbonaceous compounds on the catalyst surface, essentially after DR. As such the surface carbonatation (related to its basicity) tends to inhibit the oxygen diffusion from bulk to the surface and then to Pt particles. This surface hindrance would limit the oxidation of the methane fragments (activated on Pt) into syngas and therefore decrease the overall activity.

CHAPTER IV

Mechanistic study of the CPOM

IV.1. Study over powdered Pt/PrCeZrO and Pt/GdCeZrO catalysts

From a mechanistic point of view, it is well known and already discussed during literature analysis that synthesis gas generation may involve either a direct conversion of methane to carbon monoxide and hydrogen or a more unfavorable two-step route. The latter involves the highly exothermic complete combustion in the presence of oxygen (step1) followed by endothermic secondary steam and dry reforming of remaining hydrocarbon (step2). This sequential mechanism suffers from the need of ensuring the heat transfer from the entrance reactor zone where step 1 occurs to the remaining zone where step 2 dominates. The relative importance of both routes may depend on the catalyst structure, e.g. availability of oxygen supplied from the support lattice to metal clusters via spill-over processes.

This chapter presents TAP reactor experiments investigating mechanistic features for the partial oxidation of methane (POM) [24,195] over the two systems selected in the previous Chapter III, i.e., the bi-functional catalysts composed of Pt clusters supported over Pr and Gd doped ceria-zirconia mixed oxides, namely Pt/PrCeZrO and Pt/GdCeZrO. Furthermore, according to the fact that oxygen availability might have crucial importance, TPD experiments were performed in the TAP reactor to take benefit of the high detection sensitivity. Details on the used installation and experimental procedures were described in Chapter II. The two selected formulas are studied first as powder sample and then suppoted on the corundum single channel monolith.

IV.1.1. O_2 -TPD experiments on powder samples

Applying the TAP technique to catalysts with significant oxygen storage capacity presents major challenges that need to be addressed prior to conducting an extensive study. Pt-based catalysts are characterized by a strong adsorption of oxygen on their surface not allowing to obtain clear pulse shaped responses when the coverage of oxygen remains as low as required during conventional TAP experiments. At relatively high coverage, desorption of dissociatively adsorbed oxygen proceeds slowly leading to pronounced so-called “background” level effects. In this case the release of adsorbed molecules is only visible as continuous, elevated signal related to desorption driven by the high coverage, which itself declines only very slowly in a quasi-continuous way. Despite the fact that no quantifiable pulse response occurs, the slow desorption

under vacuum conditions alters the oxidation state of the catalyst and does not allow to establish a well defined ("absolute") oxygen saturation of the catalyst like this would be possible under atmospheric pressure conditions applying a given oxygen partial pressure. However, it is possible to achieve a dynamic saturation of the catalyst, where the final catalyst state at quasi-equilibrium depends on the catalyst temperature during saturation, oxygen pulse size and pulse frequency. For the state of dynamic saturation the rate of oxygen desorption equals the rate of oxygen adsorption form the pulse-wise supply. The latter adsorption rate is defined as the ratio of the oxygen quantity absorbed from a pulse and the time lag between two successive pulses. In order to investigate first the oxygen release from the different catalysts, oxygen TPD experiments were performed.

Figure IV.1A, B reports the TPD profiles of Pr and Gd doped powder catalysts after dynamic oxygen saturation at different temperatures.

First, it should be noted that the Gd-doped sample (Fig. IV.1B) gives rise to the low-temperature oxygen desorption, while the Pr-doped sample (Fig. IV.1A) has no significant response until 350°C. Thus, it can be concluded that the Gd-doped sample allows the formation of more weakly bound oxygen species. This kind of species is potentially more reactive and might be also more susceptible to be transferred to the Pt surface by spillover. The overall intensity observed for the Pr-doped sample is however somewhat higher than in the case of the Gd-doped sample. Comparably intense signals, especially compared to the Pt/Al_2O_3 sample without bulk storage capacity, imply that the oxygen release relates not only to the surface bound oxygen, but that additional oxygen is removed from the lattice of doped ceria-zirconia. This finding agrees with a large oxygen storage capacity known for ceria-based materials. On the other hand, different quantities of released oxygen may not just relate to the absolute storage capacity, but could be also a consequence of applying the dynamic saturation.

The amount of oxygen stored during dynamic saturation depends obviously also on the lattice mobility of oxygen. A higher mobility allows in a given time span a deeper penetration of surface-supplied oxygen into the bulk, which is in turn reflected as a higher apparent storage capacity for that active support. In this sense the Pr doped sample is expected to have higher oxygen mobility than the Gd doped one. In fact, this finding agrees well with data on the lattice mobility of oxygen measured with dynamic isotope exchange [83].

Comparison of experiments over 1.4% Pt/Al_2O_3 (Figure IV.1D) indicated no significant oxygen responses for the TPD experiment, while the oxygen desorption from bare $Pr_{0.3}Ce_{0.35}Zr_{0.35}O_x$ material proceeded very slow (Figure IV.1C). The latter observations clearly indicate the synergy between Pt and the active support concerning oxygen dynamics.

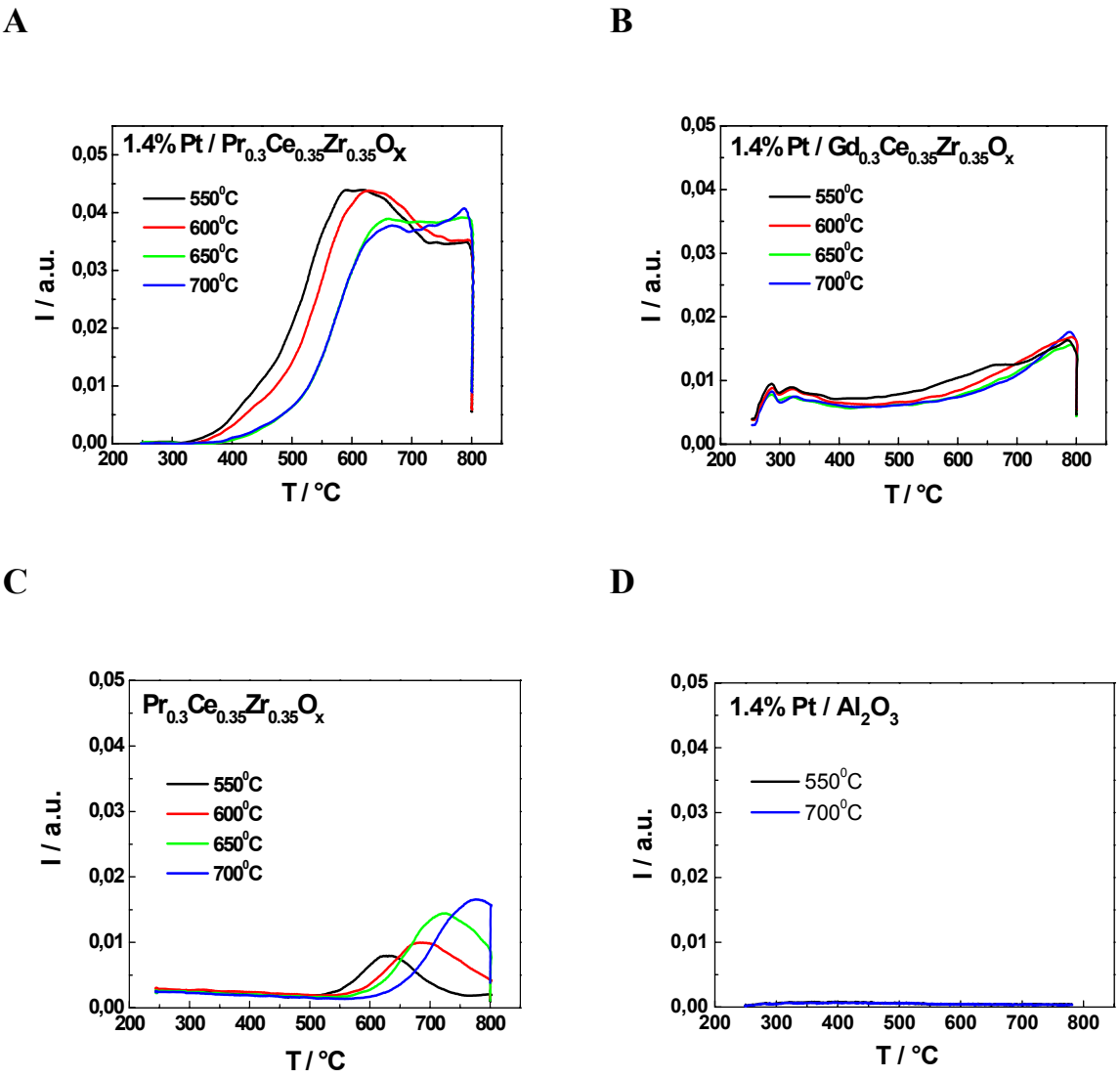

Figure IV.1: *TPD responses of a 1.4wt-% Pt / $Pr_{0.3}Ce_{0.35}Zr_{0.35}O_x$ (A), 1.4wt-% Pt / $Gd_{0.3}Ce_{0.35}Zr_{0.35}O_x$ (B), bare support (C) and 1.4wt-% Pt / Al_2O_3 (D) recorded in the TAP setup after dynamic oxygen saturation at various temperatures.*

IV.1.2. Pump-probe experiments on powder samples

A use of pump-probe experiments with a time offset of 0.5 second between oxygen (1 part) and methane (2 parts) pulses allows probing the reactivity of catalyst under different conditions and catalyst states.

Methane pulse responses scaled to the signal intensity of the inert standard argon are depicted in Figure IV.2, indicating clearly that the Gd doped sample gives rise to higher methane conversions, as also reported in Table IV.1. It is especially noteworthy that the methane conversion is lower for the case of a dynamically oxidized catalyst than that for an outgased catalyst. This observation could be related to the formation of more stable oxygen species during dynamic oxidation than those species rapidly formed during the pump oxygen pulse for the case of the outgased catalyst. This interpretation is somewhat supported by the above described TPD experiments. On the other hand, dynamic saturation leads also to oxygen storage, which then might saturate the Pt clusters on the catalyst surface by spill-over phenomena. In this way, an unusual high oxygen coverage could result, which is known to limit methane activation. In fact, it was frequently observed that oxygen has a negative order in the methane combustion kinetics over platinum catalysts. Rising the temperature to 700°C leads to methane conversions above 94%, but the high dynamics of oxygen adsorption and desorption did not allow to establish clearly distinct surface states.

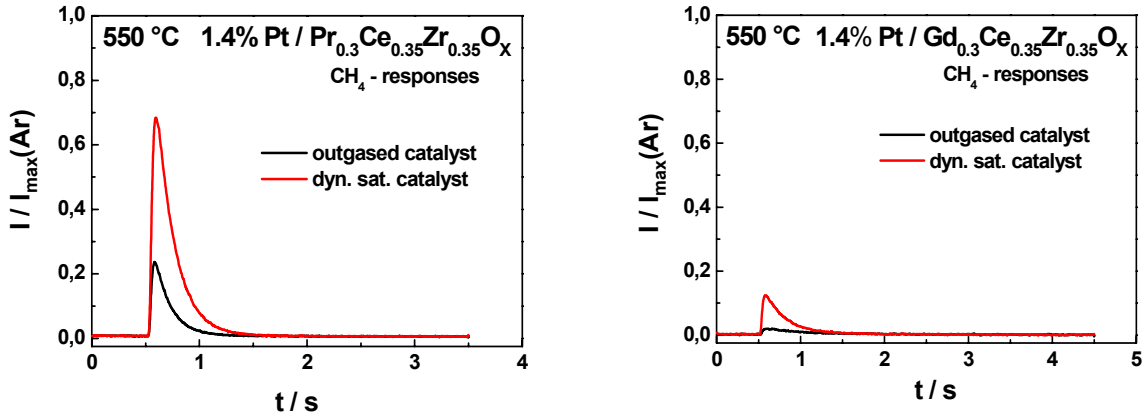

Figure IV.2: *Methane pulse responses over a 1.4 wt-% Pt / $Pr_{0.3}Ce_{0.35}Zr_{0.35}O_x$ (left) and 1.4 wt-% Pt / $Gd_{0.3}Ce_{0.35}Zr_{0.35}O_x$ (left) recorded in 1 part oxygen- 2 parts methane pump-probe TAP experiment at 550°C after dynamic oxygen saturation or outgassing.*

Table IV.1: *Methane conversions observed during pump-probe experiments at 550°C with an oxygen pump pulse followed after 0.5 s by a methane pulse at a CH_4/O_2 ratio of 1.8.*

Catalyst pretreatment	1.4 wt%Pt / $Pr_{0.3}Ce_{0.35}Zr_{0.35}O_x$	1.4 wt%Pt / $Gd_{0.3}Ce_{0.35}Zr_{0.35}O_x$
Dynamic saturation with oxygen	74	91
Outgased catalyst	91	95

Regarding the carbon dioxide and hydrogen pulse responses reported in Figures IV.3 and IV.4, the oxidized Pr sample is more selective towards hydrogen taken as representative for synthesis gas. However, it should also be noted that the hydrogen release occurred rapidly for the case of the Pr sample, while somewhat slower hydrogen release happened in the case of the Gd sample.

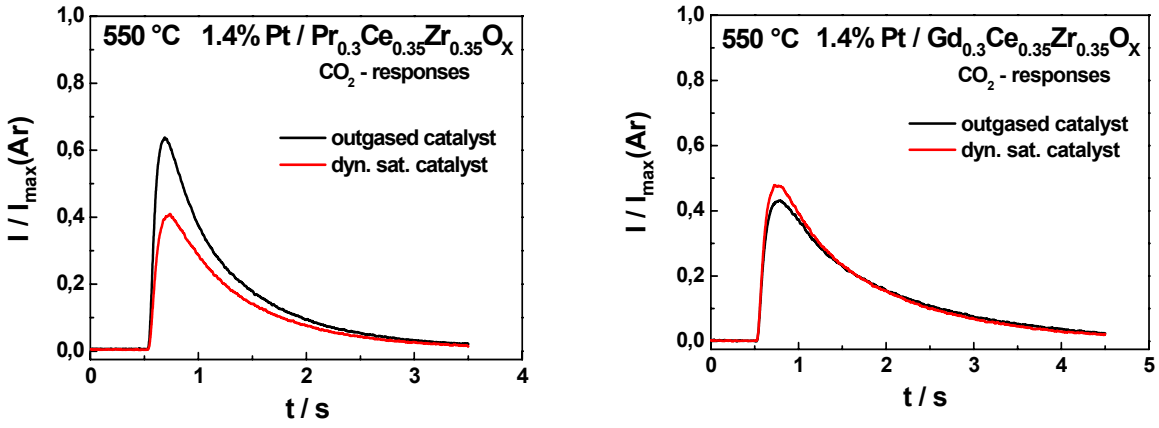

Figure IV.3: *Carbon dioxide pulse responses over a 1.4 wt-% Pt / $Pr_{0.3}Ce_{0.35}Zr_{0.35}O_x$ (left) and 1.4 wt-% Pt / $Gd_{0.3}Ce_{0.35}Zr_{0.35}O_x$ (left) recorded in 1 part oxygen- 2 parts methane pump-probe TAP experiment at 550°C after dynamic oxygen saturation or outgasing.*

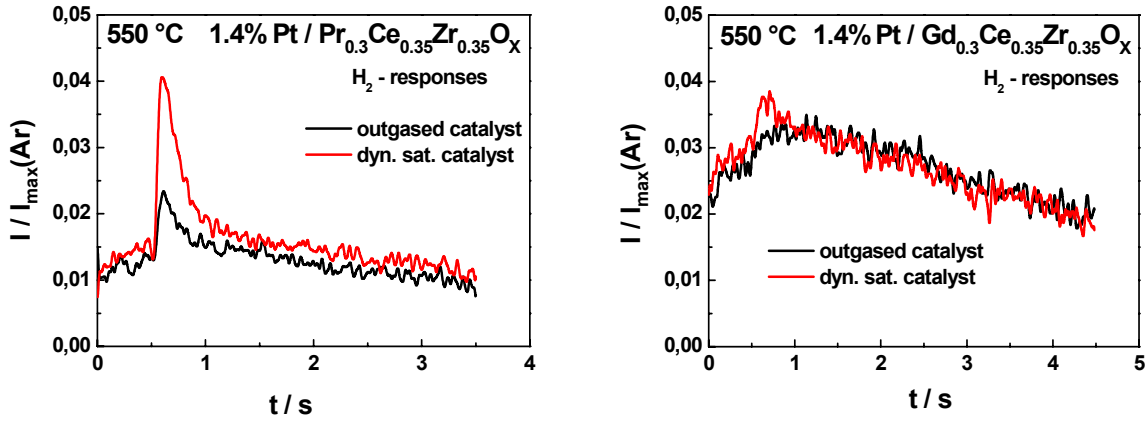

Figure IV.4: *Hydrogen pulse responses over a 1.4 wt-% Pt / $Pr_{0.3}Ce_{0.35}Zr_{0.35}O_x$ (left) and 1.4 wt-% Pt / $Gd_{0.3}Ce_{0.35}Zr_{0.35}O_x$ (left) recorded in 1 part oxygen- 2 parts methane pump-probe TAP experiment at 550°C after dynamic oxygen saturation or outgasing.*

IV.1.3. Comparison experiments with the support (without Pt), platinum black and 1.4 wt. -% Pt / Al_2O_3

For a better understanding of the catalyst nature comparison experiments over platinum black, 1.4 wt.-% Pt / Al_2O_3 and bare support were carried out in high temperature TAP reactor with the aim to:

- estimate a role of Pt and bare support in catalyst for reaction of partial oxidation of methane;
- determine effect of Pt dispersion.

Table IV.2 presents the methane conversion for oxidized catalysts of different composition. From the received data it is clear that the conversion of methane is much higher over catalysts including Pt in their formulation, while for the bare support $Pr_{0.3}Ce_{0.35}Zr_{0.35}O_x$ activity is significantly lower. The observation clearly indicated very well known fact of importance Pt in activation of methane. It should however be noted that the support itself still has an intrinsic activity, motivating a more detailed investigation under atmospheric pressure conditions.

Table IV.2: *Methane conversions observed during pump-probe experiments at 700°C with an oxygen pump pulse followed after 0.5 s by a methane pulse at a CH_4/O_2 ratio of 2 and oxidized state of catalyst.*

Catalyst	Methane conversion / %
1.4 wt%Pt / $Pr_{0.3}Ce_{0.35}Zr_{0.35}O_x$	96
$Pr_{0.3}Ce_{0.35}Zr_{0.35}O_x$	29
1.4 wt%Pt /Al_2O_3	95
Pt-black	97

The transient responses of CO, carbon dioxide, hydrogen and water on the introduction of a pulse of oxygen, followed 0.5 s later by a pulse of methane are shown in Figure IV.5. For Pt-black only products of deep oxidation were observed (Figure IV.5A), while a slow formation of CO_2 for Pt supported on the high surface area Al_2O_3 (Figure IV.5B) was detected. Data from pump-probe experiment over $Pr_{0.3}Ce_{0.35}Zr_{0.35}O_x$ show, that catalyst is selective towards H_2 and that the formation of CO_2 proceeds very slowly (Figure IV.5C). The last observation is in good agreement with TPD-O_2 data received for bare support.

Summarizing, the synergy between Pt and the active support was clearly indicated. Intrinsic fluorite-like support activity is much less than that of supported Pt but detectable.

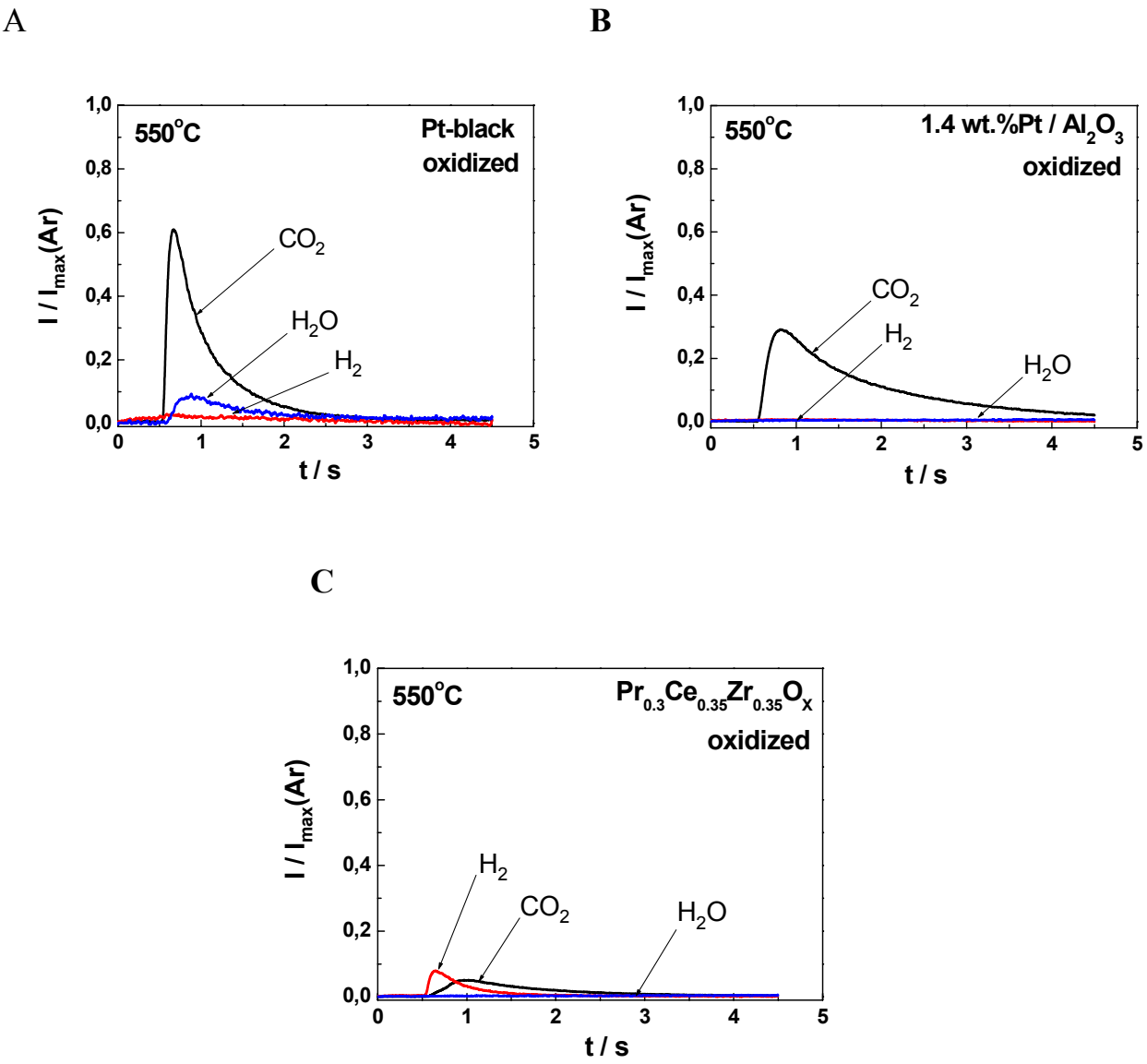

Figure IV.5: *Carbon oxide, carbon dioxide, hydrogen and water pulse responses recorded in 1 part oxygen - 2 parts methane pump-probe TAP experiment at 550°C after dynamic oxygen saturation. Over Pt-black (A), 1.4wt-% Pt / Al_2O_3 (B) and bare support (C) catalysts.*

Analyzing the pulse responses over the Pt-free catalyst support it is important to outline that a quite broad peak of carbon dioxide formation is observed. Obviously, carbon dioxide is the complementary carbon-containing product to the formation of hydrogen. The explanation for the broad CO_2 response could however be either a slow formation of CO_2 or a slow desorption associated with a strong re-adsorption.

In order to investigate the interaction of carbon dioxide and hydrogen, pulsing these two gases, as shown in Figure IV.6, has carried out separate experiments.

A B

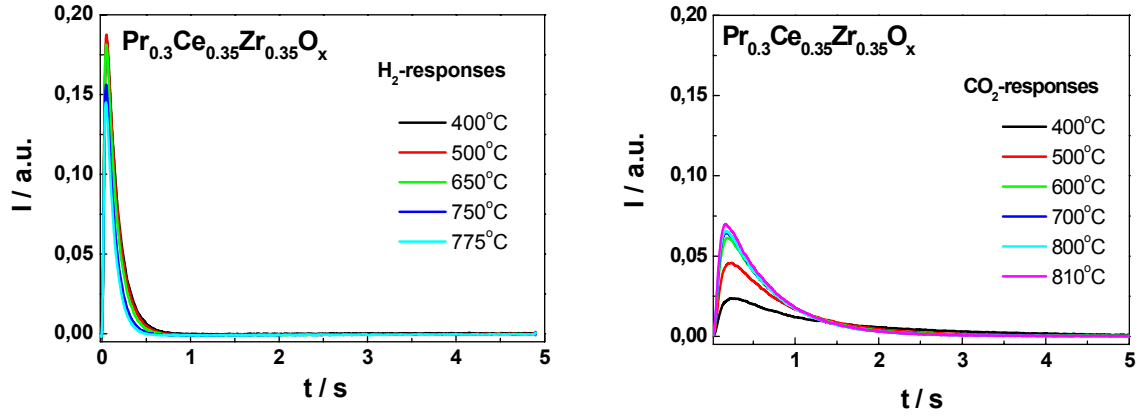

Figure IV.6: *Hydrogen (A) and carbon dioxide (B) pulse responses over a $Pr_{0.3}Ce_{0.35}Zr_{0.35}O_x$ recorded from pump-probe TAP experiment at different temperatures.*

Figure IV.6 shows a strong reversible interaction of CO_2 with the catalyst at higher temperatures. In order to determine precisely the temperature interval were a fully reversible interaction occurs, Figure IV.7A,B reports the integral of the CO_2 responses normalized to the integral of Ar responses as a function of the catalyst temperature. From the dependence of CO_2 integral over temperature it is clearly shown that interesting interval with fully reversible interaction enabling a calculation of CO_2 adsorption enthalpy according to the method of moments [186] starts for both supports at high temperature above 525°C. In turn, given the character of this interaction it is possible to analyze the data according to an analytical model and determine the difference of activation energy of the carbon dioxide desorption and adsorption, i.e. the adsorption enthalpy.

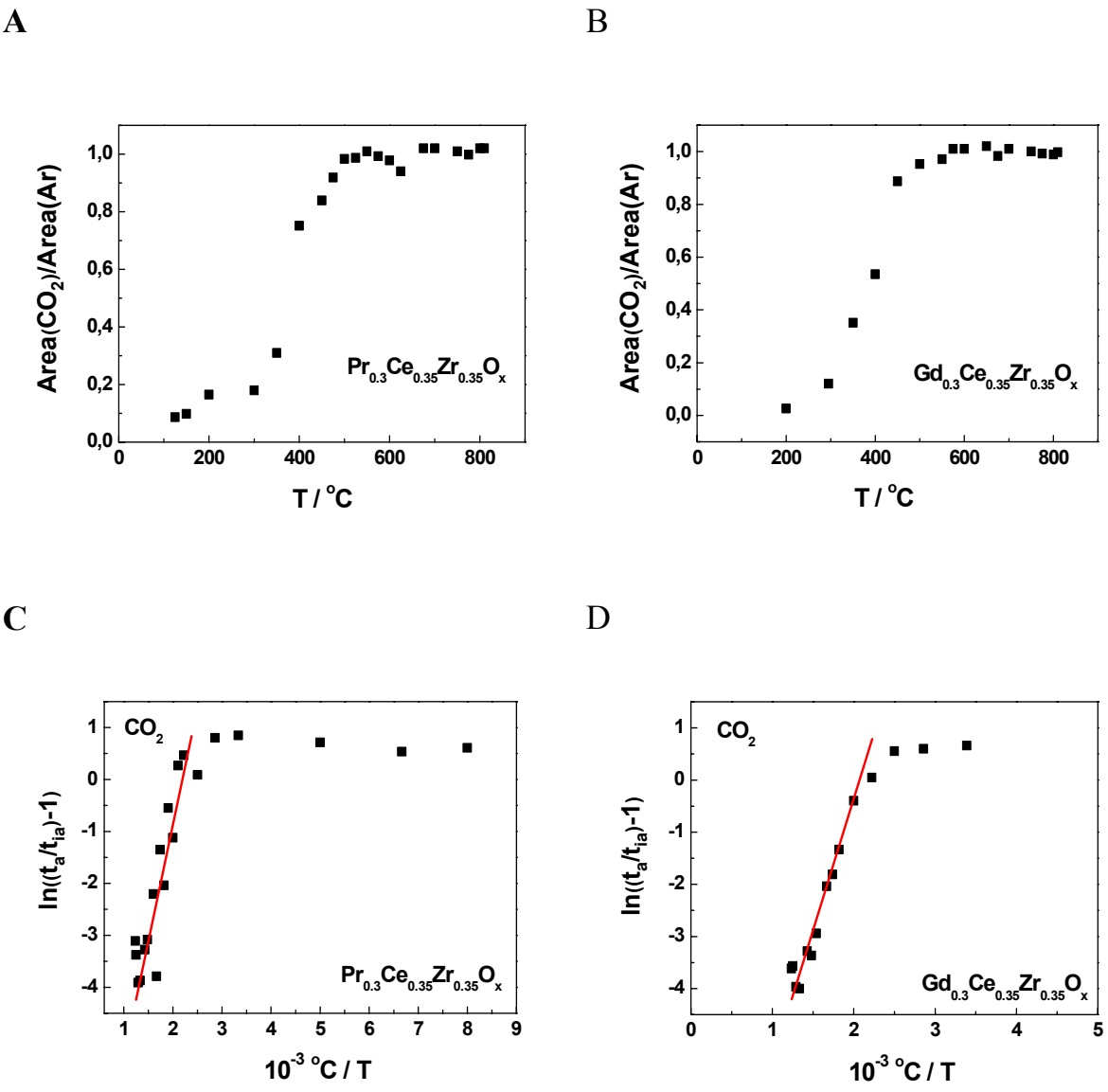

Figure IV.7: *Interaction of carbon dioxide over $Pr_{0.3}Ce_{0.35}Zr_{0.35}O_x$ (A,C) and $Gd_{0.3}Ce_{0.35}Zr_{0.35}O_x$ (B,D) support recorded at different temperatures.*

The respective data treatment making use of single-pulse experiments to characterize interactions between adsorbing molecules and the catalyst involves an integration determining the 0^{th} ($\int Intensity(t)\,dt$) and 1^{st} ($\int t\ Intensity(t)\,dt$) moment of the pulse responses and the calculation of the average residence time as ratio between the 1^{st} and 0^{th} moment. A quantification of the obtained results in terms of the heat of adsorption is possible using (***Eq.***

IV.1) derived from the analytical model for simple adsorption processes by Gleaves et al. [186]. The measured average residence time ($\bar{t}_j$) of the adsorbing molecule j is compared to the theoretical average residence time ($\bar{t}_{j,i}$) of the same molecule without interaction with the catalyst surface. The latter value is calculated from the average residence time of a non-adsorbing reference gas ($\bar{t}_i$) using ***(Eq. IV.2.)*** Herein, the mass dependency of the diffusion speed for molecules with different molar masses M is taken into account, which implies that the mass transfer must occur only by Knudsen diffusion.

$$\ln\left(\frac{\bar{t}_j}{\bar{t}_{j,i}} - 1\right) = \frac{-\Delta_{ads}H_j}{\mathrm{R}\,T} + \ln K = \frac{E_{des,j} - E_{ads,j}}{\mathrm{R}\,T} + \ln K \qquad \textit{(Eq. IV.1)}$$

$$\bar{t}_{j,i} = \bar{t}_i \sqrt{\frac{M_i}{M_j}} \qquad \textit{(Eq. IV.2)}$$

(Eq. IV.1) relates the adsorption enthalpy ($\Delta_{ads}H_j$) quantitatively to a change in the average residence time, which relates it to the difference of activation energy for desorption ($E_{des,j}$) and adsorption ($E_{ads,j}$), wherein K is defined as the ratio of the pre-exponential factors of adsorption and desorption. Thus, the heat of a completely reversible molecular adsorption can be derived from the slope of the straight line obtained by plotting the natural logarithm of the ratio $\bar{t}_j$ over $\bar{t}_{j,i}$ minus one against one over T (Figure IV.7C,D). However, the used model enforces some restrictions upon the application of this method. First, the adsorption process must be completely reversible within the investigated temperature range as can be proved by checking that the pulsed amount of reactants is completely recovered within the response. Therefore, the lower temperature limit is determined by the increase in time and the decrease in signal intensity necessary to ensure a complete detection of the pulsed molecules. An upper temperature limit often arises from the occurrence of chemical reactions, which, in turn, change the pulse response. Second, the used pulse size has to be limited to ensure that the mass transport only occurs by Knudsen diffusion.

Using ***(Eq. IV.1)*** and ***(Eq. IV.2)*** the adsorption enthalpy ($\Delta_{ads}H_j$) CO_2 was calculated for $Pr_{0.3}Ce_{0.3}Zr_{0.3}O_x$, $Gd_{0.3}Ce_{0.3}Zr_{0.3}O_x$ and Pt/Al_2O_3 catalysts (Table IV.3).

Table IV.3: *The calculated adsorption enthalpy ($\Delta_{ads}H_j$) CO_2 for $Pr_{0.3}Ce_{0.3}Zr_{0.3}O_x$, $Gd_{0.3}Ce_{0.3}Zr_{0.3}O_x$ and Pt/Al_2O_3 catalysts*

Adsorption enthalpy	Powder catalyst		
	$Pr_{0.3}Ce_{0.3}Zr_{0.3}O_x$	$Gd_{0.3}Ce_{0.3}Zr_{0.3}O_x$	Pt/Al_2O_3
$\Delta_{ads}H$ (CO_2), kJ	87	88	76

The residence times of H_2 are always very close to the theoretical value when H_2 passes the catalyst without interaction. Then, at temperatures above 500°C, reaction starts and the areas decline due to hydrogen consumption (Figure IV.8A,B). Thus, it can be concluded that hydrogen has either the problem of being not readily adsorbed on the catalyst support or that it desorbs very rapidly due to a very weak interaction. It is most likely that hydrogen does not adsorb on the support because of a weak interaction with the oxide (Figure IV.8C,D). Once at higher temperature the oxygen mobility is increased, hydrogen starts to interact and is being oxidized. The activation could proceed on defects, but there more experiments would have been needed, e.g. increasing first the temperature and then pulse back at lower temperature.

It is therefore safe to conclude that hydrogen will interact much easier with Pt than with support. This explains why hydrogen formed during activation of methane on the support can leave the catalyst within a pulse response (as observed in Figure IV.5C), while there is not much of a pulse response expectable when hydrogen is formed on Pt due to its strong interaction with the noble metal. Then, at high temperature under vacuum or with high oxygen partial pressures at ambient pressure, a slight loss of hydrogen could occur when it reacts with activated oxygen species present on the support surface.

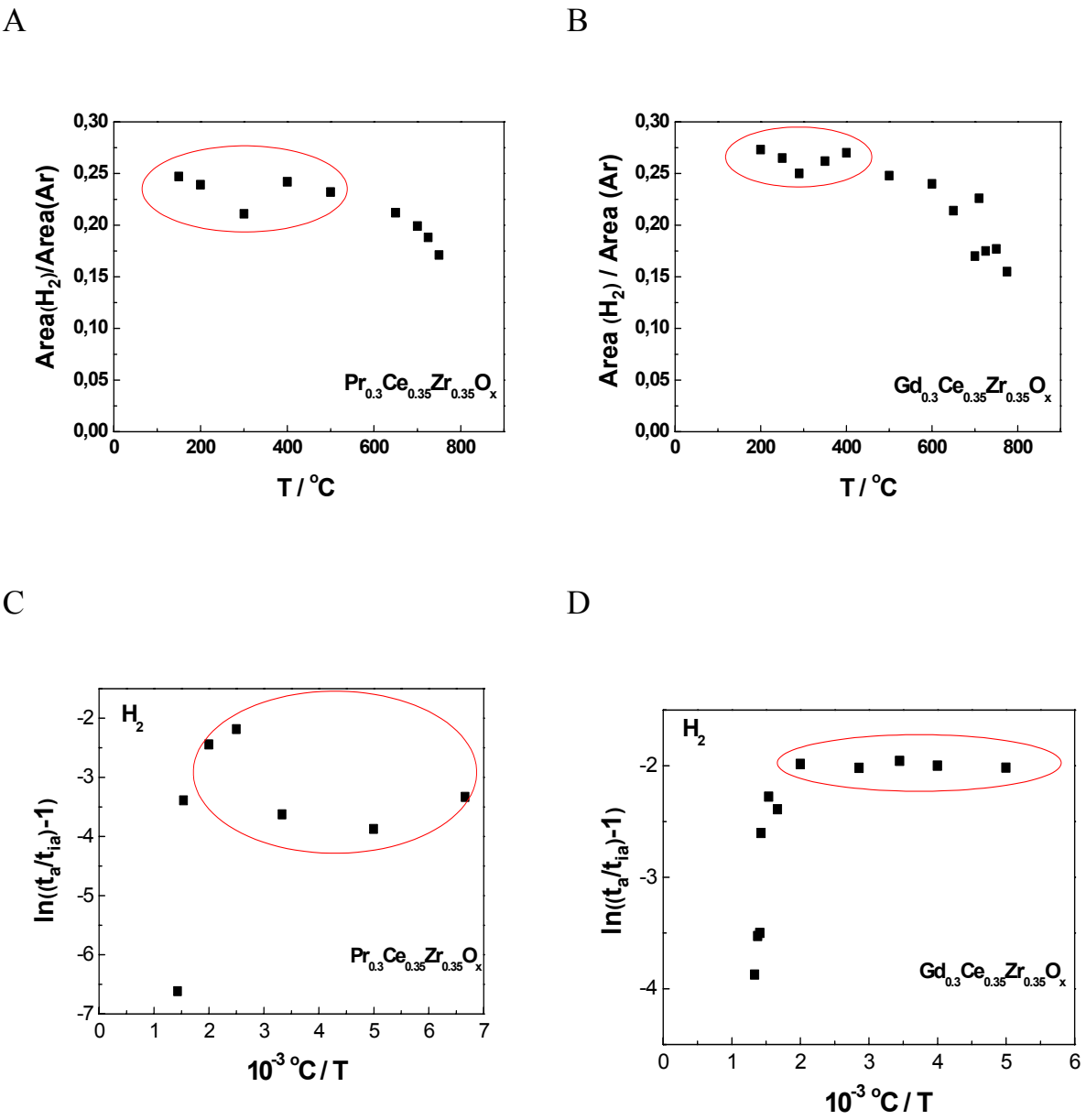

Figure IV.8: *Interaction of hydrogen over $Pr_{0.3}Ce_{0.35}Zr_{0.35}O_x$ (A,C) and $Gd_{0.3}Ce_{0.35}Zr_{0.35}O_x$ (B,D) support recorded at different temperatures.*

IV.2. TAP experiments over one channel corundum monolith catalyst

IV.2.1. Strategy for adapting TAP experiments to short contact time reactor

The investigation of the very fast oxidation steps in the formation of primary synthesis gas at atmospheric pressure remains a major challenge and no technique is presently available for tackling it. Though carried out at low pressure, using the TAP technique enables judging on the impact of the oxidation state of the catalyst on the performance. As a matter of fact, a major advantage of the TAP technique is related to the possibility of conditioning the catalyst to a defined oxidation state and to probe its reactivity with small pulses of methane hardly influencing the surface conditions. Furthermore, the TAP allows studying the reaction without significant thermal effects given the small reactant amount injected during pulsing.

Using the TAP technique with a monolithic catalyst can be considered as an original and suitable experimental strategy to explore the syngas generation at short contact time. As a matter of fact, the oxidation state profile related to the pressure pulse profile when submitting a reactant pulse-wise over the catalyst is comparable to the situation at atmospheric pressure in a short contact time reactor. Furthermore, the monolithic catalyst allows the use of smaller quantities of the highly active catalyst.

It should be first questioned why there is a specific oxidation state to be used and more specifically why equilibrated state for TAP experiment over one channel corundum monolith catalyst presents a suitable model condition to study performances?

Observing the responses to oxygen pulses it appears that the lack of rapid oxygen desorption leads to the fact that there are never substantial pulse responses over a catalyst not being equilibrated. On the other hand, pulsing methane allows to obtain pulse responses. Therefore it is obvious that the adsorption of oxygen is very fast and in any case faster than the conversion of methane. Thus, at atmospheric pressure, the inlet of a synthesis gas generator will always be strongly oxidized to a level probably not too far from the equilibrated catalyst state under TAP conditions. Focusing however on the generation of syngas by primary reaction steps, all formations of water and carbon dioxide should be avoided or minimized, even at a very oxidized state (represented by the TAP O_2 equilibrated conditions). Failing to minimize the formation of CO_2 and H_2O, those undesired products will have to be converted downstream via

the much slower secondary reforming reactions, which will require to enlarge very unfavorably the reactor to a great extent.

Therefore, it is obvious that the first hard criterion in choosing a catalyst for syngas generator is its performance in the O_2 equilibrated state, i.e. avoiding CO_2 and H_2O formation and maximizing the H_2 and CO production. This could even be so important that catalysts without activity in the oxidized state become acceptable.

Regarding the impact of the oxygen desorption on the further experimental strategy it is important to note that the reactivity of both Pt based catalysts imposes to conduct methane partial oxidation experiments at temperatures above 500°C for ensuring a sufficient reactivity. Obviously, oxygen desorption under these conditions disallows to adjust a static surface coverage or static oxygen saturation. On the other hand, exactly the obvious ability of storing oxygen implying a complication for the experiments seems to relate to the superior catalytic performance of these catalysts compared to catalyst using Pt on an inactive support. Thus, it is obviously required to develop an experimental strategy allowing to establish the catalyst reactivity as a function of the oxidation state.

Analyzing possibilities to perform reproducible experiments with a catalyst having a highly dynamic behavior, three defined and distinct surface states can be identified:

- First, it is comparably easy to obtain an “outgased state” of the catalyst. Here the catalyst is treated at high temperature and a maximum of oxygen is removed without applying a reducing agent. This catalyst state would be essentially representative of what occurs in the reforming section downstream of the reactor where no oxygen is present, thus is essentially relevant assuming a total oxidation / reforming reaction scheme. However, the current work focuses on a real partial oxidation scheme and it is obvious that this state is therefore less relevant for the investigation.
- Second, it is possible to focus on an “oxidized state”, which is essentially achieved under TAP conditions by applying the dynamic saturation introduced in the previous description of the TPD experiments. Indeed, studying this state presents an interest as extreme situation comparing the catalyst performance here to that of the formerly introduced “outgased state” presenting the complementary extreme. It should be clear that this state could be representative for the catalyst at the reactor inlet where the oxygen concentration is the highest. Targeting on the partial oxidation of methane at

atmospheric pressure, the lack of selectivity in this state will lead to extensive CO_2 and H_2O formation, requiring further reforming steps. Furthermore, strong heat effects with extensive hot spots would result in bad performances and possibly catalyst degradation. Therefore, the investigation of this catalyst state was considered to be beyond the scope of this work for the same reason as for the “outgased state”.

- Finally, it is possible to condition the catalyst by a long series of sequential oxygen and methane pulses in a ratio of 1:2 until stable performance is achieved. Applying this procedure leads obviously to a catalyst state in the TAP reactor quite close to the state of a catalyst operating at ambient pressure for the partial oxidation of methane. Accordingly, this state of the sample defined by the reaction itself is referred to as "working state".

Mechanistic information is easily obtained by studying the impact of slight variations from the “working state”. Thus, changing slightly the oxidation state is achieved by admitting a well defined number of oxygen pulses to the catalyst at “working state”. Establishing the impact of the additional oxygen proceeds by recording initially the catalytic performance for pump-probe experiments reestablishing the “working state” at longer operation and comparison to those final results at “working state”.

Following the above outlined experimental strategy exploiting the “working state” and controlled deviation from it, an extensive experimental campaign comparing a Pr and a Gd doped catalyst were performed. The “working state” was achieved using pump-probe experiments with a time offset of 0.5 second between an oxygen (1 part) and methane (2 parts). Differently oxidized states of catalyst were reached by submission of a different number of oxygen pulses at the same intensity than that used in the pump-probe experiments prior to immediate returning to those pump-probe experiment and exploiting the first 24 pulse responses to probe for the altered reactivity of the catalyst.

IV.2.2. Influence of the oxidation state for the Pr-doped catalyst

The responses of methane as reactant and hydrogen, carbon dioxide and carbon monoxide as products as a function of deviation from the “working state” are depicted in Figure IV.9 applying the above outlined experimental strategy to a Pr-doped sample. The chosen reaction

temperature for the methane conversion was 700°C. It is obvious that the responses of unconverted methane (Figure IV.9A) decrease only slightly with the number of oxygen pulses admitted onto the catalyst to increase its degree of oxidation. However, as indicated by the declining hydrogen (Figure IV.9B) and carbon monoxide (Figure IV.9D) responses and the increasing response for carbon dioxide, the selectivity towards syngas decrease with the number of additionally injected oxygen. Thus, this catalyst is very sensitive to oxygen pre-pulses as only 5 pulses cause a significant decline in synthesis gas selectivity and a rise in selectivity towards carbon dioxide (Figure IV.9C). Moreover, the formation of carbon monoxide proceeds very slowly as indicted by the broad signal observed at "working state". Furthermore, a considerable carbon monoxide intensity is already observed at zero time where only oxygen is pulsed. This finding relates clearly to the conversion of CH_x species on the catalyst surface originated from the previous methane pulse in the pump-probe sequence. It is currently not entirely clear if under ambient pressure conditions, a too slow carbon monoxide formation and release would infer CH_x species accumulation and build-up into carbonaceous residues; however the large presence of CH_x species on the catalyst at the "working state" is clearly confirmed for the Pr doped sample. By comparing the pulse responses of carbon dioxide and carbon monoxide it might be even speculated that both compounds could be primary products. However, this point cannot be resolved by comparing the height normalized carbon dioxide responses depicted in the inset as the formation rate of carbon dioxide increases only slightly with increasing number of oxygen pre-pulses.

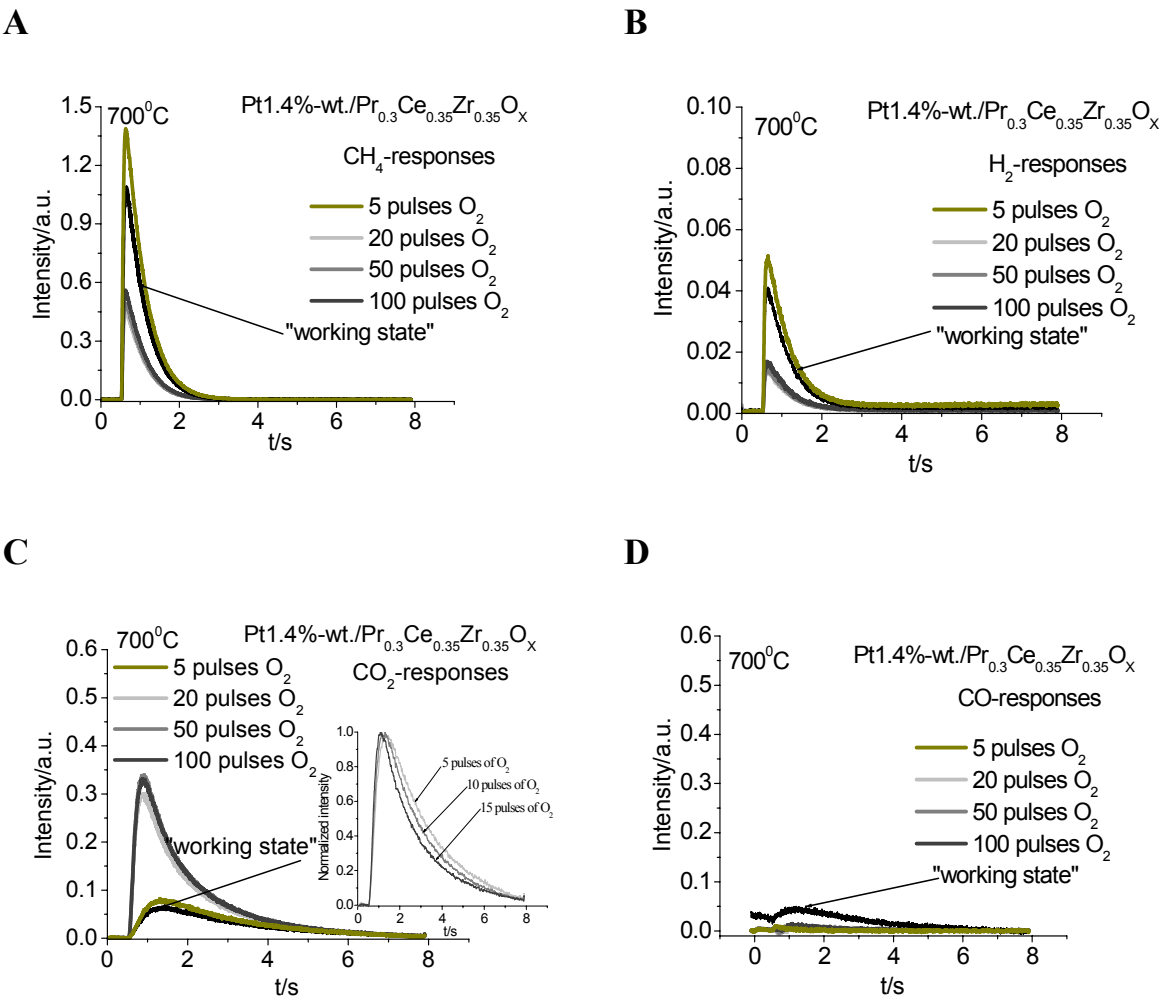

Figure IV.9: *Methane-a, hydrogen-b, carbon dioxide-c, carbon oxide-d pulse responses over a 1.4 wt-% Pt / $Pr_{0.3}Ce_{0.35}Zr_{0.35}O_x/Al_2O_3$ recorded in 1 part oxygen- 2 parts methane pump-probe TAP experiment at 700°C after 5-100 oxygen pre-pulses and "working state".*

Figure IV.9 presents also data recorded after a larger number of O_2 pre-pulses, namely 20, 50 and 100. The results indicate that even at a higher degree of oxidation, this catalyst produces stable hydrogen yields. However, it should be noted that in both cases with less and more oxygen pre-pulses the formation of CO remains relatively a slow process. Moreover, the slow formation of CO was also observed for the experiments over powdered catalysts, where no significant CO formation was observed during all experiments.

The origin for this finding is not entirely clear, but both the presence of carbon residues on the surface and/or a stabilizing effect of the active catalyst support storing excess oxygen after its spillover could contribute to inhibit the CO formation and its release in the gas phase.

IV.2.3. Influence of the oxidation state for the Gd-doped catalyst

The dependence of activity and selectivity on the oxidation state of the Gd-doped catalyst (modified by series of pre-pulses of oxygen after reaching the "working" state) is presented in Figure IV.10.

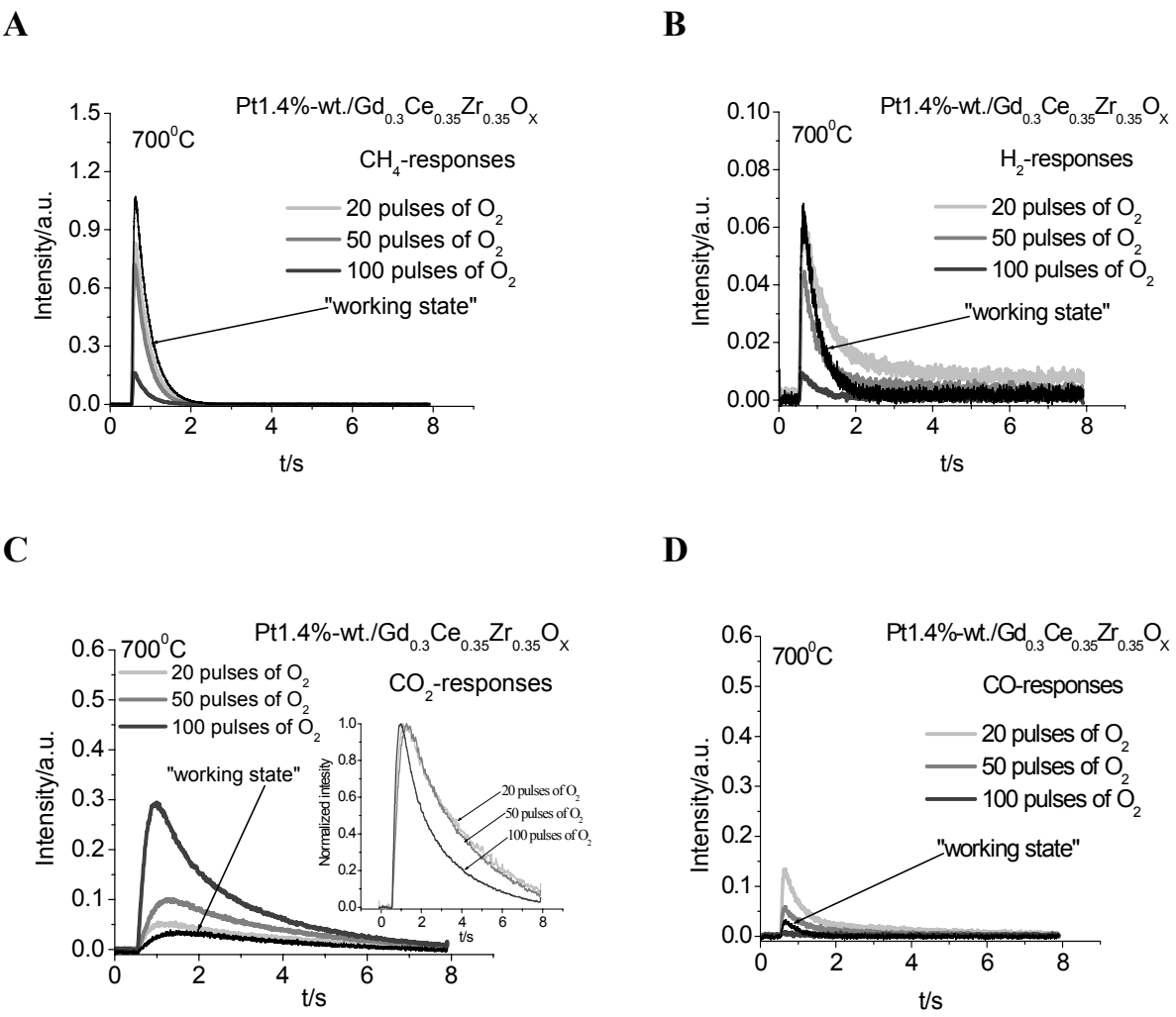

Figure IV.10: *Methane –a, hydrogen-b, carbon dioxide-c, carbon oxide-d pulse responses over a 1.4 wt-% Pt / $Gd_{0.3}Ce_{0.35}Zr_{0.35}O_x/Al_2O_3$ recorded in 1 part oxygen- 2 parts methane pump-probe TAP experiment at 700°C after 20-100 oxygen pre-pulses and "working state".*

From these results, the following statements can be formulated:

- At variance with the previous Pr doped catalyst, significant pulse responses are recorded for all expected products including carbon monoxide. This finding confirms that

the formation of carbon monoxide proceeds on this catalyst much more rapidly than for the Pr-doped sample.

- By comparing the shape of pulse responses for carbon monoxide and carbon dioxide, it comes clearly that the CO response is a sharp signal, which develops as soon as methane is pulsed, without significant tailing, while the CO_2 one develops more slowly and presents a significant tailing. As such, CO appears unambiguously as a primary product, while CO_2 would be more a secondary one, even if some contribution of a primary route cannot be excluded.

- It is remarkable that the formation of hydrogen and carbon monoxide seems to proceed almost simultaneously. Obviously, the methane decomposition does not lead to the accumulation of significant amounts of carbonaceous species on the surface of this catalyst. Accounting for the features revealed by TPD experiments, it seems likely that the fast conversion of carbonaceous ad-species to carbon monoxide for this case of the Gd-doped system relates to the action of the weakly bound oxygen species.

- The influence of the oxidation state on the performance (as a function of the number of pre-pulses of oxygen) reveals a complex behavior: the formation of hydrogen and carbon monoxide is favored by a slightly more oxidized state (after 20 O_2 pre-pulses) than the "working" state. Oxidizing more the surface (50 oxygen pre-pulses) leads however to a significant decline in the formation of selective products paralleled with a strong rise in activity. Submitting 100 oxygen pre-pulses finally leads to an almost complete conversion, but at practically zero selectivity to synthesis gas. In parallel and logically, observing the height normalized carbon dioxide responses shows a significantly faster formation of carbon dioxide under these conditions, implying a different reaction scheme.

The cause for this change in the reaction scheme could in fact be related to an increase in the oxygen coverage on the Pt surface itself, due to an inhibition of the usual back-spillover allowing uptake of excess oxygen from the Pt surface. This indirect effect could be related to the accumulation of surface ad-species (carbonate-like) on the support and the limited bulk oxygen mobility of the Gd doped support, which would lead to a saturation (over-oxidation) of near-surface regions.

IV.2.4. Effect of the time offset between oxygen and methane pulses

Experiments with different time lag between the oxygen and the methane pulses were performed to vary the time span available for surface processes, also modifying the oxygen coverage on the Pt surface. Based on the above presented results it is assumed that the selectivity to synthesis gas is strongly influenced by the extent that spillover processes, onward and backward, can proceed and therefore modify the oxygen coverage on the Pt surface. As however the spillover seems to proceed very rapidly when the catalyst is in the "working state", it was required to inject additional oxygen in order to decrease the spillover rate by increasing the oxygen activity on the support surface until the selectivity to synthesis gas started to decline. In the case of the Pr doped catalyst 5 oxygen pre-pulses were used, while for the Gd doped system 75 pre-pulses were applied.

The impact of delay between O_2 and CH_4 pulses has been studied for both catalysts using time lags of 0.1, 0.5 and 1s. Figure IV.11 and Figure IV.12 allow comparing the selectivity to the products constituting synthesis gas for both catalysts as a function of the oxygen and methane pulses offset.

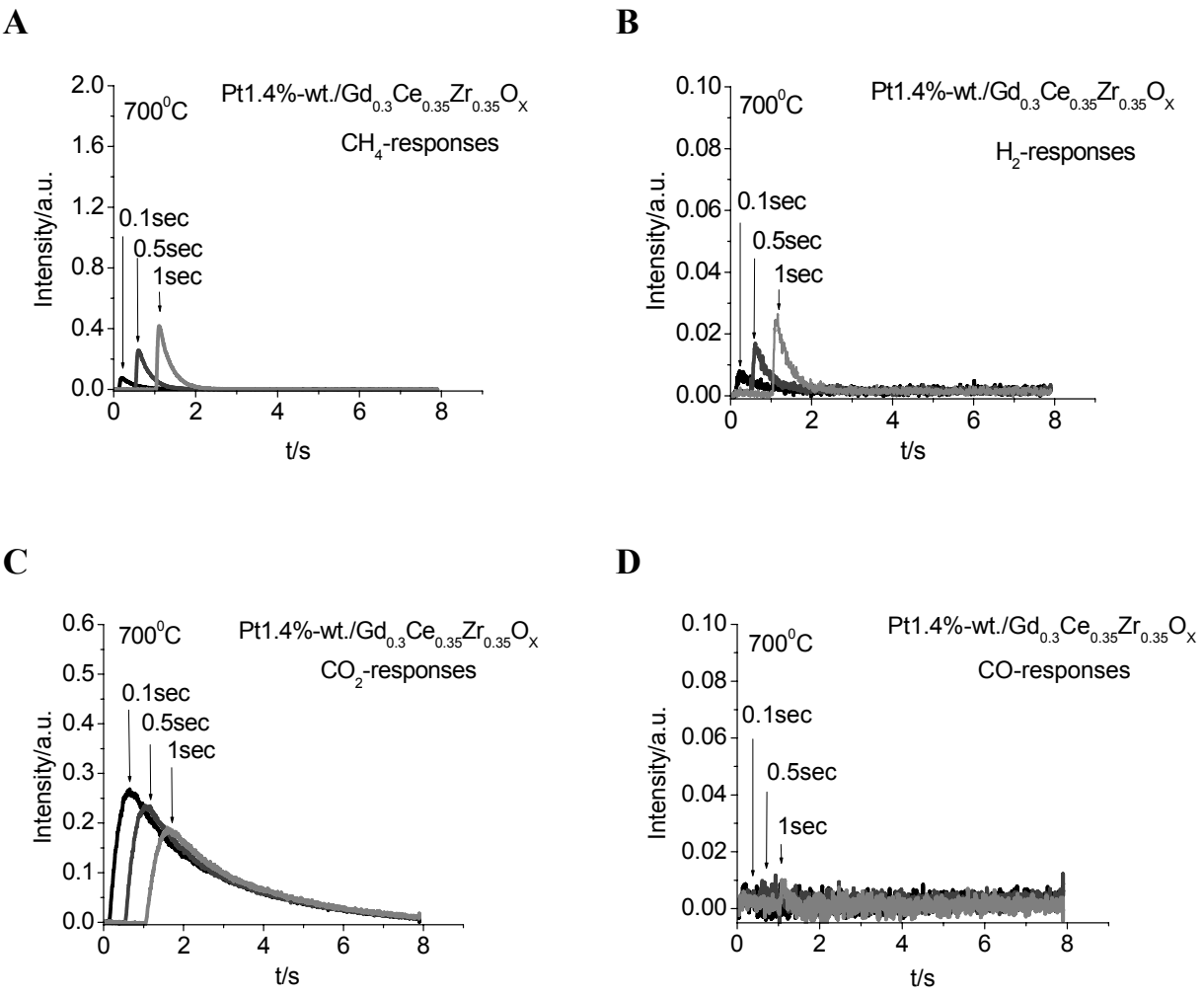

Figure IV.11: *Methane –a, hydrogen-b, carbon dioxide-c, carbon oxide-d pulse responses over a 1.4 wt-% Pt / $Gd_{0.3}Ce_{0.35}Zr_{0.35}O_x/Al_2O_3$ recorded in 1 part oxygen- 2 parts methane pump-probe TAP experiment at 700°C after 75 oxygen pre-pulses.*

As can be seen in Figure IV.11, the selectivity for Gd doped catalyst is very sensitive towards the time lag between the pulses as a short time span considerably decreases selectivity towards syngas at the benefit of carbon dioxide. In contrast, only a relatively small change in selectivity is observed for the case of the Pr doped catalyst (Figure IV.12).

On the basis of this observation, it could be proposed that the Pr-doped catalyst is more stable at given process conditions, most likely as the large bulk oxygen mobility of this material allows to store excess oxygen which might "poison" the Pt surface during oxygen concentration peaks. In turn, the sensitivity of Gd-doped catalyst to oxygen concentration (for short time offset)

could be related to the existence of a pool of short-lived oxygen species close to the Pt surface, able to react with methane decomposition adspecies, rapidly after its injection. As proposed before, the limited oxygen mobility in the Gd doped support lattice would not permit to decrease or eliminate this pool of highly reactive oxygen around the Pt surface.

Furthermore, it is interesting to note that in the case of the Pr doped sample, similar differences as for the Gd-doped one are revealed between the shape of the carbon monoxide (sharp) and carbon dioxide (wide) responses. This demonstrates that as for the Gd doped catalyst carbon monoxide appears as a primary product while carbon dioxide would be essentially a secondary product.

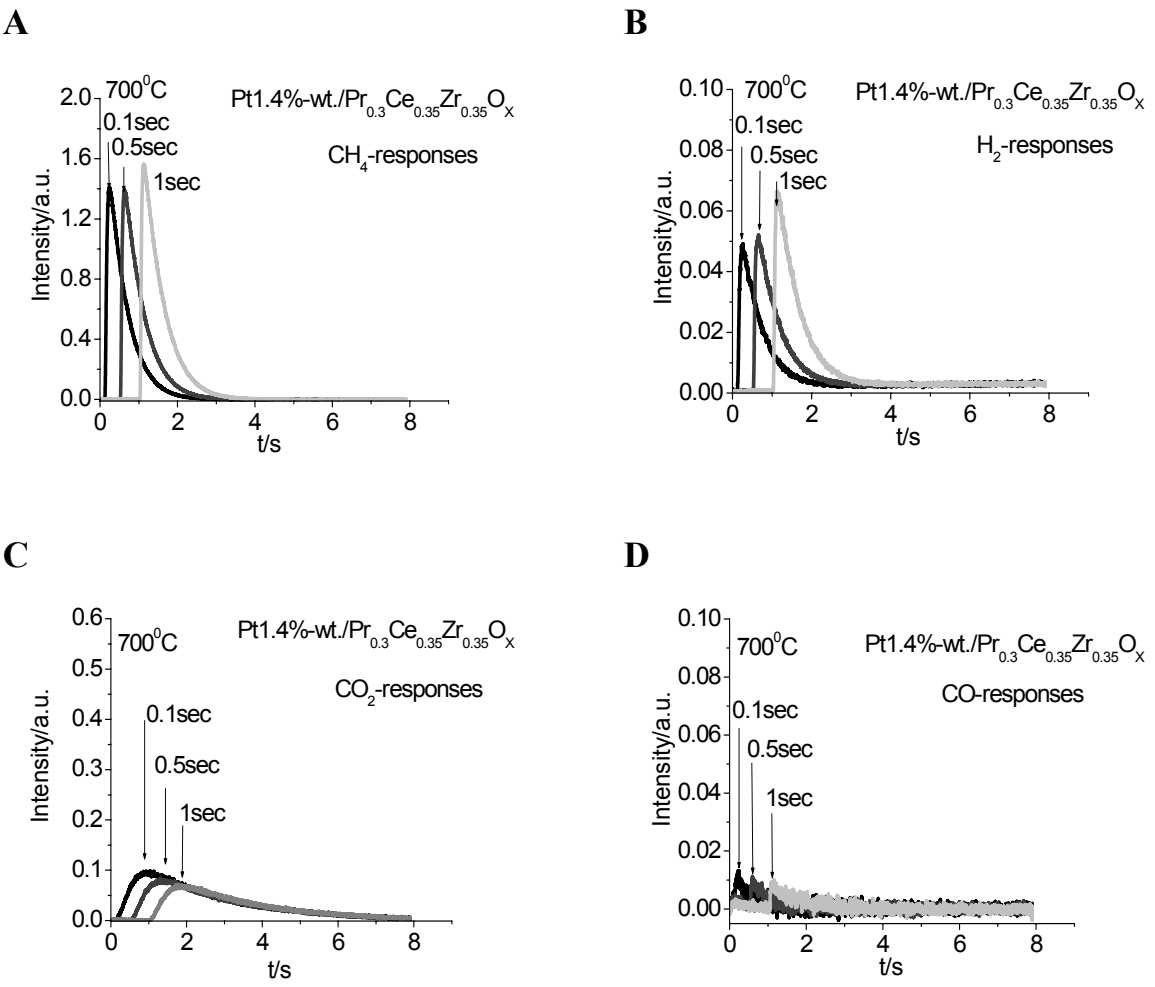

Figure IV.12: *Methane –a, hydrogen-b, carbon dioxide-c, carbon oxide-d pulse responses over a 1.4 wt-% Pt / $Pr_{0.3}Ce_{0.35}Zr_{0.35}O_x/Al_2O_3$ recorded in 1 part oxygen- 2 parts methane pump-probe TAP experiment at 700°C after 5 oxygen pre-pulses.*

Main mechanistic features summary.

Assembling all the information outlined above, it is obvious that the interplay between the oxygen spillover between Pt and the active support and the oxygen mobility in the lattice are crucial for the efficiency of the catalyst.

As hydrogen is rapidly formed in all cases, it can be considered as a primary product originating from a very rapid dissociation of methane on the Pt surface and not requiring any presence of oxygen.

In the case of the Gd-doped catalyst, the presence of a moderate quantity of oxygen on the Pt surface is highly beneficial to achieve a rapid formation of carbon monoxide (which for both catalysts appears as a primary product). On the other hand, both hydrogen and carbon monoxide are readily oxidized into secondary products (water and carbon dioxide, respectively) when a too high oxygen coverage is attained.

The oxygen mobility in the support lattice seems to control the oxygen surface coverage on Pt by storing or not the excess of oxygen coming from the gas phase in the bulk of the support. Here, Pr doped ceria-zirconia is shown to store more efficiently these excess of oxygen than the Gd doped system.

Thus, the ideal system would offer a high mobility of oxygen in the lattice but with a restricted pool of weakly bound oxygen for favoring the selective oxidation of CH_x species into carbon monoxide.

IV.3. Relaxation experiments

For gaining more information on the steady state of the catalytic surface at different partial pressures of components, relaxation experiments have been carried out at atmospheric pressure by admitting abruptly the reacting CPOM mixture over a pre-oxidized sample and observing the establishment of the steady state. Figures IV.13 - IV.14 report typical results of such experiments at 650^{o}C and contact time 15 ms. Smaller contact time did not give significant changes in the observed relaxation curves.

Relaxation experiments at atmospheric pressure were carried out in the quartz reactors of small volume as described in Chapter II. After oxygen pre-treatment the reactor was purged by helium flow (control by zero line on the oxygen detector), then He flow was replaced abruptly (by means of a 4-ways switch valve) by the reaction feed of desirable composition. The gas hold-up related to tubing and reactor (charged with a single channel monolith) void-volume for a flow rate of 30 l/h was evaluated to 2 – 4s.

As can be seen in Figure IV.13, the steady-state regime was established after relatively long (up to 600s) relaxation times for CO and H_2 concentrations, including a marked maximum at around 100 s, while the CO_2 concentration leveled off more rapidly, after around 100 s on stream.

By observing in more details the relaxation curves for the tested systems, it comes that for all gases (reactants and products) the steady state establishes slightly earlier for the Pr-doped catalyst as compared to the Gd-doped one, which is in line with a higher oxygen storage capacity and a faster diffusion within the mixed oxide, as revealed by the TAP experiments.

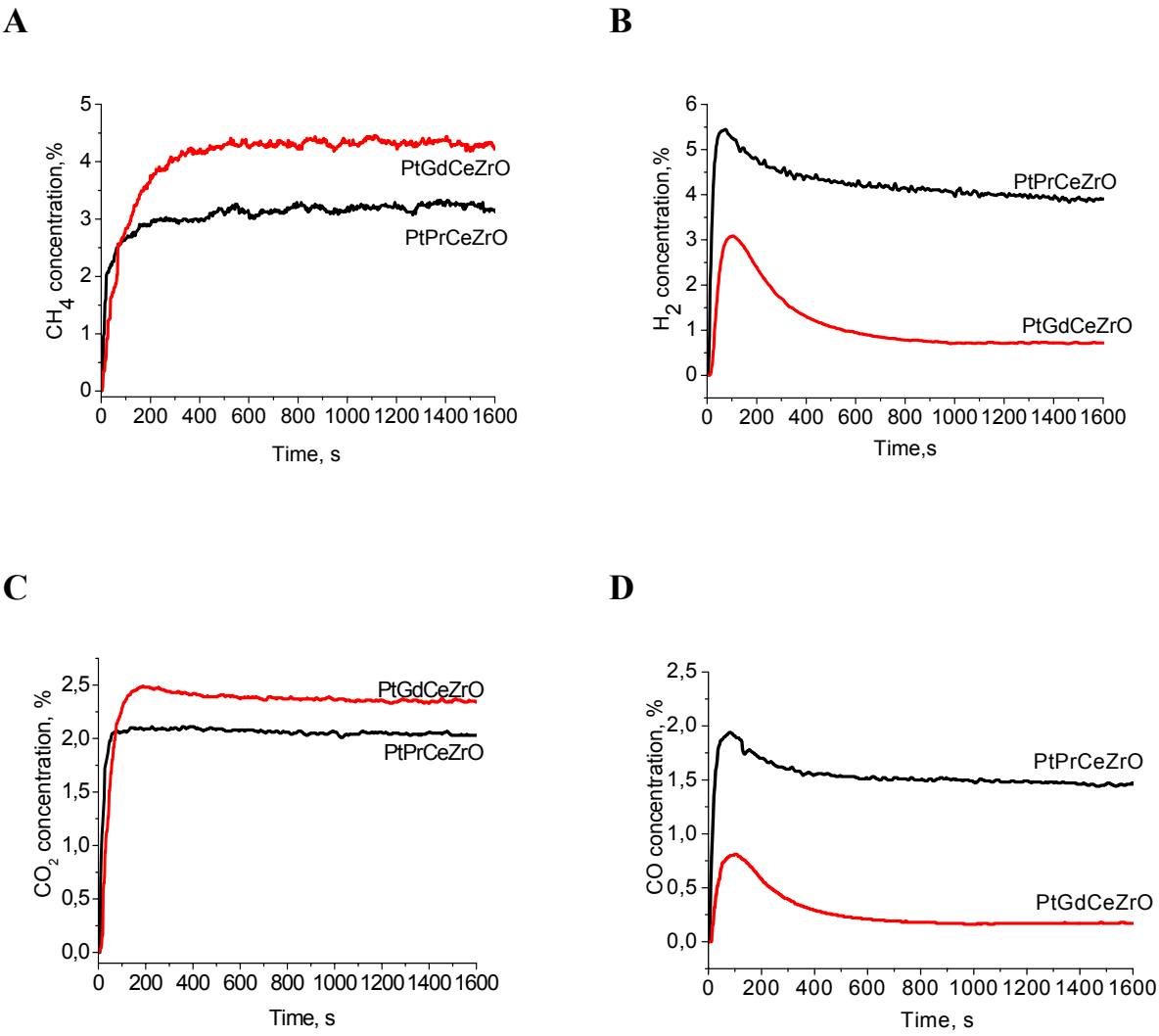

Figure IV.13: *Dynamic change of concentrations at initial moment of the CPOM reaction. Contact time 15 ms, 650°C, initial feed: 7%CH4 + 3,5%O (N_2 – balance).*

Figure IV.14 focuses on the initial dynamics (from 0 to 50 s) of the transient profiles. The following features can be outlined:

- Methane (Figure IV.14A) appears in the gas phase immediately after the switch for both samples, but at a slower rate with the Gd-doped system. This indicates a stronger interaction with the Pt surface, i.e. a larger accumulation of CH_x fragments.

This stronger interaction of methane with the preoxidized surface for Gd-doped system was also revealed in the TAP experiments (very small response of methane after 100 oxygen pulses over "working" surface (Figure IV.10A) as compared to a larger response for the Pr-doped system in Figure IV.9A).

- CO and H_2 (Figures IV.14B and D) appear in the gas phase simultaneously with the methane release for the Pr-doped system (after about 2 s) but with a delay of about 10 s for the Gd-doped sample. In turn, despite the limited resolution of the curves, CO_2 is released in the gas phase after about 6 s for both systems, though at a much slower rate for the Gd-doped system.

This observation confirms that the initial oxidation processes for a pre-oxidized surface are the selective oxidation of CH_x on Pt phase into CO and possibly the oxidation/decomposition of surface carbonaceaous adspecies (carbonates and/or formates on the mixed oxide surface) by weakly bonded oxygen. However, for the case of the Gd-doped system, the build-up of a larger pool of these active oxygen species due to a slower diffusion to the bulk delays the formation of the selective syngas products (H_2 and CO).

Again these statements are in line with the TAP observations.

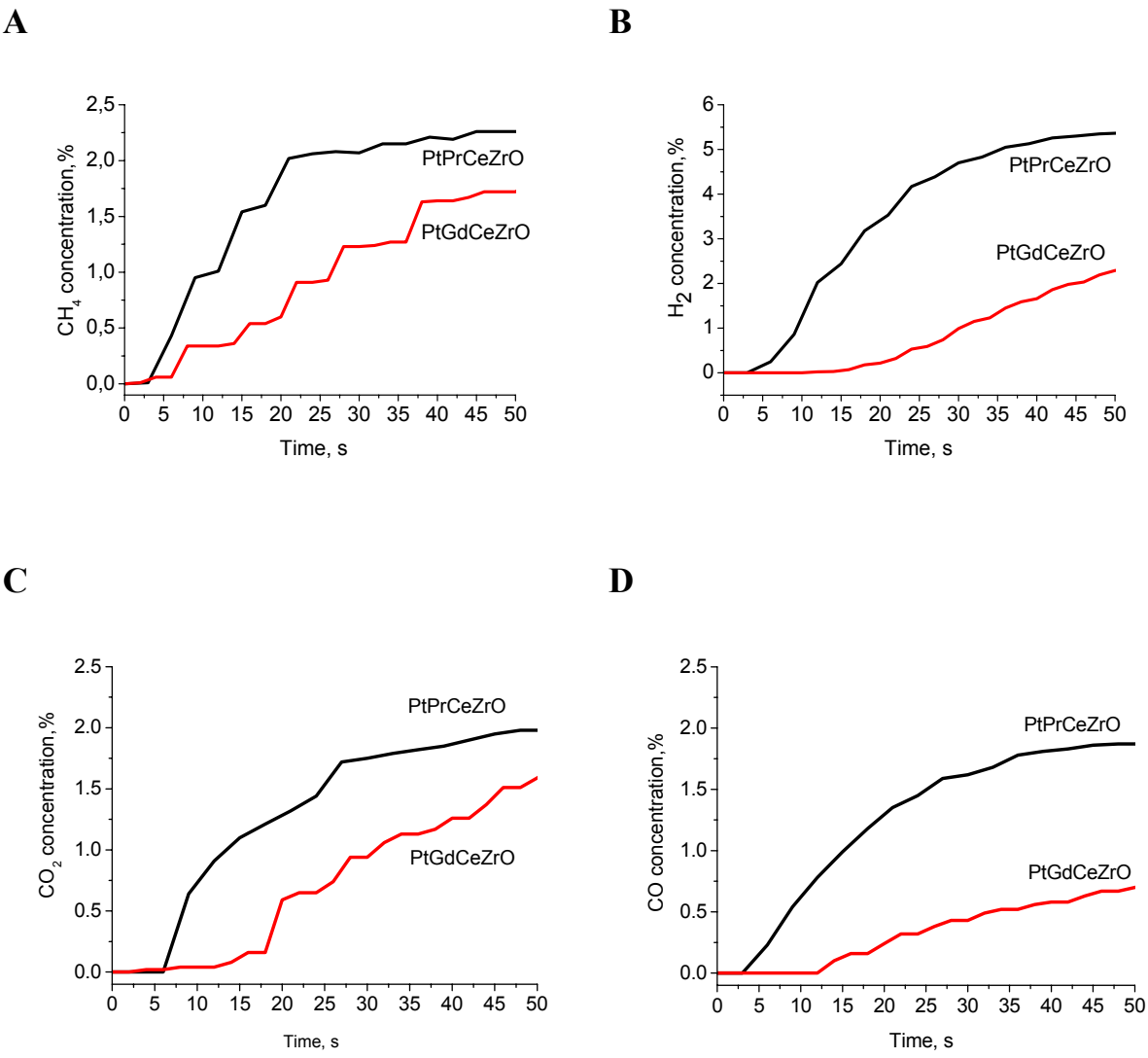

Figure IV.14: *Dynamic change of concentrations at initial moment of the CPOM reaction. Contact time 15ms, 650°C, initial feed: 7%CH4 + 3,5%O (N_2 – balance).*

IV.4. Conclusions

The impact of the oxidation state of the tested catalysts differs as a function of the dopant promoting the ceria/zirconia solid solution supporting Pt as active metal.

In the case of Pr as dopant, a minimum selectivity is preserved in all studied cases using the "working state" of the catalyst as origin. A significant and fast hydrogen release is observed, which only slightly varies as a function of the oxidation state of the sample altered by pre-

injected oxygen. Furthermore, the quasi-co-feeding of oxygen and methane by admitting both reactants at very short time offset does not lead to a total loss of selectivity.

The weakness of the Pr doped sample relates clearly to the relatively slow formation of carbon monoxide as compared to the Gd-based system. This difference might come from a largest accumulation of active oxygen around the Pt particles for the Gd-doped system (due to a slower bulk diffusion) which would facilitate the partial oxidation of the CH_x adspecies formed on the Pt surface. This presence of CH_x at the "working state" is clearly confirmed for the Gd doped sample. As such, the activity of the Pr doped catalyst is clearly lower than that of the Gd doped catalyst, which may be slightly observed in terms of hydrogen release, but which becomes much more obvious when focusing on the formation of carbon monoxide as primary product.

It can be also stressed that the absolute degree of oxidation may differ for the "working state" of both catalysts. This relates to the characteristics of the catalyst itself: due to the constant desorption of oxygen at working temperature, no fixed oxidation state may be adjusted. However, the action of oxygen integrated into the catalyst, i.e., the oxygen introduced by pulse pre-injection achieving a certain degree of sample oxidation should be clearly differentiated from the action of oxygen co-injected with methane or at a very short time offset. This latter remark is well illustrated for the case of the Gd doped sample and confirms well the unique features revealed by the TAP technique.

Furthermore, it needs to be reminded that the specificities of using a channel substrate in a TAP experiment might also impact on the results. By using a catalytic zone expanded over several millimeters, the oxidation state of the catalyst is deeply altered between the channel entry and exit. Given the observed higher sensibility of the Gd-doped catalyst to the oxidation state, this monolithic catalyst could be more affected by the oxygen concentration profile typical for the TAP technique. In order to account for this specificity and to complete the pool of information gained during this mechanistic study, ongoing work focuses now on exploring performances of thinner catalytic zones in the absence of a structural support.

However, the deep agreement and complementarity between TAP experiments carried out at low pressure and kinetic relaxation analysis carried out at atmospheric pressure demonstrate the interest and efficiency to combine these methods for CPOM mechanism study.

CHAPTER V

Kinetic experiments at ambient pressure over structured catalysts based on CeO_2-ZrO_2 mixed oxides

V.1. Context and operating conditions

This chapter presents kinetic data collected at atmospheric pressure for the two selected catalysts Pt/Ce-Zr-(Pr, or Gd)-O) supported on a single channel of corundum monolith. The influence of process parameters, such as flow rate, temperature, different dopant (Pr or Gd), ratio CH_4/O_2, addition of CO_2 to the gas feed and feed preheating, on activity and selectivity of catalysts were investigated. Pt-free systems (Ce-Zr mixed oxide coated on corundum substrate) were studied as well to highlight the crucial role of Pt both for the steam and dry reforming in the oxygen lean zone (closed to reactor outlet) but also for the oxidation of the selective primary products in the presence of oxygen (close to reactor inlet). From this point of view, some economical and catalytic benefits of combining the Pt and the structured substrate will be proposed.

The flow set-up (IRCELYON) described in Chapter II was used in the present study. The catalytic partial oxidation of methane and the dry reforming reaction was carried out in a plug-flow quartz reactor with 8 mm inner diameter. The void space between the catalyst channel and the reactor walls was filled with an α-Al_2O_3 fiber mat to force the reactant flow through the inner void of the catalytic channel and avoid the gas stream contact with the external monolith surface. Thus, approximately half of the total catalyst quantity deposited on the substrate is contacted by the reacting flow. As such the results characteristic of the inner part of a single channel can be straightforwardly used for modeling of the full sized monolith performance.

The channel wall temperature was measured at the outside surface as this approach avoids flow perturbation in the catalytic zone and a representative temperature reading is ensured by the external thermal insulation achieved with the ceramic fiber material. Temperatures in the inlet and outlet sections of the single monolithic channel were measured with a thermocouple and recorded during reaction. Additionally, a displaceable thermocouple located in a well parallel attached to one triangle side along the channel allowed measuring the temperature profile of channel during the CPOM testing as well. Throughout the experiments the oven temperature was varied in the range of 700 – 850°C. The catalyst performance was studied at different oxidation states (as adjusted by oxidizing pretreatment or equilibration by a prior reaction run).

Pretreatments of the catalyst were carried out in situ at 800°C for 1h in a flow of 20% of O_2 and 80% of N_2. Alternatively, the catalyst was operated at the reaction temperature with the feed stream until reaching the steady state. Then, the reaction mixture (6,6% CH_4, 3,3% O_2, N_2 - balance) was fed with a flow rate in the range of 100 – 1400 ml/min, i.e. a contact time of 1 – 15 ms estimated using only the channel walls volume.

Given the exothermic character of the CPOM, it was not possible to achieve isothermal conditions over the catalytic zone. However, temperature spikes were absent and typical axial temperature profiles reported in the following indicated for the catalytic zone a steady temperature rise along the flow direction. Blank experiments verified that homogeneous reactions did not occur under the studied conditions. The reactant and product compositions were analyzed by micro-GC as described in Chapter II.

The preparation and dimension of the studied structured samples Pt/PrCeZrO and Pt/GdCeZrO are described in Chapter II.

V.2. Effects of dopants on steady-state kinetic performances

The present work focused on the effects of the two dopants, Pr and Gd of the ceria-zirconia mixed oxide on the catalyst CPOM properties carried out at steady state. Temperature profiles and the gas phase temperature were measured for both catalysts (Figure V.1). From the inlet section of the single monolith to the outlet, the temperature profiles indicate an increase of the catalyst temperature. This indicates that the exothermic oxidation reactions occurred along the reactor with a net heat release.

For the catalyst doped by Pr (Figure V.1A) relatively flatter temperature profile is obtained with a T difference between the inlet and outlet of 60°C, as compared with the Gd doped system giving a larger temperature gradient of about 70°C.

It was checked also that the reaction rates were not limited by thermodynamics from the Arrhenius behavior of reaction rates. Therefore the temperature dependence in the present and further chapters will be presented as a function of the outlet temperature.

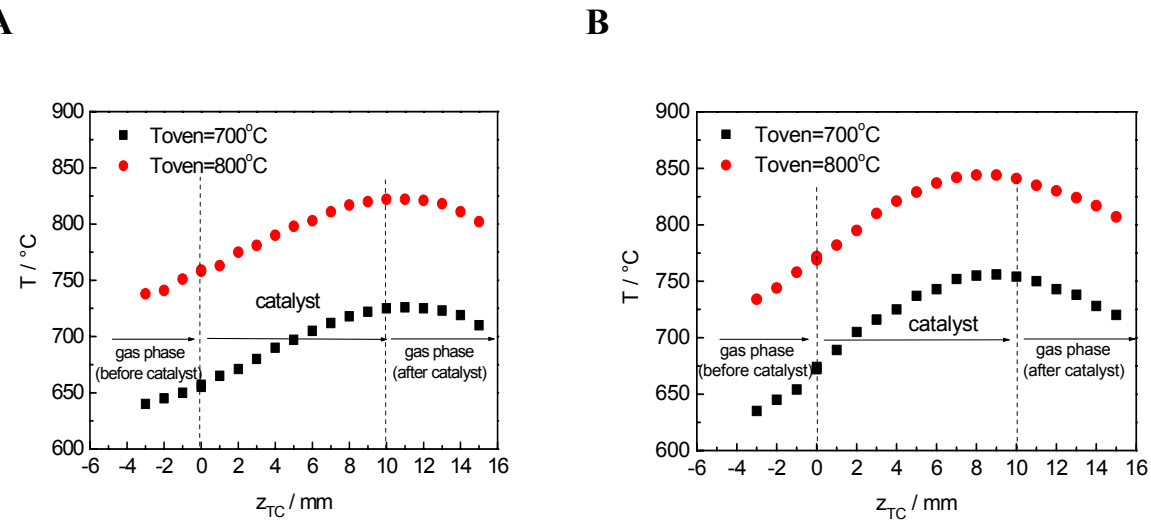

Figure V.1: *Temperature profile of 1.4-wt.% $Pt/Pr_{0.3}Ce_{0.35}Zr_{0.35}O_x$ channel (A) and 1.4-wt.% $Pt/Gd_{0.3}Ce_{0.35}Zr_{0.35}O_x$ channel (B). The flow rate – 750 ml/min, channel length – 10mm. Composition feed – 7%CH_4 + 3.5%O_2 (N_2 – balance).*

The temperature dependence of methane and oxygen conversions along with CO and H_2 selectivity is shown in Figure V.2A,B for the two Pr or Gd doped catalysts (at a feed rate of 750 ml/min). The conversion of reactants especially for methane varies only weakly with temperature for both catalysts. It should be stressed, that oxygen conversions are far from complete at the studied experimental conditions; thus a simple oxygen depletion (i.e., a mass transfer limitation) cannot explain the stagnant methane conversion. More in details, oxygen conversions for the catalyst with Pr are higher than those observed with the Gd doped one.

In contrast, the CO and to a lower extent the H_2 selectivities increase with temperature. Hydrogen selectivity remains rather limited under the present experimental conditions and little dependant on the dopant nature, while CO selectivity is clearly higher for the Pr doped catalyst.

According to O_2-TPD data, the presence of weakly bound oxygen species for the Gd doped catalyst could account for the lower CO selectivity of that catalytic system, assuming that weakly bound oxygen could very rapidly oxidize the initially formed CO. In fact, a comparable trend is observed for the H_2 selectivity and it seems reasonable to assume that hydrogen is even more readily oxidized to water, in line with the TAP study showing that the hydrogen formation is fast under vacuum conditions with limited oxygen coverage.

A **B**

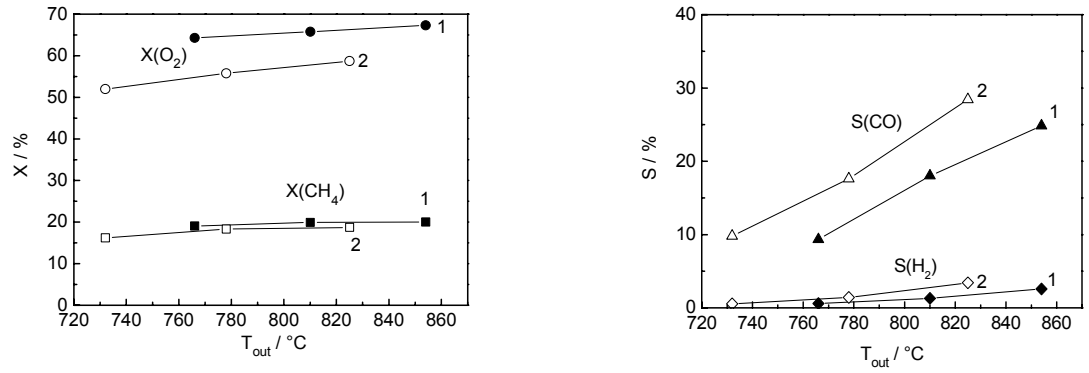

Figure V.2: *Temperature dependence of methane, oxygen conversion (A) and CO, H_2 selectivities (B) for 1.4%wt.-Pt/$Gd_{0.3}Ce_{0.35}Zr_{0.35}O_x$ channel (1) and 1.4%wt.-Pt/$Pr_{0.3}Ce_{0.35}Zr_{0.35}O_x$ channel (2). Composition feed - 7%CH_4+3.5%O_2 in N_2.Channel length - 10 mm. Contact time 1.9 ms (750 ml/min).*

It was decided to carry further on with a more detailed study using the Pr doped catalyst, as this system seems more selective towards syngas formation.

V.3. Characterization of catalysts

Our initial plan was to thoroughly characterize the selected CPOM systems structured on single channel monolith, before and after kinetic testing. However, most of the conventional characterization techniques being not adapted to the monolith support, it was decided to prepare a powder form of these selected formulations, to test them under similar conditions as the structured forms and to characterize them before and after testing, after having validated the procedure. These powder forms of the selected systems will be referred to as "reference powder systems".

V.3.1. Preparation of reference powder systems

The structured support was replaced by α-Al_2O_3 particles sieved in the size range of 100-200 microns and further on impregnated with the same active phase formula as for the selected structured systems. Additional catalytic experiments were conducted with this powder material under the same operating conditions as for the monolith based systems.

After chemical analysis, this reference powder catalyst was found to present the same chemical composition, but with a higher fraction of active phase with respect to the α-alumina concentration: 50 versus 10wt.% on α-Al_2O_3 particles and on structured corundum, respectively. However, the reference powder systems performed essentially in the same way as the structured ones and therefore were considered as a suitable system for advanced characterization.

V.3.2. BET analysis

The BET surface areas of Pt/PrCeZrO and Pt/GdCeZrO supported on the α-Al_2O_3 particles after calcination at 900°C and α-Al_2O_3 annealed at 1300°C are listed in Table V.1. The α-Al_2O_3 support has a surface area of 3 m^2/g, while the 1.4wt.%-Pt/$Pr_{0.3}Ce_{0.35}Zr_{0.35}O_x$/α-$Al_2O_3$ reference powder catalyst has a surface area of 21 m^2/g, which is one of the highest values among all the powder catalyst samples. Besides this, the surface area of the reference systems decreases from 21 m^2/g to 15 m^2/g by changing from Pr to Gd as dopant.

Table V.1: *BET surface area of the α-Al_2O_3 and the Pt/PrCeZrO and Pt/GdCeZrO supported on the α-Al_2O_3 powder catalyst*

Sample	BET surface area (m^2/g)
Pt/$Pr_{0.3}Ce_{0.35}Zr_{0.35}O_x$/α-$Al_2O_3$	21.1[a]
Pt/$Gd_{0.3}Ce_{0.35}Zr_{0.35}O_x$/α-$Al_2O_3$	15.4[a]
α-Al_2O_3	3

[a] Relative to the total weight (alumina + coating)

V.3.3. XRD analysis

The XRD patterns of the reference samples doped by Gd or Pr before and after CPOM reaction are presented in Figure V.3. No significant differences can be observed between the two catalysts, as well as no major evolution of the patterns can be detected after the reaction.

The cerium-zirconium support, with a ratio Ce:Zr=1, is present as a pure cubic phase for all samples. Broad diffraction peaks were detected in all cases, indicating the presence of small oxide particles. For all cases reflexes corresponding to platinum in cubic phase can be observed. The relatively weak and broad Pt related reflexes indicate that the respective supported nano-particles are reasonably small with a size close to 4nm, being the lower size detectable by XRD.

The pattern corresponding to the sample doped by Pr after reaction shows some additional reflexes, because of some SiC particles which were not completely removed from the spent sample after having been added for diluting the catalyst bed.

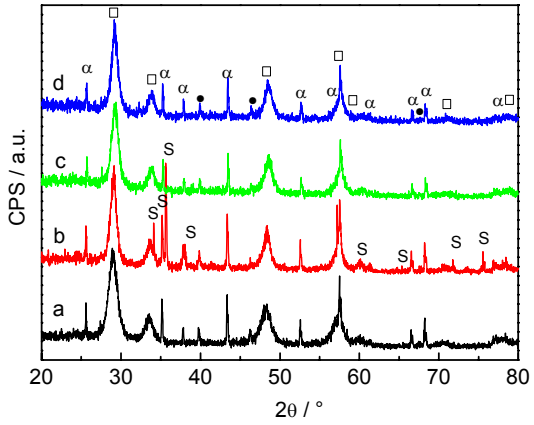

Figure V.3: *XRD patterns of catalysts a, b - $Pt/Pr_{0.3}Ce_{0.35}Zr_{0.35}O_x/\alpha\text{-}Al_2O_3$ and c, d - $Pt/Gd_{0.3}Ce_{0.35}Zr_{0.35}O_x/\alpha\text{-}Al_2O_3$, where is a, c –before reaction CPOM, b, d after reaction (α-corundum, α - Al_2O_3;* □ - cubic phase; • - *Pt; S – SiC traces).*

V.3.4. Raman spectroscopy

Figure V.4 shows the Raman spectra of the reference catalysts with the same fraction of Ce and Zr doped by Pr. Two samples are investigated, one before and another one after the CPOM reaction at 800°C. Both spectra of the fresh and spent catalyst after reaction reveal the presence of a strong band at around 470 cm^{-1}, which is assigned to the F_{2g} Raman active mode of a material with cubic fluorite-type structure (space group *Fm3m*). The band is irrespective of the state of the catalyst (before and after reaction). According to literature, a band at ca. 468 cm^{-1} is assigned to first order anion-lattice associated vibration [196], whose characteristic frequency displays low sensitivity to changes in Ce/Zr composition near the unity [197]. However, broad bands at 203 and 273 cm^{-1} are detected in the Raman spectrum of both samples of catalyst, which is characteristic of tetragonal zirconia phase (space group $P4_{2/nmc}$) [198,199]. Kim et. al. [200] have observed two strong bands at 263 and 148 cm^{-1} in the pure tetragonal ZrO_2. However, in our case the shift in frequencies is more probably related to defect sites, i.e. oxygen vacancies, in the mixed oxides. Supposing the presence of tetragonal ZrO_2 is not in agreement with XRD data,

where such a phase is not observed. The sample state clearly evolves during reaction and the broad bands below 300 cm^{-1} are more intense for the catalyst after reaction. This could be probably related to a slight demixing of the Ce/Zr compound close to the surface once a reducing atmosphere would impact more severely on ceria than zirconia. On the other hand, an additional creation of oxygen vacancies during reaction is highly probable, which would also explain the observed frequency shift. A band can also be observed at 590 cm^{-1} due to the LO mode of CeO_2, which appears because of relaxation symmetry rules [201].

Due to the broadness and overlapping of the bands of ZrO_2 and CeO_2, it is difficult to say whether there is a co-presence of a tetragonal and a cubic phase and the absence of such a phase in XRD makes an explanation of the observed changes by oxygen vacancy creation more probable.

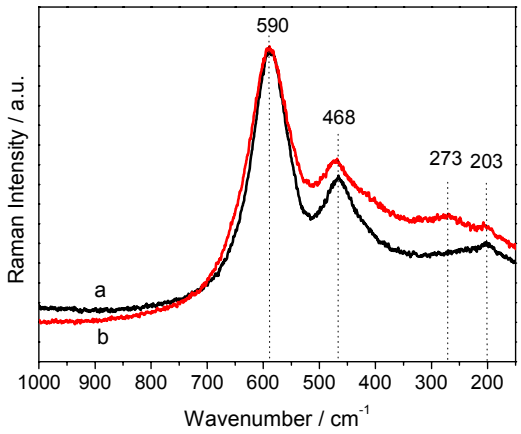

Figure V.4: *Raman spectra of the fresh 1.4-wt.% Pt/$Pr_{0.3}Ce_{0.35}Zr_{0.35}O_x$/α-$Al_2O$ catalyst (a) and a sample after reaction at 800°C (b).*

V.3.5. XPS analysis

XPS analysis was carried out for the reference samples, PtPrCeZrO/α-Al_2O_3 and PtGdCeZrO/α-Al_2O_3, before and after reaction at 800°C. The spectra for each sample do not show appreciable differences before or after reaction.

The analysis of the Pt spectral regions in all samples was complicated by the fact that in addition to the small platinum overall concentration (1.4 %wt.) the Pt 4f peaks (71 and 74 eV)

are masked by the preponderance of the Al 2p one (73eV), while at the same time the only other relatively sensitive Pt peak, Pt 4d, is partially masked by the strong Zr 3p peaks. This is why virtually no platinum was detected in three of the samples; only the gadolinium-based one after high temperature reaction exhibited a small measurable quantity of Pt. Hence, no reliable information on the chemical state of platinum could be obtained.

A quantitative analysis (Table V.2, Table V.3) shows there is more than 50 at.% oxygen in all samples, which is in line with the binding energy values revealing that the three major over-layer elements, praseodymium (gadolinium), cerium and zirconium are mainly in their oxide states. A slight increase (~ 2 at.%) in oxygen is noted after reaction, together with an increase in carbon. This latter observation could be related to the formation of surface carbonates.

Table V.2: *Binding energies of surface elements (eV) referenced to C 1s at 284,6 eV*

Sample	Pt 4f $_{5/2}$	O 1s	C1s	Pr 3d $_{5/2}$	Gd 4d	Ce 3d $_{5/2}$	Zr 3d $_{5/2}$	Al 2p
$Pt/Pr_{0.3}Ce_{0.35}Zr_{0.35}O_x/\alpha\text{-}Al_2O_3$		529.3	284.6	933.4		822.2	181.7	74.2
$Pt/Pr_{0.3}Ce_{0.35}Zr_{0.35}O_x/\alpha\text{-}Al_2O_3$ **After reaction**		529.2	284.6	933.0		822.0	181.5	74.3
$Pt/Gd_{0.3}Ce_{0.35}Zr_{0.35}O_x/\alpha\text{-}Al_2O_3$		529.2	284.6		141.2	822.0	181.5	74.1
$Pt/Gd_{0.3}Ce_{0.35}Zr_{0.35}O_x/\alpha\text{-}Al_2O_3$ **After reaction**	70.6	529.2	284.6		141.0	822.0	181.4	74.2

Table V.3: *Data of quantitative surface analysis (in atomic percentages)*

Sample	Pt	O	C	Pr	Gd	Ce	Zr	Al
$Pt/Pr_{0.3}Ce_{0.35}Zr_{0.35}O_x/\alpha\text{-}Al_2O_3$	nd	51.4	3.1	15.5		10.6	7.4	11.9
$Pt/Pr_{0.3}Ce_{0.35}Zr_{0.35}O_x/\alpha\text{-}Al_2O_3$ **After reaction**	nd	53.7	6.8	12.8		9.7	7.6	9.4
$Pt/Gd_{0.3}Ce_{0.35}Zr_{0.35}O_x/\alpha\text{-}Al_2O_3$	nd	56.6	7.7		6.2	9.3	6.6	13.7
$Pt/Gd_{0.3}Ce_{0.35}Zr_{0.35}O_x/\alpha\text{-}Al_2O_3$ **After reaction**	0.05	58.4	8.1		5.9	10.7	7.2	9.6

nd: not determined due to low concentration and peaks overlaps (see text above)

In order to monitor the variation of the atomic surface composition, the fraction of Pr (Gd), Ce and Zr over the sum of these elements were calculated before and after reaction (Table V.4).

For the praseodymium-based sample, the fraction of cerium is close to its nominal ratio in the mixed oxide bulk in both cases before and after reaction. On the other hand the surface seems to be slightly enriched in praseodymium and depleted in zirconium, by comparing surface and nominal (bulk) composition. After reaction this is still the case, with however, a small decrease in the praseodymium content and a corresponding increase in the zirconium content. Nevertheless, the surface composition is still well away from the nominal bulk ratio. In the case of the gadolinium-based sample, it is the zirconium content that is the closest to the nominal bulk ratio, while, the surface is enriched in cerium and depleted in gadolinium. While the reaction does not affect the zirconium content, the overall cerium ratio decreases slightly and is offset by a corresponding increase in gadolinium concentration.

Table V.4: *Atomic ratios of the different elements compared to the nominal ratios of Pr or Gd / Ce / Zr = 0.30 / 0.35 / 0.35*

Sample	Pr / Ce / Zr	Gd / Ce / Zr
$Pt/Pr_{0.3}Ce_{0.35}Zr_{0.35}O_x/\alpha\text{-}Al_2O_3$	0.46 / 0.32 / 0.22	
$Pt/Pr_{0.3}Ce_{0.35}Zr_{0.35}O_x/\alpha\text{-}Al_2O_3$ **after reaction**	0.42 / 0.32 / 0.25	
$Pt/Gd_{0.3}Ce_{0.35}Zr_{0.35}O_x/\alpha\text{-}Al_2O_3$		0.28 / 0.42 / 0.30
$Pt/Gd_{0.3}Ce_{0.35}Zr_{0.35}O_x/\alpha\text{-}Al_2O_3$ **after reaction**		0.25 / 0.45 / 0.30

Considering that the overall aluminum content should be more or less constant throughout the used catalyst samples since alumina is the support, the atomic ratios of the different elements to aluminum were calculated (Table V.5). An increase in the atomic concentrations of all the other elements in the surface layer after reaction was noted.

Table V.5: *The atomic ratios of the different elements to aluminium*

Sample	Pt / Al	O / Al	C / Al	Pr / Al	Gd / Al	Ce / Al	Zr / Al
$Pt/Pr_{0.3}Ce_{0.35}Zr_{0.35}O_x/\alpha\text{-}Al_2O_3$		4.33	0.26	1.31		0.9	7.40
$Pt/Pr_{0.3}Ce_{0.35}Zr_{0.35}O_x/\alpha\text{-}Al_2O_3$ **after reaction**		5.71	0.73	1.36		1.03	7.56
$Pt/Gd_{0.3}Ce_{0.35}Zr_{0.35}O_x/\alpha\text{-}Al_2O_3$		4.13	0.56		0.45	0.68	6.57
$Pt/Gd_{0.3}Ce_{0.35}Zr_{0.35}O_x/\alpha\text{-}Al_2O_3$ **after reaction**	0.01	6.07	0.84		0.61	1.11	7.22

According to Shelef et. all [202] the ratio of Ce^{4+} to Ce^{3+} oxides were estimated by using the single Ce 3d photo emission peak at 917eV. Thus the percentage of cerium in the Ce^{4+} state was around 90% in all cases, with a slight increase for both samples after reaction (Table V.5). The latter finding shows indeed that the catalyst sample kept a rather oxidized state during the reaction. Nevertheless, samples were transferred to XPS in air atmosphere and one might suspect re-oxidation at that moment. However, as shown by the O_2-TPD study presented before, such a re-oxidation depends strongly on the temperature and is expected to be slow at room temperature. This is in line the TAP investigation having shown that the oxygen activation on the catalyst was faster than that of methane. On the other hand, this underlines also the importance of investigating the catalyst performance in a rather oxidized state, where the present samples showed distinct differences.

Table V.6: *The percentage of cerium in the Ce^{4+} state to Ce^{3+}*

Sample	Ce^{4+} / Ce^{3+}
$Pt/Pr_{0.3}Ce_{0.35}Zr_{0.35}O_x/\alpha\text{-}Al_2O_3$	0.93
$Pt/Pr_{0.3}Ce_{0.35}Zr_{0.35}O_x/\alpha\text{-}Al_2O_3$ **after reaction**	0.95
$Pt/Gd_{0.3}Ce_{0.35}Zr_{0.35}O_x/\alpha\text{-}Al_2O_3$	0.89
$Pt/Gd_{0.3}Ce_{0.35}Zr_{0.35}O_x/\alpha\text{-}Al_2O_3$ **after reaction**	0.92

V.3.6. TEM analysis

Figure V.5 presents TEM images of catalysts where Pt was supported on $Pr_{0.3}Ce_{0.35}Zr_{0.35}O_x/\alpha\text{-}Al_2O_3$, $Gd_{0.3}Ce_{0.35}Zr_{0.35}O_x/\alpha\text{-}Al_2O_3$ or bare $\gamma\text{-}Al_2O_3$. The catalysts either doped by Pr or Gd (Figure V.5 A-B) exhibit a higher dispersion and lower agglomeration of the Pt particles than the $Pt/\gamma\text{-}Al_2O_3$ catalyst (Figure V.5 C). The latter observation could relate to the fact that Pt supported on the doped cerium-zirconium oxide is probably kept in a more oxidized state [176], which would at higher temperature inhibit the sintering of metallic particles generally observed on interaction-free supports like alumina.

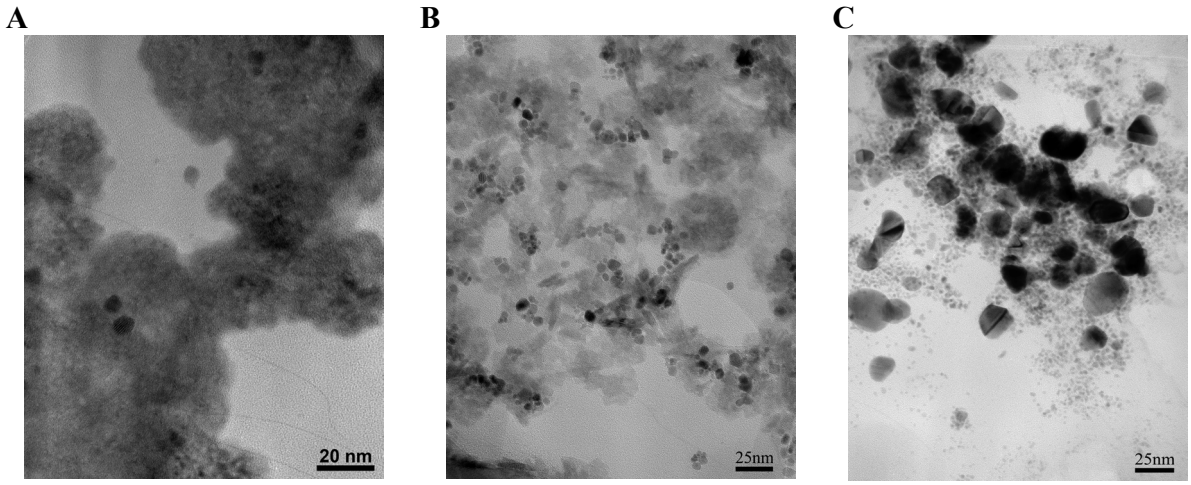

Figure V.5: *TEM images of samples: (A) - $Pt/Pr_{0.3}Ce_{0.35}Zr_{0.35}O_x/\alpha\text{-}Al_2O_3$, (B) - $Pt/Gd_{0.3}Ce_{0.35}Zr_{0.35}O_x/\alpha\text{-}Al_2O_3$ and (C) – $Pt/\gamma\text{-}Al_2O_3$.*

V.4. Influence of gas phase preheating

The target of experiments using the flow installation at atmospheric pressure is to determine the catalyst performance in the kinetic regime and to use it in a mathematical modeling for estimating the kinetic parameters. Experiments were carried out at high flow rate in order to avoid external mass transfer limitations for the fast CPOM reaction. It should be stressed that the external diffusion path length in the monolith channel is comparably large as compared to that in inter particle voids of a conventional fixed-bed reactor. However, high flow rates lead to a strong convective heat removal from the catalytic zone by the diluted reactant mixture, as long as the reactant flow is not sufficiently pre-heated. This is observable as the temperature of

the catalyst inlet section decreases significantly with increasing feed flow rate when contacting an initially cold gas mixture.

The impact of feed gas preheating well before the inlet part of the catalyst was investigated by installing an additional preheating oven immediately before the reactor oven. As can be seen in Figure V.6, in the absence of preheating (Figure V.6 A) the temperature difference between inlet and outlet of the catalytic channel was about 70°C. With preheating kept at 725°C, a more flat temperature profile was observed (Figure V.6 B) and the temperature gradient between inlet and outlet decreased to 30-25°C for a reactant flow rate of 750 ml/min and temperature of experiment 700 and 800°C. Thus, the gas phase temperature upstream of the inlet part of the single channel catalyst reached, or was very close to, the desirable temperature of experiment after installing of this additional preheating oven.

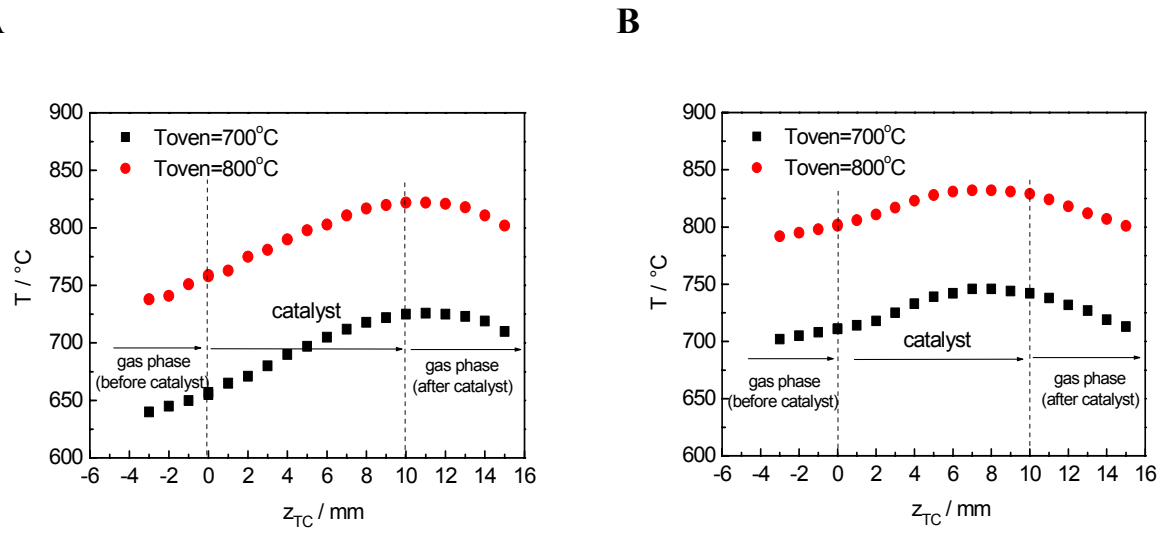

Figure V.6: *Temperature profile of a 1.4-wt.% $Pt/Pr_{0.3}Ce_{0.35}Zr_{0.35}O_x$ channel without preheater (A) and with preheater at T=725°C (B). Flow rate – 750ml/min, channel length – 10mm at 700°C and 800°C. Feed composition - 6.6%CH_4 + 3.3%O_2 (N_2 - balance).*

Although the preheating should not have direct impact on the catalytic action, a change of the observed overall conversion and selectivity is expected with applying more isothermal conditions over the catalytic section.

Changes in conversion and selectivity after applying the additional preheating are presented in Figure V.7.

It should be first noted that only very small amounts of carbon monoxide and hydrogen are formed at 700°C, which makes syngas quantification quite uncertain by micro-GC analysis. For this reason the effect of preheating will not be discussed for that temperature. In turn, at higher temperature (800°C) the selectivity towards syngas products is significantly improved after preheating, while O_2 and CH_4 conversion change only slightly.

Furthermore, for the experiments with preheating, it is important to stress that there is a transient behavior in selectivity right after the stepwise increase of temperature. Clearly CO and H_2 selectivity decline slightly during about 30 min, before leveling off. Given that the element balances are well closed once a steady operation is achieved but that there is a clear deficit in oxygen during the transient, it seems obvious that there is an oxygen take-up by the catalyst during the transient period corresponding to an increased syngas selectivity. Such a transient behavior was not observed for experiments without preheating, probably due to the fact that the catalyst temperature was not homogeneous enough for a clear observation of strongly temperature dependant effects.

TPD data presented in chapter IV (mechanistic study) clearly indicated that the oxygen release from the $Pr_{0.3}Ce_{0.35}Zr_{0.35}O_x$ proceeds essentially in the temperature range between 600 and 800°C and that there is a strong temperature impact on the oxygen uptake in this T range as well. Accordingly, the transient in selectivity above reported strongly confirms of the major role of the oxygen storage capacity for the employed mixed oxide catalyst even at atmospheric pressure operation.

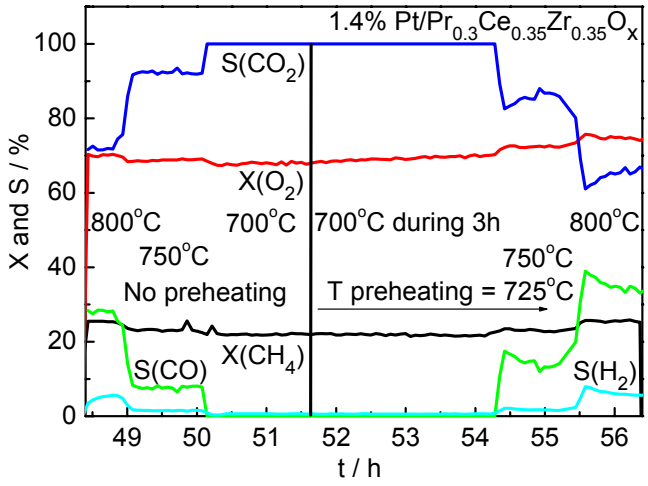

Figure V.7: *Catalytic activity of 1.4-wt.% $Pt/Pr_{0.3}Ce_{0.35}Zr_{0.35}O_x$ channel. Flow rate – 100 ml/min, channel length – 20 mm at different temperatures. Composition feed – 6.6%CH_4 + 3.3%O_2 (N_2 - balance). Temperature of preheating 725°C.*

V.5. Effect of process parameters

The effect of different process parameters (catalyst temperature, contact time, inlet CH_4/O_2 ratio and the effect of CO_2 addition to gas feed) on the catalytic performance (conversion and selectivity) was studied for the single monolith channel coated with the 1.4%$Pt/Pr_{0.3}Ce_{0.35}Zr_{0.35}O_x$ catalyst, as the most efficient system for CPOM.

V.5.1. Effect of temperature and reactant space-time

V.5.1.1. Temperature effects

Catalytic partial oxidation tests were performed with feed streams (CH_4 = 6.6 %, CH_4/O_2 = 2, N_2 to balance) in the temperature range of 700 – 850°C with flow rates varying from 400 ml/min to 1400 ml/min.

Figure V.8 reports the temperature dependence as a function of the outlet temperature of the catalyst, given that the previously presented temperature profiles indicated the highest temperatures towards the channel outlet.

As can be seen, methane and oxygen conversions increase only slightly over the investigated T range. The apparent activation energy for methane conversion rate was evaluated

to approximately 17 kJ mol^{-1}, i.e. a value far too low for the difficult process of methane activation. This indicates therefore that the reaction rates are widely determined by transport phenomena.

However, in the mean time, hydrogen and carbon oxide selectivities vary strongly with catalyst temperature. The formation rate of H_2 and CO thus appears to be determined significantly by the kinetics of catalytic reactions, in contrast to the conversion of methane and oxygen. This seems in so far plausible as the selectivity towards syngas depends essentially on surface processes, logically less or not influenced by the mass transfer limitations, at variance with reactants conversion.

Identical trends were also found by C.R.H. de Smet et al. [42], Heitnes et al. [203] and by Hickman and Schmidt [73] using Pt and Pt/10%Rh gauzes.

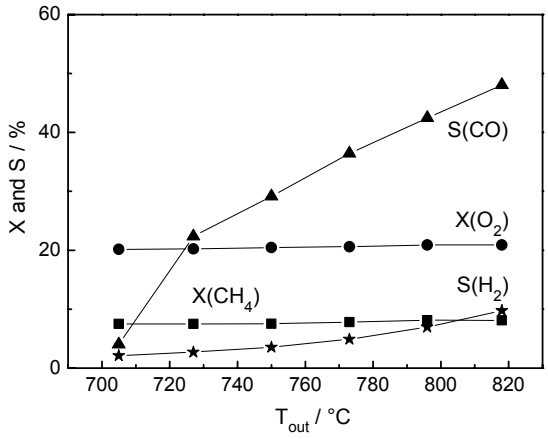

Figure V.8: *Temperature dependence of reactants conversion and CO, H_2 selectivity over 1.4-wt.% $Pt/Pr_{0.3}Ce_{0.35}Zr_{0.35}O_x$ channel. Flow rate – 1200 ml/min, channel length – 10 mm. Composition feed – 6.6%CH_4 + 3.3%O_2 (N_2 - balance).*

V.5.1.2. Space-time effects

The effect of space-time (W/F) on methane and oxygen conversion and on H_2 and CO selectivity was studied by varying the flow rate at constant catalyst weight, as reported in Figure V.9 at 850°C.

As can be seen, both the conversion of CH_4 and O_2 and the CO and H_2 selectivity slowly increase with space-time.

By checking easily that the conversion profiles do not linearly extrapolate to zero at zero W/F value, this clearly confirms that even at very high flow rates such as 600 to 1400 ml/min the presence of external mass transfer limitations is highly probable.

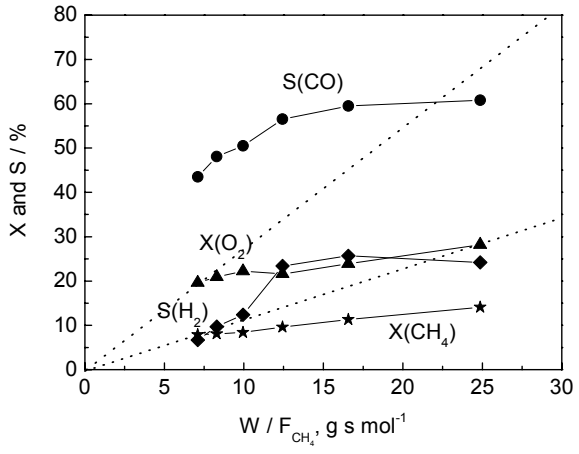

Figure V.9: *Space-time dependence of reactant conversions and CO, H_2 selectivities over 1.4-wt.% Pt/$Pr_{0.3}Ce_{0.35}Zr_{0.35}O_x$ channel. At temperature 850 °C, channel length – 10 mm. Composition feed – 6.6% CH_4 + 3.3% O_2 (N_2 - balance).*

Concerning product selectivities, it could be proposed that hydrogen and carbon oxide are secondary products in the space-time window, which was explored in the present study. This means that catalytic partial oxidation of methane reaction would occur through the indirect mechanism.

In this context it is important to note that the presence of oxygen usually suppresses steam and dry reforming reactions on supported Pt. However, the limited syngas selectivity indicates that a higher fraction of oxygen is converted in total oxidation than which is supplied in the gas phase with a methane to oxygen ratio of 2:1. Furthermore, the molecular mass dependency of the diffusion coefficients (taken Knudsen diffusion as extreme case) explains that methane diffusion is faster than oxygen diffusion. Both elements and the high probability of mass transfer limitations point towards a strong oxygen depletion at the catalytic surface and would explain the discrepency of observing an indirect syngas formation in the presence of oxygen in the gas

phase. This suggests that indeed reforming reactions could occur within pores where oxygen is absent The latter discussion clearly holds for external mass transfer limitations probed by the variation of the gas velocity, but it cannot be excluded that even internal mass transfer limitations could be present as well. On the other hand, internal diffusion limitations might be less probable due to the thin catalyst layer deposited on the monolith substrate given that the effective pore length remains relatively short in the present case.

V.5.2. Influence of CH_4/O_2 feed ratio

The influence of the CH_4/O_2 ratio was investigated by varying the oxygen and methane concentration in the range 1.8 - 3.3 vol.% and 6.6 - 8.2 vol.% respectively, at 1200 ml/min and an oven temperature of 850°C.

As shown in Figure V.10, the conversion of CH_4 decreases slowly by increasing methane-to-oxygen inlet ratio while the oxygen conversion remains practically constant. The CO and H_2 selectivity increases slightly by increasing methane-to-oxygen inlet ratio. Note at this stage that methane and oxygen conversion should have changed more significantly under kinetic control, unless zero order for both reactants.

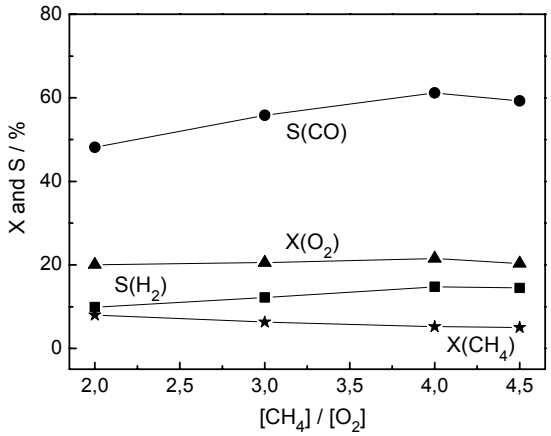

Figure V.10: *Effect of CH_4/O_2 ratio on reactant conversions and CO and H_2 selectivity over a 1.4-wt.% $Pt/Pr_{0.3}Ce_{0.35}Zr_{0.35}O_x$ channel. Experimental conditions were a temperature of 850 °C, a flow rate of 1200 ml/min and a channel length of 10 mm.*

V.5.3. Effect of CO_2 addition to the feed stream

In order to check the potential influence of dry reforming at very short contact times, $CH_4/O_2/CO_2$ mixtures with N_2 as balance were fed with reactant ratios of 2/1/0, 2/1/0.74 and 2/1/2 by varying CO_2 inlet concentration from 0 to 4 vol.%, at a flow rate of 1200 ml/min and oven temperature of 850°C.

Figure V.11 reports the conversion of reactants and syngas product selectivities as a function of CO_2 concentration in the feed. Obviously, the methane conversion does not at all depend on the carbon dioxide inlet partial pressure, while the oxygen conversion and hydrogen selectivity present a very weak dependence. However, the CO selectivity increases while the H_2 selectivity slightly decreases by increasing CO_2 inlet partial pressure. This might result from the occurrence of reverse WGS reaction, forming some additional CO from CO_2 and H_2.

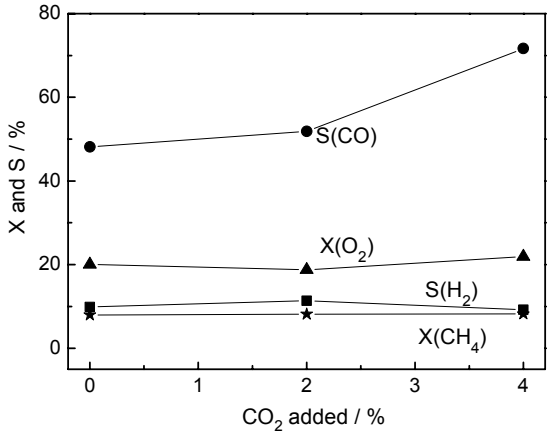

Figure V.11: *Effect of CO_2 concentration added to the feed on reactant conversion and CO and H_2 selectivity over a 1.4-wt.% $Pt/Pr_{0.3}Ce_{0.35}Zr_{0.35}O_x$ coated channel. Temperature: 850°C, flow rate: 1200 ml/min and channel length: 10 mm.*

These experiments with added CO_2 confirmed that the rate of CH_4 activation is independent of the nature and amount of the reforming co-reactant. On the other hand, according to the likely presence of mass transfer limitations (Figure V.9), adding CO_2 was not expected to influence methane activation as the activation with CO_2 (dry reforming) is considerably slower than the competing activation by O_2 (partial oxidation).

V.6. Catalytic properties of the support (doped mixed oxide coated channel without Pt)

V.6.1. Objective

Redox properties, thermal stability, structure and oxygen storage capacity of the complex Ce-Zr mixed oxides have been extensively studied by different scientific groups as described in the literature review (Chapter I). Most of the effort was to some extent dedicated to the use of Ce-Zr oxides as catalyst support for the NO_x abatement. However, their behavior and role in the POM process stays a matter of debate. Thus, if a clear impact of the support on the catalytic performance is recognized, the precise way along which the noble metal (Pt) and the support (Pr-Ce-Zr-O_X /Gd-Ce-Zr-O_X) interact remains to be determined. To tackle this question, a detailed knowledge of the support catalytic properties is a prerequisite, which is the object of that chapter.

As such, the complex Pt-free (Pr/Gd)-Ce-Zr oxide coated on the single channel of corundum monolith was investigated in the process of CPOM.

V.6.2. Effect of space time

Figure V.12 shows the methane and oxygen conversion as a function of the reactant space-time, which was varied by changing the total flow-rate. The following statements can be derived:

- Upon increasing W/F, the methane and oxygen conversions first increase linearly with W/F and can be extrapolated to zero conversion at zero space time. It can therefore be concluded that the oxygen and methane conversion in the low W/F domain, means at high flow rates, are established in the kinetic regime. At higher W/F values, i.e. lower flow rates, the loss of linearity strongly suggests, as observed in the presence of Pt, that the reaction proceeds in the so-called diffusion regime. Mass transfer limitations might limit keep the effective activities below the intrinsic catalytic performance.
- By comparing with the data reported in Figure V.9, the activity of the mixed oxide support material is clearly lower than that of the Pt – supported catalyst, as expected.

- Since mass transfer limitation can be safely excluded only at the highest flow rates, it was decided to account like for the case of Pt containing systems, for mass transfer terms during the modeling of studied process for the estimations of coefficients in the kinetic expression presented in a further chapter.

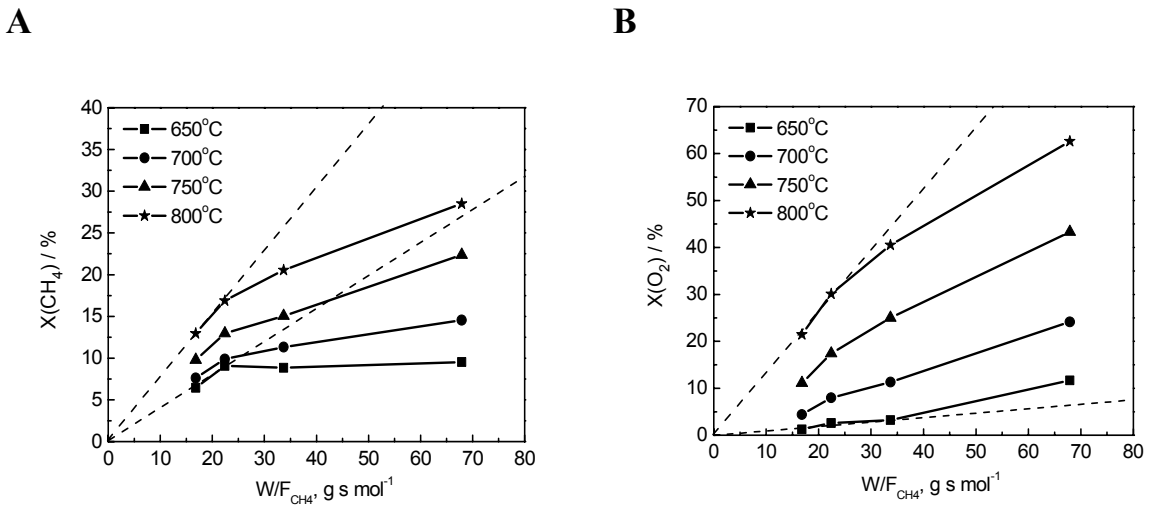

Figure V.12: *Methane and oxygen conversion as a function of the reactant space-time for $Pr_{0.3}Ce_{0.35}Zr_{0.35}O_x$ coated on a channel at different temperature. Channel length – 10mm. Composition feed – 6.6%CH_4 + 3.3%O_2 (N_2 - balance).*

V.6.3. Temperature profile

The temperature profile was also established along the monolith coated with the supports with the two different dopants under CPOM conditions.

The following features are revealed in Figure V.13:

- The same type of T profile is observed for both compositions under the studied conditions:
- Either with an oven temperature fixed at 700 or 800°C, the temperature of the monolith remains under the oven temperature, at variance with what was observed in the presence of Pt in Figure V.6, which combined endo and exothermic domains. In addition, the endothermic profile becomes progressively more marked along the catalytic zone.

- The resulting temperature drop appears slightly less pronounced for the Gd doped support as compared to the Pr doped one:

- for Gd, at oven temperature of 800°C: drop from 777°C to 769°C, and at 700°C, drop from 682°C to 675°C

- for Pr, at oven temperature of 800°C: drop from 778°C to 763°C and at 700°C: drop from 683°C to 672°C.

These observations indicate therefore a much lower heat release in the absence of Pt in the catalytic systems and a slightly lower activity of the Pr doped system as compared to the Gd based one as shown in the following.

A **B**

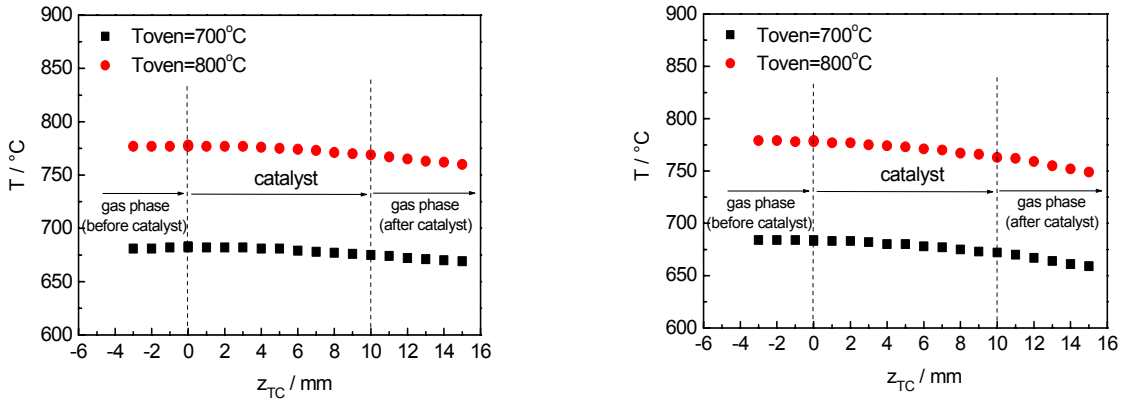

Figure V.13: *Temperature profile of $Pr_{0.3}Ce_{0.35}Zr_{0.35}O_x$ channel (A) and $Gd_{0.3}Ce_{0.35}Zr_{0.35}O_x$ channel (B). The flow rate – 100 ml/min, channel length – 10mm. Composition feed – 7%CH_4 + 3.5%O_2 (N_2 - balance).*

V.6.4. Temperature effect

Figure V.14 shows the dependence of reactant conversion and product selectivity on the outlet temperature for the monoliths coated with the two different mixed oxides, however the concentration of CO at low temperature was very low and difficult detectable by used micro-GC:

- At 400 ml/min, a relatively high selectivity to carbon monoxide and hydrogen is observed as compared to the results obtained in the presence of Pt.

- Reactant conversions and hydrogen selectivity increase with temperature.
- As for the CO selectivity, it tends to decrease slightly with temperature, at least for the Pr doped system. The simultaneous increase of hydrogen formation might indicate the occurrence of WGS. However, the opposite trends are not of the same intensity. In addition, the reverse effects would have been observed if related to WGS since this equilibrium is displaced towards CO at increasing temperature.

On the other hand, one might assume that the rise in hydrogen selectivity with temperature could be explained either by steam reforming or by carbon dioxide reforming, i.e. dry reforming, of methane being both favored at higher temperature.

For this reason, as done for the Pt containing systems, it was decided to investigate the dry reforming activity of the Pt free mixed oxides. Furthermore, this property is of crucial importance as the reaction over the support only leads to the formation of some CO and H_2, but there is a need for additional reforming to convert the complementary produced CO_2 and H_2O.

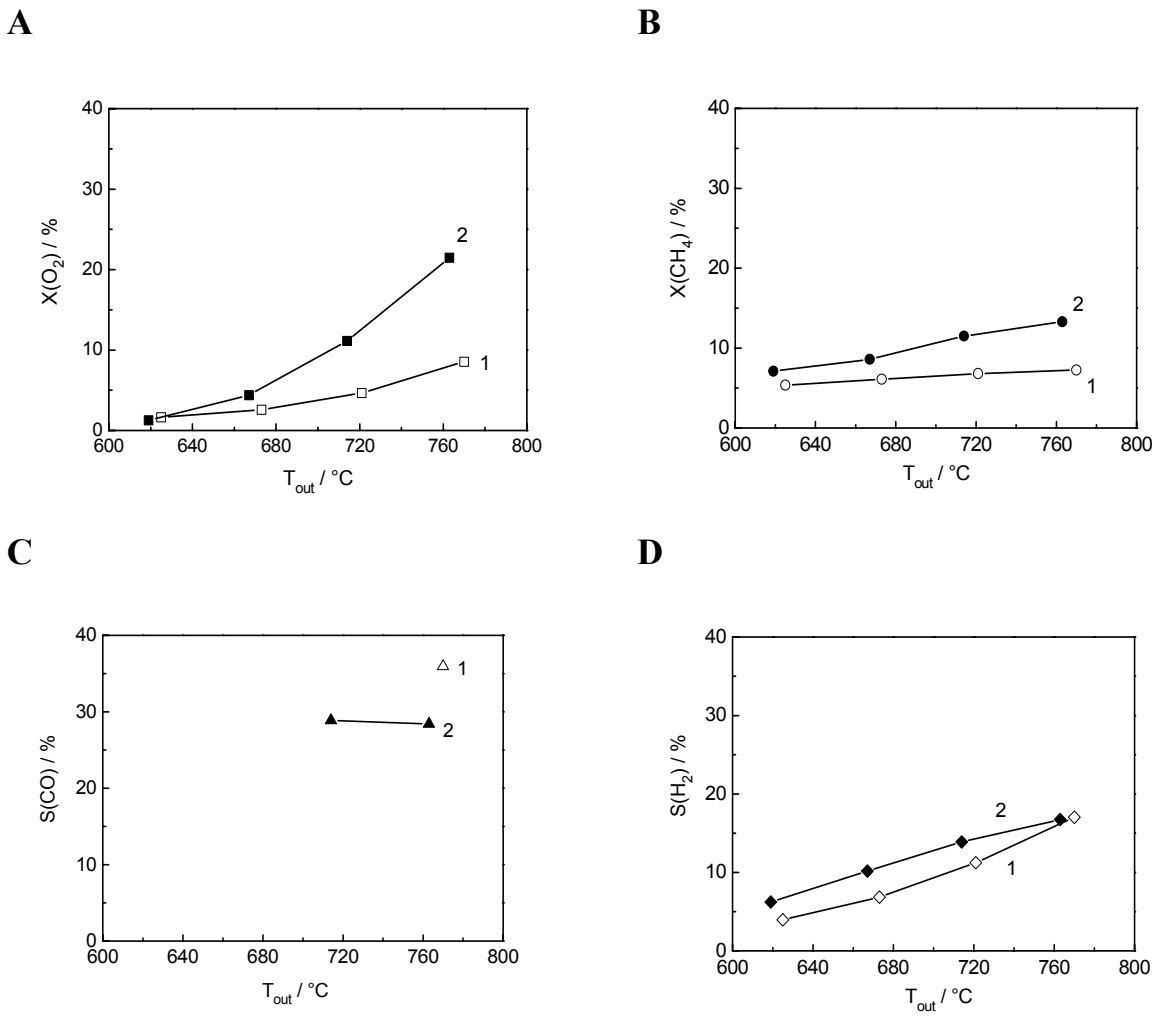

Figure V.14: *O_2 and CH_4 conversion and CO, H_2 selectivity in CPOM over $Gd_{0.3}Ce_{0.35}Zr_{0.35}O_x$ (1) and $Pr_{0.3}Ce_{0.35}Zr_{0.35}O_x$ (2). Flow rate – 400 ml/min, channel length – 10mm. Composition feed – 7%CH_4 + 3.5%O_2 (N_2 - balance).*

V.6.5. Dry reforming experiments

The dry reforming experiments were carried out over the channels coated with the Pt-free mixed oxides under the same experimental conditions as for the Pt containing systems. In the absence of Pt, no significant activity was observed as indicated by the missing hydrogen peak in the GC analysis.

TAP data showed that carbon dioxide could adsorb on the mixed oxide surface; but from steady-state experiments it seems that adsorbed CO_2 can not activate methane at comparable

reaction rates, while the methane activation clearly proceeds rapidly in case of adsorbed oxygen for the partial oxidation reaction.

V.7. New concept derived from steady-state experiments summary

From the main features revealed by steady-state experiments, it can be concluded that Pt is required for the steam/dry reforming activity of the catalyst, since it has been shown that the reforming on the Pt-free support is inefficient. On the other hand, despite the beneficial action of the mixed oxide support, it comes that the presence of Pt in the inlet zone of the catalyst, where high oxygen partial pressures still exist, leads to an over-oxidation of the desired products CO and H_2. It might be therefore proposed a new structured catalyst concept with a Pt concentration being very low at the monolith inlet and increasing along the flow direction. In this way, the mixed oxide intrinsic activity for syngas formation in the presence of O_2 would be exploited at the monolith inlet, while in a downstream section, once O_2 concentration is lowered, Pt added to the catalyst would favor both the direct partial oxidation at low oxygen pressure and the dry/steam reforming with the remaining methane.

This concept might also involve a favorable heat and volume management, since the initial catalyst section without Pt would be only slightly overheated, while the reforming section with Pt could be shortened, as only a smaller quantity of CO_2 and H_2O would need to be reformed.

The next chapter presents additional experiments based on this new reactor concept.

V.8. Catalysts stability with time on stream

On the basis of the previously presented concept, a new combination of active components supported on the single corundum monolith channel was prepared with Pt added to the doped mixed oxide only partially, i.e. in the downstream segment. This new catalyst was tested and compared under the same CPOM conditions with the previously reported system having an homogeneous concentration of Pt along the monolith coating.

Thus, the two tested systems can be described as follows:

- 1.4%wt.-Pt/$Pr_{0.3}Ce_{0.35}Zr_{0.35}O_x$ (20mm) ;
- $Pr_{0.3}Ce_{0.35}Zr_{0.35}O_x$ (10mm) + 1.4%wt.-Pt/$Pr_{0.3}Ce_{0.35}Zr_{0.35}O_x$ (10mm).

Stability tests were performed with single channels of corundum monolithic substrates at constant temperature of 800°C, atmospheric pressure, with a flow rate of 100ml/min and a CH_4/O_2 ratio = 2 during 26h on stream (Figure V.15).

A **B**

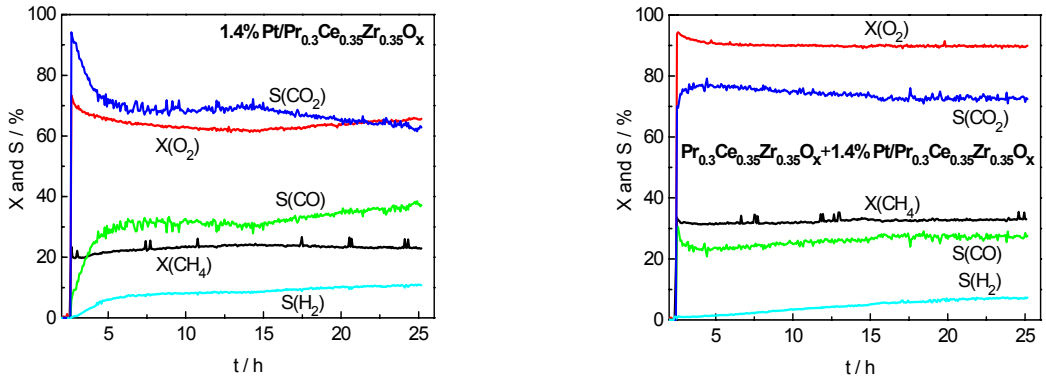

Figure V.15: *Catalytic performance for 1.4%wt.-Pt/$Pr_{0.3}Ce_{0.35}Zr_{0.35}O_x$ (A) and $Pr_{0.3}Ce_{0.35}Zr_{0.35}O_x$+1.4%wt.-Pt/$Pr_{0.3}Ce_{0.35}Zr_{0.35}O_x$ (B) during stability test.*

It should be noted first that for both combinations, O, C and H balances were closed to 100% ± 2% all over the testing period.

As can be seen from the concentration profiles, the performances of both fresh catalysts change significantly along the testing period. However the system without Pt in the inlet part (Figure V.15 B) stabilizes much more rapidly than the Pt gradient-free system (Figure V.15 A). Thus, even during 26h in stream this latter system did not reach the steady state. This observation might be related to thermal effects as explained before (Figure V.7), with much stronger exotherm in the first part of the monolith for the Pt-gradient free system.

Interestingly, the methane and oxygen conversions were higher for the Pt-gradient system while the final syngas selectivity remained slightly lower. The results can be analyzed in more details as follows:

Case of the Pt gradient free system. It can be noted that after 15h on stream, the oxygen concentration which was rather low initially started to slowly increase while methane conversion was decreasing and syngas selectivity increasing. Due to the high thermal gradient, the amount of lattice stored oxygen might have been depleted or the platinum nano clusters might have been

agglomerated under the thermal impact in the first part of the monolith. In both cases, the catalytic nano structure could have evolved towards a less performing system like a Pt/Al_2O_3 catalyst in the inlet section dedicated essentially to combustion reactions. This would explain the higher oxygen conversion observed. In turn this faster depletion of the oxygen content in the gas phase makes the "reforming" section longer and more efficient, which explains the improved syngas selectivity after long term testing.

Case of the Pt gradient system. The newly proposed configuration with a Pt gradient along the flow direction has a clear advantage in terms of relative activity and catalyst performance stability. The slightly lower syngas selectivity is most likely related to the arbitrarily selected length ratio between the zone without and with Pt content. Given the present observations, it seems advisable to shorten the length of the zone without Pt to the benefit of a longer zone containing Pt allowing a more efficient reforming.

However, a further optimization of the length ratio was beyond the scope of the present work, as a rational approach requires knowing the kinetics of the involved reaction. In turn, it was preferred to focus on a kinetic study presented in the next chapter of this work.

V.9. Switch experiment

In order to gain a better understanding of the role played by oxygen mobility at the Pt/mixed oxide interface the Pt gradient free system was first brought to steady state operation and a switch experiment was carried out.

A fresh catalyst was kept on CPOM stream during 48 h till steady-state was reached, to then switched to a N_2 purge flow for 30 min and thereafter instantaneous switched back to the initial feed stream (Figure V.16).

After switching from N_2 purge back to the CPOM stream, the H_2 selectivity was temporarily decreased and recovered only slowly to the initial steady-state values. One likely explanation is that during N_2 purge, the catalyst surface was partially re-oxidized because of oxygen diffusion from the mixed oxide bulk to its surface. On the other hand, the continuous purge with nitrogen might have also decreased the degree of surface oxidation by favoring oxygen desorption as shown previously from O_2-TPD experiments at 800°C. It can therefore be speculated that the rate of oxygen diffusion from the bulk to the surface is higher than the surface

desorption of oxygen under the prevailing conditions, which might be the case for these doped mixed oxide based systems.

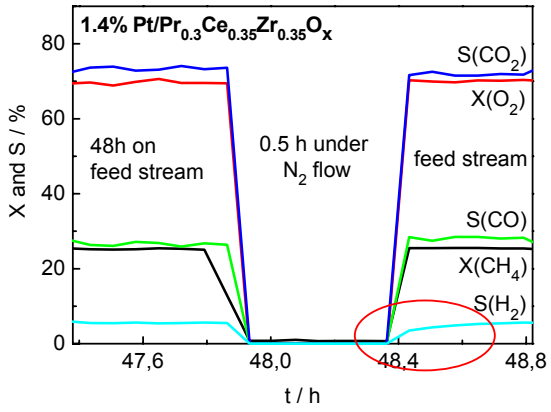

Figure V.16: *Catalytic activity of 1.4-wt.% $Pt/Pr_{0.3}Ce_{0.35}Zr_{0.35}O_x$ channel. Flow rate – 100ml/min, channel length – 20mm and 800°C. Composition feed – 6.6%CH_4 + 3.3%O_2 (N_2 - balance).*

Figure V.17 presents the catalytic performance of the catalyst after oxygen in-situ pretreatment. It is clear that the hydrogen selectivity was slowly increased during 1.5 h after start up followed by a very slow decrease probably related to a slight growth of the Pt nano-clusters. For this experiment with oxygen pretreatment the behavior of the hydrogen selectivity in the initial time span after start up (Figure V.17) was comparable to that in the case of switch experiments after nitrogen purging (Figure V.16). Data of the TAP study presented in Chapter IV showed that the catalyst in its oxidized state presented a better selectivity at only slightly lower activity as compared to its reduced state. According to these last observations it can be supposed, as speculated above, that during the nitrogen purge, the catalyst surface is partially oxidized by the oxygen migration from bulk to despite oxygen desorption.

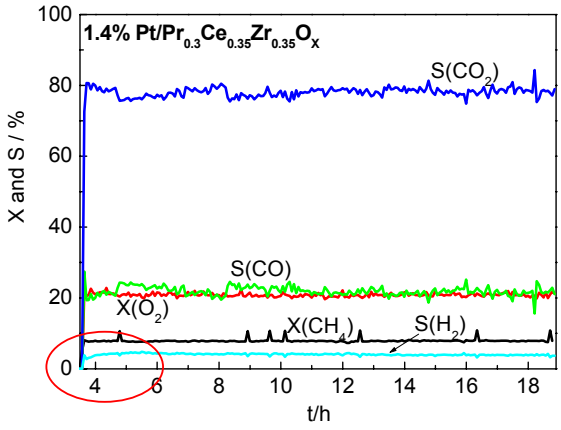

Figure V.17: *Catalytic activity of 1.4-wt.% Pt/$Pr_{0.3}Ce_{0.35}Zr_{0.35}O_x$ channel after oxygen pretreatment. Flow rate – 750 ml/min, channel length – 10mm and 800°C. Composition feed – 6.6%CH_4 + 3.3%O_2 (N_2 - balance).*

V.10. Conclusion

The catalytic partial oxidation of methane was studied at atmospheric pressure over catalysts with active components comprising Pt/Ce-Zr-(Pr, or Gd)-O supported on single corundum monolith channels. The catalyst temperature of the inlet and outlet section of catalyst was measured directly. By checking carefully temperature profiles, it is shown that the presence of an additional feed preheating tended to flatten the temperature profile within the monolith.

Many parameters like the effect of temperature, flow rate, CH_4/O_2 ratio, addition of CO_2 to the reactant feed, preheating and dopant on the catalytic performance were studied as well.

The catalyst doped by Pr was found to give the best performance for syngas production. It was shown that CO, CO_2, H_2 and H_2O were the main products at oxygen conversions lower than 100%, however with a relatively high selectivity to total oxidation products. However, the methane and oxygen conversions did not alter in that way as it would be expected when the reaction would proceed under kinetic control. Both the methane and oxygen conversion rates were most probably strongly influenced by mass transport phenomena, as was demonstrated by the fact that methane and oxygen conversions are hardly temperature dependent. The selectivity to CO was varied considerably with temperature, which showed the significant influence of the surface chemistry in its formation step. Increasing methane to oxygen ratio in the gas stream to the inlet increased CO and H_2 selectivities as well. CO_2 addition to the feed did not show any

changes of methane conversion, while the oxygen conversion and hydrogen selectivity had a very weak dependence. The CO selectivity increased with increasing carbon dioxide inlet partial pressure, pointing probably to a certain relevance of dry (CO_2) reforming of methane and / or the reversed water-gas shift reaction.

The catalytic properties of support and interaction of support with Pt was studied as well. It was shown that in presence of O_2 some CO and H_2, but also larger quantities of CO_2 and H_2O could be produced by reaction over the support. However, the support did not show sufficient efficiency in the dry reforming reaction. Taking the received data in account, it was suggested to explore a structure catalyst where the first section of it should be only mixed oxide for producing some CO and H_2 in dominating presence of gas phase oxygen and in second section where less oxygen is remaining to add Pt for favoring the reforming activity. Experiments could demonstrate that the suggested configuration of a structured catalyst performed with good results in terms of stability on stream. Nevertheless, addition major optimization is needed to adjust relative length of the different sections.

The characterization of the catalysts was carried out before and after reaction. XRD data showed the dominance of the cubic phase for all complex oxide samples. Raman spectra revealed also the presence of tetragonal ZrO_2, which is not in agreement with XRD data. However, due to the broadness and overlapping of the bands of ZrO_2 and CeO_2, it was complicated to definitively prove a co-presence of a tetragonal and a cubic phase. Comparison with TEM data revealed the higher dispersion and lower tendency to sintering of Pt particles for the catalyst with mixed oxide support as compared to a bare γ-Al_2O_3. XPS spectra showed that the catalyst samples remain in a rather oxidized state during reaction. The change in the atomic surface composition of elements in the catalysts before and after reaction was determined and calculated as well. XPS data were found perfectly in line with the kinetic observations collected during transient operations (switch from inert to CPOM feed gas). The latter showed that during N_2 purging, the catalyst was re-oxidized by the bulk oxygen diffusing from the mixed oxide. The obtained data was further used for carrying out a kinetic parameter estimation by numerical modeling presented in the next chapter.

CHAPTER VI

Mathematical modeling of the CPOM over single monolith channels

VI.1. Context

As was noted in the literature overview two distinct mechanisms are proposed for explaining the formation of syngas.

- The indirect pathway postulates that CH_4 is first totally oxidized to CO_2 and H_2O (in a strongly exothermic reaction) and then reformed to produce syngas (by strongly endothermic reactions). One major proof of the existence of such exothermic – endothermic sequence has been the observation sharp hot spots temperatures at the entrance of the reactor, which can cause detrimental effects on the stability of the catalytic material and can cause severe heat transport limitations [16].
- The direct pathway postulates the formation of H_2 and CO as primary products, eventually further oxidized into CO_2 and H_2O, depending on process conditions (contact time, O/C ratios etc. The main evidence in favor of a direct path is the observation of syngas at extremely short contact times, in the presence of unreacted oxygen [21].

However, the fast rate at which the CPOM reaction is proceeding makes mass transport limitations likely to occur, thus masking the intrinsic catalyst performance. In order to minimize mass transfer limitations several experimental reactor configurations have been used to study the reaction kinetics of the CPOM at short residence times and high temperatures. These configurations have in common that they employ the catalytic material in a structured configuration being in contrast to fixed beds used in conventional reactors. A catalytic annular reactor was applied by Beretta et al. [204] to study the intrinsic kinetics of the CPO reaction. In the presence of heat-transport limitations, de Smet et al. [42] developed an experimental reactor, containing a single Pt gauze as catalyst. Heat-transport limitations were first explicitly taken into account and later experimentally quantified by measuring the catalyst temperature with a spot-welded thermocouple attached to the Pt gauze. It was demonstrated that experiments could not be performed at conditions where both conversion and selectivities are determined by chemical phenomena alone. Moreover, taking into account the relevant transport phenomena, de Smet et.

al. [42] developed a reactor model to obtain the intrinsic kinetic parameters of the CPOM reaction on the Pt gauze.

The present Chapter reports on the development of a kinetic model for the catalytic partial oxidation of methane over a single monolith channel in the presence of unavoidable transport phenomena. Experimental data used for mathematical modeling have been presented in Chapter V. Experiments were performed studying the influence of the catalyst temperature, the reactant space-time and the inlet CH_4/O_2 ratio. The relative importance of dry reforming was studied as well. The aim of present study is to provide a comprehensive kinetic mechanism that can account for synthesis gas production.

VI.2. Operating conditions of kinetic tests

The kinetic tests were performed over the best performing system, i.e., a PtPrCeZrO single monolith channel of 10mm length in the plug-flow reactor as described in Chapter II. All experiments were performed at atmospheric pressure. A typical run consisted of varying the oven temperature from 700 up to 850°C, with 1h dwell steps at temperature increments of 25-50°C. At each temperature, conversions and selectivities were estimated from repeated analysis once stable values were measured. Typically the catalyst showed stable operation once an induction period of 20min was passed and performance data could be averaged over the remaining 40min. Nevertheless, prior to kinetic investigations, the catalyst underwent a standard conditioning procedure consisting of repeated runs at a fixed low flow rate of 100 ml min^{-1}, feeding a diluted gas mixture with a composition of 7 vol.% CH_4, a O_2/CH_4 ratio of 0.5 and N_2 added to balance. The catalyst conditioning was complete when stable performances were reached at each temperature in the whole range. To operate far from thermodynamic control, kinetic experiments were performed at higher values of flow rates than the conditioning one.

VI.3. 1 D mathematical reactor model

A one-dimensional heterogeneous model accounting for the interfacial concentration gradients has been used for the analysis of the experimental results [205]. The radial temperature gradients were not calculated, as the outside wall temperature was measured with a thermocouple

(Figure VI.1) and it was assumed that this corresponds to the actual catalyst temperature. The axial profile was also measured and is shown in Figure V.6-B. By applying high flow rates rather isothermal conditions are obtained. Axial dispersion in the monolith channel operated in the laminar flow regime can be neglected due to the very high superficial velocities applied in these experiments [206]. The one-dimensional heterogeneous model is used to simulate a single monolith channel.

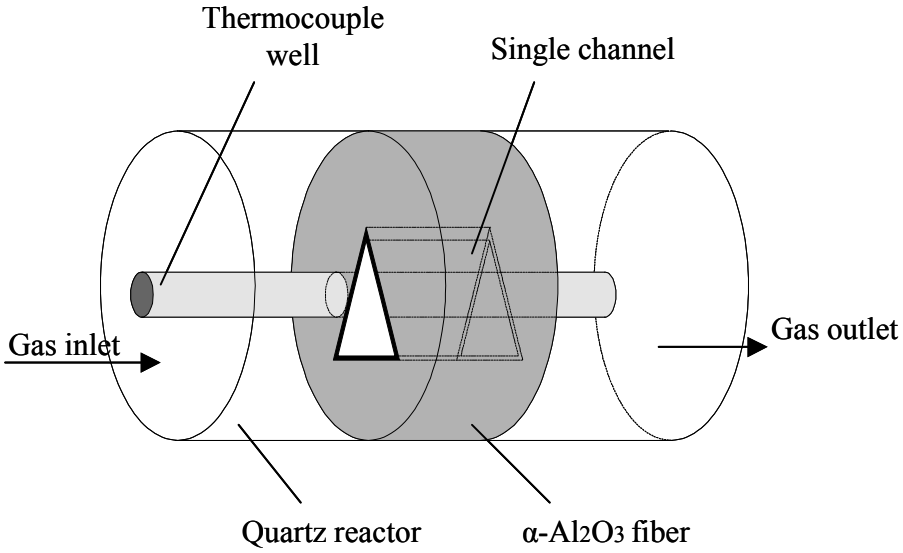

Figure VI.1: *Scheme of the quartz reactor charged with a single monolithic channel*

Adopting the above hypotheses leads to the mathematical equations reported in the following Table VI.1. The coefficients for mass transfer in the monolith reactor are calculated according to the relations proposed by Groppi et al. [207, 208]. The correlations for mass transfer are given in Table VI.2. The Sherwood number Sh_T is the *Sh* number for constant wall temperature, Sh_H refers to a constant wall heat flux. The actual *Sh* number is calculated using the interpolation formula of Brauer and Fetting [209], rearranged into (***Eq. VI.4)***. The density of the mixture has been calculated according to the law for ideal gases. Due to the small flow resistance of monoliths the pressure drop over the reactor is negligible and therefore the momentum equation has not been taken into account. The binary molecular diffusion coefficients are calculated from the Füller-Schettler-Giddings relation [210] and then the Wilke equation is used to calculate the diffusivities of the mixture [210].

Table VI.1. *Model equations*

$\frac{dF_j}{dz} = 3 d_i R_j$	mol/s m_r	***Eq. VI.1***
$R_j = k_{g,j}\left(C_j - C_j^{\,s}\right)$	mol/s m^2_{cat}	***Eq. VI.2***
Initial conditions:		
z =0 : $C_j = C_j^0$		***Eq. VI.3***

Table VI.2. *Mass transfer correlations for a triangular monolith channel*

- Triangular monolith channel:	
$2Sh = Sh_H - Da\frac{Sh_H}{Sh_T} + \sqrt{\left(\left(Sh_H - Da\frac{Sh_H}{Sh_T}\right)^2 + 4DaSh_H\right)}$	***Eq. VI.4***
$Sh_H = 1.89 + 8.933\left(\frac{1000}{l*}\right)^{-0.5386}\exp\left(-\frac{6.7275}{l*}\right)$	***Eq. VI.5***
$Sh_T = 2.47 + 6.854\left(\frac{1000}{l*}\right)^{-0.5174}\exp\left(-\frac{42.49}{l*}\right)$	***Eq. VI.6***
$l* = \mathrm{Re}\,Sc\frac{d_h}{l}$	***Eq. VI.7***

VI.3.1 Solution procedure

The set of equations to be solved consists of ordinary non-linear first-order differential equations that form a set of initial value problem coupled to non-linear algebraic equations. It should be noted that the differential equations reflect the change in species concentrations, which can be accessed as stoichiometic coefficient weighted linear combination of the reaction rates for the microkinetic steps considered. The set of differential algebraic equations (DAE) were numerically integrated using the ODEPACK library [211]. A number of physical properties and other variables (e.g. ρ, u, ΔH) depend on the temperature, pressure or flow composition. These

are updated after each integration step in a separate subroutine. All this is implemented in a FORTRAN code.

VI.4. Experimental results

Table VI.3 summarizes the range experimental conditions investigated.

Table VI.3: *Experimental conditions of kinetic experiments*

Range of variation parameter	Feed: 6.6%CH_4 + 3.3%O_2 (N_2 - balance)
Oven temperature / °C	700 ÷ 850
Flow rate / ml/min	400 ÷ 1400
CH_4/O_2	2 ÷ 4.5
Concentration CO_2 added in the feed / %	0 ÷ 4

In the range of conditions studied, CO, CO_2 and H_2O were the main reaction products, while the selectivity to H_2 remained relatively low. The H_2 selectivity for all the applied conditions is plotted in Figure VI.2 and shows an exponential increase with temperature. It becomes clear from Figure VI.2 that the hydrogen selectivity was below 15% for the majority of conditions and reached peak values of 25%.

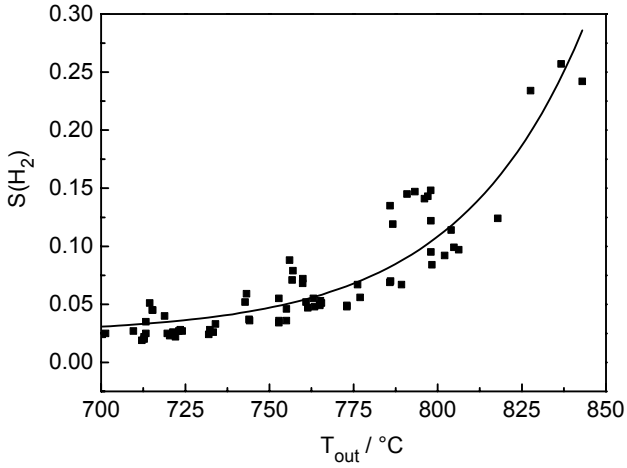

Figure VI.2: *Dependence of H_2 selectivity from temperature for the applied conditions*

VI.5. Kinetic modeling

Comparing coarsely the experimental results in this work to those reported in literature revealed large similarities with those used by de Smet et al. [43] in a modeling study. On the other hand, there is the major difference that de Smet et al. did not observe any hydrogen production over their Pt gauze catalyst at temperatures below 1000°C preventing these authors to determine kinetic parameters for the hydrogen production. Nevertheless, the proposed kinetic scheme and kinetic parameters was considered highly suitable as a starting point for the kinetic description of the data in this work. The steps in the reaction model (mechanism) initially proposed by de Smet et al. [43] are summarized in Table VI.4.

Table VI.4: *Reaction mechanism used by de Smet et al. [43]*

Reaction			A or s^0 (Pa^{-1} s^{-1}or s^{-1})	E_{act} (kJ mol^{-1})	Rate equation	Step
$O_{2,g} + 2*$	→	$2O*$	0.023	0	$K_1P_{O2}\theta_*$	1
$CH_{4,g} + 2O*$	→	$C* + 2H_2O_{,g} + *$	$2.4\ 10^5$	48.2	$K_2P_{CH4}\theta_*\theta_O$	2
$C* + O*$	→	$CO* + *$	$1\ 10^{13}$	62.8	$K_3\theta_C\theta_O$	3
$CO* + O*$	→	$CO_{2,g} + 2*$	$1\ 10^{13}$	100	$K_4\theta_{CO}\theta_O$	4
$CO*$	→	$CO_{,g} + *$	$1\ 10^{13}$	126	$K_5\theta_{CO}$	5a
$CO_{,g} + *$	→	$CO*$	0.84	0	$K_6P_{CO}\theta_*$	5b

* denotes a Pt active site.

All reaction steps were considered irreversible, except the sorption step (5) of carbon monoxide. Moreover, all reactions were considered to be first order in reactants and adsorbed species. Lacking experimental data the hydrogen production has been neglected as pointed out before. In fact these authors assumed even that the activation proceeds in an oxidative step leading immediately to the formation of water. The pre-exponential factor and the apparent activation energy for the methane activation step were estimated by a regression analysis of the experimental CO selectivities. All the other kinetic parameters of the remaining 4 steps were fixed at values obtained from the literature. The above reaction model gave an adequate description of their experimental data [43].

In the present work, the above model could describe most of the data in this study adequately (estimated kinetic parameters are indicated in Table VI.4), except the data concerning the CO_2 addition. Remarkably, it should be mentioned that de Smet et al. [43] never performed CO_2 addition experiments. Despite the reasonable fit for methane and oxygen conversion as well as for the carbon oxide selectivity in cases without CO_2 addition, there is an obviously need to extend the suggested five–step reaction model (Table VI.4).

The latter model identified as partially suitable was kept as starting point for a kinetic description of data in the present work. However, for fitting all the data in this study, several steps had to be formulated reversible. In order to take into account the addition of CO_2 in the reactant feed, step 4 has been assumed reversible. In order to account for a reversibility of the initial carbon species oxidation the step 3 was also considered as reversible. Furthermore, TAP experiments [24] have shown that oxygen adsorption on platinum is reversible at the reaction temperatures investigated and the TPD study presented in the former chapter on mechanistic investigations supported this for the case of the investigated catalyst under the applied reaction conditions. The extended reaction network used in this work is reported in Table 5a and involved steps are the following:

Oxygen Adsorption. The first step in the reaction mechanism concerns the activation of oxygen through dissociative adsorption. According to Williams et al. [212], the adsorption rate can be assumed to be first order in the fraction of vacant surface sites θ*, which implies that the rate-determining step in the adsorption involves the interaction of molecular oxygen with a single catalytic site. Oxygen adsorption is considered to be competitive, in contrast to the mechanism proposed by Hickman and Schmidt [213].

Methane Adsorption. In agreement with theoretical calculations of Au et al. [214], methane adsorption under the present conditions is considered to be oxygen-assisted, directly resulting in adsorbed hydroxyl species that recombine instantaneously to gaseous water. Thus a dissociative adsorption of methane, resulting in the formation of a surface carbon species and gaseous water, is taken into account in step 2.

Reaction 2 is obviously not an elementary step, but proceeds through a number of intermediates such as adsorbed CH_x (x=1,3) fragments and adsorbed OH species. Molecular methane adsorption on the Pt surface is considered to be reversible and in quasi equilibrium. The abstraction of the first hydrogen atom by adsorbed oxygen species is considered as the rate-determining step in methane decomposition. The subsequent abstraction of hydrogen atoms from adsorbed CH_x fragments, and the recombination of hydroxyl species to water, is potentially very fast. As a result, no CH_x species appear as surface intermediates in the kinetic model.

Carbon Monoxide and Carbon Dioxide Production. Steps 3 to 5 concern paths toward carbon monoxide and carbon dioxide. Reaction 3 describes the formation of adsorbed CO species, which is generally considered to be very fast [213]. Adsorbed CO species are converted to CO_2 in step 4, which desorbs instantaneously. CO_2 adsorption is not taken into account in the kinetic model, since the heat of adsorption of CO_2 on Pt is very low [215]. Finally, CO desorption and adsorption are described in the kinetic model by steps 5a and 5b.

Table VI.5a: *POM reaction scheme over supported Pt adapted from the proposition of de Smet et al. to account for reversible oxygen adsorption, carbon species oxidation and CO_2 formation*

Reaction			A or s^0 (Pa^{-1} s^{-1}or s^{-1})	E_{act} (kJ mol^{-1})	Step
$O_{2,g} + 2*$	→	$2O*$	0.11	0	1a
$2O*$	→	$O_{2,g} + 2*$	$1.7\ 10^{13}$	200	1b
$CH_{4,g} + 2O*$	→	$C* + 2H_2O_{,g} + *$	$2.4\ 10^{5}$	48.2	2
$C* + O*$	→	$CO* + *$	$1\ 10^{13}$	62.8	3a
$CO* + *$	→	$C* + O*$	$1\ 10^{11}$	184	3b
$CO* + O*$	→	$CO_{2,g} + 2*$	$1.9\ 10^{9}$	30	4a
$CO_{2,g} + 2*$	→	$CO* + O*$	$6.3\ 10^{2}$	28	4b
$CO*$	→	$CO_{,g} + *$	$1\ 10^{13}$	126	5a
$CO_{,g} + *$	→	$CO*$	0.84	0	5b

* denotes a Pt active site or a site located on the ceria, see discussion

Table VI.5b: *POM reaction scheme over supported Pt proposed in this study accounting for hydrogen production*

Reaction			A or s^0 (Pa^{-1} s^{-1}or s^{-1})	E_{act} (kJ mol^{-1})	Step
$O_{2,g}$ + 2*	→	2O*	0.68	0	1a
2O*	→	$O_{2,g}$ + 2*	$1.0\ 10^{14}$	200	1b
$CH_{4,g}$ + 5*	→	C* + 4H*	$9.35\ 10^{3}$	125.2	2
C* + O*	→	CO* + *	$1\ 10^{13}$	62.8	3a
CO* + *	→	C* + O*	$1\ 10^{11}$	184	3b
CO* + O*	→	$CO_{2,g}$ + 2*	$3.2\ 10^{13}$	37.4	4a
$CO_{2,g}$ + 2*	→	CO* + O*	$9.9\ 10^{3}$	10	4b
CO*	→	$CO_{,g}$ + *	$1\ 10^{13}$	126	5a
$CO_{,g}$ + *	→	CO*	0.71	0	5b
2H*	→	$H_{2,g}$ + 2*	$1.0\ 10^{14}$	159.7	6a
$H_{2,g}$ + 2*	→	2H*	0.02	0	6b
2H* + O*	→	$H_2O_{,g}$ + 3*	$1.0\ 10^{13}$	20	7a
$H_2O_{,g}$ + 3*	→	2H* + O*	$1.0\ 10^{6}$	69	7b

* denotes a Pt active site or a site located on the ceria, see discussion

As mentioned before and detailed in a later paragraph, the reaction scheme adapted from de Smet et al. in Table VI.5a allows a reasonable description of the methane conversion and carbon oxide selectivities observed. On the other hand, the hydrogen production is not described and the experimental results indicated a selectivity of up to 25%. In order to account for the hydrogen production, a second kinetic scheme using elements of the work from Hickman and Schmidt [213] was established and is summarized in Table VI.5b.

Table VI.6a: *Matrix indicating the required linear combination relating the reaction rates to the change in species concentration or coverage for the microkinetic model presented in table 5a.*

	1a	1b	2	3a	3b	4a	4b	5a	5b
$O_{2,g}$	-1	1							
O*	2	-2	-2	-1	1	-1	1		
$CH_{4,g}$			-1						
C*			1	-1	1				
CO*				1	-1	-1	1	-1	1
$CO_{2,g}$						1	-1		
CO_g								1	-1
$H_2O_{,g}$			2						

Table VI.6b: *Matrix indicating the required linear combination relating the reaction rates to the change in species concentration or coverage for the microkinetic model presented in table 5b.*

	1a	1b	2	3a	3b	4a	4b	5a	5b	6a	6b	7a	7b
$O_{2,g}$	-1	1											
O*	2	-2		-1	1	-1	1					-1	1
$CH_{4,g}$			-1										
C*			1	-1	1								
CO*				1	-1	-1	1	-1	1				
$CO_{2,g}$						1	-1						
H*			4							-2	2	-2	2
$H_{2,g}$										1	-1		
$H_2O_{,g}$												1	-1
CO_g								1	-1				

The reversible steps 1, 3, 4, 5 are identical to those included in the adapted scheme following de Smet et al. presented in Table VI.5a. The essential difference in this scheme from Table VI.5b over that previous presented in Table VI.5a is found in step 2 now considering a dissociation of methane into a carbon species and adsorbed hydrogen as proposed by Hickman and Schmidt [213]. Consequently, step 6 accounts for reversible hydrogen release and step 7 accounts for its reversible oxidation to gaseous water. In fact, without anticipating the discussion, the rapid release of hydrogen observed during TAP experiments supports formulating step 2 in the present form, while the increasing catalyst activity adding more oxygen pre-pulses is more contradicting a methane activation without participation of oxygen.

Parameter fitting according to the newly proposed reaction scheme in Table VI.5a was restricted to a minimum using literature data and other criteria to estimate parameters. Hickman and Schmidt [213] give rate parameters for the reverse reaction of step 3, which has been included in our mechanism (3b). Only the parameters of steps 1a, 4a and 4b have been optimized through regression analysis of 70 data points. Note that only 5 parameters have been adjusted.

The (partial) description of results by the model adapted from de Smet et al. (considered steps and estimated kinetic parameters as given in Table VI.5a) is depicted showing the experimentally observed performances (points) along with the model predicted ones (lines) in Figure VI.3a and by the respective parity plots for the methane conversion and carbon monoxide selectivity in Figure VI.4a. Resulting from the fact that this model does not account for a hydrogen release the oxygen consumption is over-estimated and the calculated resulting oxygen conversions do not correspond to the measured oxygen conversion. Hence, the Figure VI.3a below shows only the experimental oxygen conversion and the hydrogen selectivity was not included in Figure VI.4a. An adequate description of both the methane conversion and the CO selectivity are obtained.

Extending the reaction scheme adapted from de Smet et al. [43] to the mechanism given in Table VI.5b allowed to account for a hydrogen production. However, as only one step was replaced (step 2) and two more were added (steps 6 and 7) several parameters could remain fixed to values determined for the above discussed scheme outlined in Table VI.5a. This relates to the steps 3a, 3b and 5a. Other parameters needed only an adjustment of the frequency factor, which was the case for steps 1a, 1b, 5b. This relates to the fact that changing step 2 from an “oxygen assisted” one to a step without oxygen participation required obviously to adapt to the different needs in oxygen consumption. The parameters of the “new” steps 2, 6 and 7 were obviously newly estimated, but also the parameters of the step 4 relating to CO oxidation had been estimated once more.

All fitted kinetic parameters are given in Table VI.5b along with a comparison of the experimentally observed performances (points) and the model predicted ones (lines) in Figure VI.3b and the respective parity plots for the methane conversion and carbon monoxide and hydrogen selectivity in Figure VI.4b as a measure of the fitting quality.

The main result of using the new reaction scheme is a reasonable description of the hydrogen production and a better description of the oxygen conversion depicted in Figure VI.3b. Nevertheless, especially at high residence times (W/F) there is a major deviation in the model predicted oxygen conversion against the experimental one. Initially only one type of active site is assumed, although this will be discussed in more details in the next section.

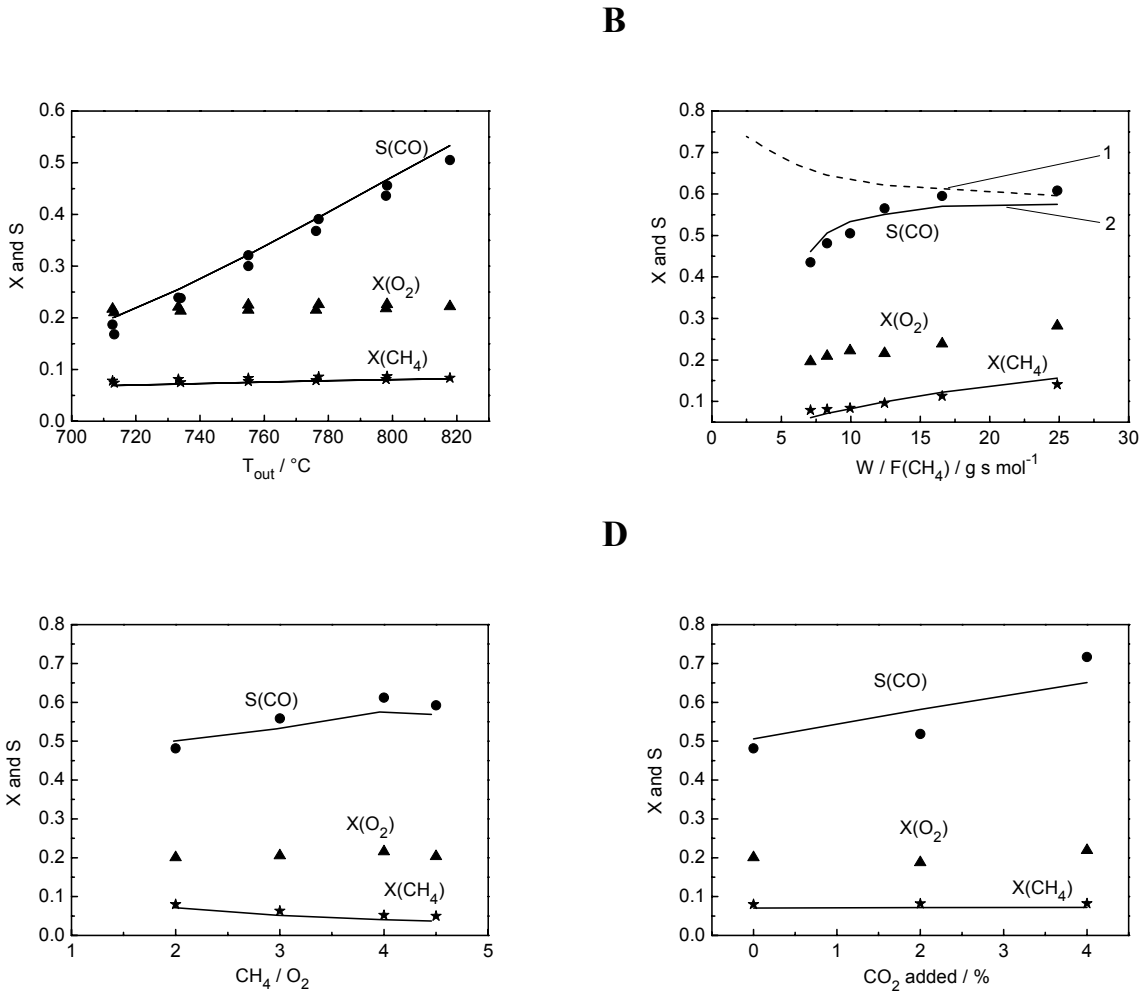

Figure VI.3a: *Experimental and calculated data at different process parameters using the mechanism proposed by de Smet et al.. Trace 1 denotes the CO selectivity if the temperature would remain constant and trace 2 outlines the CO selectivity at the experimentally measured temperatures altered by the convective contribution.*

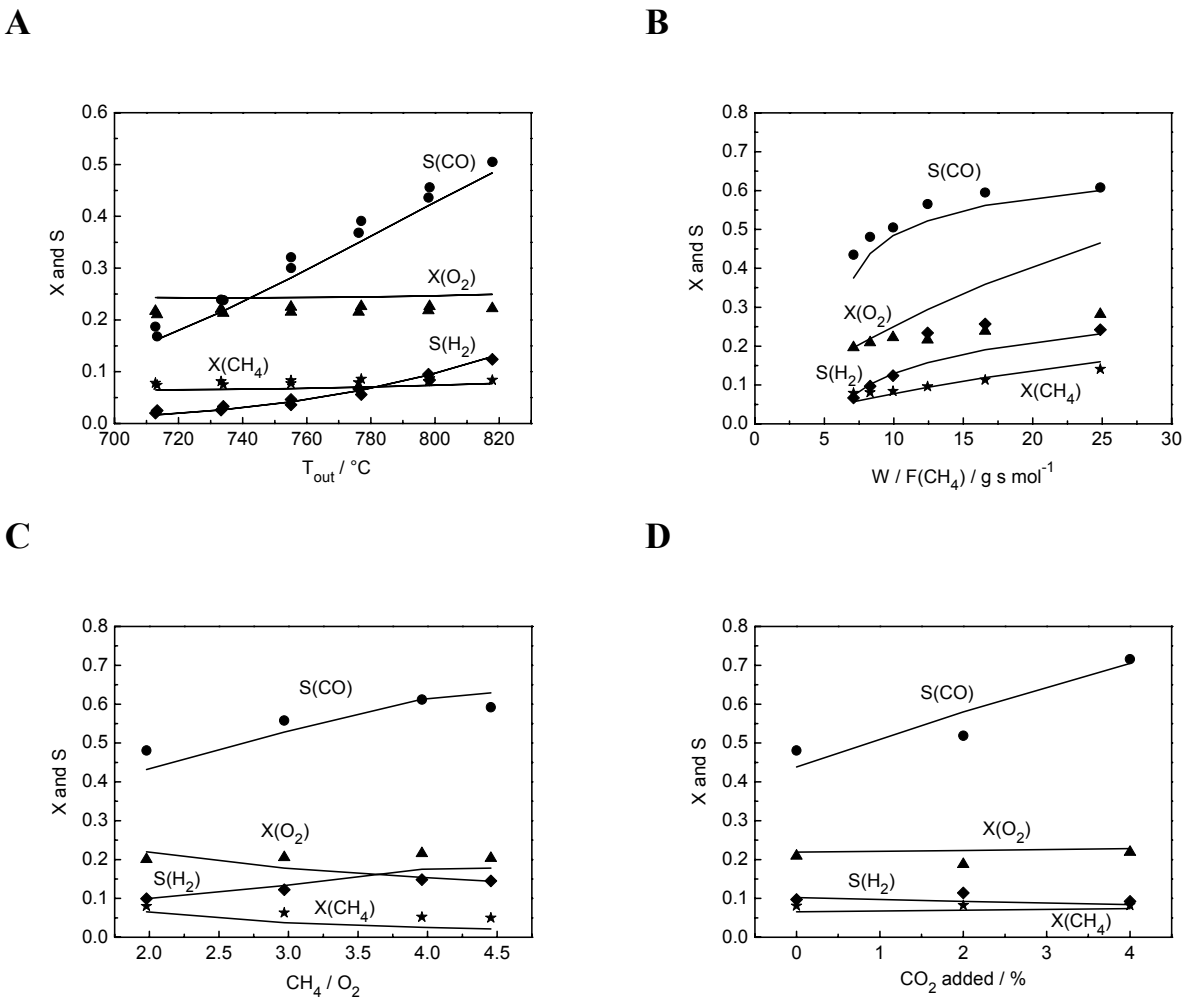

Figure VI.3b: *Experimental and calculated data at different process parameters using the mechanism proposed in this work*

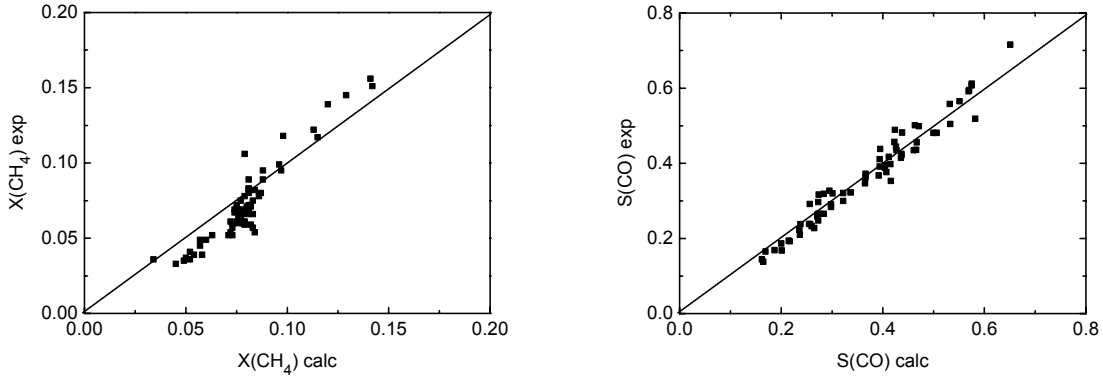

Figure VI.4a: *Parity plot for the methane conversion and the CO selectivity of experimental and calculated values (according to the kinetic parameters given in table 5a)*

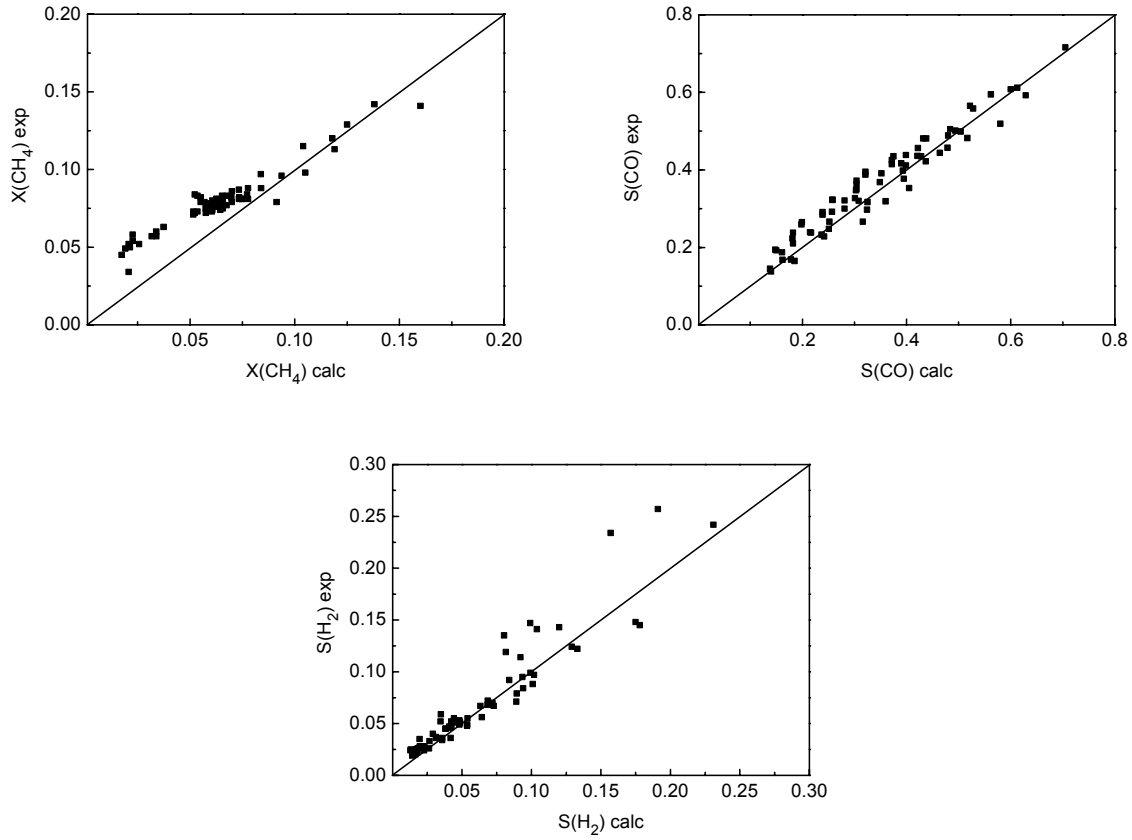

Figure VI.4b: *Parity plot for the methane conversion, the CO and H_2 selectivity of experimental and calculated values (according to the kinetic parameters given in Table VI.5b)*

VI.6. Discussion

The above section on kinetic modeling indicated that a reasonable description was achieved. Nevertheless, the proposed models in Table VI.5a and VI.5b have some fundamental differences requiring an appropriate discussion in the following.

VI.6.1. Evaluation of the different proposed models

As can be seen in Figures VI.3a and VI.4a the modified "oxygen assisted" CPOM mechanism originally proposed by de Smet et al. [43] describes adequately the CH_4 conversion and CO selectivity data over the Pt/PrCeZrO/α-Al_2O_3 monolith catalyst. The extension (Table VI.5a) to the original scheme (Table VI.4) was found necessary to describe experiments with CO_2 addition not performed in the de Smet et al. work. As was noted before, de Smet et al. studied the reaction in a continuous flow reactor set-up with a single wire Pt gauze as catalyst [42,43]. It seems logical that readsorption could be underrepresented under these conditions and that might have prevented the authors to discriminate the steps newly added in this work. In fact these steps were apparently not needed to describe the smaller base of experimental data with their proposed reaction network. However, the new experiments with carbon dioxide addition to the feed indicated that several steps in the carbon oxide formation proceed in fact reversibly.

The global rate coefficient for dissociative adsorption of methane is the product of the equilibrium coefficient for molecular adsorption and the rate coefficient of the rate-determining step. The activation energy of the rate-determining step thus can be written as:

$$E_{act} = E^{global} - \Delta H^0_{ads} \qquad \textit{Eq. VI.8}$$

where E^{global} is the global activation energy of dissociative methane adsorption, and ΔH^0 is the standard adsorption enthalpy of methane. Substitution of the estimated global activation energy, 48.2 kJ mol^{-1}, and the standard adsorption enthalpy of methane, ΔH =-25.1 kJ /mol [215], results in an activation energy of the rate-determining step of 73.3 kJ mol^{-1}.

In the literature, no data were found regarding the activation energy of oxygen-assisted methane adsorption. The calculated value, however, is higher than the reported activation energy

of 43.1 kJ mol^{-1} [216] for dissociative methane adsorption into adsorbed carbon and hydrogen species.

The second further extended model (Table VI.5b) allowed both a satisfying prediction of the H_2 selectivity and a reasonable prediction of the O_2 conversion. New parameter estimation could be limited to newly introduced reaction steps and a reevaluation of the parameters for the reversible CO oxidation in step 4.

On the other hand the major change for this model is the assumption of a "non oxygen assisted" activation of methane as proposed by Hickman and Schmidt [213]. Assuming an activation of methane via the formation of a carbon species and adsorbed hydrogen rapidly releasable to gas-phase agrees well with the observed pulse shaped rapid formation of H_2 in TAP experiments over this catalyst [217]. In turn, this is somewhat contradictory to the rising catalyst activity with increasing amount of pre-adsorbed oxygen reported in the same work. Moreover, the least satisfying description of the model is observed for the oxygen conversion at long contact times (high W/F) without observing a strong detrimental impact on the prediction of other reaction observables. Both deviations could be rationalized to some extend assuming that oxygen is also activated or stored on another less reactive site, at a lower rate than that for the now assumed single site. Under TAP conditions this second type site would become active only at more pronounced oxygen pre-adsorption and at ambient pressure its impact would increase with rising contact time. In fact assuming such a second type site is even reasonable given the previously demonstrated participation of oxygen on the support or even in its bulk, leading to a small catalytic activity of the support material under atmospheric pressure. Despite being out of the scope of the present kinetic investigation focusing on description of the dominating reactions (most probably proceeding on Pt sites) the above suggests a deeper discussion on the role of ceria in the mechanistic scheme.

VI.6.2. Role of ceria

Whereas the assumption of a single active site for methane and oxygen activation seems quite relevant over pure Pt catalysts (gauzes), although in their original reaction mechanism Hickman and Schmidt [213] proposed different sites for methane and oxygen, it is certainly not the case for a Pt/PrCeZrO/α-Al_2O_3 monolith catalyst. The ceria can activate CO and water as

well and adsorb different reaction intermediates such as hydroxyl groups and carbonates. This will lead to parallel reactions pathways for the oxidation of methane over these catalysts. This has been demonstrated in the case of three-way catalysts [218].

Steady-state kinetics will not be able in most cases to unequivocally discriminate between these different pathways due to the strong coupling of the kinetic constants in these similar paths. However, by comparing results (including the values of the kinetic parameters) of experiments over platinum and Pt/PrCeZrO/α-Al_2O_3 monolith catalysts the role of the support can be unraveled. Therefore in this work we compare our results over Pt/PrCeZrO/α-Al_2O_3 single channel of monolith to the results of de Smet et al. over a Pt gauze [43]. Both sets of data have been obtained under rather similar conditions under mass transfer limitations, although over different catalyst geometries. Moreover both data sets have been analyzed and modeled through a similar sequence of elementary steps.

From Figure VI.3a it is observed that the CO selectivity increases from 20 – 50% over a temperature interval of 100°C. In the case of the Pt gauze this increase is lower from 20 – 35% only. The CO selectivity depends on the ratio of the CO desorption rate and the CO oxidation rate to CO_2, i.e. R5 and R4. The temperature dependence of the CO selectivity depends thus on the ratio of the activation energies of these two rates. Thus E5/E4 (Pt/PrCeZrO/α-Al_2O_3) and with E5 fixed at 126 kJ/mol this becomes E4 (Pt/PrCeZrO/α-Al_2O_3) < E4 (Pt gauze). This is indeed the case shown in Tables VI.4 and VI.5. Thus the ceria effectively lowers the activation barrier of the CO_2 production rate. Indeed Nibbelke et al. [218] found from transient experiments of CO oxidation over a Pt/Rh/Ce/Al catalyst that a parallel CO_2 route involving species adsorbed on ceria exists. They proposed the following reaction step:

$$CO* + Os \rightarrow CO_{2,g} + * + s$$

Where * represents a Pt site and s is a ceria site. They have estimated an activation energy for this step of 11 kJ/mol. The value obtained in our study of 30 kJ/mol is in between the values of the pathway over Pt and the ceria-catalyzed route, thus indicating that both routes play a role for CO_2 production over the Pt/Ce/Al catalyst.

Figure VI.3a-b shows an increasing CO selectivity with increasing space-time quite contrary to the effect observed over the Pt gauze. In the previous Chapter V it was explained that

this was due to the variation of the catalyst temperature with changing flow rates. Therefore the dotted line 1 in Figure VI.3a-b is a simulation with a constant catalyst temperature of 850°C. Now the CO selectivity decreases with increasing space-time indicating that CO is the most important primary product in the partial oxidation of methane. These results are well in line with TAP studies (Chapter IV) as well as steady state experiments [219].

Similar methane conversions are obtained for the Pt/PrCeZrO/α-Al_2O_3 catalyst and the Pt gauze at apparently very different W/F values (5-25 vs. 10 - 130 g s mol^{-1}). The number of surface Pt atoms of the gauze has been estimated to be 4-6 nmol using data from [220] corrected for the different gauze diameters. The monolith contains approximately 30 nmol of surface platinum atoms (D~50%). The actual space-times with respect to the number of surface platinum atoms in both reactors are thus very similar.

Figure VI.3a-d shows that addition of CO_2 to the feed lead to a higher CO selectivity. Unfortunately, these experiments have not been reported by de Smet et al. [43] over the Pt gauze. In our case the CO_2 co-feeding experiments can be accounted for in the model by assuming a dissociation of CO_2 into adsorbed CO and O. Carbon dioxide dissociation over platinum is debated in the literature. Tol et al. [221] reported that CO_2 does not dissociate over Pt but Huinink [222] has observed oxygen exchange of CO_2. TAP experiments over Pt/Al_2O_3 using labeled CO_2 showed that there is no occurring of CO_2 dissociation or a direct reaction between CO_2 and adsorbed carbon neither [223]. However, similar TAP experiments over Pt/ZrO_2 showed that CO_2 dissociations occurs where the oxygen vacancy on the ZrO_2 catalyze this step [223]. In this case CO_2 dissociations involves sites on the ceria.

The value of the oxygen sticking coefficient of 0.11 over Pt/PrCeZrO/α-Al_2O_3 is almost an order of magnitude higher than over Pt reported in the range of 0.01 [43]. This is in agreement with an activation of oxygen on the ceria.

VI.6.3. Rate-determining step

Using Campbell's definition for the degree of rate control [224]:

$$X_{rc,i} = \left(\frac{k_i}{r}\right)\left(\frac{\delta r}{\delta k_i}\right) \qquad \textit{Eq. VI.9}$$

the rate-controlling steps can be established. In (***Eq. VI.9)*** where $X_{rc,i}$ is the degree of rate control and *r* is the overall rate, the partial derivative is taken holding constant the equilibrium constant for step *i* and the rate constants k_j for all other steps *j*. Table VI.7a gives the $X_{rc,i}$ as defined by (***Eq. VI.9)*** above for the 5 reversible reaction steps from Table VI.5a for the 4 principal gas phase species. These coefficients can vary between –1 – +1. A high absolute value indicates that the step has a large contribution to the overall reaction rate [224]. Note that step (1) has been taken reversible by introducing a small rate constant for the reverse step. Within a certain range of values this did not influence the modeling results.

Table VI.7a *Degree of rate control ($X_{rc,i}$) for the 5 reversible reaction steps from Table 5a for the CH_4, O_2, CO and CO_2 gas phase species*

Step	CH_4	O_2	CO	CO_2
1	0.06	0.00	0.47	-0.45
2	0.51	0.55	-0.28	0.27
3	0.01	0.00	0.09	-0.08
4	-0.04	0.02	-0.43	0.41
5	0.00	0.00	0.00	0.00

Table VI.7b *Degree of rate control ($X_{rc,i}$) for the 7 reversible reaction steps from Table VI.5b for the CH_4, O_2, CO, CO_2, H_2 and H_2O gas phase species*

Step	CH_4	O_2	CO	CO_2	H_2	H_2O
1	0.85	0.97	-0.51	0.40	-0.78	0.09
2	-0.41	-0.47	0.29	-0.23	0.44	-0.05
3	0.15	0.06	0.42	-0.33	0.68	-0.08
4	-0.08	-0.03	-0.41	0.32	0.08	-0.01
5	0.06	0.02	0.34	-0.27	-0.06	0.01
6	0.07	0.03	-0.04	0.03	0.83	-0.09
7	-0.06	-0.02	0.06	-0.05	-0.74	0.08

From Table VI.7a it follows that the production of CO in the reaction scheme proposed in Table VI.5a depends mainly on three steps. Higher CO production rates can be obtained by

either increasing the methane activation step (1), or lower the oxygen activation step (2) or lower the adsorbed CO oxidation rate (4). On the other hand changing the CO desorption rate (5) does not influence the CO production rate.

Table VI.7b shows the data for performing a similar analysis for the case to the reaction scheme presented in Table VI.5b. In fact, it is clear that the adsorption of oxygen (step 1) followed by the oxidation of the carbon species (step 3) has a high impact on the formation of the selective products like CO and H_2. In the case of CO these two steps dominate even over the oxidation of adsorbed CO and its release to the gas phase oxygen has a still smaller impact.

There is a substantial difference for the hydrogen formation as the sorption has the strongest impact here and the oxidation of hydrogen has approximately the same importance as the oxygen adsorption. Nevertheless, considering the importance of the oxygen adsorption, thus the local oxygen coverage, and the above discussed role of ceria sites, it becomes clear why an oxygen exchange between Pt and ceria sites, i.e. the oxygen storage capacity of the support has such a prominent importance for the catalyst performance.

The microkinetic model offers thus an aid in catalyst development. On the other hand developing kinetic models based on rate-equation containing a single RDS will not capture all the details of the partial oxidation of methane mechanism.

VI.6.4. Influence of mass transfer limitations

Similar to the findings of de Smet et al. [43] we obtained higher methane and oxygen conversions and better CO selectivity in simulations in the absence of diffusion limitations.

VI.7. Conclusions

In present chapter the kinetics of the partial oxidation of methane has been studied over a Pt/PrCeZrO/α-Al_2O_3 supported on a triangular monolith. By running high flow velocities and using a suitable preheating, nearly isothermal conditions were obtained inside the monolith channel. Furthermore the catalyst temperature was measured directly by placing a thermocouple at the outside of the monolith.

By using a one-dimensional model that takes the mass transfer limitations into account it was possible to determine the intrinsic kinetics. A microkinetic model based on 5 elementary

steps for the oxidation of methane over platinum has shown already a reasonable description of the CH_4 conversion and CO selectivity. A further extended microkinetic model based on 7 elementary steps has been validated and this model allowed at short contact time a satisfying description of the experimental data. Nevertheless, at longer contact times, slower steps not consider in the present scheme gain apparently in relative importance. On the other hand, much more experimental data beyond the scope to this work would be needed to ensure proper parameter estimation for these extra steps. The same applies to reinforcing the estimation of parameters for the hydrogen production requiring e.g. an addition of hydrogen to the reactant mixture.

The data over the Pt/PrCeZrO/α-Al_2O_3 catalyst have been compared to literature data over a Pt gauze. In this way the role of ceria can be unraveled. Ceria provides a parallel reaction pathway for the oxidation of CO with a much lower energy barrier than over Pt. The microkinetic model takes into account the co-feeding of carbon dioxide thus the methane dry reforming. This occurs through the dissociation of carbon dioxide catalyzed by ceria. A reaction path analysis has revealed the main reaction steps for the production of carbon monoxide.

VI.8. Notation

C_j molar concentration of species j (mol/m_f^3)

d_h hydraulic diameter (m)

D molecular diffusion coefficient (m^2/s)

Da Damköhler number, $Da = \dfrac{r_j \delta_{wash} d_h}{4 C_j D}$

E_{act} activation energy (J/mol)

F_j molar flow rate of species j (mol/s)

k_j mass transfer coefficient from gas to solid interface for species j (m_f^3/m_s^2 s)

L reactor length (m)

Pr Prandtl number, $\mathrm{Pr} = \dfrac{C_p \mu}{\lambda_e}$

R gas constant (J/mol K)

R_j rate of disappearance of component j (mol/m^2_{cat} s)

R overall reaction rate

Re Reynolds number, $\mathrm{Re} = \frac{\rho u d_h}{\mu}$

Sc Schmidt number, $Sc = \frac{\mu}{\rho D}$

Sh Sherwood number, $Sh = \frac{k_g d_h}{D}$

T temperature (K)

u gas velocity (m/s)

V reactor volume (m_r^3)

W catalyst mass (kg)

X_{CH4} CH_4 conversion

z distance inside the monolith (m)

δ_{wash} thickness of the washcoat (m_s)

ΔH_R enthalpy of reaction (J/mol)

ΔS_R entropy of reaction (J/mol K)

λ_e effective thermal conductivity of the solid phase (J/m s K)

μ viscosity of the gas mixture (Pa s)

ρ density of the gas mixture (kg/m_f^3)

ρ_s catalyst density (kg/m_s^3)

Superscripts

0 inlet

p inside solid phase washcoat or particle)

s surface

Subscripts

j component or species

f fluid phase

r reactor

s solid phase

CHAPTER VII

General conclusion and perspectives

VII.1. General conclusion

VII.1.1. Background

The main goal of this research project was to elucidate mechanistic and kinetic features of the partial oxidation of methane (CPOM) reaction over structured catalysts based on the Pt supported on doped ceria-zirconia oxides. In order to investigate materials relevant for a future industrial application, it was decided to prepare and test single monolith channels coated with optimized substrates in the catalytic partial oxidation of methane at short contact times. This choice was motivated by an attempt to minimize the influence of mass and heat transfer under industrial conditions, but it should also be noted that the size of these structures are not down-scalable to the same extent as it is required for the flow rates under laboratory conditions.

Following the selection of the most promising catalyst composition, it was attempted to elucidate the reaction mechanism in view of the impact of oxygen species and its mobility in the surface/bulk of the supporting mixed oxides displaying a fluorite structure.

From the kinetic experiments over the studied structured catalyst, it was demonstrated that Pt is required to promote reforming reactions and that the doped CeO_2-ZrO_2 support itself has a significant activity in the oxidative activation of methane. Nevertheless, it was still possible to achieve a satisfying mathematical description of the experimental kinetic data with a model accounting essentially for active sites belonging to the Pt phase. This can be simply related to the fact that the activity of Pt sites remained significantly higher than that of the support. This finding is important to stress as the TAP investigations carried out on the mot performing systems indicate that a higher degree of oxidation for the mixed oxide support decreases the rate of methane activation. Thus, it is observed that the activation rates over the mixed oxides based systems are lower than those measured over a catalyst with an inactive oxide support, like a conventional Pt/Al_2O_3 catalyst. Obviously, this explains why the new formulas investigated in the present work prevent the formation of detrimental hot spot, which is one of the main problems in CPOM.

The main research strategy and the detailed objectives of this thesis were formulated after analyzing the state of the art reported in literature, attempting to answer still open and unsolved questions:

- Effect of different dopants and process parameters on the performance of single monolith channels with catalytic wall coatings comprising Pt as noble or Ni as base metal supported on doped CeO_2-ZrO_2 mixed oxides, under short contact time operating conditions. Thus it was undertaken to understand which factors, e.g. surface or bulk (or storage) effects determine the state of Pt necessarily contained in the catalyst composition.
- After various formulations screening and selection of the most performing ones, it was attempted to identify the key mechanistic features of CPOM over the selected systems in order to clearly reveal the interaction between the CeO_2-ZrO_2 mixed oxides and the supported Pt phase.
- The final goal of the project was to set-up a micro-kinetic model able to predict the performances of the best structured catalytic system over a wide range of process parameters. The key mechanistic features were used to identify the main pseudo-elementary steps of the process and formulate the related rate equations of a robust predictive model.

VII.1.2. Summary of the main experimental results

VII.1.2.1. Selection of catalyst formulations

From literature analysis and from preliminary lab-scale results, it was decided to screen monolithic catalysts based on CeO_2-ZrO_2 mixed oxide, pure or doped by Pr and Gd, as support and comprising an active phase being either lanthanum nickelate, pure or promoted by Pt, or Pt, pure or promoted by La. This screening under CPOM conditions allowed us to derive the following conclusions:

- The monolithic catalysts based on CeO_2-ZrO_2 mixed oxide support, optionally doped with Pr or Gd, and Pt as active component have been identified as the most promising formulas in CPOM. They were found to better perform in an oxidized state than the systems using lanthanum nickelate, pure or promoted by Pt, supported on a CeO_2-ZrO_2 mixed oxide, which require a pre-reduction to perform satisfactorily.
- The behavior of the studied catalysts in CPOM does not only depend on the chemical composition but also in a large extent on the pretreatment.

- Testing the selected catalysts in the dry reforming process with different process parameters showed that the catalyst doped by Pr had a better activity and selectivity. This phenomenon could be correlated to the bulk oxygen mobility of these systems.

VII.1.2.2. Mechanistic study of CPOM in the TAP reactor

The objective of TAP reactor experiments was to investigate detailed mechanistic features of CPOM over the previously selected catalysts, under conditions allowing fine tuning of the catalysts redox state. This presents a special challenge for these materials being bi-functional catalysts composed of Pt clusters supported on reducible ceria-based mixed oxide supports doped by Pr and Gd. A special attention was paid to the crucial role of oxygen species concentration linked to oxygen mobility for the catalytic performance, and the main features from this TAP study can be resumed as follows:

- TPD profiles of Pr and Gd doped samples are distinctively different because the Gd doped sample gives rise to low temperature oxygen desorption, while the Pr doped sample has no significant response until 350°C. Gd doping allows obviously the formation of adsorption sites carrying more weakly bound oxygen species then those formed on a Pr doped sample.
- Methane conversion is found lower for a dynamically oxidized catalyst (series of preinjected oxygen pulses) than for an outgased i.e., partially reduced system. This observation is probably related to the formation of oxygen species during the dynamic saturation which are more stable than those formed during the oxygen pump-pulse rapidly interacting with the outgased catalyst.
- From pump-probe experiments (alternating methane and oxygen pulses) after oxygen preinjection, the oxidized Pr doped powder sample was identified as more selective towards hydrogen. It should also be noted that the hydrogen release occurred more rapidly for the case of the Pr sample than for the Gd sample.
- From TAP study over a single monolith channel it was found that Pr preserves minimum syngas selectivity in all studied cases. The weakness of the Pr doped sample relates to the relatively slow formation of CO. It might be due to a build-up of carbonaceous species during atmospheric pressure operation. Such an

accumulation of CH_x species on the catalyst surface would inhibit its activity. The presence of CH_x species at the "working state" (i.e., after reaching a pseudo steady state close to the operating system at atmospheric pressure) is clearly confirmed for the Gd doped sample.

- The activity of the Pr doped catalyst is clearly lower than that of the Gd doped catalyst, for H_2 formation but mainly for the primary formation of CO.
- The Gd doped sample showed a complex behavior of performances as a function of the catalyst's oxidation state. The Gd-doped catalyst seems more selective towards synthesis gas at the "working state", but its selectivity suffers from an injection of additional oxygen. The Pr-doped catalyst reveals a more stable behavior showing no major loss in selectivity when the "working state" becomes altered or when oxygen and methane become injected with shorter time offset.

In a summary, the TAP study clearly revealed the impact of the oxidation state on the syngas formation. The responses by pulsing quasi simultaneously methane and oxygen ("working state") over catalytic single monolith channel were shown to be highly sensitive to the nature of the dopants added to the fluorite structured ceria/zirconia solid solution supporting the Pt phase.

From a methodological point of view, this work represents the first study using the TAP technique with short contact time and negligible thermal effect for investigating the CPOM reaction over a single monolith channel. The primary syngas gas formation was probed, while this demonstration remains an unachieved challenge for the very fast oxidation steps at atmospheric pressure.

VII.1.2.3. Kinetic study at atmospheric pressure

The direct use of the rate constants established from TAP data for a comprehensive kinetic model was judged not relevant enough because the state of the catalyst under vacuum conditions was hardly comparable to the one at atmospheric conditions, especially for oxygen storage capacity and mobility. Therefore a kinetic study was carried out at atmospheric pressure, revealing the following main features:

- Mass and heat transfer phenomena play an important role under the studied conditions. Accordingly, the reactor configuration and reactant preheating for kinetic experiments were optimized and the obtained temperature profile along the channel was reasonably flattened.
- The individual effect of process parameters, such as temperature, flow rate, CH_4/O_2 ratio, and addition of CO_2 to the reactant feed, preheating and dopant on the catalytic performance was studied for the Pt catalysts doped by Pr and Gd.
- The Pr doped catalyst showed better catalytic performances for the syngas production. It was demonstrated that CO, CO_2, H_2 and H_2O were the main products at oxygen conversions lower than 100%.
- From the changes in methane and oxygen conversion as a function of temperature and contact time, it was concluded that the rates of reactant conversion were strongly influenced by mass transfer phenomena.
- The reaction carried out over the Pt-free support led to a formation of some CO and H_2, but also to comparatively large quantities of CO_2 and H_2O. In turn, the support did not show significant efficiency in the dry reforming reaction.

From these statements, a new channel configuration with a first section coated only with the mixed oxide and a second one downstream with added Pt was designed and tested. As a matter of fact, it was foreseen that a first syngas production would occur in the first section where the O_2 concentration is still high, while the Pt containing section would favor the steam and dry reforming of the remaining methane to syngas with the water and carbon dioxide formed in the first section. This new configuration gave promising results in terms of stability on stream, but further optimization by adjusting the length of the different sections is needed to improve the syngas yield.

VII.1.2.4. Kinetic model

A micro-kinetic model describing CPOM over a Pt/PrCeZrO/α-Al_2O_3 catalyst supported on a single triangular monolith channel was successfully developed, by combining and improving existing models from the literature. Its main characteristics can be listed as follows:

- A one-dimensional model was modified to take the mass transfer limitations into account. As a result it was possible to estimate all the parameters of the intrinsic kinetics. A microkinetic model based on 5 elementary steps for the oxidation of methane over platinum showed in a first approach an already reasonable description of CH_4 conversion and CO selectivity.
- The data obtained over the Pt/PrCeZrO/α-Al_2O_3 catalyst has been compared to literature data over a Pt gauze. In this way the role of ceria was unraveled. Ceria provides a parallel reaction pathway for the oxidation of CO with a much lower energy barrier than over Pt.
- Contrary to the existing models, the microkinetic model developed in this study allows to take into account the co-feeding of carbon dioxide thus the methane dry reforming. This occurs through the dissociation of carbon dioxide catalyzed by ceria. A reaction path analysis has revealed the main reaction steps for the production of carbon monoxide.
- An extended microkinetic model based on 7 elementary steps was finally validated and this model allowed a satisfying description of the experimental data gained at short contact time. Nevertheless, at longer contact times, slower steps not considered in the present scheme might become important for the robustness of the model.

VII.2. Perspectives

Many aspects of the CPOM over a doped Pt / CeO_2-ZrO_2 catalyst coated on a single monolith channel could be investigated. However, other challenges beyond the scope of the present work were identified and some suggestions presented below would contribute to improve the developed kinetic model.

A central point in the formulation of a kinetic model for the reaction is whether the activation (decomposition) of methane proceeds via an oxidative or in a non-oxidative process. Currently methane activation on Pt seems to proceed by a non-oxidative process and the activation on the support in an oxidative step, requiring to include both contributions for a further refined model. The challenge in such an investigation is related to i) Pt dispersion impacting on methane activation and ii) the clear influence of the support as well.

There is some indication in the presented TAP experiments over Pt black and Pt supported on Al_2O_3 that the over oxidation of hydrogen becomes limited using more dispersed Pt. Such an assumption could even explain why de Smet et al. did not observed hydrogen production using poorly dispersed (bulk or massive) Pt in the form of a gauze, while Hickman and Schmidt using a supported Pt catalyst noted hydrogen formation. However a direct relationship between a higher degree of Pt dispersion and a decreased secondary oxidation of adsorbed hydrogen to water might either relate to a faster hydrogen desorption (possibly local coverage effects) or to secondary reactions yielding additional hydrogen.

- Additional TAP experiments pulsing methane on the surface of catalyst are required for new insight in methane decomposition in the absence of oxygen and at different well defined Pt dispersions. Complementary experiments with small quantities of added oxygen should help as well.
- A direct investigation of hydrogen adsorption would be highly interesting but the absence of clear pulse responses under the wide range of conditions explored in this work suggest more studies with other techniques like H_2-TPA / TPD or a calorimetric work potentially also using pulse-wise hydrogen addition to yield more kinetic information.
- The addition of CO_2 to the reactant feed performing the kinetic study at ambient pressure was found highly beneficial as it allowed the estimation of more kinetic parameters compared to studies reported in literature. The addition of water for investigating hydrogen production, would provide the same benefits. Similarly, the addition of hydrogen to the reactant mixture during the steady-state kinetic experiments at atmospheric pressure should allow to refine the kinetic model, also accounting for the experimentally established activity of the CeO_2-ZrO_2 support. The way that oxygen, needed for the oxidative activation of methane on the support, is activated either directly on the support or on Pt and then supplied to the support, also deserves further investigation.
- Obviously, a more profound investigation comparing the results of O_2-TPD, O_2-TPA and isotopic exchange experiments with the base support, the Pt modified support and Pt supported on Al_2O_3 could also provide valuable information.

Finally, the validation of this kinetic model with experimental data obtained at pilot scale level would be the ultimate proof of its robustness.

REFERENCES

[1] S. Cornot-Gandolphe. Changes in world gas reserves and resources // J. Energy Explore. Exploit. - 1995. - V. 13 - P. 3 -17.

[2] British Petroleum. Review of World Gas, B.P. Gas International - London, 1987.

[3] Y. Liu, T. Hayakawa, T. Ishii, M. Kumagai, H. Yasuda, K. Suzuki, S. Hamakawa and K. Murata. Methanol decomposition to synthesis gas at low temperature over palladium supported on ceria-zirconia solid solutions // Appl. Catal. - A: Gen. - 2001. - V. 210. - P. 301 - 314.

[4] S. Murcia-Mascaros, R.M. Navarro, L. Gomez-Sainero , U. Costantino, N. Nocchetti and J.L.G.Fierro. Oxidative Methanol Reforming Reactions on CuZnAl Catalysts Derived from Hydrotalcite-like Precursors // J. Catal. - 2001. - V. 198. – P. 338 - 347.

[5] R. Lago, G. Bini, M.A. Pena and J.L.G. Fierro. Partial Oxidation of Methane to Synthesis Gas Using $LnCoO_3$ // J. Catal. – 1997. – V. 167. – P. 198 – 209.

[6] N. Nichio, M. Casella, O. Ferretti, M. Gonzalez, C. Nicot, B. Moraweck and R. Frety. Partial oxidation of methane to synthesis gas. Bihaviour of different Ni supported catalysts // Catal. Lett. – 1996. – V. 42. – P. 65 – 72.

[7] A.A. Lemonidou, A.E. Stabouli, G.J. Tjatjopoulos and I.A. Vasalos. Partial oxidation of methane to synthesis gas over unpromoted and (0.1-0.5 wt%) Ni-promoted cacium aluminate catalysts // Catal. Lett. – 1997. – V. 43. – P. 235 – 240.

[8] S. Tang, J. Lin and K. Tan. Partial oxidation of methane to syngas over Ni/MgO, Ni/CaO and Ni/CeO_2 // Catal. Lett. – 1998. – V. 51. – P. 169 – 175.

[9] D.A. Hickman, E.A. Haupfear and L.D. Schmidt. Syngas formation by direct oxidation of methane over Rh monoliths // Catal. Lett. – 1993. – V. 17. – P. 223.

[10] F. Fischer and H. Tropsch. // Brennstoff-Chem – 1928. – V. 9. – P. 39.

[11] T. Sodesawa, A. Dobash and F. Nozaki. Catalytic reaction of methane with carbon dioxide // React. Kinet. Catal. Lett. – 1979. - V. 12. – P. 107 – 111.

[12] A. Guerrero-Ruiz, I. Rodriguez-Ramos and A. Sepúlveda-Escribano. // J. Chem. Soc., Chem. Commun. – 1993. – P. 487.

[13] A.M. Gadalla and M.E. Sommer. Synthesis and characterization of catalysts in the system Al_2O_3-MgO-NiO-Ni for methane reforming with CO_2 // J. Am. Ceram. Soc. – 1989. – V. 72. – P. 683 – 687.

[14] A.M. Gadalla and M.E. Sommer. Carbon dioxide reforming of methane on nickel catalysts // Chem. Eng. Sci. – 1989. –V. 44. – P. 2825 – 2829.

[15] O. Yamazaki, T. Nozaki, K. Omata and K. Fujimoto. Reduction of carbon dioxide by methane with Ni-on-MgO-CaO containing catalysts // Chem. Lett. – 1992. – V. 21. – P. 1953.

[16] P.D.F. Vernon, M.L.H. Green, A.K. Cheetham and A.T. Ashcroft. Partial oxidation of methane to synthesis gas, and carbon dioxide as an oxidising agent for methane conversion // Catal. Today – 1992. – V. 13. – P. 417 – 426.

[17] J.R. Rostrup-Nielsen and J.-H. Bak Hansen. CO_2-Reforming of methane over transition metals // J. Catal. – 1993. – V. 144. – P. 38 - 49.

[18] J.T. Richardson and S.A. Paripatyadar. Carbon dioxide reforming of methane with supported rhodium // Appl. Catal. – 1990. – V. 61. – P. 293 – 309.

[19] J.S.H.Q. Perera, J.W. Couves, G.Sankar and J.M. Thomas. The catalytic activity of Ru and Ir supported on Eu_2O_3 for the reaction, $CO_2 + CH_4 = 2H_2 + 2CO$: a viable solar-thermal energy system // Catal. Lett. – 1991. – V. 11. – P. 219 – 225.

[20] P. Pantu, G.R. Gavalas. Methane partial oxidation on Pt/CeO_2 and Pt/Al_2O_3 catalysts // Appl. Catal. A: Gen. – 2002. – V. 223. – P. 253 – 260.

[21] D.A. Hickman, L.D. Schmidt. Production of syngas by direct catalytic oxidation of methane // Science – 1993. - V. 259. – P. 343 – 346.

[22] K.H. Hofstad, J.H.B.J Hoebink, A. Holmen, G.B. Marin. Partial oxidation of methane to synthesis gas over rhodium catalysts // Catal. Today – 1998. – V. 40. – P. 157-170.

[23] E.P.J. Malens, J.H.B.J Hoebnik, G.B. Marin. The reaction mechanism of the partial oxidation of methane to synthesis gas: a transient kinetic study over rhodium and a comparison with platinum // J. Catal. – 1997. - V. 167. – P. 43 – 56.

[24] M. Fathi, F. Monnet, Y. Schuurman, A. Holmen, C. Mirodatos. Reactive oxygen species on platinum gauzes during partial oxidation of methane into synthesis gas // J. Catal. – 2000. - V. 190. – P. 439 – 445.

[25] M. Fathi, E. Bjorgum, T. Viig, O.A. Rokstad. Partial oxidation of methane to synthesis gas: elimination of gas phase oxygen // Catal. Today – 2000. – V. 63. – P. 489 – 497.

[26] H.C. Yao, Y.F. Yu Yao. Ceria in automotive exhaust catalysts I: oxygen storage // J. Catal. – 1984. - V. 86. – P. 254 – 265.

[27] A. Holmgren, B. Andersson. Oxygen storage dynamics in $Pt/CeO_2/Al_2O_3$ catalysts // J. Catal. – 1998. - V. 178. – P. 14 – 25.

[28] K. Otsuka, K. Wang, E. Sunada, I. Yamanaka. Direct partial oxidation of methane to synthesis gas by cerium oxide // J. Catal. – 1998. - V. 175. – P. 152 – 160.

[29] H. He, H.X. Dai, L.H. Ng, K.W.Wong, C.T. Au. Pd-, Pt-, and Rh-loaded $Ce_{0.6}Zr_{0.35}Y_{0.05}O_2$ three-way catalysts: an investigation on performance and redox properties // J. Catal. – 2002. - V. 206. – P. 1 – 13.

[30] K. Otsuka, Y. Wang, M. Nakamura. Direct conversion of methane to synthesis gas through gas-solid reaction using CeO_2-ZrO_2 solid solution at moderate temperature // Appl. Catal. A: Gen. – 1999. – V. 317 – 324.

[31] D. Neumann, M. Kirchhoff and G. Veser. Catalytic partial oxidation of methane over a 4% Rh/α-Al_2O_3 catalyst: Part I: Kinetic study in annular reactor // Catal. Today – 2004. – V. 98. – P. 565 – 574.

[32] P. Aghalayam, Y.K. Park and D.G. Vlachos. Partial oxidation of light alkanes in short contact time microreactors // Catalysis – 2000. – V. 15. – P. 98 - 134.

[33] L. Basini, K. Aasberg-Petersen, A. Guarinoni and M. Ostberg. Catalytic partial oxidation of natural gas at elevated pressure and low residence time // Catal. Today - 2001 – V. 64. – P. 9 -20.

[34] E.P.J. Mallens, J.H.B.J. Hoebink and G.B. Marin. The Reaction mechanism of the partial oxidation of methane to synthesis gas: a transient kinetic study over rhodium and a comparison with platinum // J. Catal. – 1997. - V. 167 – P. 43 - 56.

[35] I. Tavazzi, A. Beretta, G. Groppi and P. Forzatti. Development of a molecular kinetic scheme for methane partial oxidation over a $Rh/\alpha\text{-}Al_2O_3$ catalyst // J. Catal. – 2006. - V. 241. - P. 1 – 13.

[36] D. Wang, O. Dewaele, A.M. De Groote and G.F. Froment. Reaction mechanism and role of the support in the partial oxidation of methane on Rh/Al_2O_3 // J. Catal. – 1996. – V. 159. – P. 418 - 426.

[37] R. Schwiedernoch, S. Tischer, C. Correa and O. Deutschmann. Experimental and numerical study on the transient behavior of partial oxidation of methane in a catalytic monolith // Chem. Eng. Sci. – 2003. – V. 58. – P 633 - 642.

[38] O.V. Buyevskaya, D. Wolf and M. Baerns. Rhodium-catalyzed partial oxidation of methane to CO and H_2. Transient studies on its mechanism // Catal. Lett. – 1994. – V. 29 - P. 249 – 260.

[39] Z. Tian, O. Dewaele and G.B. Marin. The state of Rh during the partial oxidation of methane into synthesis gas // Catal. Lett. – 1999. – V. 57. - P. 9 - 17.

[40] E. Ruckenstein and H.Y. Wang. Effect of support on partial oxidation of methane to synthesis gas over supported rhodium catalysts // J. Catal. – 1999. – V. 187. - P. 151 - 159.

[41] A. Beretta, P. Baiardi, D. Prina, and P. Forzatti. Analysis of a catalytic annular reactor for very short contact times // Chem. Eng.Sci. - 1999. – V.54. – P. 765.

[42] C.R.H. de Smet, M.H.J.M. de Croon, R.J. Berger, G.B. Marin and J.C. Schouten. An experimental reactor to study the intrinsic kinetics of the catalytic partial oxidation of methane in the presence of heat-transport limitations // Appl. Catal. A: General – 1999. - V.187. – P. 33 - 48.

[43] C.R.H. de Smet, M.H.J.M. de Croon, R.J. Berger, G.B. Marin and J.C. Schouten. Kinetics for the partial oxidation of methane on a Pt gauze at low conversions // AIChE J. – 2000. – V. 46. – P. 1837 – 1849.

[44] M. Maestri, A. Beretta, G. Groppi, E. Tronconi and P. Forzatti. Comparison among structured and packed-bed reactors for the catalytic partial oxidation of CH_4 at short contact times // Catal. Today – 2005. - V. 105. - P. 709 - 717.

[45] K.L. Hohn and L.D. Schmidt. Partial oxidation of methane to syngas at high space velocities over Rh-coated spheres // Appl. Catal. A: Gen. – 2001. – V. 211. - P. 53 - 68.

[46] A.P.E. York, X. Tiancun, M.L.H. Green. Brief overview of the partial oxidation of methane to synthesis gas // Top. Catal. – 2003. – V. 22. – 345 – 358.

[47] H. Liander. Utilization of natural gases for the ammonia process // Trans. Faraday Soc. – 1929. - V. 25. – P. 462 – 472.

[48] C. Padovani and P. Franchetti. // Giorn. Chem. Ind. Appl. Catal. – 1933. – V. 15. – P. 429.

[49] M. Prettre, Ch. Eichner and M. Perrine. Catalytic oxidation of methane to carbon monoxide and hydrogen // Trans. Faraday Soc. – 1946. - V. 42. – P. 335 - 340.

[50] V.R. Choudhary, S.R. Sansare, A.S. Mamman. Low-temperature selective oxidation of methane to carbon monoxide and hydrogen over cobalt-MgO catalysts // Appl. Catal. A: Gen. – 1992. - V. 90. – P. L1 - L5.

[51] V.R. Choudhary, V.H. Rane, B. Prabhakar. Low temperature oxidative conversion of methane to syngas over NiO-CaO catalyst // Catal. Lett. – 1992. – V. 15. – P. 363 - 370.

[52] V.R. Choudhary, A.M. Rajput, V.H. Rane. Low temperature oxidative conversion of methane to synthesis gas over Co-rare-earth oxide catalysts // Catal. Lett. – 1992. – V. 16. – P. 269 - 272.

[53] V.R. Choudhary, V.H. Rane, A.M. Rajput. Selective oxidation of methane to CO and H_2 over unreduced NiO-rare-earth oxide catalysts // Catal. Lett. – 1993. – V. 22. – P. 289 - 297.

[54] W.J.M. Vermeiren, E. Blomsma, P.A. Jacobs. Catalytic and thermodynamic approach of the oxyreforming reaction of methane // Catal. Today – 1992. – V. 13. – P. 427 – 436.

[55] T. Zhu and M. Flytzani-Stephanopoulos. Catalytic partial oxidation of methane to synthesis gas over Ni-CeO_2 // Appl. Catal. A: Gen. – 2001. - V. 208. – P. 403 - 417.

[56] W. Chu, Q. Yan, S. Liu and G. Xiong. // Stud. Surf. Sci. Catal. – 2000. - V. 130D. – P. 3573.

[57] W. Chu, Q. Yan, X. Liu, Q.Li, Z.Yu and G. Xiong. Rare earth promoted nickel catalysts for the selective oxidation of natural gas to syngas // Stud. Surf. Sci. Catal. – 1998. – V. 119. – P. 849 – 854.

[58] V.A. Tsipouriari and X.E. Verykios. Kinetic study of the catalytic partial oxidation of methane to synthesis gas over Ni/La_2O_3 catalyst // Stud. Surf. Sci. Catal. – 1998. – V. 119. – P. 795 – 800.

[59] Y.Lu, Y.Liu and S. Shen. Design of stable Ni catalysts for partial oxidation of methane to synthesis gas // J. Catal. – 1998. – V. 177. – P. 386 – 388.

[60] S.Liu, G.Xiong, H.Dong, W.Yang, S.Sheng, W.Chu and Z.Yu. // Stud. Surf. Sci. Catal. – 2000. - V. 130D. – P. 3567.

[61] D.B. Meadowcroft. Low-cost oxygen electrode material // Nature – 1970. – V. 226. – P. 847.

[62] T. Seiyama. Total oxidation of hydrocarbons on perovskite oxides // Catal. Rev.-Sci. Eng. – 1992. – V. 34. – P. 281-300.

[63] J.W. Nam, H. Chae, S.H. Lee, H. Jung, K.Y. Lee. Methane dry reforming over well-dispersed Ni catalyst prepared from perovskite-type mixed oxides // Stud. Surf. Sci. Catal. – 1998. - V. 119. – P. 843 – 848.

[64] T. Hayakawa, H. Harihara, A.G. Andersen, A.P.E. York, K. Suzuki, H. Yasuda, K. Takehira. A sustainable catalyst for the partial oxidation of methane to syngas: Ni/$Ca_{1-x}Sr_xTiO_3$, prepared in situ from perovskite precursors // Chem. Int. Ed. Eng. – 1996. – V. 35. – P. 192 - 195.

[65] W. Chu, W.G. Yan, X. Liu, Q. Li, Z.L. Yu, G.X. Xiong. Rare earth promoted nickel catalysts for the selective oxidation of natural gas to syngas // Stud. Surf. Sci. Catal. – 1998. – V. 119. - 849-854.

[66] Z. Zhang, X.E. Verikios. Carbon dioxide reforming of methane to synthesis gas over Ni/La_2O_3 catalysts // Appl. Catal. A: Gen. – 1996. - V. 138. – P. 109 - 133.

[67] P. Chen, H.B. Zhang, G.D. Lin, K.R. Tsai. Development of coking-resistant Ni-based catalyst for partial oxidation and CO_2-reforming of methane to syngas // Appl. Catal. A: Gen. – 1998. - V. 166. – P. 343 - 350.

[68] A.T. Ashcroft, A.K. Cheetham, J.S. Foord, M.L.H. Green, C.P. Grey, A.J. Murrel and P.D.F. Vernon. Selective oxidation of methane to synthesis gas using transition metal catalysts // Nature – 1990. – V. 344. – P. 319 – 321.

[69] P.D.F. Vernon, M.L.H. Green, A.K. Cheetham and A.T. Ashcroft. Partial oxidation of methane to synthesis gas // Catal. Lett. – 1990. – V. 6. – P. 181 – 186.

[70] P.D.F. Vernon, M.L.H. Green, A.K. Cheetham and A.T. Ashcroft. Partial oxidation of methane to synthesis gas, and carbon dioxide as an oxidising agent for methane conversion // Catal. Today – 1992. – V. 13. – P. 417 – 426.

[71] S.C. Tsang, J.B. Claridge and M.L.H. Green. Recent advances in the conversion of methane to synthesis gas // Catal. Today – 1995. – V. 23. – P. 3 – 15.

[72] J.B. Claridge, M.L.H. Green, S.C. Tsang, A.P.E. York, A.T. Ashcroft and P.D. Battle. A study of carbon deposition on catalysts during the partial oxidation of methane to synthesis gas // Catal. Lett. – 1993. – V. 22. – P. 299 – 305.

[73] D.A. Hickman, L.D. Schmidt. Syngas Formation by Direct Catalytic Oxidation of Methane // J. Catal. – 1992. – V. 138. – P. 267 – 282.

[74] K. Heitnes, S. Lindberg, O.A. Rokstad, A. Holmen. Catalytic partial oxidation of methane to synthesis gas using monolithic reactors // Catal. Today – 1994. – V. 21. – P. 471 – 480.

[75] K. Heitnes, S. Lindberg, O. A. Rokstad, A. Holmen. Catalytic partial oxidation of methane to synthesis gas // Catal. Today – 1995. – V. 24. – P. 211 – 216.

[76] A.G. Dietz, L. D. Schmidt. Effect of pressure on three catalytic partial oxidation reactions at millisecond contact times // Catal. Lett. – 1995. – V. 33. – P. 15 – 29.

[77] K. Heitnes, T. Sperle, O.A. Rokstad, A. Holmen. Partial oxidation of methane to synthesis gas over a Pt/10% Rh gauze // Catal. Lett. – 1997. – V. 45. – P. 97 – 105.

[78] R.P. O'Connor, E.J. Klein, L.D. Schmidt. High yields of synthesis gas by millisecond partial oxidation of higher hydrocarbons // Catal. Lett. – 2000. – V. 70. – P. 99 – 107.

[79] Johnson –Matthey. http://www.johnsonmattheyny.com

[80] M. Flytzani-Stephanopoulos and G. E. Voecks. Autothermal reforming of aliphatic and aromatic hydrocarbon liquids // Int. J. Hydrogen Energy – 1983. – V. 8. – P. 539 – 548.

[81] R. Krüger, A. Voß. Systemanalytischer Vergleich inovativer Kraftstoffe und Antriebssysteme // VDI-Berichte – 2000. – V. 1565. - P. 493 – 528.

[82] J. Kašpar, P. Fornasiero, M. Graziani. Use of CeO_2-based oxides in the three-way catalysis // Catal. Today – 1999. – V. 50. – P. 285 – 298.

[83] V.A. Sadykov, T.G. Kuznetsova, Yu. V. Frolova-Borchert, N.V. Mezentseva, G.M. Alikina, A. I. Lukashevich, et. al. Fuel-rich methane combustion: Role of the Pt dispersion and oxygen mobility in a fluorite-like complex oxide support // Catalysis Today – 2006. - V. 117. – P. 475 – 483.

[84] M. Mogensen, N.M. Sammes, G.A. Tompsett. Physical, chemical and electrochemical properties of pure and doped ceria // Solid State Ionics. - 2000. – V. 129. – P. 63 –94.

[85] K. Takanabe, K. Aika, K. Seshan, L. Lefferts. Sustainable hydrogen from bio-oil – steam reforming of acetic acid as a model oxygenate // J. Catal. – 2004. – V. 227 – P. 101 – 108.

[86] M. Ozava, M. Kimura, A. Isogai. The application of Ce---Zr oxide solid solution to oxygen storage promoters in automotive catalysts // J. Alloys Comp. – 1993. - V. 193. - P. 73 –75.

[87] T. Murota, T. Hasegawa, S. Aozasa, H. Matsui, M. Motoyama. Production method of cerium oxide with high storage capacity of oxygen and its mechanism // J. Alloys Comp. – 1993. - V. 193. - P. 298 – 299.

[88] Y. Yashima, T. Hirose, S. Katano, Y. Suzuki, M. Kakihana, M. Yoshimura. Structural changes of ZrO_2-CeO_2 solid solutions around the monoclinic-tetragonal phase boundary // Phys. Rev. B. – 1995. – V. 51. – P. 8018 – 8025.

[89] Y. Yashima, K. Marimoto, N. Ishizawa, M. Yoshimura. Diffusionless tetragonal-cubic transformation temperature in zirconia-ceria solid solution // J. Am. Ceram. Soc. – 1993. - V. 76. – P. 2865 - 2868.

[90] Y. Yashima, K. Marimoto, N. Ishizawa, M. Yoshimura. Zirconia-ceria solid solution synthesis and the temperature-time-transformation diagram for the 1:1 composition // J. Am. Ceram. Soc. – 1993. - V. 76. – P. 1745 - 1750.

[91] S. Meriani. Metastable tetragonal CeO_2-ZrO_2 solid solution // J. De Physique. – 1986. – V. 47. – P. C1.485 – C1.489.

[92] H. Shui-gen, L. Lin. Phase diagram calculation and fabrication of multi-component zirconia-based ceramics // J. Shanghai University. – 2005. – V. 9. – P. 358 – 360.

[93] E. Tani, M. Yoshimura, S. Somiya. Revised phase diagram of the system ZrO_2-CeO_2 below 1400°C // J. Am. Ceram. Soc. – 1983. - V. 66. – P. 506 - 1750.

[94] Y. Yashima, H. Arashi, M. Kakihana, M. Yoshimura. Raman scattering study of cubic-tetragonal phase transition in $Zr_{1-x}Ce_xO_2$ solid solution // J. Am. Ceram. Soc. – 1994. - V. 77. – P. 1067 - 1071.

[95] P. Fornasiero, G. Balducci, R. Di Monte, J. Kašpar, V. Sergo, G. Gubitosa, A. Ferrero, M. Graziani. Modification of the redox behaviour of CeO_2 induced by structural doping with ZrO_2 // J. Catal. – 1996. – V. 164. – P. 173 - 183.

[96] V. Longo and D. Minichelli. // J. Am. Ceram. Soc. 1973. – V**. 56.** - P. 1186.

[97] A. Kawabata, S. Hirano, M. Yoshinaka, K. Hirota and O. Yamaguchi. Solid solutions of metastable tetragonal ZrO_2 and Ce_3ZrO_8 in the system ZrO_2-CeO_2 // J. Mater. Sci. – 1996. – V. 31. – P. 4945 – 4949.

[98] A. I. Leonov, A. B. Andreeva, and E. K. Keler. Influence of the gas atmosphere on the reaction of zirconium dioxide with oxides of cerium // Izv. Akad. Nauk SSSR, Neorg. Mater. –1966. – V. 2. – P. 137–144.

[99] M. Pijolat, M. Prin, M. Soustelle, O. Touret and P. Nortier. Thermal stability of doped ceria: experiment and modeling // J. Chem. Soc., Faraday Trans. – 1995. – V. 91. – P. 3941 – 3948.

[100] P. Fornasiero, R. Di Monte, G. Ranga Rao, J. Kašpar, S.Meriani, A. Trovarelli, M. Graziani. Rh-loaded CeO_2-ZrO_2 solid solutions as highly efficient oxygen exchangers: dependence of the reduction behavior and the oxygen storage capacity on the structural properties // J. Catal. – 1995.- V. 151. – P. 168 – 177.

[101] C.E. Hori, H. Permana, K.Y.S. Ng, A. Brenner, K. More, K.M. Rahmoeller, D. Belton. Thermal stability of oxygen storage properties in a mixed CeO_2-ZrO_2 system // Appl. Catal. B: Environ. – 1998. – V. 16. – P. 105 – 117.

[102] A. Trovarelli, F. Zamar, J. Llorca, C. de Leitenburg, G. Dolcetti, J. Kiss. Nanophase fluorite-structured CeO_2-ZrO_2 catalysts prepared by high-energy mechanical milling // J. Catal. – 1997. – V. 169. – P. 490 - 502.

[103] U.S. Patent 3 330 697. Method of preparing lead and alkaline earth titanates and niobates and coating method using the same to form a capacitor / M. P. Pechini, filed 08.1963, patented 11.07.1967.

[104] S.P. Simner, P-W. Wu, B. Dunn. Solution processing approaches for solid electrolytes and electrode materials // J. Mater. Res. – 1998. - V. 13. – 4. - P. 866 - 874.

[105] M. Liu, D. Wang. Preparation of $La_{1-z}Sr_zCo_{1-y}Fe_yO_{3-x}$ thin films, membranes and coatings on dense and porous substrates // J. Mater. Res. – 1995. - V. 10. – 12. – P. 3210 - 3221.

[106] P.A. Lessing. Mixed-cation oxide powders via polymeric precursors // Ceram. Bull. – 1989. – V. 68. – 5. - P. 1002 - 1007.

[107] J. Ma, M. Yoshimuro, M. Kakihana, M. Yashima. Synthesis of ZrO_2-Y_6WO_{12} solid solution powders by a polymerized complex method // J. Mater. Res. – 1998. – V. 13. – 4. - P. 939 - 943.

[108] V. Perrichon, A. Laashir, S.Abouarnadasse, O. Touret and G. Blanchard. Thermal stability of a high surface area ceria under reducing atmosphere // Appl. Catal. A: Gen. – 1995. – V. 129. – P. 69 - 82.

[109] C. de Leitenburg, A. Trovarelli, F. Zamar, S. Maschio, G. Dolcetti, J. Llorca. A novel and simple route to catalysts with high oxygen storage capacity: the direct room-temperature synthesis of CeO_2-ZrO_2 solid solutions // J. Chem. Soc., Chem. Commun. – 1995. – V. 21. – P. 2181 – 2182.

[110] E. Rogemond, N. Essayem, R. Fréty, V. Perrichon, M. Primet,S. Salasc, M. Chevrier, C. Gauthier, F. Mathis. Measurement of the ceria surface area of a three-way commercial catalyst after laboratory and engine bench aging // Stud. Surf. Sci. Catal. – 1998. – V. 116. - P. 137 - 146.

[111] G.Balducci, P.Fornasiero, R.Di Monte, J.Kašpar, S.Meriani, M.Graziani. An unusual promotion of the redox behaviour of CeO2-ZrO2 solid solutions upon sintering at high temperature // Catal. Lett. – 1995. – V. 33. – P. 193 - 200.

[112] A. Trovarelli, C. de Leitenburg, and G. Dolcetti. Design better cerium-based oxidation catalyst // Chemtech. – 1997. – V. 27. – P. 32 - 37.

[113] J.P. Cuif, G. Blanchard, O. Touret, A. Seigneurin, M. Marczi and E. Quémeré. // Soc. Autom. Eng. – 1996. - P. 961906.

[114] J. Kašpar, P. Fornasiero, G. Balducci, R. Di Monte, N. Hickey and V. Sergo. Effect of ZrO_2 content on textural and structural properties of CeO_2-ZrO_2 solid solutions made by citrate complexation route // Inorganica Chimica Acta – 2003. – V. 349. – P. 217 - 226.

[115] J. Kašpar, R. Di Monte, P. Fornasiero, M. Graziani, H. Bradshaw, and C. Norman. Dependency of the Oxygen Storage Capacity in Zirconia-Ceria Solid Solutions upon Textural Properties // Top.Catal. – 2001. - V.16/17. – P. 83.

[116] R. Di Monte and J. Kašpar. Nanostructured CeO_2-ZrO_2 mixed oxide // J. Mater. Chem., - 2005. – V. 15. – P. 633 - 648.

[117] E. Rohart, O. Larcher, S. Deutsch, C. Hedouin, H. Aimin, F. Fajardie, M. Allain, and P. Macaudiere. From Zr-rich to Ce-rich: thermal stability of OSC materials on the whole range of composition // Top.Catal. – 2004. – V. 30/31. – P. 417 - 423.

[118] S. Rossignol, F. Gerard, and D. Duprez. Effect of the preparation method on the properties of zirconia–ceria materials // J. Mater. Chem. – 1999. - V. 9 – P. 1615 - 1620.

[119] A.L. Quinelato, E.Longo, E.R. Leite, M.I.B. Bernardi, and J.A. Varela. Effect of ceria content on the sintering of ZrO_2 based ceramics synthesized from a polymeric precursor // J. Mater. Sci. – 2001. - V. 36. – P. 3825 - 3830.

[120] O.A. Kirichenko, G.W. Graham, W. Chun, and R.W. McCabe. Effect of coprecipitation conditions on the surface area, phase composition, and reducibility of CeO_2-ZrO_2-Y_2O_3 materials for automotive three-way catalysts // Stud. Surf. Sci. Catal. – 1998. – V. 118. – P. 411-420.

[121] J.G. Duh, H.T. Dai and B.S. Chiou. Sintering, Microstructure, Hardness and Fracture Toughness Behaviour of Y_2O_3-CeO_2-ZrO_2 // J. Am. Ceram. Soc. – 1988. – V. 71. - P. 813-819.

[122] J.G. Duh, H.T. Dai and W.Y. Hsu. Synthesis and Sintering Behaviour in CeO_2-ZrO_2 Ceramics // J. Mater. Sci. – 1988. – V. 23. - P. 2786-2791.

[123] J.Z. Shyu, W.H. Weber, and H.S. Gandhi. Surface characterization of alumina-supported ceria // J. Phys. Chem. – 1988. – V. 92. – P. 4964 – 4970.

[124] T. Miki, T. Ogawa, A. Ueno, S. Matsuura, M. Sato, Chem. Lett. –1988. – P. 565.

[125] R. Di Monte, P. Fornasiero, J. Kašpar, P. Rumori, G. Gubitosa, and M. Graziani. $Pd/Ce_{0.6}Zr_{0.4}O_2/Al_2O_3$ as advanced materials for three-way catalysts - Part 1. Catalyst characterisation, thermal stability and catalytic activity in the reduction of NO by CO // Appl. Catal. B: Environ. – 2000. - V. 24. – P. 157 -167.

[126] R. Di Monte, P. Fornasiero, J. Kašpar, M. Graziani, J.M. Gatica, S. Bernal, and A. Gomez Herrero. Stabilisation of nanostructured $Ce_{0.2}Zr_{0.8}O_2$ solid solution by impregnation on Al_2O_3: a suitable method for the production of thermally stable oxygen storage/release promoters for three-way catalysts // Chem. Commun. - 2000. – V. 21. - P. 2167 - 2168.

[127] R. Di Monte, P. Fornasiero, S. Desinan, J. Kašpar, J. M. Gatica, J. J. Calvino and E. Fonda. Thermal stabilization of $Ce_xZr_{1-x}O_2$ oxygen storage promoters by addition of Al_2O_3: effect of thermal aging on textural, structural, and morphological properties // Chem. Mater. – 2004. – V. 16. – P. 4273 - 4285.

[128] M. Fernández-García, A. Martínez-Arias, A. Iglesias-Juez, C. Belver, A.B. Hungría, J.C. Conesa and J. Soria. Structural Characteristics and Redox Behavior of CeO_2–ZrO_2/Al_2O_3 Supports // J. Catal. – 2000. – V. 194. - P. 385 - 392.

[129] M. Fernández-García, A. Martínez-Arias, A. Iglesias-Juez, A.B. Hungría, J.A. Anderson, J.C. Conesa and J. Soria. New $Pd/Ce_xZr_{1-x}O_2/Al_2O_3$ three-way catalysts prepared by microemulsion Part 1. Characterization and catalytic behavior for CO oxidation // Appl. Catal. B: Environ. – 2001. – V. 31. - P. 39 - 50.

[130] A.I. Kozlov, D.H. Kim, A. Yezerets, P. Andersen, H.H. Kung, and M.C. Kung. Effect of preparation method and redox treatment on the reducibility and structure of supported ceria–zirconia mixed oxide // J. Catal. – 2002. – V. 209. – P. 417 - 426.

[131] J. Kašpar and P.Fornasiero. Nanostructured materials for advanced automotive de-pollution catalysts // J. Solid State Chem. – 2003. – V. 171. – P. 19 - 29.

[132] J. Kašpar and P. Fornasiero. "Structural properties and thermal stability of ceria-zirconia and related materials" in: "Catalysis by Ceria and Related Materials"// A.Trovarelli (Ed.), Chap.6, Imperial College Press, London – 2002. - P. 217 - 241.

[133] C. Janvier, M. Pijolat, F. Valdivieso, M. Soustelle, and C. Zing. Thermal stability of $Ce_{1-x}Zr_xO_2$ solid solution powders // J. European Ceram. Soc. – 1998. – V. 18. – P. 1331 - 1337.

[134] R. Di Monte and J. Kašpar, J. Mater. Chem. – 2004. - DOI:10.1039/B414244F.

[135] J.M.Dominguez, J.L.Hernandez, and G.Sandoval. Surface and catalytic properties of Al_2O_3–ZrO_2 solid solutions prepared by sol–gel methods // Appl. Catal. A: Gen. – 2000 – V. 197. – P. 119 - 130.

[136] L. Gao, Q. Liu, J.S. Hong, H. Miyamoto, S.D.De la Torre, A. Kakitsuji, K. Liddell, and D.P. Thompson. Phase transformation in the Al_2O_3/ZrO_2 system // J. Mater. Sci. – 1998. – V. 33. – P. 1399 – 1403.

[137] T. Horiuchi, Y. Teshima, T. Osaki, T. Sugiyama, K. Suzuki, and T. Mori. Improvement of thermal stability of alumina by addition of zirconia // Catal. Lett. – 1999. – V. 62. – P. 107 - 111.

[138] J. Soria, J.M. Coronado, and J.C. Conesa. Spectroscopic study of oxygen adsorption on CeO_2/α-Al_2O_3 catalyst supports // J. Chem. Soc. - Faraday Trans. – 1996. – V. 92. – P. 1619 - 1626.

[139] R. Di Monte, P. Fornasiero, J. Kašpar, P. Rumori, G. Gubitosa, and M. Graziani. Stabilisation of nanostructured CeO_2–ZrO_2 solid solutions by addition of Al_2O_3: a suitable way for production of thermally stable oxygen storage/release promoters for three-way catalysts // Appl. Catal. B: Environ. – 2001. – V. 140. – P. 229 - 236.

[140] A. Piras, A. Trovarelli, and G. Dolcetti. Remarkable stabilization of transition alumina operated by ceria under reducing and redox conditions // Appl. Catal. B: Environ. – 2000. – V. 28. - L77 – L81.

[141] G. Ranga, J. Kašpar, R. Di Monte, S.Meriani and M.Graziani. NO Decomposition over Partially Reduced Metallized CeO_2-ZrO_2 Solid Solution // Catal. Lett. – 1994. – V 24. – P. 107 – 112.

[142] H. Vidal, J. Kašpar, M. Pijolat, G. Colon, S. Bernal, A.M. Cordon, V. Perrichon, F. Fally. Redox behavior of CeO_2–ZrO_2 mixed oxides I. Influence of redox treatments on high surface area catalysts // Appl. Catal. B: Environ. – 2000. – V. 27. – P. 49 - 63.

[143] H. Vidal, J. Kašpar, M. Pijolat, G. Colon, S. Bernal, A.M. Cordon, V. Perrichon, F. Fally. Redox behavior of CeO_2–ZrO_2 mixed oxides II. Influence of redox treatments on high surface area catalysts // Appl. Catal. B: Environ. – 2001. – V. 30. – P. 75 - 85.

[144] R.T. Baker, S. Bernal, G. Blanco, A.M. Cordon, J.M. Pintado, J.M. Rodriguez-Izquierdo, F. Fally, V. Perrichon. Reversible changes in the redox behaviour of a $Ce_{0.68}Zr_{0.32}O_2$ mixed oxide: effect of alternating the re-oxidation temperature after reduction at 1223 K // Chem. Commun. – 1999. - P. 149 - 150.

[145] N. Izu, T. Omata, and S. Otsuka-Yao-Matsuo. Oxygen release behaviour of $Ce_{(1-x)}Zr_xO_2$ powders and appearance of $Ce_{(8-4y)}Zr_{4y}O_{(14-\delta)}$ solid solution in the ZrO_2–CeO_2–$CeO_{1.5}$ system // J. Alloys Comp. – 1998. – V. 270. – P. 107 – 114.

[146] S. Otsuka-Yao, H. Morikawa, N. Izu, and K. Okuda. Oxygen evolution properties of CeO_2-ZrO_2 powders as automotive exhaust sub-catalysts and the phase diagrams // Nippon Kinzoku Gakkaishi – 1995. – V. 59. – P. 1237 - 1246.

[147] H. Kishimoto, T. Omata, S. Otsuka-Yao-Matsuo, K. Ueda, H. Hosono, and H. Kawazoe. Crystal structure of metastable k-CeZrO phase possessing an ordered arrangement of Ce and Zr ions // J. Alloys Comp. – 2000. – V. 312. – P. 94 - 103.

[148] Y. Nagai, T. Yamamoto, T. Tanaka, S. Yoshida, T. Nonaka, T. Okamoto, A. Suda, and M. Sugiura. X-ray absorption fine structure analysis of local structure of CeO_2-ZrO_2 mixed oxides with the same composition ratio (Ce/Zr = 1) // Catal. Today – 2002. – V. 74. – P. 225 - 234.

[149] A. Suda, Y. Ukyo, H. Sobukawa, and M. Sugiura. Improvement of oxygen storage capacity of CeO_2–ZrO_2 solid solution by heat treatment in reducing atmosphere // J. Ceram. Soc. of Japan – 2002. – V. 110. – P. 126 – 130.

[150] J.C. Conesa. Computer modeling of local level structures in (Ce,Zr) mixed oxide // J. Phys. Chem. B. – 2003. - V. 107. – P. 8840 - 8853.

[151] P. Vidmar, P. Fornasiero, J. Kašpar and M. Graziani. Effects of trivalent dopants on the redox properties of $Ce_{0.6}Zr_{0.4}O_2$ mixed oxide // J. Catal. – 1997. - V. 171. - P. 160 - 168.

[152] B. Harrison, A.F. Diwell and C. Hallett. Plat. Met. Rev. – 1988. – V. 32. - P. 73 - 83.

[153] T.Ozaki, T.Masui, K.Machida, G.Adachi, T.Sakata, and H.Mori. Redox behavior of surface-modified CeO_2-ZrO_2 catalysts by chemical filing process // Chem. Mater. – 2000. - V. 12. – P. 643 - 649.

[154] C.E. Hori, A.Brenner, K.Y.S. Ng, K.M. Rahmoeller, and D. Belton. Studies of the oxygen release reaction in the platinum-ceria-zirconia system // Catal. Today. – 1999. – V. 50. – P. 299 - 308.

[155] M. Boaro, C. de Leitenburg, G. Dolcetti, and A. Trovarelli. The dynamics of oxygen storage in ceria–zirconia model catalysts measured by CO oxidation under stationary and cycling feedstream compositions // J. Catal. – 2000. – V. 193. – P. 338 - 347.

[156] P. Fornasiero, T. Montini, M. Graziani, J. Kašpar, A.B. Hungria, A. Martinez-Arias, and J.C. Conesa. Effects of thermal pretreatment on the redox behaviour of Ce0.5Zr0.5O2: isotopic and spectroscopic studies // Phys. Chem. Chem. Phys. - 2002. – V. 4. – P. 149 - 159.

[157] K. Yamada, H. Tanaka, M. Yamamoto. Oxygen storage capacity on cerium oxide – preciouse metal system // SAE Technical Paper Series 970464 - 1997.

[158] B.K. Cho. Chemical modification of catalyst support to enhancement of transient catalytic activity: nitric oxide reduction by carbon monoxide over rhodium // J. Catal. – 1991. – V. 131. – P. 74 – 87.

[159] P. Shuk, M. Greenblatt and M. Croft. Hydrothermal synthesis and properties of mixed conducting $Ce_{1-x}Tb_xO_{2-\delta}$ solid solutions // Chem. Mater. – 1999. V. 11. - P. 473 - 479.

[160] C.K. Narula, L.P. Haack, W. Chun, H.-W. Jen and G.W. Graham. Single-phase PrO_y-ZrO_2 materials and their oxygen storage capacity: a comparison with single-phase CeO_2-ZrO_2, PrO_y-CeO_2, and PrO_y-CeO_2-ZrO_2 materials // J. Phys. Chem. B – 1999. - V. 103. - P. 3634 - 3639.

[161] R.D. Shannon and C.T. Prewitt. Effective ionic radii in oxides and fluorides // Acta Crystallographica B. – 1969. - V. 25. - P. 925 - 946.

[162] Y. Zhang, A. Andersson and M. Muhammed. Nanophase catalytic oxides: I. Synthesis of doped cerium oxides as oxygen storage promoters // Appl. Catal. B: Environ. – 1995. – V. 6. - P. 325 - 337.

[163] C. Lammonier, A. Bennani, A. D'Huysser, A. Aboukaïs and G. Wrobel. Evidence for different copper species in precursors of copper-cerium oxide catalysts for hydrogenation reactions: an X-ray diffraction, EPR and X-rayphotoelectron spectroscopy study // J. Chem. Soc. Faraday Trans. – 1996. – V. 92. - P. 131 - 136.

[164] S. Imamura, M. Shono, N. Okamoto, A. Haneda and S. Ishida. Effect of cerium on the mobility of oxygen on manganese oxides // Appl. Catal. A: Gen. – 1996. - V. 142 - P. 279 - 288.

[165] A. Trovarelli. Catalytic properties of ceria and CeO_2-containing materials // Catal. Rev. Sci. Eng. – 1996. - V. 38. – P. 439 - 520.

[166] S. Bernal, J.J. Calvino, M.A. Cauqui, J.M. Gatica, C.L. Cartes, J.A.P. Omil, and J.M. Pintado. Some contributions of electron microscopy to the characterization of the strong metal–support interaction effect // Catal. Today. – 2003. – V. 77. – P. 385 - 406.

[167] A.Trovarelli. Catalysis by Ceria and Related Materials // Imperial College Press, London. – 2002. - P. 1 - 500.

[168] R.Di Monte and J.Kašpar. On the role of oxygen storage in three-way catalysis // Top. Catal. – 2004. – V. 28. – P. 47 - 58.

[169] A. Trovarelli, G. Dolcetti, C. de Leitenburg, J. Kašpar, P. Finetti, and A. Santoni. Rh-CeO_2 interaction induced by high-temperature reduction - characterization and catalytic behavior in transient and continuous conditions // J. Chem. Soc. Faraday Trans. – 1992. – V. 88. – P. 1311 – 1319.

[170] C. de Leitenburg and A. Trovarelli. Metal-support interactions in Rh/CeO_2, Rh/TiO_2 Rh/Nb_2O_5. Catalysts as inferred from CO_2 methanation activity // J. Catal. – 1995. -V. 156. – P. 171 - 174.

[171] G. Ranga Rao, P. Fornasiero, R. Di Monte, J. Kašpar, G. Vlaic, G. Balducci, S. Meriani, G. Gubitosa, A. Cremona, and M. Graziani. Reduction of NO over partially reduced metal-loaded CeO_2–ZrO_2 solid solutions // J. Catal. – 1996. – V 162. – P. 1 - 9.

[172] C. de Leitenburg, A. Trovarelli, and J. Kašpar. A temperature-programmed and transient kinetic study of CO_2 activation and methanation over CeO_2 supported noble metals // J. Catal. – 1997. – V. 166 – P. 98 - 107.

[173] A. Galdikas, D. Duprez, and C. Descorme. A novel dynamic kinetic model of oxygen isotopic exchange on a supported metal catalyst // Appl. Surf. Sci. – 2004. – V. 236 - P. 342 - 355.

[174] M. Fernandez-Garcia, A. Martinez-Arias, L.N. Salamanca, J.M. Coronado, J.A. Anderson, J.C. Conesa, and J. Soria. Influence of ceria on Pd activity for the CO + O_2 reaction // J. Catal. – 1999. - V. 187. – P. 474 - 485.

[175] S. Golunski, R. Rajaram, N. Hodge, G.J. Hutchings, and C.J. Kiely. Low-temperature redox activity in co-precipitated catalysts: a comparison between gold and platinum-group metals // Catal. Today – 2002. – V. 72. – P. 107 - 113.

[176] V.A. Sadykov, Yu.V. Frolova-Borchert, N.V. Mezentseva, G.M. Alikina, A.I. Lukashevich, E.A. Paukshtis, V.S. Muzykantov, L.Ch. Batuev, T.G. Kuznetsova, E.M. Moroz, D.A. Zyuzin, V.P. Kol'ko, E.B. Burgina, V.V. Kriventsov, D.I. Kochubei, E. Kemnitz, K. Scheurell. Nanocrystalline catalysts based on CeO_2-ZrO_2 doped by praseodymium or gadolinium: synthesis and properties // Mater. Res. Soc. Symp. Proc. – 2006. - 0900-O10-04.1.

[177] T.G. Kuznetsova, V.A. Sadykov, E.M. Moroz, S.N. Trukhan, E.A. Paukshtis,V.N. Kolomiichuk, E.B. Burgina, V.I. Zaikovskii, M.A. Fedotov, V.V. Lunin, E. Kemnitz, Preparation of Ce-Zr-O composites by a polymerized complex method // Stud. Surf. Sci. Catal. – 2002. – V. 143. – P. 659 - 667.

[178] S. Brunauer, P.H. Emmet and E. Teller. Adsorption of gases in multimolecular layers // J. Am. Chem. Soc. – 1938. – V. 60. - P. 309 – 319.

[179] J.W. Niemantsverdriet. Microscopy and imaging in “Spectroscopy in catalysis” (Second Edition) // Wiley-VCH Verlag GmbH, Weinheim – 2000. - P. 167 - 200.

[180] A. Stefanescu, A.C. van Veen, C. Mirodatos, J.-C. Beziat, E. Duval-Brunel. Wall coating optimization for microchannel reactors // Catal. Tod. – 2007. – V. 125. - P. 16 - 23.

[181] J.W. Niemantsverdriet. The Vibrational Spectroscopies In “Spectroscopy in Catalysis (Second Edition)” // Wiley-VCH Verlag GmbH, Weinheim – 2000. - P. 201 - 229.

[182] M.P. Seah. Practical surface analysis by auger and X-ray photoelectron spectroscopy (D. Briggs and M.P. Seah, eds.) // John Wiley &Sons. - 1983.

[183] J.F. Moulder, W.F. Stickle, P.E. Sobol, K.D. Bomben. Handbook of X-ray photoelectron spectroscopy // Perkin-Elmer Corporation, Physical Electronics Division, Eden Prairie Minnesota - 1992.

[184] H. Kobayashi, M. Kobayashi. Tansient response method in heterogeneous catalysis // Catal. Rev. – 1974. – V. 10. – P. 139 - 176.

[185] C.O. Bennett. The transient method and elementary steps in heterogeneous catalysis // Catal. Rev. – 1976. – V. 13. – P. 121 - 148.

[186] J.T. Gleaves, J.R. Ebner, T.C. Kuechler. Temporal analysis of products (TAP) – a unique catalyst evaluation system with submillisecond time resolution // Catal. Rev.- Sci. Eng. – 1988. – V. 30. – P. 49 – 116.

[187] O. Hinrichsen, A.C. van Veen, H.W. Zanthoff, M. Muhler. TAP reactor studies in in-situ spectroscopy in heterogeneous catalysis (ed. James F. Haw) // ISBN 3-527-30248-4, Wiley-VCH Verlag GmbH, Weinheim. – 2002. – P. 237 - 269.

[188] J.R. Ebner, J.T. Gleaves, T.C. Kuechler, T.P. Li. Studies of binary oxide catalysts for the ammoxidation of methanol to hydrogen cyanide // Symposium on Chemicals from Syngas and Methanol Presented before the Division of Petroleum Chemistry, Inc. American Chemical Society, New York Meeting. - 1986.

[189] J.T. Gleaves, G.S. Yablonskii, P. Phanawadee, Y. Schuurman. TAP-2: An interrogative kinetics approach // Appl. Catal. - 1997. – V. 160 – P. 55 - 88.

[190] A. Slagtern, Y. Schuurman, C. Leclercq, X. Verykios, C. Mirodatos. Specific features concerning the mechanism of methane reforming by carbon dioxide over Ni/La_2O_3 catalyst // J. Catal. – 1997. – V. 172. – P. 118 – 126.

[191] P. Aghalayam, Y.K. Park, N. Fernandes, V. Papavassiliou, A.B. Mhadeshwar and D.G. Vlachos. A C1 mechanism for methane oxidation on platinum // J. Catal. – 2003. - V. 213. – P. 23 – 38.

[192] S. Pavlova, N. Sazonova, V. Sadykov, S. Pokrovskaya, V. Kuzmin, G. Alikina, A. Lukashevich and E. Gubanova. Partial oxidation of methane to synthesis gas over corundum supported mixed oxides: One channel studies // Catal. Tod. - 2005. – V. 105. – P. 367 - 371.

[193] V.A. Sadykov, S.N. Pavlova et al. Selective oxidation of hydrocarbons into synthesis gas at short contact times: Design of monolith catalysts and main process parameters // Kinetics and Catalysis – 2005. – V. 46 – P. 227 - 250.

[194] S.N. Pavlova, N.N. Sazonova, V.A. Sadykov, O.I. Snegurenko, V.A. Rogov, E.M. Moroz, I.A. Zolotarsky, A.V. Simakov, V.N. Parmon. Selective catalytic oxidation of methane to syngas over supported mixed oxides comprising Ni and Pt // Kinetics and Catalysis. – 2004. – V. 45. – P. 1 – 10.

[195] M. Soick, O. Buyevskaya, M.Höhenberger, D. Wolf. Partial oxidation of methane to synthesis gas over Pt/MgO. Kinetics of surface processes // Catal. Tod. – 1996. – V. 32 – P. 163 - 169.

[196] J.R. Ferraro, K. Nakamoto, Introductory Raman Spectroscopy, Academic Press, New York - 1994.

[197] M. Fernández-García, A. Martínez-Arias, A. Iglesias-Juez, A.B. Hungría, J.A. Anderson, J.C. Conesa, J. Soria. Thermal behavior of $(Ce,Zr)O_x$ / Al_2O_3 complex oxides prepared by a microemulsion method // Phys. Chem. Chem. Phys. - 2002. – V. 4. – P. 2473 - 2481.

[198] E.F. Lopez, V.S. Escribiano, M. Panizza, M.M. Carnasciali, G. Busca. Vibrational and electronic spectroscopic properties of zirconia powders // J. Mater. Chem. – 2001. – V. 11 - P. 1891 - 1897.

[199] S. Wang, W. Wang, J. Zuo, Y. Qian. Study of the Raman spectrum of CeO_2 nanometer thin films // Mater. Chem. Phys. – 2001. - V. 68. – P. 246 – 248.

[200] D. Kim, H. Jung, I. Yang, J. Raman spectroscopy of tetragonal zirconia solid solutions // Am. Ceram. Soc. – 1993. – V. 76. – V. 2106 - 2108.

[201] X.-M. Lin, L.-P. Li, G.-S. Li, W.-H. Su. Transport property and Raman spectra of nanocrystalline solid solutions $Ce_{0.8}Nd_{0.2}O_{2-\delta}$ with different particle size // Mater. Chem. Phys. – 2001. – V. 69. – P. 236 - 240.

[202] M. Shelef, L.P. Haack, R.E. Soltis, J.E. Devries, E.M. Logothetis, An XPS study of interactions in thin films containing a noble metal with valence-invariant and reducible oxides // J. Catal.– 1992. – V. 137. – P. 114 – 126.

[203] K.H. Hofstad, O.A. Rokstad and A. Holmen. Partial oxidation of methane over platinum metal gauze // Catal. Lett. – 1996 – V. 36 – P. 25 – 30.

[204] A. Beretta, P. Baiardi, D. Prina, P. Forzatti. Analysis of a catalytic annular reactor for very short contact times // Chem. Eng. Sci. – 1999. – V. 54. – P. 765 – 773.

[205] G.F.Froment, K.B. Bischoff. Chemical reactor analysis and design , 2nd ed. Wiley – 1990. – 704 pages.

[206] S.T. Sie. Miniaturization of hydroprocessing catalyst testing systems: Theory and practice // AIChE J. – 2004. – V.42. – P. 3498 – 3507.

[207] G. Groppi, A. Belloni, E. Troncani, P. Forzatti. A comparison of lumped and distributed models of monolith catalytic combustors // Chem. Eng. Sci. – 1995. – V. 50. – P. 2705-2715.

[208] R.E. Hayes, S.T. Kolaczkowski. Introduction to catalytic combustion // Gordon and Breach Science Publishers – 1997. – Ps. - 681.

[209] H.W. Brauer and F. Fetting. Stofftransport bei wandreaktion im einlaufgebiet eines stromungsrohres // Chem. Ing. Technol. – 1966. – V. 38. – P. 30 - 35.

[210] R.C. Reid, J.M. Prausnitz, B.E. Poling. The properties of gases and liquids", 4th ed., New York: McGraw Hill. – 1998.

[211] A.C. Hindemarsh. ODEPACK, A systematized collection of ODE solvers // Elsevier. – 1983. – P. 55 – 64.

[212] W.R. Williams, C.M. Marks, L.D. Schmidt. Steps in the reaction $H_2+O_2 \leftrightarrow H_2O$ on Pt: OH desorption at high temperatures // J. Phys. Chem. – 1992. – V. 96. – P. 5922 – 5931.

[213] D.A. Hickman, L.D. Schmidt. Step in CH_4 oxidation on the Pt and Rh surface: high-temperature reactor simulations // AIChE J. – 1993. – V. 39. – P. 1164 – 1177.

[214] C.-T. Au, C.-F. Ng, M.-S. Liao. Methane dissociation and syngas formation on Ru, Os, Rh, Ir, Pd, Pt, Cu, Ag and Au : a theoretical study // J. Catal. – 1999. – V. 185. – P. 12 – 22.

[215] E. Shustorovich. The bond-order conservation approach to chemisorption and heterogeneous catalysis: applications and implications // Adv. Catal. – 1990. – V. 37. – P. 101 – 164.

[216] A.B. Anderson, J.J. Moloney. Activation of methane on iron, nickel, and platinum surfaces. A molecular orbital study // J. Phys. Chem. – 1988. – V. 92. – P. 809 – 812.

[217] E.L. Gubanova, A. van Veen, C. Mirodatos, V.A. Sadykov, N.N. Sazonova // Влияние подвижности кислорода сложного оксидного носителя на механизм парциального окисления метана (in Russian, reading to "Influence of the oxygen mobility in complex oxide supports on the mechanism of the partial oxidation of methane") Russ. Chem. J. - 2008. - V. 52. - P. 21 – 31.

[218] R.H. Nibbelke, A.J.L. Nievergeld, J.H.B.J. Hoebink, G.B. Marin. Development of a transient kinetic model for the CO oxidation by O_2 over a $Pt/Rh/CeO_2/\gamma\text{-}Al_2O_3$ three-way catalyst // Appl. Catal. B: Environ. – 1998. – V. 19. – P. 245-259.

[219] F. Monnet, Y. Schuurman, F. Cadete Santos Aires, J.C. Bertolini, C. Mirodatos. Silicon nitride supported platinum catalysts for the partial oxidation of methane at high temperatures // Catal. Today. – 2001. – V. 64 – P. 51 - 58.

[220] E.Bergene, O.Tronstad, and A.Holmen. Surface areas of Pt-Rh catalyst gauzes used for ammonia oxidation // J. Catal. – 1994. – V. 146. – P. 141 - 147.

[221] M.F.H. van Tol, A. Gielbert, B.E. Nieuwenhuys. The adsorption and dissociation of CO_2 on Rh // Appl. Surf. Sci. – 1993. – V. 67 – P. 166 - 178.

[222] J.P. Huinink, Doctorate Thesis, Eindhoven University of Technology, The Netherlands, 1995.

[223] A.M. O'Connor, Y. Schuurman, J.R.H. Ross, C. Mirodatos. Transient studies of carbon dioxide reforming of methane over Pt/ZrO_2 and Pt/Al_2O_3 // Catal. Today – 2006. – V. 115. – P. 191-198.

[224] C.T. Campbell. Future directions and industrial perspectives micro- and macro-kinetics: their relationship in heterogeneous catalysis // Topics Catal. – 1994. – V.1 – P. 353 - 366.

TITRE en français :

Étude expérimentale et modélisation de l'oxydation partielle du méthane en gaz de synthèse sur réacteur catalytique monolithique à temps court

---

RESUME en français :

Cette étude a pour objectif principal de développer un réacteur structuré de type monolithe pour atteindre des performances élevées en oxydation partielle du méthane en gaz de synthèse. Les catalyseurs étudiés sont à base de Pt et Ni comme métaux noble et non noble, respectivement, supportés sur un oxyde mixte CeO_2-ZrO_2 et déposés sur les parois d'un monolithe en corundum. Le rôle de différents dopants introduits dans le support oxyde mixte du catalyseur vis à vis du stockage-déstockage d'oxygène a été élucidé et l'influence des conditions opératoires et des paramètres du procédé sur les performances d'un élément mono canal du monolithe a été précisée. Une étude mécanistique a révélé d'importants facteurs comme la nature et la dynamique des espèces de surface et de cœur et montré que l'interaction entre le Pt et l'oxyde mixte CeO_2-ZrO_2 déterminait l'activité du catalyseur. Des expériences cinétiques ont démontré que le Pt est requis pour les réactions de reformage mais que le support CeO_2-ZrO_2 dopé pouvait présenter une activité non négligeable pour l'activation oxydante du méthane. Une modélisation mathématique des données expérimentales a été réalisée avec un modèle prenant en compte essentiellement l'activité du Pt. Cette dernière a été trouvée très supérieure à celle du support. Cependant des expériences en réacteur TAP ont montré qu'une oxydation du catalyseur permettait une vitesse d'oxydation du méthane supérieure.

TITRE en anglais :

Experimental study and mathematical modeling of catalytic partial oxidation of methane to synthesis gas over monolith catalyst at short contact times

---

RESUME en anglais :

Main objective of the thesis was to develop a structured reactor for the efficient catalytic partial oxidation of methane (CPOM) to synthesis gas. The investigated catalysts comprised Pt as noble or Ni as base metal supported on CeO_2-ZrO_2 mixed oxides introduced as wall coatings of corundum monolith substrates. It was possible to elucidate the effect of different dopants modifying the mixed oxide and to establish the impact of process parameters on the CPOM performance of single monolith channels at short contact times. A mechanistic study revealed important factors, e.g. surface (species) or bulk (storage) effects, in the interaction between the CeO_2-ZrO_2 mixed oxide and Pt, playing a key role as the most active sites. Kinetic experiments lead to the insight that Pt is required for reforming reactions and showed a significant reactivity of the doped CeO_2-ZrO_2 support in the oxidative methane activation. A mathematical description of the experimental data was achieved with a model accounting mainly for the activity of Pt. The activity of Pt sites was found significantly higher than that of the support although TAP investigations indicated that a more oxidized catalyst shows lower methane activation rates.

DISCIPLINE :

Chimie – Génie des procédés

MOTS-CLES :

Catalytic partial oxidation of methane, synthesis gas, $CeZrO_x$ support, structured catalyst, short contact times, reaction mechanism, kinetic study

---

INTITULE ET ADRESSE DE L'U.F.R. OU DU LABORATOIRE :

Institut de Recherche sur la Catalyse et l'Environnement de Lyon, IRCELYON
2, avenue Albert Einstein, 69626 VILLEURBANNE, FRANCE